

**EXCITED STATE PI ELECTRON DONOR - ACCEPTOR INTERACTIONS: THE
INFLUENCE OF ELECTRONIC STRUCTURE ON THE PHYSICAL PROPERTIES AND
PROCESSES OF DIBENZOYLMETHANATOBORON DIFLUORIDE / BENZENE
EXCIPLEXES**

by

Carl Ingemar Johansson

B.Sc. (Hon.), Simon Fraser University, 1987

A THESIS SUBMITTED IN PARTIAL FULFILLMENT OF THE
REQUIREMENTS FOR THE DEGREE OF
DOCTOR OF PHILOSOPHY
in the Department
of
Chemistry

© Carl I. Johansson 1994

SIMON FRASER UNIVERSITY

December 1994

All rights reserved. This work may not be reproduced in
whole or in part, by photocopy or other means, without
permission of the author.

Approval

Name: Carl Ingemar Johansson
Degree: Doctor of Philosophy
Title of thesis: Excited State π Electron Donor - Acceptor Interactions: The Influence of Electronic Structure on the Physical Properties and Kinetic Processes of Dibenzoylmethanatorboron Difluoride / Benzene Exciplexes.

Examining Committee:

Chair: Dr. Saul Wolfe

Dr. Y. L. Chow
Senior Supervisor

Dr. B. Mario Pinto

Dr. Paul Percival

Dr. Ross Hill
Internal Examiner
Department of Chemistry

Dr. Jack Saltiel
External Examiner
Department of Chemistry
Florida State University

Date of Approval: December 7, 1994

PARTIAL COPYRIGHT LICENSE

I hereby grant to Simon Fraser University the right to lend my thesis, project or extended essay (the title of which is shown below) to users of the Simon Fraser University Library, and to make partial or single copies only for such users or in response to a request from the library of any other university, or other educational institution, on its own behalf or for one of its users. I further agree that permission for multiple copying of this work for scholarly purposes may be granted by me or the Dean of Graduate Studies. It is understood that copying or publication of this work for financial gain shall not be allowed without my written permission.

Title of Thesis/Project/Extended Essay:

Excited State π Electron Donor-Acceptor Inter-
actions: The Influence of Electronic Structure
on the Physical Properties and Processes of
Dibenzogluconato boron Difluoride / Benzene Exciplexes

Author: _____

" (signature)

(name)

December 8, 1994

(date)

Abstract

The photocycloaddition of dibenzoylmethanoboron difluoride (DBMBF₂), and allied β-diketonatoboron difluoride complexes, with olefins and enones is known to be initiated from DBMBF₂'s singlet excited state where an excited state complex (exciplex) intermediate was proposed; however, this intermediate could not be detected spectroscopically. In contrast, singlet excited DBMBF₂ interacts with various substituted benzenes to show a strong exciplex emission in nonpolar to aprotic polar solvents where no photocycloaddition was observed. Taking advantage of the strong exciplex emission and lack of photoreactivity, the DBMBF₂ / benzene system was chosen as a model to study the interaction between singly excited β-diketonatoboron difluoride complexes with electron π donors.

Steady state fluorescence studies have illustrated that the DBMBF₂ / benzene exciplex can be generated from either excitation of the ground state DBMBF₂ or its electron - donor complex with benzenes. Emission solvatochromism studies, with a carefully selected set of solvents, illustrated that the degree of electron transfer (ET) within these exciplexes ranges from complete to negligible ET, which is correlated to the benzene's oxidation potential. This variation in exciplex dipolar character was rationalized by a valence bond-like function for the interaction between the charge transfer, |A⁻D⁺⟩, and locally excited, |*AD⟩, configurations: $\Psi_{\text{ex}} = a |A^{-}D^{+}\rangle + c |*AD\rangle$.

Steady state and time-resolved fluorimetry were used to examine the influence of the charge transfer and locally excited configuration on the exciplex's physical properties. The charge transfer configuration was found to control the exciplex's binding energy, hence the rate constants for exciplex formation and dissociation, and the exciplex free energy. The locally excited configuration was found to control the exciplex's radiative and radiationless processes.

Dedication

To my wife Jinping Jiang and my son Calvin Jiang Johansson.

To dad, mom and family.

To the memory of:
my sister Marianne Johansson and
Gene Roddenberry.

Acknowledgements

The author wishes to express his gratitude to:

Dr. Y.L. Chow for his continual encouragement, guidance and financial support during the course of this study.

Drs. P. Percival and B.M. Pinto for encouragement and guidance.

Dr. E.M. Voigt for her interest in the author's post-secondary education and teaching the author about EDA complexes.

Dr. S. Holdcroft for permission to use the LS-100 and electrochemical equipment.

Mr. G. Owens (mass spectroscopy), Mrs. Tracy (magnetic resonance) and Mr. P. Saunders (jack-of-all-trades) for their 'beyond the call of duty' help.

Dr. and Mrs. Cheng.

Dr. P. Wan of the University of Victoria (Department of Chemistry) for permission to use the PTI LS-1 system.

Dr. D. Shukla of the University of Victoria (Department of Chemistry) for help in fine tuning the LS - 1.

Mr. Jonathan 'Sweet Cheeks' Male

Mr. & Mrs. Marcel 'Bumchimp' Veronesi.

Members of Dr. Chow's group, past and present, for valuable advice and friendship.

Financial support from Simon Fraser University and the Department of Chemistry is gratefully acknowledged.

TABLE OF CONTENTS

Title Page	i
Approval	ii
Abstract	iii
Dedication	vi
Acknowledgements	vii
Table of Contents	viii
List of Tables	xiv
List of Figures	xvii
List of Abbreviations	xxiii
List of Symbols	xxvi

CHAPTER ONE

INTRODUCTION : β -DIKETONATOBORON COMPLEXES

1.1	General	1
1.2	Photochemistry/physics	4
1.3	Motivation and Thesis Overview	6

CHAPTER TWO

THEORETICAL ASPECTS

2.1	Classical Marcus Theory of Electron Transfer	9
2.2	Bimolecular Photoinduced Electron Transfer	18
2.3	Molecular Complexes	20
	2.3.1 Electron Donor - Acceptor Complex	21
	2.3.2 Exciplexes	26
2.4	Solvatochromism and Exciplex Dipolar Character	34

2.5	Polarographic and Excited State Energies	48
-----	--	----

CHAPTER THREE

SPECTROSCOPIC AND REDOX PROPERTIES OF β -DIKETONATOBORON COMPLEXES

3.1	Introduction	52
3.2	UV - Visible Absorption - Results and Discussion	52
3.3	Luminescence	61
3.3.1	Introduction	61
3.3.2	Results and Discussion	62
3.3.2.1	General	63
3.3.2.2	Nature of the Singlet and Triplet States	71
3.4	Redox Potentials of β -Diketonatoboron Complexes	75
3.4.1	Introduction	75
3.4.2	Results and Discussion	75
3.4.2.1	Changes on Complexation	75
3.4.2.2	Relationship to Electronic Structure	79
3.4.2.3	Relationship with Excitation Energies	80
3.5	Conclusions	83

CHAPTER FOUR

ELECTRON DONOR - ACCEPTOR COMPLEXES

4.1	Introduction	84
4.2	Results and Discussion	84

CHAPTER FIVE

GENERAL MECHANISTIC OVERVIEW

5.1	Introduction	97
5.2	Results and Discussion	100
5.2.1	Reaction Intermediate	100
5.2.2	Reaction Order	104
5.2.2.1	Stoichiometric Expressions	104
5.2.2.2	DBMBF ₂ / Substituted Benzene Complex Stoichiometry	106
5.2.3	Reaction Scheme	108

CHAPTER SIX

THE NATURE OF THE EXCIPLEX

6.1	Introduction	110
6.2	Results and Discussion	110
6.2.1	DBMBF ₂ / Substituted Benzene Exciplex Dipolar Character	110
6.2.2	Solvatochromic Analysis	116
6.2.3	Solvent Effect on Exciplex CT Character	122
6.2.4	Exciplex Wavefunction and Frontier Orbitals	124
6.2.5	β -Diketonatoboron Complex and Exciplex CT Character	129
6.2.6	Final Comments	133

CHAPTER SEVEN

EXCIPLEX BINDING ENERGY IN CYCLOHEXANE

7.1	Introduction and Mathematical Formulae	135
7.1.1	General	135
7.1.2	Formulae for the Determination of Exciplex Binding	

	Energies	138
7.2	Results and Discussion	141
	7.2.1 Exciplex Binding Energy	142
	7.2.2 Steric Effects on the Ground and Excited State	
	Surfaces	148
	7.2.3 Stabilization of Weak CT Exciplexes	152

CHAPTER EIGHT

KINETIC AND THERMODYNAMIC PARAMETERS OF DBMBF₂ / BENZENE

EXCIPLEXES IN CYCLOHEXANE

8.1	Introduction and Mathematical Models	156
8.2	Results and Discussion	158
	8.2.1 Exciplex Process Rate Constants in Cyclohexane	158
	8.2.2 Exciplex and Excited EDA Complex	172
	8.2.3 Thermodynamic Properties	176

CHAPTER NINE

EXCIPLEX RADIATIVE AND RADIATIONLESS PROCESSES IN CYCLOHEXANE

9.1	Introduction and Mathematical Models	182
	9.1.1 General	182
	9.1.2 Emission Probability	182
	9.1.3 Radiationless Probability	185
9.2	Results and Discussion	187
	9.2.1 General	187
	9.2.2 Exciplex Radiative Probability	188
	9.2.3 Exciplex Radiationless Probability	199

CHAPTER TEN

FLUORESCENCE QUENCHING DYNAMICS IN ACETONITRILE

10.1	Introduction	206
10.2	Results and Discussion	208
10.2.1	Substituted Benzene Electron Donors	208
10.2.2	Exergonic Region	214
10.2.3	Endergonic Region	223

CHAPTER ELEVEN

EXPERIMENTAL

11.1	General	228
11.2	Chemicals	228
11.3	Boron Complexes	229
11.3.1	Dibenzoylmethantoboron Difluoride (DBMBF ₂)	229
11.3.2	4-Methoxy-4'-t-butyl-dibenzoylmethanatoboron difluoride (MBDBF ₂)	229
11.3.3	Other β - diketonatoboron Complexes	230
11.4	EDA Complexes	230
11.4.1	Sample Preparation	230
11.4.2	Association Equilibrium Constants	232
11.4.3	Enthalpy of EDA Complex Formation	232
11.5	Steady State Fluorimetry	233
11.5.1	Instrument and Setup	234
11.5.2	Sample Preparation and Conditions	235
11.5.3	Exciplex Emission and Resolution of Unresolved Fluorescent Bands	237
11.5.4	Fluorescence Quenching in Acetonitrile	238

11.5.5	Exciplex Enthalpy of Formation	240
11.5.6	Fluorescence Center of Gravity	240
11.5.7	Exciplex Fluorescence Quantum Yield ($\Phi_{\text{ex}}^{\infty}$)	244
11.5.8	Excited State Energies and Fluorescence Quantum Yields	245
11.5.9	Total Emission and Phosphorescence	247
11.6	Time - Resolved Fluorimetry	248
11.6.1	Time - Correlated Single Photon Counting	248
11.6.2	The LS - 1	248
11.6.3	Calibration and Time Resolution	249
11.6.4	Data Analysis	251
11.7	UV - Vis Absorption	253
11.8	Cyclic Voltammetry	253
11.9	Fitting of Exciplex Dipole Moment to Theory	256
11.10	Estimation of Errors	257
	REFERENCES	261

LIST OF TABLES

Table 1.1:	Dipole Moments of Some β -Diketonatoboron Complexes	4
Table 2.1:	Selected Solvatochromic Dyes and Their Properties	37
Table 2.2:	Common Assumptions Applied in Deriving Solvatochromic Equations	47
Table 3.1:	UV-Vis Spectroscopic Data for the Principle Absorption Bands of Some β -Diketonatoboron Complexes	59
Table 3.2:	Fluorescence Lifetimes and Quantum Yields of Emission of Various β -Diketonatoboron Complexes	64
Table 3.3:	The Lowest Spectroscopic Singlet and Triplet Energies for Various β -Diketonatoboron Complexes	65
Table 3.4:	Redox Potentials of Some Boron Complexes in Acetonitrile	77
Table 4.1:	DBMBF ₂ / Substituted Benzene EDA Complex Formation Enthalpies and Association Equilibrium Constants in Cyclohexane and Acetonitrile	88
Table 5.1:	Bimolecular Quenching Processes	98
Table 6.1:	DBMBF ₂ / Substituted Benzene Exciplex Emission Maxima in Various Solvents	112
Table 6.2:	DBMBF ₂ / Substituted Benzene Exciplex Dipolar Nature	120
Table 6.3:	β -Diketonatoboron / p-Xylene Exciplex Fluorescence Maximum in Neat p-Xylene	131
Table 6.4:	DBMBF ₂ , BABF ₂ , and AABF ₂ / p-Xylene Exciplex Emission Maxima in Various Solvents: Influence of Acceptor	134
Table 6.5:	Comparison of Exciplex Charge Transfer fraction Obtained from Solvatochromic Analysis and the Slope of Figure 6.5.	134

Table 7.1:	DBMBF ₂ / Benzene Exciplex Enthalpies of Formation in Cyclohexane	145
Table 8.1:	Observed λ_1 Characteristic Value for DBMBF ₂ Fluorescence Quenching by Benzenes in Oxygen Free Cyclohexane at 23 °C	160
Table 8.2:	Evaluated Kinetic Rate Constants of some DBMBF ₂ / Benzene Exciplexes in Degassed Cyclohexane at (296 K)	169
Table 8.3:	Comparison of the Lifetimes of the DBMBF ₂ / Benzene and Excited EDA Complex in Argon Degassed cyclohexane at 23 °C	174
Table 8.4:	Thermodynamic Properties of Some DBMBF ₂ / Benzene Exciplexes in Cyclohexane Under Argon	178
Table 9.1:	DBMBF ₂ / Benzene Exciplex Fluorescence Quantum Yields (Φ_{ex}^{∞}) in Argon Purged Argon	189
Table 9.2:	DBMBF ₂ / Substituted Benzene Exciplex Radiative and Radiationless Rate Constants in Cyclohexane and Aromatic Solvents; Comparison of Observed and Calculated Radiative Rate Constants	191
Table 10.1:	Fluorescence Quenching Parameters of Singlet Excited DBMBF ₂ by Benzenes in Aerated Acetonitrile	211
Table 10.2:	Fluorescence Quenching Parameters of Singlet Excited DBMBO by Benzenes in Aerated Acetonitrile	213
Table 10.3:	Fluorescence Quantum Yields of DBMBF ₂ / Benzene Exciplexes in Aerated Acetonitrile	216
Table 10.4:	Evidence for Diffusion Controlled Fluorescence Quenching of Singlet Excited DBMBF ₂ by Benzenes	221
Table 11.1:	Other β -Diketonatoboron Complexes and Their Source	231
Table 11.2:	Parameters Determined in the Gaussian Fitting of DBMBF ₂ 's Fluorescence in Figure 11.5	241

Table 11.3:	Lifetime Standards Used in Evaluating the PTI LS-1	250
Table 11.4:	Cyclic Voltammetry Calibration	255
Table 11.5:	Memory Listing	258
Table 11.6:	Calculation of the Overlap Integral for DBMBF ₂ / Benzene Exciplexes	259

LIST OF FIGURES

- Figure 2.1: Free Energy Surfaces for the Precursor and Successor Complexes as a Function of the Nuclear Coordinates of the Complexes and Solvent. 11
- Figure 2.2: The Intersection of Displaced Free Energy Parabolas as a Function of Increasing Exothermicity. **a:** $\Delta G_{ET}^{\circ} = 0$; **b:** $\Delta G_{ET}^{\circ} > \lambda$; **c:** $\Delta G_{ET}^{\circ} = \lambda$; **d:** $\Delta G_{ET}^{\circ} \ll \lambda$. 16
- Figure 2.3: Hypothetical effect of donor - acceptor distance on the electron transfer within a precursor complex. The solid lines represent ET at a donor - acceptor distance of 3.5 Å ($\lambda = 0.5$ eV, $\kappa_{el}v_n = 10^{13}$ s⁻¹) and 7.0 Å ($\lambda = 1.5$ eV, $\kappa_{el}v_n = 10^{11}$ s⁻¹). 17
- Figure 2.4: Unfavorable charge transfer interaction between a ground state donor and acceptor. 18
- Figure 2.5: A Simple MO Picture for the Interaction of a Singly Excited Acceptor with a Ground State Donor. 28
- Figure 2.6: Simulated Exciplex Dipole Moment and Resonance Interaction Energy of a Hypothetical Exciplex with a Wavefunction Described by $\Psi_{EX} = a |A^{\cdot-}D^{\cdot+}\rangle + b |A^*AD\rangle$. The Calculation Assumed a Configuration Overlap of 0.03, an Acceptor Singlet Energy of 3.0 eV, a Constant Donor IP of 8.5 eV and a Maximum Exciplex Dipole Moment of 13 Debyes. 35
- Figure 2.7: Schematic Representation of the Relative Change in the Excited and Ground State Energy Levels as a Function of their Dipole Moments. 36
- Figure 2.8: The Ground and Excited State Non - Equilibrium Free Energies (F_g and F_e , respectively) vs. the Solvation Coordinate (z). The

	Absorption (\uparrow) and Relaxed Emission (\downarrow) Processes are Shown.	
	Adapted from Reference 79	39
Figure 2.9:	Illustration of the Ideal Relative Orientation of the Ground and Charge Transfer Dipole Moments of Two π Systems. EWG and EDG Represent Electron Withdrawing and Donating Groups, Respectively.	44
Figure 2.10:	Relationship of Molecular Orbitals with Electrochemical and Spectroscopic Properties where the Energy Level Ordering has been Exaggerated. Adapted from Loufty and Loufty [95].	51
Figure 3.1:	Relationship Between λ_{\max} of Various β - Diketonatoboron Complexes [(\blacksquare) BF_2 ; (\square) BM ; (\bullet) BO] vs. the λ_{\max} of Their Parent β - Diketones in Acetonitrile.	56
Figure 3.2:	The UV - Vis Absorption Spectra of Some β - Diketonatoboron Complexes in Acetonitrile; (a) DBMBF_2 (1.05×10^{-5} M); (b) BABF_2 (3.14×10^{-5} M).	57
Figure 3.3:	UV - Vis Absorption Spectrum of DBMBN (1.75×10^{-5} M) in Acetonitrile. Note the Weak Absorption Band at Beyond the Principle Absorption Band (cf. Figure 3.2a).	58
Figure 3.4:	Fluorescence Excitation and Emission Spectra (Corrected and Normalized) of DBMBF_2 (8.0×10^{-7} M) and DBMBM (5.0×10^{-7} M) in Acetonitrile Under Argon. For Excitation Spectra λ_{mon} was 440 nm and for Emission Spectra λ_{ex} was 365 nm. The Excitation and Emission Slit Widths were 2 and 4 nm, Respectively.	66
Figure 3.5:	Total Emission Spectra (Uncorrected) of Some β -Diketonatoboron Complexes in Methylcyclohexane Glass at 77 K. BABF_2 (2.8×10^{-4} M). Note that BABF_2 also shows Phosphorescence Emission. The Peak Near 335 nm is the Rayleigh Band.	68
Figure 3.6:	Illustration of a Cyclic Voltammogram for a Reversible Redox Couple.	76

- Figure 3.7: Hückel LCAO - MO Description of the β - Diketone Fragment. The Size of the Orbital Indicates the Relative Magnitude of the Coefficient. 80
- Figure 3.8: Relationship Between the Singlet and Triplet Energies (Table 3.3) and the Redox Potentials (Table 3.4) of Various β - Diketonatoboron Complexes. The Open Squares Represent those Complexes where the E_S was Estimated from their UV - Vis Absorption. 82
- Figure 4.1: EDA Complex UV-Vis Absorption Bands Observed Between DBMBF₂ (0.009 M) and Benzenes in Acetonitrile; Benzenes are PMB (a: 0 M; b: 0.06 M; c: 0.08 M; d: 0.11 M; e: 0.15 M; f: 0.20 M), Durene (a: 0 M; b: 0.11 M; c: 0.12 M; d: 0.16 M; e: 0.22 M; f: 0.31 M), and p-Xylene (a: 0 M; b: 0.08 M; c: 0.19 M; d: 0.32 M; e: 0.46 M; f : 0.63 M). 86
- Figure 4.2: Benesi - Hildebrand plots for DBMBF₂ / Substituted Benzene EDA Complexes in Acetonitrile at Ambient Temperature (cf. Figure 4.1). 87
- Figure 4.3: Ground State Association Enthalpic Plots (eq 4.2) Monitored at 420 nm. Concentrations : [DBMBF₂] = 9 mM; [o-Xylene] = 0.248 M; [Mesitylene] = 0.389 M; [PMB] = 0.259 M. 90
- Figure 4.4: Correlation of DBMBF₂ / Substituted Benzene EDA Complex Formation Enthalpy (in eV units) in Acetonitrile vs. Donor's IP. 93
- Figure 4.5: Examples of Excited EDA Complex Emission in Cyclohexane. [DBMBF₂] = 1.1 x 10⁻⁵ M. A: [Durene] = 0.134 M; Excitation Wavelengths: (a) 365 nm; (b) 390 nm; (c) 400 nm. B: [Mesitylene] = 0.204 M; Excitation Wavelengths: (a) 365 nm; (b) 350 nm; (c) 390 nm; (d) 400 nm. 95

- Figure 4.6: Examples of Excited EDA Complex Emission in Acetonitrile where $[DBMBF_2] = 9 \text{ mM}$ and $\lambda_{\text{ex}} = 400 \text{ nm}$. $[p\text{-Xylene}] = 0.298 \text{ M}$. $[PMB] = 0.254 \text{ M}$. 96
- Figure 5.1: Fluorescence (uncorrected, $\lambda_{\text{ex}} = 365 \text{ nm}$) Quenching of Singlet Excited $DBMBF_2$ ($1 \times 10^{-5} \text{ M}$) by Benzenes in Cyclohexane. A: o-Xylene; (a) 0 M; (b) 0.05 M; (c) 0.11 M; (d) 0.15 M; (e) 0.21 M. B: 1,2,3,4 - Tetramethylbenzene; (a) 0 M; (b) 0.04 M; (c) 0.09 M; (d) 0.13 M; (e) 0.20 M. 101
- Figure 5.2: Fluorescence Excitation Spectra of the $DBMBF_2$ ($1 \times 10^{-5} \text{ M}$) / Durene (0.153 M) System. A: Excitation Spectrum Monitored at $DBMBF_2$ (410 nm); B: Excitation Spectrum Monitored at the Exciplex (550 nm). 102
- Figure 5.3: $DBMBF_2$ ($1 \times 10^{-5} \text{ M}$) - Benzene Exciplex Stoichiometric Plots in Cyclohexane. Plots of $\ln(I_{\text{ex}} / I_{\text{A}})$ vs. $\ln[D]$ (eq 5.2). 107
- Figure 6.1: A Plot of the $DBMBF_2$ / Substituted Benzene Exciplex Fluorescence Maximum in Cyclohexane ($h\nu_{\text{max}}$) Against the Difference in the Redox Potentials of the Donor (E_{ox}) and Acceptor (E_{red}); E_{ox} values for Table 6.2. The Inclined Solid Line was Calculated According to eq 6.1b. The Horizontal Solid Line Represents the Singlet Energy of $DBMBF_2$ in Cyclohexane ($E_S = 3.24 \text{ eV}$, Table 3.3). 115
- Figure 6.2: Plot of the Theoretical (F_3 , eq 2.11) Against Dimroth and Reichardt's Empirical Polarity Scale (E_T). The Solid Line is the Best Fit Through the 'Ideal' Solvents. 117
- Figure 6.3: Representative Solvatochromic Plots (eq 2.51) for the $DBMBF_2$ / Substituted Benzene Exciplex Fluorescence with PMB, p - Xylene, Toluene and Benzene as Electron Donors. 118

- Figure 6.4: Relationship Between the Observed and Estimated Gas Phase Exciplex Dipole Moment and the Donor's Ionization Potential. The Dashed Line Represents the Best Fit of Equations 2.36 and 2.37 with an Overlap Integral Value of 0.037. 125
- Figure 6.5: Frontier Orbital Interpretation of Variable Exciplex Dipolar Character. The Acceptor MO's are Denoted by **a** and the Donor by **b** where the Prime (') Denotes the LUMO. 126
- Figure 6.6: Correlation of Exciplex Fluorescence Maximum with Redox Potentials in p-Xylene. X Represents F, Oxalyl and Manonyl Ligands. Data from Table 6.3. 132
- Figure 7.1: Potential Energy Scheme for Excited State Complexes (Exciplexes and Excimers) as a Function of Donor - Acceptor Distance. 136
- Figure 7.2: Illustration of the Change in the Exciplex / *A Fluorescence Intensities for an Exciplex Passing from a Reversible to an Irreversible Reaction. 140
- Figure 7.3: Variation in the Exciplex / DBMBF₂ (4.3 x 10⁻⁶ M) Fluorescence Intensities with Temperature in Cyclohexane Under Argon. Donors: 4 - t - Butyl - o - xylene (0.18 M) {Temperatures (°C) : (a) 14.5, (b) 21.6, (c) 29.1, (d) 35.6, (e) 40.1, (f) 46.3 and (g) 54.9}; 1,2,4 - Trimethylbenzene (0.18 M) {Temperatures (°C) : (a) 13.3, (b) 17.7, (c) 22.0, (d) 29.0, (e) 35.8, (f) 41.5, (g) 46.4, (h) 53.5 and (i) 59.8}. 143
- Figure 7.4: Variation of the Exciplex / DBMBF₂ Fluorescence Intensities with Temperature (eq 7.3). Donors: t - Butylbenzene (**a**); 1,2,4 - Trimethylbenzene (**b**); 5 - t - Butyl - o -Xylene (**c**);

	HMB (d). Note that the Three Regions (Reversible, Intermediate and Irreversible) are Displayed.	144
Figure 7.5:	Correlation Between the Exciplex's Franck - Condon Ground State Complex Energy and Charton's Steric Parameter (ν_c).	150
Figure 8.1:	Fluorescence Decay Examples of DBMBF ₂ / Benzene Exciplexes in Degassed Cyclohexane (296 K). Donors: (a) Benzene (1.8 M); (b) p-Xylene (0.23 M). The First Symmetrical Peak is the Lamp Profile. The Residuals (RESID) and the Autocorrelation (ACORR) are shown below the Fluorescence Decay Trace.	164
Figure 8.2:	Typical Examples of the Fit of the Observed Exciplex Lifetimes as a Function of the Donor Concentration. The Solid Line Represents the Best Fit of Eq 8.6.	171
Figure 8.3:	The influence of the exciplex's decay rate constant (Σk_{dex}) on the observed exciplex lifetime. The lines were calculated using eq 8.6 with the following parameters: $1/\tau_m = 4.3 \times 10^9 \text{ s}^{-1}$; $k_{ex} = 5 \times 10^7 \text{ s}^{-1}$; $k_{ex} = 7.5 \times 10^9 \text{ M}^{-1} \text{ s}^{-1}$.	172
Figure 8.4:	The Influence of the Exciplex's Decay Rate Constant (k_{ex}) on the Observed Exciplex Lifetime. The Lines were Calculated Using Eq 8.6 with the Following Parameters: $1/\tau_m = 4.3 \times 10^9 \text{ s}^{-1}$; $\Sigma k_{dex} = 5 \times 10^7 \text{ s}^{-1}$; $k_{ex} = 7.5 \times 10^9 \text{ M}^{-1} \text{ s}^{-1}$.	173
Figure 8.5:	In Phase Mixing of the π_{CH_3} with the Benzene Ring π System; Only the Ipso Carbon π Orbital is Shown for Clarity.	181
Figure 9.1:	Plot of Φ_{ex}^{∞} vs. donor's IP.	190
Figure 9.2:	Relationship Between Exciplex Radiative Rate Constant and its Emission Maximum in Cyclohexane. Methyl Benzenes (●) and t-Butyl Benzenes (O).	194

- Figure 9.3: Correlation Between the Radiative Rate Constants for DBMBF₂ / Benzene Exciplexes in Cyclohexane Calculated from |*AD> Contribution to the Exciplex Wavefunction to that Observed. The Error Bars are not Shown for Clarity. The Inset Shows the Relationship of k_f^{ex} with Respect to c^2 . Symbols : (■) DBMBF₂ / Methyl Benzene Exciplexes; (□) DBMBF₂ / Methyl Benzene Exciplexes Corrected for Solvent Induced Polarization; (O) DBMBF₂ / t - Butyl Benzene Exciplexes; (Δ) DBMBF₂ / t - Butyl Benzene Exciplexes Corrected for Solvent Induced Polarization. 196
- Figure 9.4: The Engleman - Jortner Pictorial Description of the Radiationless Process; The Strong (a) and Weak Coupling (b) Limits. 200
- Figure 9.5: Relationship between DBMBF₂ / benzene exciplex radiationless rate constant and contribution of |*AD> to the exciplex's wavefunction. Closed squares represent methylbenzene donors and the open circles represent hindered benzene donors. The coefficient c^2 was obtained from Table 6.2 and k_{nr}^{ex} from Table 9.2. The solid line is the best fit through the closed squares and the dashed line is best line through the open circles that is parallel to the solid line; the last point was ignored. 204
- Figure 10.1: Plots of eq 10.1 (Stern-Volmer equation) for the Fluorescence Quenching of Singlet Excited DBMBF₂ by Benzenes in Aerated Acetonitrile. [DBMBF₂] = 2 x 10⁻⁶ M, λ_{ex} = 365 nm and slits 4 nm. 210
- Figure 10.2: Semilog plot (Rehm - Weller plot) for the fluorescence quenching of singly excited DBMBF₂ (circles; squares for hindered benzenes) and DBMBO (triangles) by benzenes in acetonitrile (aerated, 23 ± 2 °C). The solid line is represents the calculated k_{obs} from the PET model of Rehm and Weller. Inset shows the change in

	the fluorescence quenching distance with electron transfer exothermicity. Exciplex emission is denoted by open circles and triangle.	215
Figure 10.3:	Best fit of the Kuzmin Model to the Observed Fluorescence Quenching of Singlet Excited DBMBF ₂ by Benzenes in Aerated Acetonitrile.	227
Figure 11.1:	Relationship of Excitation / Emission to Detector Orientation Used in Fluorescence Studies.	234
Figure 11.2:	Plot of Relative Fluorescence Intensity of DBMBF ₂ vs. [DBMBF ₂] in Aerated Acetonitrile.	236
Figure 11.3:	Algorithm for the Resolution of the Overlapping DBMBF ₂ and its Exciplex Fluorescence.	239
Figure 11.4:	Deconvolution of DBMBF ₂ Fluorescence Profile (Aerated Acetonitrile) into Five Gaussian. The Solid Line Represents the Summation of the Gaussian Curves.	242
Figure 11.5:	Comparison of the Observed (Solid Line) and Calculated (Dashed Line) of DBMBF ₂ Fluorescence Profile in Aerated Acetonitrile.	243
Figure 11.6:	The Ratio of $\Phi_{ex}^{\infty} / \Phi_F$ vs. Benzene Concentration in Argon Purged Cyclohexane. Donors are: (■) Benzene; (□) Toluene; (●) Durene.	246
Figure 11.7:	Schematic Overview of the LS - 1 Single Photon Counter. Adapted from References 148 and 233.	249
Figure 11.8:	Illustration of the Cyclic Voltammetry Set-up.	254
Figure 11.9:	Exciplex Dipole Moment Calculation Program Listing	258

LIST OF ABBREVIATIONS

2,3-DMN	2,3-Dimethoxynaphthalene
AAB ϕ_2	Acetylacetonatoboron diphenyl
AABC	Acetylacetonatoboron catecholate
AABF ₂	Acetylacetonatoboron difluoride
AABM	Acetylacetonatoboron malonate
AABN	Acetylacetonatoboron naphthadiolate
AABO	Acetylacetonatoboron oxalate
AAH	Acetylacetone
ACHBF ₂	2-Acetylcyclohexanonatoboron difluoride
ACHH	2-Acetylcyclohexanone
BABC	Benzoylacetonatoboron catecholate
BABF ₂	Benzoylacetonatoboron difluoride
BABM	Benzoylacetonatoboron malonate
BABN	Benzoylacetonatoboron naphthadiolate
BABO	Benzoylacetonatoboron oxalate
BAH	Benzoylacetone
CRIP	Contact radical ion pair
CT	Charge transfer
DA	Donor-acceptor
DBMBAc ₂	Dibenzoylmethanatoboron bisacetate
DBMBC	Dibenzoylmethanatoboron catecholate
DBMBF ₂	Dibenzoylmethanatoboron difluoride
DBMBM	Dibenzoylmethanatoboron malonate
DBMBN	Dibenzoylmethanatoboron naphthadiolate
DBMBO	Dibenzoylmethanatoboron oxalate

DBMB ϕ_2	Dibenzoylmethanatoboron diphenyl
DBMH	Dibenzoylmethane
DCM	1,2-Dichloromethane
D-t-BBF $_2$	2,2,6,6-Tetramethyl-3,5-heptanedionatoboron difluoride
DW	Durbin-Watson
EA	Electron affinity
EDA	Electron donor-acceptor complex
ET	Electron transfer
e.u.	Entropy units
FWHM	Full width at half maximum
HMB	Hexamethylbenzene
HOMO	Highest occupied molecular orbital
IP	Ionisation potential
LCAO	Linear combination of atomic orbitals
LE	Locally excited
LUMO	Lowest unoccupied molecular orbital
μL	Microlitre
MBDBC	4-Methoxy-4'-t-butyl-dibenzoylmethanatoboron catecholate
MBDBF $_2$	4-Methoxy-4'-t-butyl-dibenzoylmethanatoboron difluoride
MBDBM	4-Methoxy-4'-t-butyl-dibenzoylmethanatoboron malonate
MBDBN	4-Methoxy-4'-t-butyl-dibenzoylmethanatoboron naphthadiolate
MBDBO	4-Methoxy-4'-t-butyl-dibenzoylmethanatoboron oxalate
MBDH	4-Methoxy-4'-t-butyl-dibenzoylmethane
Me-AABF $_2$	2-Methylacetylacetonatoboron difluoride
Me-C $_6$ H $_{11}$	Methylcyclohexane
NMR	Nuclear magnetic resonance
o-DMB	o-Dimethoxybenzene

PET	Photoinduced electron transfer
PMB	Pentamethylbenzene
rf	Radio frequency
SCE	Saturated calomel electrode
Sol	Solvent molecule
SSRIP	Solvent separated radical ion pair
TCB	Tetracyanobenzene
TMB	Tri or tetramethylbenzene

LIST OF SYMBOLS

α_e	Excited state polarizability.
α_g	Ground state polarizability.
α_{ex}	Exciplex polarizability.
a	$ A^-D^+\rangle$ configuration coefficient; acceptor's HOMO.
a^*	Corresponding no-bond excited configuration coefficient.
a'	Acceptor's LUMO.
A	Acceptor, Einstein's coefficient for spontaneous emission.
A_A^0	Acceptor's integrated fluorescence area in the absence of donor.
AD	Donor-acceptor complex: no-bond configuration.
A^-D^+	Donor-acceptor complex: dative configuration; Exciplex charge transfer configuration.
A^+D^-	Exciplex reverse charge transfer configuration.
$*AD$	Exciplex locally excited configuration, centered on the acceptor.
A^*D	Exciplex locally excited configuration, centered on the donor.
$A^{\delta-}D^{\delta+}$	Exciplex: mixture of A^-D^+ and $*AD$ configurations.
β	Beta, experimental parameter in eq 2.6 and efficiency of SSRIP formation.
b	Dative ($ A^+D^-\rangle$) configuration coefficient.
b^*	Corresponding excited dative configuration coefficient.
B_{op}	van der Zwan and Hynes' polarizability function.
B_{or}	van der Zwan and Hynes' orientation function.
χ	Supermolecular orbital.
c	$ *AD\rangle$ configuration coefficient.
c^*	Corresponding excited configuration coefficient.
C	Coulombic energy.
C_{2v}	Second order proper axis of rotation with a vertical mirror plane.

C_s	Molecule with only a mirror plane.
Δe	Fraction of electron transferred.
ΔG_{ET}^\ddagger	Activation energy for electron transfer.
ΔG_{ET}^0	Free energy of electron transfer.
$\Delta G_{ET}^\ddagger(0)$	Intrinsic activation energy for electron transfer.
ΔG_{ex}	Free energy for exciplex formation.
$\Delta \Delta G_{solv}$	Difference between the solvation energies of a cation and an anion.
ΔG_{solv}^+	Solvation free energy of a cation.
ΔG_{solv}^-	Solvation free energy of an anion.
$\Delta h\nu$	Difference in gas phase absorption and emission energies.
ΔH_a	Enthalpy for EDA formation.
ΔH_{ex}	Enthalpy for exciplex formation.
$\Delta \lambda$	Difference in UV-Vis absorption λ_{max} .
ΔS_{ex}	Entropy for exciplex formation.
$\Delta S_{solvent}$	Change in solvent degrees of freedom upon complex formation.
$\Delta S_{trans/rot}$	Change in translational and rotational degrees of freedom upon complex formation.
$\Delta S_{vib/int-rot}$	Change in vibration internal rotational degrees of freedom upon complex formation.
ΔU	Difference in excited and ground state free energies of solvation.
d	$ A^*D\rangle$ configuration coefficient; donor's HOMO.
d^*	Corresponding excited configuration coefficient.
d'	Donor's LUMO.
D	Donor.
D_{in}	Dielectric constant inside the Onsager cavity.
D_{DA}	Sum of diffusion coefficients for donor and acceptor..
ϵ	Dielectric constant or molar extinction coefficient.

ϵ_A	Acceptor A's molar extinction coefficient.
ϵ_{DA}	EDA complex's molar extinction coefficient.
ϵ_{ho}	HOMO's energy.
ϵ_{lu}	LUMO's energy.
ϵ_{max}	Molar extinction coefficient at λ_{max} .
ϵ_0	Permeability constant.
e	No-bond (IAD)) configuration coefficient.
e^*	Corresponding excited configuration coefficient.
E_{CT}	Energy of charge transfer configuration.
E_{LE}	Energy of locally excited configuration.
E_S	Singlet energy.
E_T	Triplet energy.
$E_{N_T}^N$	Symbol for Dimroth and Reichardt's empirical polarity scale.
E_{Ref}	Reference potential.
E_{ox}	Oxidation potential.
E_{red}	Reduction potential.
E_{EX}	Exciplex energy.
E_{A_A}	Electron affinity of acceptor.
E_N	EDA complex energy.
E_V	Franck-Condon excited EDA complex energy.
E_0	Energy of the no-bond configuration.
E_1	Energy of the dative configuration.
ϕ	Angle between two vectors; phenyl substituent.
Φ^*A	Quantum yield of singly excited acceptor's emission.
Φ_{ex}	Quantum yield of exciplex fluorescence.
Φ_{ex}^∞	Limiting quantum yield of exciplex fluorescence.
Φ_F	Quantum yield of fluorescence.

F_e	Free energy of the excited state solute-solvent system.
F_e^{eq}	Equilibrated F_e .
F_g	Free energy of the ground state solute-solvent system.
$F_g(t)$	Free energy of the ground state solute-solvent as a function of time.
F_g^{neq}	Non-equilibrated F_g .
F_1	Solvent reorientation function.
F_2	Solvent polarizability function.
F_3	Modified reorientation-polarizability function for exciplex solvatochromism for a non-polarizable dipole.
F_4	Modified reorientation-polarizability function for exciplex solvatochromism for a polarizable dipole.
γ	Efficiency of exciplex formation from the encounter complex.
h	Planck's constant.
$h\nu_F^o$	Gas phase emission energy.
$h\nu_F$	Emission energy.
$h\nu_f^{ex}$	Exciplex emission energy.
$h\nu$	Photon energy.
$h\nu_{Abs}^o$	Gas phase absorption energy.
$h\nu_{Abs}$	Absorption energy.
H	Electronic Hamiltonian.
H	Configuration interaction integral.
H_{rp}	Electronic coupling.
H_{rp}^o	Intrinsic electronic coupling.
I	Fluorescence intensity.
I^o	Fluorescence intensity in the absence of quencher.
I_{ex}^o	Exciplex emission intensity in the absence of oxygen.
I_{ex}	Exciplex emission intensity.

I_A°	Acceptor's fluorescence intensity in the absence of oxygen.
I_A	Acceptor's fluorescence intensity.
I_{trp}	Triplex emission intensity.
IP	Ionization potential.
IP_D	Donor's ionization potential.
J	Coulombic Integral.
κ_{el}	Transmission coefficient.
k_B	Boltzmann's constant.
$(k_{bet})_{ss}$	Rate constant for back electron transfer within the SSRIP.
k_{cc}	Rate constant for non-relaxed exciplex formation from the encounter complex.
k_{-cc}	Rate constant for the reverse step of k_{cc} .
k_{diff}	Rate constant for bimolecular diffusion.
k_{-diff}	Rate constant for the separation of an encounter complex.
k_{et}	Rate constant for electron transfer.
k_{-et}	Rate constant for back electron transfer.
k_{ex}	Rate constant for exciplex formation.
k_{-ex}	Rate constant for exciplex dissociation.
k_f	Rate constant for fluorescence.
k_f^{ex}	Rate constant for exciplex fluorescence.
k_{nr}	Rate constant for the sum of all non-radiative processes.
k_{nr}^{ex}	Rate constant for the sum of all exciplex non-radiative processes.
k_{obs}	The observed rate constant obtained from steady state fluorescence quenching experiments.
k_{sep}	Rate constant for the separation of a SSRIP to free ions.
k_{solv}	Rate constant for the conversion of an exciplex to a SSRIP.
K	Exchange integral.

K_a	Equilibrium constant for EDA complex formation.
K_{SV}	Stern-Volmer constant.
$\lambda_{1,2}$	Characteristic values.
λ_{max}	UV-Vis absorption or emission maximum.
λ	Reorganization energy.
λ_{in}	Inner reorganization energy.
λ_{out}	Outer reorganization energy.
μ_e	Excited state dipole moment of a solute or an exciplex.
μ_g	Ground state dipole moment of a solute or a Franck-Condon ground state complex derived from an exciplex.
$\mu(t)$	Time dependent dipole moment.
μ_{ex}	Exciplex dipole moment due to charge transfer interactions.
μ_{ex}^o	Gas phase exciplex dipole moment due to charge transfer interactions.
M_{if}	Transition dipole moment between initial (i) and final (f) states.
M_{ex}	Exciplex transition dipole moment due to charge transfer interactions.
π^*	Antibonding π MO.
$\pi \rightarrow \pi^*$	Excitation of a bonding π electron to an antibonding π MO.
π, π^*	Excited state prepared from excitation of a bonding π electron to an antibonding π MO.
ν_{ave}	Fluorescence center of gravity.
ν_{el}	Frequency of passage through the transition state due to electronic coupling.
ν_n	Frequency of passage through the transition state.
n, π^*	Excited state prepared from excitation of a nonbonding electron to an antibonding π MO.
$n \rightarrow \pi^*$	Excitation of a nonbonding electron to an antibonding π MO.
N_A'	Avogadro's number divided by 1000.

r_A	Electron acceptor's radius.
r_D	Electron donor's radius.
r_{DA}	Electron donor-acceptor's interseparation distance.
r_o	Electron donor-acceptor's interseparation contact distance.
R_{DA}	Fluorescence quenching distance.
R_E	Exciplex Franck-Condon ground state repulsion energy.
R_E^o	Exciplex Franck-Condon ground state repulsion energy in the absence of solvent effects.
R_{eff}	Effective fluorescence quenching distance.
R_{VDW}	Van der Waals fluorescence quenching distance.
σ	Exciplex donor-acceptor distance.
$\Sigma e r$	Electron dipole moment operator.
Σk_{dm}	Sum of all the decay rate constants of a species in its lowest singlet excited state.
Σk_{dex}	Sum of all the decay rate of an exciplex; does not include the exciplex dissociation rate constant.
$S_1 \rightarrow T_1$	Radiationless transition between the lowest singlet and triplet states.
$S_{vib.}$	Vibrational entropic term.
τ_{ex}	Lifetime of a singlet exciplex.
τ_{ex}^*	Lifetime of a singlet exciplex which includes the exciplex dissociation rate constant.
τ_m	Lifetime of a species in its lowest singlet excited state.
T	Temperature.
v_c	Charton's steric parameter.
$U_{Dest.}$	Excited state destabilization energy due to interaction with the ground state.
$U_{Stab.}$	Excited state stabilization energy due to interaction between configurations.
U_e^o	Solute's gas phase energy in its lowest singlet excited state.

U_g°	Solute's gas phase energy.
V	Radiationless operator.
V_M	Molecular volume.
V_{VDW}	Van der Waals volume.
w_r	Work to bring reactants from infinity.
$*X$	Unknown excited state species.
Ψ_{EX}	Exciplex wavefunction.
$^1\Psi_{EX}$	Singlet exciplex wavefunction.
$^3\Psi_{EX}$	Triplet exciplex wavefunction.
Ψ_N	EDA complex ground state wavefunction.
Ψ_V	EDA complex excited state wavefunction.
$[*A]^{\circ}$	Excited state steady state concentration of A in the absence of quencher.
$[*A]$	Excited state steady state concentration of A in the presence of quencher.

“Do not seek to follow in the footsteps of the men of old; seek what they sought.”

Matsuo Basho

1644-1694

CHAPTER ONE

INTRODUCTION : β -DIKETONATOBORON COMPLEXES

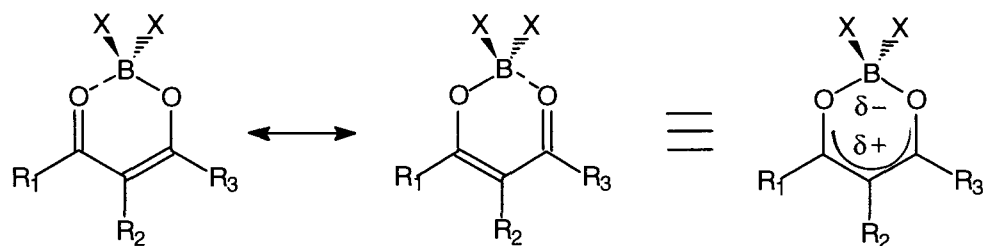
1.1 General

The chemistry of alkaline and transition metal chelates with β -diketone ligands is well investigated and is still enjoying considerable interest in the literature [1-7]. For transitional metal complexes, such as $\text{Cu}(\text{acetylacetonate})_2$, the electron density of the β -diketonate ligand is polarized away from the metal; that is, the metal donates electron density to the β -diketonate ligand [1-3]. In contrast, β -diketone complexes with the elements P, Si and B the β -diketonate ligands are electropositive (see below) [1].

Of particular interest are the β -diketonatoboron complexes and, in particular, β -diketonatoboron difluoride complexes due to their potential as a new electron acceptor series for photoinduced electron transfer (PET) reactions [8], then synthetic accessibility [9,10] and their relative stability [9-11]. Phosphorous complexes are known to be unstable in contact with atmospheric moisture and slowly decompose under inert atmospheres [12] whereas the boron analogs are stable indefinitely exposed to air [9-11]. β -Diketonatoboron difluoride complexes are readily prepared in good yields (typically 80+% overall yield) from their corresponding β -diketone with boron trifluoride etherate [8-10].

The first reported synthesis of a β -diketonatoboron complex was described in 1905 by Diltey et al. [13]. Since then, more than 100 analogs have been prepared [14-24] and the chelated structure of β -diketonatoboron complexes (Scheme 1.1) has been demonstrated and characterized by numerous physical methods: IR [9,10,17a,23]; UV-Vis absorption [9,10,14a-e, 17a]; ^1H NMR [9,10,17a,c]; ^{13}C NMR [10,18]; ^{11}B NMR [9,10]; ^{19}F NMR [10]; mass spectroscopy [14g]; X-ray crystallography [19-21]; cyclic voltammetry [10, 18]; ESR [22]; photoelectron spectrometry [24]; dipole moment [10, 17b]; xerography [15].

Scheme 1.1



X	β -Diketone	R ₁	R ₂	R ₃	Abbreviation
F	AAH	CH ₃	H	CH ₃	AABF ₂
F	D-t-BBH	t-Butyl	H	t-Butyl	D-t-BBF ₂
F	ACH	R ₁ = R ₂ = CH ₂ (CH ₂) ₂ CH ₂		CH ₃	ACHBF ₂
F	Me-AAH	CH ₃	CH ₃	CH ₃	Me-AABF ₂
F	BAH	CH ₃	H	Phenyl	BABF ₂
F	MBDH	4-t-Butyl ϕ	H	4-MeO ϕ	MBDBF ₂
F	DBMH	ϕ	H	ϕ	DBMBF ₂
Oxalate	DBMH	ϕ	H	ϕ	DBMBO
Malonate	DBMH	ϕ	H	ϕ	DBMBM
Catechol	DBMH	ϕ	H	ϕ	DBMBC
2,3-Dihydroxy - naphthalene	DBMH	ϕ	H	ϕ	DBMBN
Acetate	DBMH	ϕ	H	ϕ	DBMBAc ₂

$\phi \equiv$ phenyl

The aromatic character of β -diketonatoboron complexes, initially proposed by Calvin and Wilson [25], has aroused considerable interest and debate in the literature [1-3,9,10,17c,26]. Chemically, the endowment of a certain amount of aromatic character to β -diketonatoboron complexes is suggested by i) their significant resistance to hydrolysis relative to other boron complexes [11] and ii) that the chelated ring undergoes electrophilic substitution reactions [25,26]. However, the question of ring current in β -diketonates has not been completely confirmed by physical methods. X-ray diffraction studies [19-21] indicate that the β -diketonate ligand is planar where the B — O, C — O and C — C bond lengths are equal; this implies resonance within the chelated ring. A detailed NMR study by Brown and Bladon [10] has shown that the proton resonances of the ligand's substituent groups are chemically equivalent and shifted down field relative to their parent β -diketones. In particular, the methine proton chemical shift moves significantly down field upon complexation. In addition, a comparative study of the ^{19}F analog, relative BF_4^- , indicated a symmetrical environment. In another NMR study by Balaban et al., it was concluded that there is no ring current in β -diketonatoboron complexes [17c]. In a comparison of ^1H NMR shifts between beryllium and boron complexes, Balaban et al. found that they exhibit similar NMR characteristics (e.g., methine proton chemical is shifted down field relative to the parent β -diketone and equivalent ligand substituent chemical shifts) although aromatic behavior is impossible for beryllium β -diketonate complexes. In particular, the change in the methine proton chemical shift, relative to the parent β -diketone, was attributed to the sensitivity of the chelated ring to electrostatic influences as was first proposed by Smith and Wilkins [29]. As a final note, a ^{10}B and ^{11}B isotope IR study by Kopteva et al. [23] was able to identify the B — O and B — F vibrational stretching bands. In this study, β -diketonatoboron complexes are suggested to have asymmetrical structures as shown on the left of Scheme 1.1

In addition to the spectroscopic evidence for the chelated structure shown in Scheme 1.1, the structure is further supported by dipole moment measurements. Table

1.1 lists dipole moments for some β -diketonatoboron complexes [10,17b], which are significantly larger than the dipole moments of the corresponding β -diketones [30]. Since the coordinated B — O results in a semipolar bond, the dipole moment group value for the B — O is 3.5 D [30b]. Therefore, using the parent β -diketones as a basis (Table 1.1) the β -diketonatoboron complexes are predicted to have dipole moments greater than 6 D; this prediction is reasonably followed by the experimental values shown in Table 1.1.

Table 1.1: Experimental Dipole Moments of Some β -Diketonatoboron Complexes

Complex	μ_g (D)	Complex	μ_g (D)
DBMBF ₂	6.7 ± 0.3 ^a	AABF ₂	7.6 ± 0.3 ^a
DBMBC	6.3 ± 0.1 ^b	AABC	5.5 ± 0.1 ^b
DBMB ϕ_2	5.6 ± 0.1 ^b	AAB ϕ_2	4.9 ± 0.1 ^b
DBMH ^a	3.0 ± 0.1 ^c	AAH ^a	2.8 ± 0.1 ^c

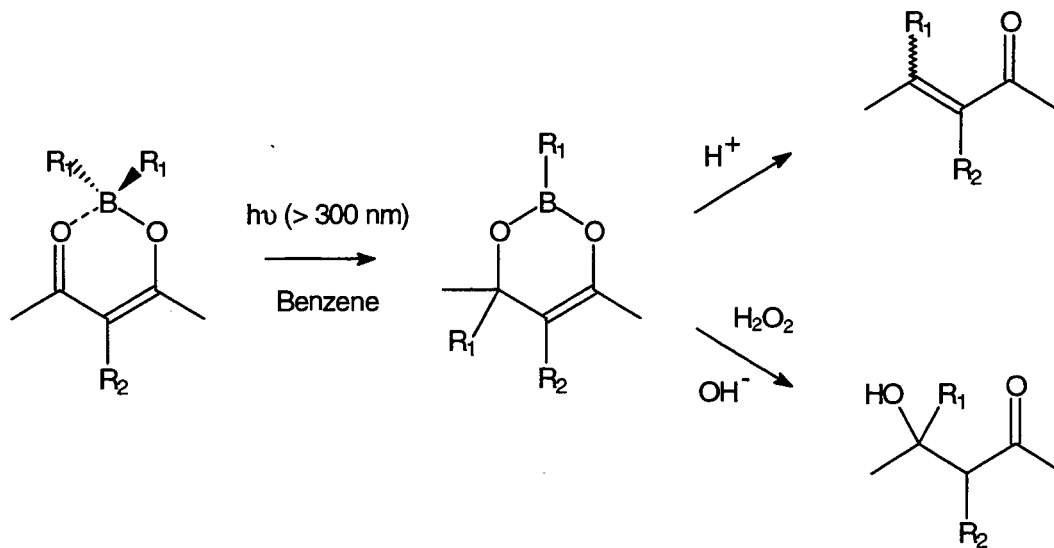
^a Reference 10. ^b Reference 17b ^c Values for *cis*-enol tautomer, reference 30.

1.2 Photochemistry / physics

The photochemistry and photophysics of β -diketonatoboron have not received much attention in the literature. Dialkylboryl acetylacetonone undergoes a photoinduced intramolecular alkyl migration reaction (Scheme 1.2) [31]. The mechanism is believed to involve photorearrangement where the boron-alkyl bond is homolytically broken and the alkyl radical migrates to one of the carbonyl carbons or undergoes hydrogen abstraction.

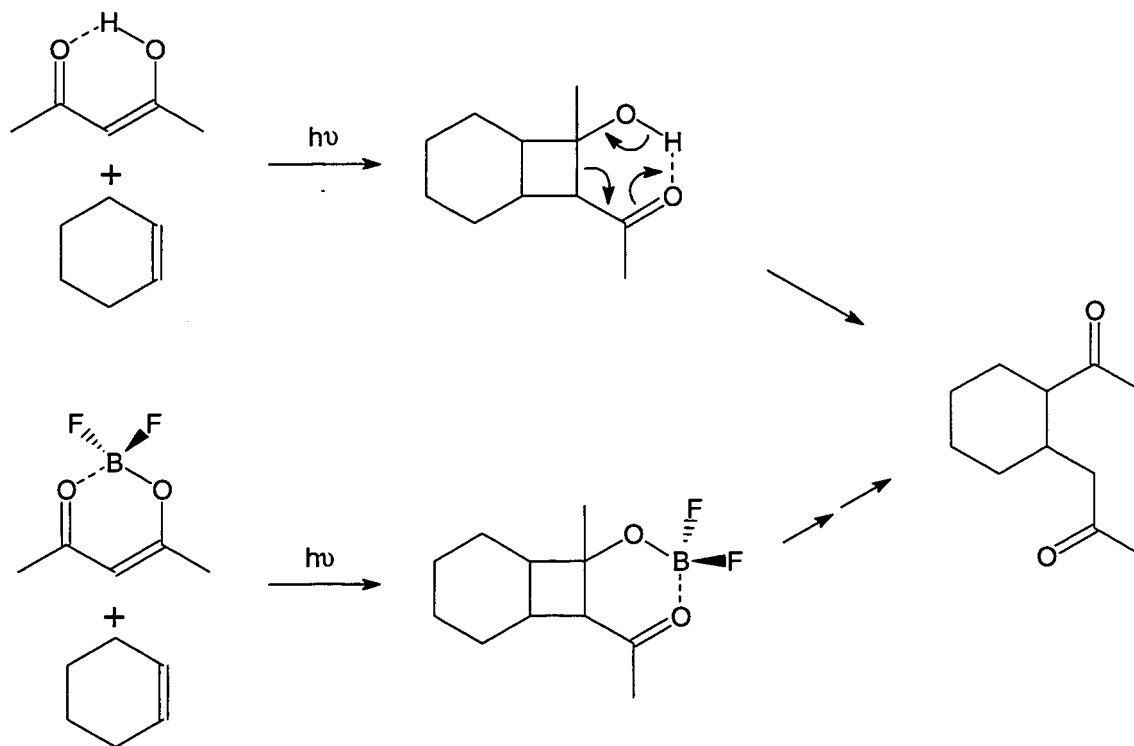
Recently, Chow's group demonstrated that β -diketonatoboron difluorides are a new class of PET electron acceptors which either undergo 2+2 photocycloaddition [32] or

Scheme 1.2



sensitize cation radical dimerization reactions [8,33]. The dibenzoylmethanatoboron difluoride (DBMBF₂) was used as a representative model for the photochemistry of β -diketonatoboron complexes. The 2+2 photocycloadditions of singlet excited DBMBF₂ with electron poor olefins resembles, only in the resulting isolated 1,5- β -diketone product, the de Mayo reaction [34] as shown in Scheme 1.3. The de Mayo reaction is believed to be an excited triplet state reaction (triplet state AAH) [35] whereas Chow and Cheng have shown that DBMBF₂ reacts from its excited singlet state [8,36]. The de Mayo reaction is considered one of the few synthetically useful photochemical reactions for natural product synthesis; for example, it has been used in the synthesis of the protanoic acid skeleton [34]. However, the de Mayo reaction is generally sluggish and long photolysis times are necessary, hence other photoreaction side products can accumulate and reduce the chemical yield. The modification of the β -diketone with the BF₂ moiety is a significant improvement since the photolysis time is significantly reduced and the photoreaction is cleaner (cf. Scheme 1.3).

Scheme 1.3



For electron rich olefins, singlet excited DBMBF₂ sensitizes olefin cation radical dimerization by photoinduced electron transfer [8,36]. It is generally accepted that PET involves electron transfer with an encounter complex (donor-acceptor distance of ca. 7 Å) to produce a solvent separated radical ion pair (SSRIP) [8], which either undergoes back electron transfer or separation into free radical ions. From this point radical cation chain reactions can be envisioned [8,36].

1.3 Motivation and Thesis Overview

Extensive investigations of the photochemical reactions of singlet excited DBMBF₂ have shown that the photoreaction between DBMBF₂ and olefins depends on the

quencher's properties; i.e., the switch between 2+2 photocycloaddition and sensitized cation radical dimerization reactions depends on the quencher's electron donating ability [8,32,36]. The intermediate steps between the initial promotion of DBMBF₂ to its singlet state and the isolation of reaction products was not entirely clear where most of the mechanistic interpretation was inferred from the literature. In contrast, the interaction of singlet excited DBMBF₂ with benzene and pyridine did not show any photoreaction. However, this interaction did show an emission from an intermediate suspected to be an exciplex (excited state complex) derived from singlet excited DBMBF₂ [36].

It was recognized that a photophysical investigation was needed to achieve a better understanding of the β-diketonatoboron complex photochemistry. In particular, it would be desirable to determine what driving forces and transients are involved. To achieve this, the fluorescence quenching of singlet excited DBMBF₂ by benzenes was the initial starting point on the basis that an exciplex intermediate was proposed. Many photoreactions are postulated to proceed by way of an exciplex intermediate. It is, therefore, extremely important to be able to demonstrate and characterize these exciplexes. The DBMBF₂ / benzene exciplex serves as a model system for the DBMBF₂ / olefin system.

The interaction of singlet excited DBMBF₂ with benzenes was examined in various solvents ranging from nonpolar (cyclohexane) to polar (acetonitrile); the most extensive study was performed in cyclohexane. It was found that singlet excited DBMBF₂ does indeed form exciplexes with ground state benzenes and that the exciplex properties (i.e., dipolar nature, reaction kinetics, radiative & radiationless rates and the thermodynamic values) are significantly dependent on the electron donation potential's of the benzenes, as measured by their ionisation potentials (IP). In particular, the exciplex dipolar character could be varied from an common highly polar exciplex (i.e., essentially a contact radical ion pair) to a less common nonpolar exciplex. The trend in exciplex dipolar character can be rationalized by frontier orbital interaction between the highest occupied molecular orbitals (HOMO) of DBMBF₂ and benzene. The variable exciplex dipolar character provided an

opportunity to examine its influence on the physical properties of DBMBF₂ / benzene exciplexes in solution.

CHAPTER TWO

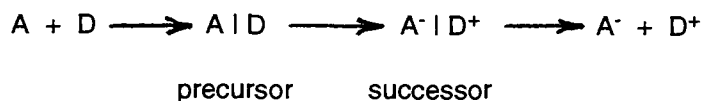
THEORETICAL ASPECTS

Electron transfer (thermal and photoinduced) [37], exciplex formation [38] and electron donor-acceptor complex (EDA complex) formation [39] are important processes in many photoinitiated reactions and currently hold considerable theoretical and experimental interest in the literature. The interplay between these processes is governed by the interaction between the donor-acceptor's frontier molecular orbitals is the decisive factor controlling the feasibility of these processes. For the interaction of singlet excited DBMBF₂ with electron donors, understanding of these processes is required as a precursor to discussion of the experimental results.

2.1 Classical Marcus Theory of Electron Transfer

Electron transfer (ET) reactions are simplest chemical reactions on the basis that no chemical bonds are broken and formed [37]. Electron transfer reactions can be separated into two classes, thermal ET and photoinduced ET (PET) where for the latter class the driving force is provided by the absorption of light by a substrate or complex. Electron transfer theory exists on many levels of sophistication, however, a short review of relevant formulae, assumptions and physical implications of the classical theory of Marcus is adequate for the study presented here [37,40].

The classical theory of Marcus for a bimolecular ET reaction between an electron donor (D) and acceptor (A) considers the diffusion of the D and A together to form a precursor complex in which the electron is then transferred. The resulting radical ion pair is called the successor complex.



Marcus defines the ET above as outer sphere where there is weak electronic coupling between D and A such that they retain their molecular identities and properties; the vertical dash | symbolizes the weak coupling between the donor and the acceptor [37,40d]. It is important to note that the weak electronic coupling between the donor and acceptor is a strict requirement since strong electronic coupling results in bond formation, that is, molecular complex formation, and Marcus' theory breaks down; molecular complexes will be discussed in section 2.2.

The initial reaction state (precursor complex) will have an energy surface consisting of a large number of coordinates (nuclear and solvent). However, the reaction can be depicted as a slice along the reaction path (a one dimensional surface) as shown in Figure 2.1 [37,41]. The identical but displaced parabolas in Figure 2.1 for the complexes is an assumption of Marcus' theory and has been supported by molecular dynamics studies [42]. The intersection of the two parabolas in Figure 2.1 defines the activation free energy for the ET process (ΔG_{ET}^\ddagger). From simple geometrical considerations [43] it can be shown that the relationship between ΔG_{ET}^\ddagger and ΔG_{ET}^o is given by eq 2.1

$$\Delta G_{ET}^\ddagger = (\lambda + \Delta G_{ET}^o)^2 / 4\lambda + W_r \quad (2.1)$$

W_r is the electrostatic work to bring the reactants together to form the precursor complex; this term is neglected if atleast one of the reactants is neutral. λ is called the reorganization energy and its relationship to the free energy parabolas is shown in Figure 2.1. Note that this simple relationship fails either if the parabolas are different or if the electronic coupling is large. For the latter point, the electronic coupling is denoted by H_{rp} in Figure 2.1 where the difference between the parabolas intersection point and the actual

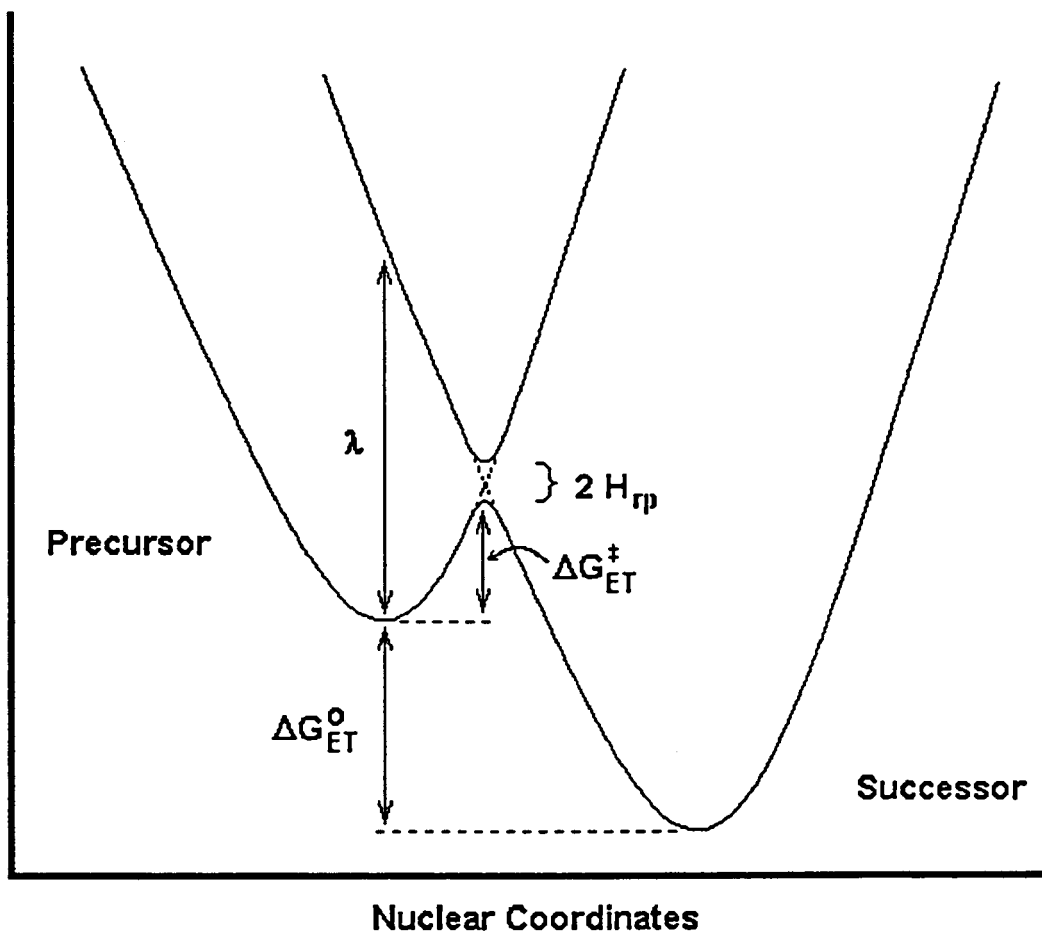


Figure 2.1: Free Energy Surfaces for the Precursor and Successor Complexes as a Function of the Nuclear Coordinates of the Complexes and Solvent.

transition point is equal to H_{TP} ; ΔG_{ET}^{\ddagger} (true) = ΔG_{ET}^{\ddagger} (eq 2.1) - H_{TP} . Equation 2.1 is unlike other free energy relationships since this relationship is a quadratic free energy relationship.

Electron transfer is assumed instantaneous relative to the nuclear motion of the reactants and solvent. For successful electron transfer, the solvent and reactants must 'reorganize' to a transition state configuration where the precursor and successor have similar energies within $k_B T$ (k_B is the Boltzmann constant). This Franck-Condon factor strongly influences the reaction rate since unless $-\Delta G_{ET}^{\circ}$ approaches λ the reaction rate is negligible even if the reaction is strongly exothermic ($\Delta G_{ET}^{\circ} \ll 0$).

The reorganization energy can be broken into two terms, the complex's (inner) and the solvent's (outer) reorganization energies [37, 40] (eq 2.2).

$$\lambda = \lambda_{in} + \lambda_{out} \quad (2.2)$$

The solvent-independent term λ_{in} arises from the structural differences between the equilibrium configuration of the precursor and successor states. λ_{in} is usually treated harmonically such that it is a measure of the changes in the bond force constants and bond lengths before and after the electron is transferred. Calculations have shown that λ_{in} is typically small (0.1-0.3 eV) and negligible for rigid molecular systems (aromatics). The λ_{out} term arises from the solvent's orientation and polarization around the complexes before the electron is transferred. Marcus has derived a simple expression for λ_{out} assuming linear response theory [37,40].

$$\lambda_{out} = \frac{(\Delta e)^2}{4\pi\epsilon_0} \left[\frac{1}{2r_D} + \frac{1}{2r_A} - \frac{1}{r_{DA}} \right] \left[\frac{1}{n^2} - \frac{1}{\epsilon} \right] \quad (2.3)$$

Δe represents the charge transferred, n is the solvent's refractive index and ϵ is the solvent's bulk dielectric constant. The symbols r_D , r_A and r_{DA} represent the donor's radius,

acceptor's radius and the DA center to center radius, respectively, where the derivation of eq 2.2 assumes that the donor, acceptor and complex are spherical in shape. The values for λ_{out} in polar solvents like acetonitrile range from 1.0 to 1.5 eV and are nearly zero for nonpolar solvents. Because the outer reorganization energy term dominates the overall reorganization energy, the reaction coordinate is sometimes labelled as the solvent coordinate; the consequence of λ_{out} dominating the total reorganization energy is that the parabolas will be nearly identical in shape (cf. Figure 2.1).

Using classical transition-state theory, the first order rate constant for forward ET (i.e., ET from precursor to the successor), k_{et} , is given by [37,40]

$$k_{et} = \kappa_{el} \nu_n \exp \{-\Delta G_{ET}^{\ddagger} / k_B T\} \quad (2.4)$$

where, typically, ν_n would represent the frequency of passage through the transition state ($\approx 10^{13} \text{ s}^{-1}$) and κ_{el} would represent the transmission coefficient. In electron transfer theory the product $\kappa_{el} \nu_n$ can be reinterpreted as (within the framework of the Landau-Zener treatment of avoided crossing) [41,44]

$$\kappa_{el} \nu_n = \frac{2 \nu_n [1 - \exp(-v_{el} / 2\nu_n)]}{2 - \exp(-v_{el} / 2\nu_n)} \quad (2.5)$$

$$\text{where } v_{el} = (2\pi^2 H_{rp}^2 / h) / (4\pi\lambda k_B T)^{1/2}$$

Two limiting cases can be identified on the basis of eqs 2.4 and 2.5.

- (I) Electronic coupling ($H_{rp} \approx 10 \text{ cm}^{-1}$) is very weak; $v_{el} \ll 2\nu_n$ and $\kappa_{el} = (v_{el} / \nu_n) \ll 1$:

$$k_{\text{et}} = v_{\text{el}} \exp \{-\Delta G_{\text{ET}}^{\ddagger} / k_{\text{B}}T\}$$

This is called the nonadiabatic limit where electron transfer is the rate limiting step.

- (ii) Electron coupling ($H_{\text{rp}} \approx 1000 \text{ cm}^{-1}$) is strong; $v_{\text{el}} \gg 2v_{\text{n}}$ and $\kappa_{\text{el}} = 1$:

$$k_{\text{et}} = v_{\text{n}} \exp \{-\Delta G_{\text{ET}}^{\ddagger} / k_{\text{B}}T\}$$

This is called the adiabatic limit where nuclear motion is the rate limiting step. The reaction is insensitive to the degree of electronic interaction via center-to-center DA distance, steric effects, orientation factors and medium.

The electronic coupling, H_{rp} , is expected to be a strong function of the donor-acceptor distance due to the requirement for orbital overlap. Since the orbital overlap behaves exponentially with respect to distance, H_{rp} can be cast into the form [45,46]

$$H_{\text{rp}} = H_{\text{rp}}^{\circ} \exp [-\beta (r_{\text{DA}} - r_0) / 2] \quad (2.6)$$

where r_0 is the donor-acceptor contact distance and β experimentally ranges from 0.9 to 2 \AA^{-1} . It is typically found that the formation of contact radical ion pairs (CRIP; r_{DA} ca. 3.5 \AA) results in a H_{rp} of a few hundred cm^{-1} 's whereas for solvent separated radical ion pairs (SSRIP; r_{DA} ca. 7 \AA) H_{rp} is of a few tenths cm^{-1} 's [46]. The amount of interaction to promote electron transfer is very small relative to common chemical sense; for an activationless reaction a H_{rp} of 10 cm^{-1} gives a rate of approximately 10^9 s^{-1} and for a H_{rp} of 100 cm^{-1} the electron transfer reaches the limiting adiabatic region ($k_{\text{et}} \approx 10^{13} \text{ s}^{-1}$) [45].

Equation 2.4 has an unusual prediction that the maximum rate of electron transfer is obtained when $\Delta G_{\text{ET}}^{\circ} = -\lambda$. If the free energy for ET is either greater than or less than -

λ , the rate constant for ET falls off exponentially [37,44-47]. Even for very large driving forces, $\Delta G_{ET}^{\circ} \ll -\lambda$, the rate constant for ET becomes negligible, which is due to an activation barrier. Figure 2.2 illustrates the free energy surfaces for a variety of conditions, including the activation barrier for large driving forces and shows the effect of increasing the exothermicity of ET in relation to where the free energy parabolas intersect. Figures 2.2a and b show activated ET with zero and small driving forces. Figure 2.2c shows the barrierless case where ET will reach its maximum rate. As the driving force increases (Figure 2.2d) the activation barrier returns and the rate of ET decreases. In Figure 2.2d the system is said to be in the inverted region.

The consequence of an imposed activation barrier in the inverted region at large driving forces can be illustrated by computing the rate constant for electron transfer as a function of ΔG_{ET}° for two hypothetical successor complexes, a CRIP and a SSRIP, where the rate constant is calculated from eqs 2.1 and 2.4. The calculation uses typical values derived from the literature; CRIP: $\lambda = 0.5$ eV, $\kappa_{el}v_n = 10^{13}$ s⁻¹; SSRIP: $\lambda = 1.5$ eV, $\kappa_{el}v_n = 10^{11}$ s⁻¹ [45,46]. The calculations are shown in Figure 2.3 where the computed rate for electron transfer for the formation of CRIP and SSRIP successor complexes show two downward symmetrical parabolas which are displaced from each other by the difference of their reorganization energies (1 eV). However, the parabola corresponding to the CRIP successor complex is "shallower" hence the electron transfer rate decreases more rapidly than that for the SSRIP successor. As an outcome of the difference in reorganization energies, the CRIP reaction commands the overall electron transfer reaction up to a ΔG_{ET}° of - 1.1 eV before the SSRIP reaction can eclipse the CRIP reaction beyond a ΔG_{ET}° of - 1.1 eV. In summary, as a consequence of the inverted region two reaction products are formed in a bimolecular electron transfer reaction where the driving force and reorganization energies control the eventual reaction products: CRIP vs. SSRIP. This may lead to different chemistry.

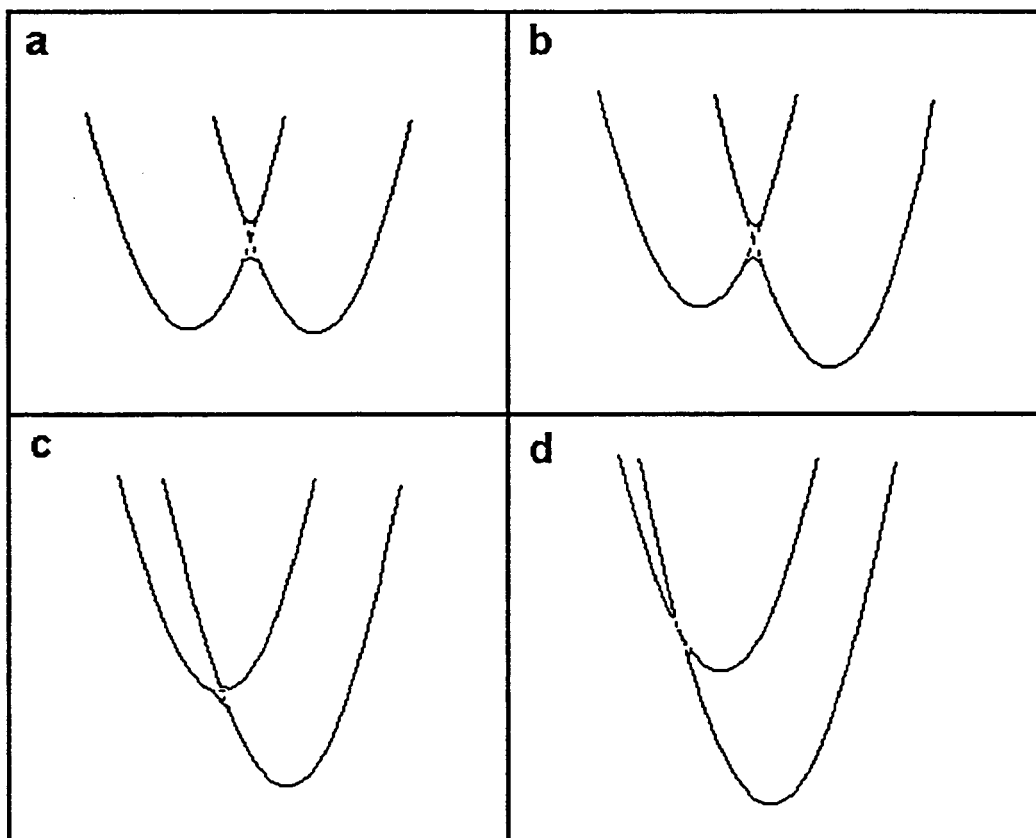


Figure 2.2: The Intersection of Displaced Free Energy Parabolas as a Function of Increasing Exothermicity. **a:** $\Delta G_{\text{ET}}^{\circ} = 0$; **b:** $\Delta G_{\text{ET}}^{\circ} > \lambda$; **c:** $\Delta G_{\text{ET}}^{\circ} = \lambda$; **d:** $\Delta G_{\text{ET}}^{\circ} \ll \lambda$.

Adapted from Bolton and Archer [48].

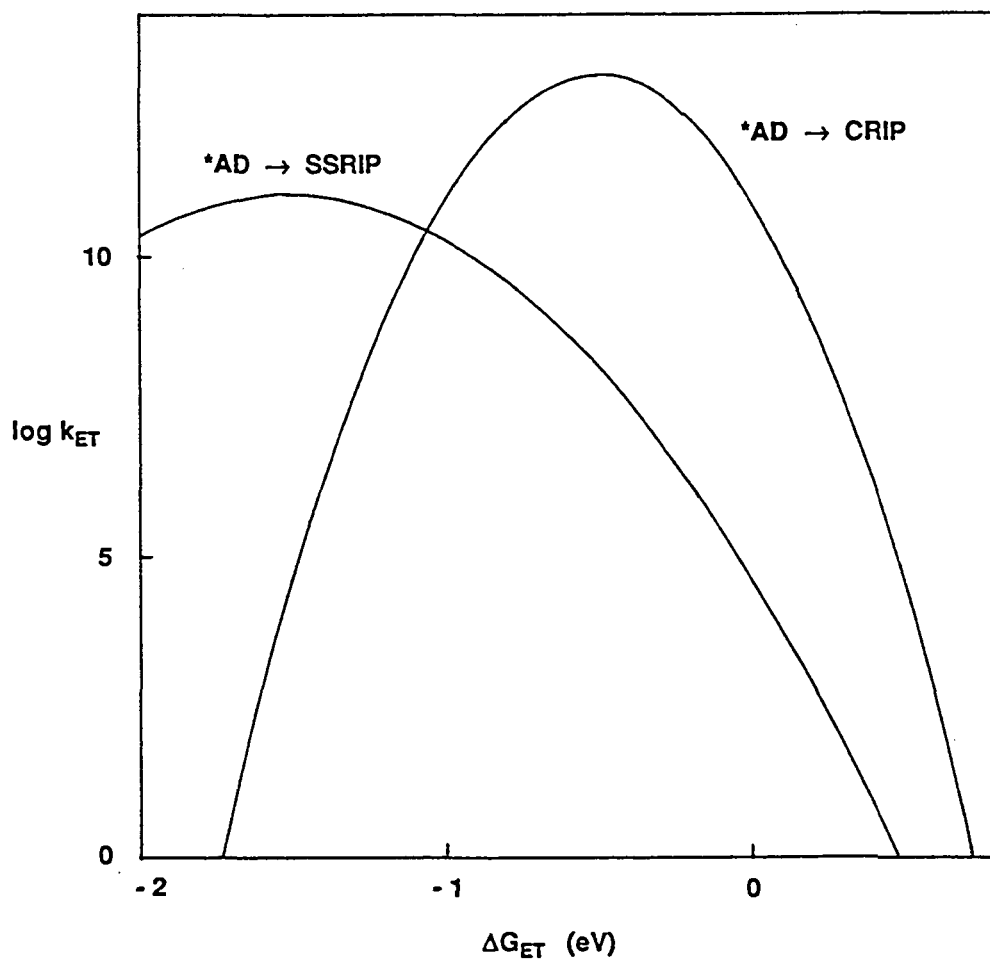


Figure 2.3: Hypothetical effect of donor - acceptor distance on the electron transfer within a precursor complex. The solid lines represent ET at a donor - acceptor distance of 3.5 Å ($\lambda = 0.5$ eV, $\kappa_{el} \nu_n = 10^{13}$ s⁻¹) and 7.0 Å ($\lambda = 1.5$ eV, $\kappa_{el} \nu_n = 10^{11}$ s⁻¹).

2.2 Bimolecular Photoinduced Electron Transfer

Organic substrates are not, in general, powerful reducing or oxidizing agents such that ET is observed with ground state reactants. Electron transfer is an endothermic process due to mismatching of the donating and accepting orbital's (HOMO \rightarrow LUMO) energies as illustrated below. HOMO-HOMO and LUMO-LUMO ET processes are not feasible on the ground state since there are no electrons in the LUMOs and that electron transfer between is not possible between closed shell HOMOs. Electron transfer can be made possible if an electron is removed from one of the HOMOs or an electron is deposited in one of the LUMOs. The most effective approach is to promote either the donor or

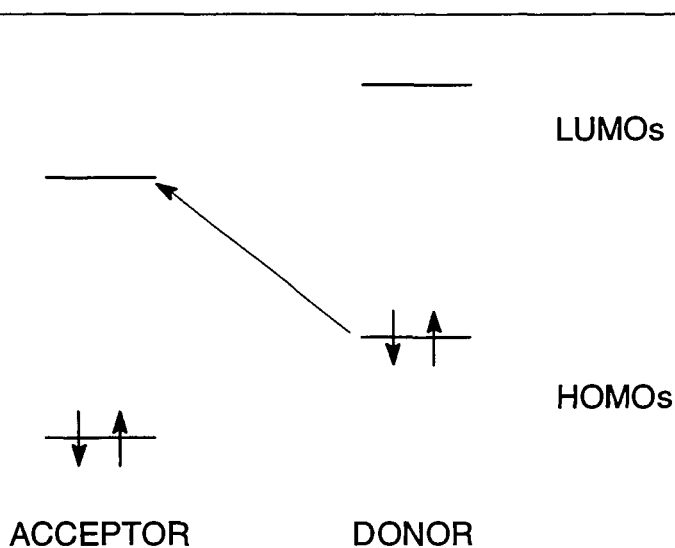


Figure 2.4: Unfavorable Charge Transfer Interaction between a Ground State Donor and Acceptor.

acceptor to its spectroscopic excited state. This process opens up the HOMO and deposits an electron in the LUMO concurrently, so that ET can proceed; this is termed photoinduced electron transfer (PET).

The free energy for PET process can be calculated from a breakdown of the process into its individual components [50]:

	Process		Energy
*A	→	A + hν	- E _S
A + e ⁻	→	A ⁻	- EA _A
D	→	D ⁺ + e ⁻	IP _D
D ⁺ + A ⁻	→	D ⁺ A ⁻	-C
*A + D	→	D ⁺ A ⁻	ΔG _{ET} ^o

$$\Delta G_{ET}^o = IP_D - EA_A - C - E_S \quad (2.7)$$

Here C represents the Coulombic energy to bring the ion pair from infinity to the successor's donor-acceptor center to center distance and E_S is the singlet energy of *A. In solution, the equivalent equation to eq 2.7 can be derived using the following relationships between gas phase potentials and redox potentials [13] where ΔG_{Sol}⁺ and ΔG_{Sol}⁻ represent the solvation energies of the cation and anion, respectively, and E_{Ref} is the reference electrode's potential.

$$E_{ox} = IP_D + \Delta G_{Sol}^+ + E_{Ref} \quad (2.8a)$$

$$E_{red} = EA_A - \Delta G_{Sol}^- + E_{Ref} \quad (2.8b)$$

Substituting eq 2.8 into eq 2.7 gives

$$\Delta G_{ET}^{\circ} = E_{ox} - E_{red} + \Delta\Delta G_{sol} - C - E_S \quad (2.9)$$

where $\Delta\Delta G_{sol} = \Delta G_{Sol}^{+} + \Delta G_{Sol}^{-}$

It should be noted that the process breakdown above assumes no electronic coupling between D and *A, as required by Marcus theory, hence the reactant properties can be used. In addition, the free energy for a thermal ET process is calculated by a similar equation where the E_S term is dropped.

Equation 2.7 predicts that PET will be feasible if the excited state energy (E_S) exceeds the sum $E_{ox} - E_{red}$ (C in polar solvents can be neglected). Since $E_{ox} - E_{red}$ are around 2 to 3 V for typical donor-acceptor pairs, the excited state energy must be greater than 3 eV. This value for E_S represents absorption in the UV region of the electromagnetic spectrum. Numerous examples of PET in a number of donor-acceptor systems have been described since the original work by Weller's and Mataga's groups [37,38,40,41, 44-48].

2.3 Molecular Complexes

Absorption and emission processes are typically discussed in terms of a single molecular entity. However, the absorption and emission process may occur from molecular complexes of 1:1 or higher stoichiometries [50-54]. Molecular complexes formed on the ground surface are known as electron donor-acceptor (EDA) complexes (other terms include charge transfer complexes and ground state complexes) and have been extensively investigated for several decades [50,51]. The name EDA complexes was coined by Briegleb and it is now the accepted term [51,52]. Molecular complexes formed on the excited state surface are known as exciplexes [53], which encompasses CRIP's and hetero-excimer (hetero -excimer was coined to represent exciplexes that do not have complete electron transfer [53]).

Molecular complexes between organic substrates can be quickly identified and characterized if they interact with light. For EDA complexes, the partners act in a cooperative fashion to absorb a photon which typically results in a new absorption band uncharacteristic of the complex component's absorption bands [50-52]. This new absorption band, and the concentration dependence thereof, is a strong experimental observation to confirm that a EDA complex exists. Similarly for exciplexes, the partners act cooperatively to emit a photon which is usually uncharacteristic of either the donor or acceptor's emission profiles [53,54]. The observation of a new emission band and the concentration dependence is strong evidence that a exciplex is being formed.

2.3.1 Electron Donor-Acceptor Complexes

Benesi and Hildebrand discovered that an aromatic solution of iodine possessed a UV-Vis absorption band uncharacteristic of either molecule [55]. They were able to demonstrate that iodine formed a weak complex with the aromatic solvent, viz.



This finding has stimulated a great deal of experimental and theoretical interest in the nature of these complexes.

The nature of EDA complexes was first qualitatively discussed by Brackman [56] where the complex was thought of as a resonance hybrid between a no-bond and dative bond: $AD \leftrightarrow A^-D^+$. In the fifties Mulliken placed Brackman's description of EDA complexes into the language of quantum chemistry [50]. Mulliken described EDA complexes as resonance between a 'no-bond' (AD) and 'dative' (A^-D^+) structure as shown below.

$$\Psi_N = e |AD\rangle + a |A^-D^+\rangle + \dots \quad (2.12)$$

$|AD\rangle$ denotes the configuration due to the interaction of intermolecular forces between A and D, hence the name no-bond configuration; $|A^-D^+\rangle$ is the charge transfer plus a covalent bond configuration, hence the name dative configuration. The $+\dots$ in the above wavefunction denotes additional but negligible terms. The interpretation of the dative bond in a EDA complex is analogous to the approximate ionic-covalent resonance description of HCl [50].

$$\Psi(\text{HCl}) \equiv x \underset{\text{(ionic)}}{|H^+, Cl^-\rangle} + y \underset{\text{(covalent)}}{|H - Cl\rangle} \quad (2.13)$$

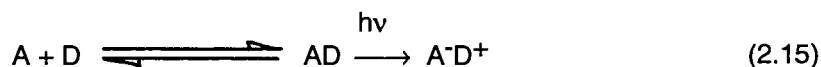
Due to the interaction of the no-bond and dative configurations, the ground configuration $|AD\rangle$ will acquire additional stabilization energy and will gain some dipolar character. For the latter point, EDA complexes of 1,3,5-trinitrobenzene with hexamethylbenzene and durene have dipole moments of 0.87 and 0.55 D [51], respectively, whereas a complete charge transfer EDA complex is expected to have a dipole moment of about 14 D [51]. Calculations have demonstrated that the major stabilization energy of EDA complexes is probably derived from the no-bond $|AD\rangle$ configuration [52,57,58]. Typically, most complexes are weak, that is, the coefficient e is significantly larger than a [51]. For example, tetracyanoethylene, a powerful ground configuration electron acceptor, forms weak EDA complexes with methyl substituted benzenes in dichloromethane solutions [51,59].

If a ground wavefunction is given by eq 2.12, it necessarily follows that there is an excited state wavefunction Ψ_V [50,51]:

$$\Psi_V = e^* |A^-D^+\rangle - a^* |AD\rangle + \dots \quad (2.14)$$

The excited EDA wavefunction shows that the excited state is destabilized by the resonance between the no-bond and dative configurations. Similarly to eq 2.12, the +.... represents other, but negligible terms. In comparing eqs 2.12 and 2.14, one finds that $e \approx e^*$ and $a \approx a^*$ (vide infra); if $e \gg a$ then $e^* \gg a^*$ for the excited state. Therefore, the ground state is essentially purely no bond structure but the excited state is essentially ionic. However, caution must be applied when discussing excited EDA states. Equation 2.12 is a description of an equilibrated ground state whereas eq 2.14 refers to the excited Franck-Condon excited state [50]. Relaxation from this Franck-Condon state may reduce or increase the coefficient a in eq 2.14.

With the correct energy of light, a weak EDA complex ($e \approx 1$ and $a < 1$) can be promoted to the excited state surface: this is shown below.



The absorption of light essentially transfers an electron from the donor D to the acceptor A hence the source of the term 'charge transfer' absorption band; it has been demonstrated that excited weak EDA complexes are adequately described as contact radical ion pairs in solution [39,50,51]. The return electron transfer process, or back electron transfer, is mostly radiationless [60].

The energy of the EDA complex (E_N) can be calculated from the wavefunction given by eq 2.12. The energy is defined as [50,51,61] shown in eq 2.16 where H ($= \langle A^{\cdot-}D^{\cdot+} | H | AD \rangle$) is the electronic coupling between the no-bond and dative configurations, E_0 ($= \langle AD | H | AD \rangle$) is the energy of the no-bond configuration, E_1 ($= \langle A^{\cdot-}D^{\cdot+} | H | A^{\cdot-}D^{\cdot+} \rangle$) is the energy of the dative configuration and S ($= \langle A^{\cdot-}D^{\cdot+} | AD \rangle$) is the orbital overlap between orbitals on A and D. The operator H is the electronic Hamiltonian operator. Note that

the EDA complex energy is approximately equal to the experimental enthalpy of complex formation, ΔH_a .

$$E_N = \frac{\langle \Psi_N | H | \Psi_N \rangle}{\langle \Psi_N | \Psi_N \rangle} \quad (2.16)$$

$$= \frac{e^2 E_0 + 2eaH + a^2 E_1}{e^2 + 2eaS + a^2}$$

By applying the variational principle [61] to eq 2.16

$$e (E_0 - E_N) + a (H - E_N S) = 0 \quad (2.17a)$$

$$e (H - E_N S) + a (E_1 - E_N) = 0 \quad (2.17b)$$

In order to have a solution, other than the trivial solution ($e = a = 0$), the secular determinant must equal to zero.

$$\begin{vmatrix} (E_0 - E_N) & (H - E_N S) \\ (H - E_N S) & (E_1 - E_N) \end{vmatrix} = 0 \quad (2.18)$$

Expanding eq 2.18 gives

$$(E_0 - E_N) (E_1 - E_N) - (H - E_N S)^2 = 0 \quad (2.19)$$

Assuming that we are dealing with weak EDA complexes such that the no-bond configuration, AD, is the major contributing factor in the stabilization of the complex, hence $e > a$ from eq 2.12. E_N can be replaced by E_0 except for $(E_0 - E_N)$. Under this assumption the energy of the EDA complex is

$$E_N = E_0 - \frac{(H - E_0S)^2}{(E_1 - E_0)} \quad (2.20)$$

and from eq 2.17a the ratio of the coefficients is

$$a / e = - (H - E_0S) / (E_1 - E_0) \quad (2.21)$$

Note that the same result for eq 2.20 would be obtained from second order perturbation theory [50]. Equations 2.20 and 2.21 show that as the dative configuration approaches the no-bond configuration, that is, as the $(E_1 - E_0)$ term becomes smaller, the extent of charge transfer is expected to increase [50,51]. Incorporating eq 2.21 into 2.20 we have

$$E_N = E_0 - (a^2 / e^2) (E_1 - E_0) \quad (2.22)$$

The equations obtained analogously for the excited state have the form.

$$E_E = E_1 + \frac{(H - E_1S)^2}{(E_1 - E_0)} \quad (2.23)$$

$$a^* / e^* = - (H - E_1S) / (E_1 - E_0) \quad (2.24)$$

If the overlap is small, from eqs 2.21 and 2.24 it can be shown that (vide infra)

$$a^* / e^* = a / e \quad (2.24)$$

The $(E_1 - E_0)$ term can be broken down as shown below. IP, EA and C above were defined earlier (eq 2.7). The symbol V represents the energy for bond formation within the

radical ion pair. As pointed out by Mulliken [50], the IP and EA are for the vertical processes.

	Process		Energy
AD		A + D	$-E_0$
A + e ⁻	→	A ⁻	$-EA_A$
D	→	D ⁺ + e ⁻	IP _D
A ⁻ + D ⁺	→	A ⁻ D ⁺	$-C + V$
*A + D	→	A ⁻ D ⁺	$E_1 - E_0$

$$E_1 - E_0 = IP - EA - C + V' \quad (2.26)$$

$$\text{where } V' = V - E_0$$

Equation 2.22 is actually a hyperbola with the asymptotes [62]

$$E_N = \pm (a^2 / e^2) (IP - EA - C + V') \quad (2.27)$$

where eq 2.26 was substituted in. If $\sqrt{E_0}$ is larger than $b \sqrt{E_1 - E_0}$ (this is usually true for weak complexes where a is less than unity and the difference $E_1 - E_0$ is near zero) then a plot of E_N (or ΔH_a) vs. IP (for a constant acceptor) is found to be linear over a limited range of IPs [62].

2.3.2 Exciplexes

Unlike an excited EDA complex discussed above, an exciplex is defined as an emissive excited molecular complex of definite stoichiometry that is dissociated or weakly

associated in its ground state [53,54]. Scheme 2.2 illustrates the formation of a 1:1 exciplex on the singlet energy surface where A and D are those defined in section 2.3.1. If the lifetime of the excited acceptor *A is sufficiently long, *A and D diffuse together to form an exciplex. The exciplex may undergo several processes: dissociation to *A and D, emission of a photon, back electron transfer, radiationless decay to the ground state A and D or to a triplet state level and to product formation [60,63].

The first example of molecular complex formation on the singlet excited state surface between two different components was reported in 1963 by Leonhardt and Weller [64]. They demonstrated that the fluorescence quenching of singlet excited perylene by N,N-dimethylaniline leads to an emissive exciplex in nonpolar solvents. Since then, many other examples have been reported and still enjoy current interest in the literature [see, e.g., 38,65-68]. Generally, exciplexes are characterized experimentally by i) a broad and featureless

Scheme 2.2



emission that is red-shifted from the predecessor's fluorescence; and ii) the absence of an EDA absorption band [53,69]. It is because of this absence of an EDA absorption band that exciplexes are considered different from their excited EDA complex counterparts. Whether the difference between exciplexes and excited EDA complexes can be due to electronic structure, geometrical orientation or specifies the preparation method of the excited state species is not entirely clear.

The stabilization of an exciplex is due to the polarizability of the excited species [i.e., *A due to half filled HOMO and lowest unoccupied molecular orbital (LUMO)] and

charge transfer interactions with another polar or polarizable species (i.e., D) [69]. This can be described in terms of a simple molecular orbital (MO) picture as shown in Figure 2.5. Figure 2.5 illustrates that the major orbital interactions occur between the LUMOs and HOMOs resulting in a new set of molecular orbitals, hence there is a net stabilization.

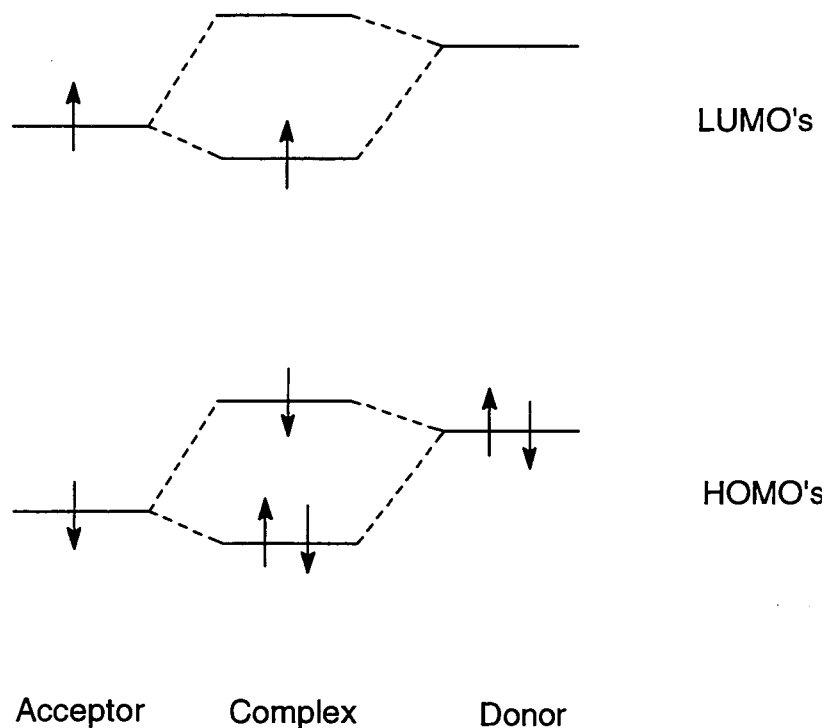


Figure 2.5: A Simple MO Picture for the Interaction of a Singlet Excited Acceptor with a Ground State Donor.

The interactions shown above demonstrate that the acceptor in the complex has gained electron density hence we could symbolize the complex has $A^{\delta-}D^{\delta+}$ where the greek lower case deltas represent partial transfer of charge. Note that the exciplex is lower in energy than a contact radical ion pair, $A^{\cdot-}D^{\cdot+}$, due to frontier orbital interactions (see below).

The free energy of exciplex formation can be broken down into individual processes as was shown for electron transfer, relative to *A [54]:

	Process		Energy
*A	\longrightarrow	A	$-E_S$
$A + e^-$	\longrightarrow	A^-	$-EA_A$
D	\longrightarrow	$D^+ + e^-$	IP_D
$A^- + D^+$	\longrightarrow	A^-D^+	$-C$
A^-D^+	\longrightarrow	$A^{\delta-}D^{\delta+}$	$-U_{stab}$
$^*A + D$	\longrightarrow	$A^{\delta-}D^{\delta+}$	ΔG_{EX}

$$\Delta G_{EX} \equiv IP_D - EA_A - C - \Delta E_S - U_{stab} \quad (2.28)$$

Equation 2.28 is nearly identical to eq 2.7 except for the last term. Therefore, exciplex formation may be more favorable thermodynamically than ET by approximately an amount- U_{stab} [70]. It should be noted that eq 2.28 is only applicable to highly polar exciplexes.

The frontier orbital interaction between an excited *A and D results in electronic coupling. Assuming the $|A^-D^+\rangle$ configuration is the lowest energy state the following wavefunction describes the electronic structure of the exciplex where the frontier orbital interaction introduces the latter four terms [69,71,72].

$$\Psi_{EX} = a |A^-D^+\rangle + b |A^+D^-\rangle + c |^*AD\rangle + d |A^*D\rangle + e |AD\rangle \quad (2.29)$$

$|A^-D^+\rangle$ and $|A^+D^-\rangle$ represent the charge transfer (dative) configurations and measure the degree of charge transfer. The $|A^-D^+\rangle$ configuration is correlated with the donation of an electron from the donor's HOMO to the acceptor's HOMO; this can be seen in Figure 2.5

where the HOMO electrons are shared hence the acceptor has a net gain. Conversely, the $|A^+D^- \rangle$ configuration is correlated with the donation of an electron from the acceptor's LUMO to the donor's LUMO. The $|^*AD \rangle$ and $|A^*D \rangle$ represent the locally excited configurations where the symbol * denotes which species contains the excitation energy. The locally excited configurations can be described as the reluctance of the acceptor or donor to share electron density.

The simplest wavefunction to describe an exciplex is the interaction between a charge transfer and locally excited configuration as shown below.

$$\Psi_{EX} = a |A^+D^- \rangle + c |^*AD \rangle \quad (2.30)$$

The charge transfer and locally excited configurations are denoted by $|A^+D^- \rangle$ and $|^*AD \rangle$, respectively, where the interaction between these two configurations is a manifestation of the donor's and acceptor's frontier HOMO interaction [71a,72]. If we assume that the $|^*AD \rangle$ contribution to the exciplex does not contribute to the observed exciplex dipole moment then the observed exciplex dipole moment is due to the magnitude of the a coefficient in eq 2.30. An evaluation of the a coefficient can be calculated from eq 2.31 [71a]

$$a^2 = \mu_{ex} / \mu_{CRIP} \quad (2.31)$$

where μ_{ex} is the observed exciplex dipole moment and μ_{CRIP} represents the dipole moment of the hypothetical contact radical ion pair with $a = 1$ and $c = 0$. From the normalization condition, $a^2 + c^2 + 2acS = 1$, the coefficient c can be calculated if the configuration overlap integral, $S = \langle A^+D^- | ^*AD \rangle$, is known; typically, S is small for exciplexes [71,72] and the normalization condition can be approximated by $a^2 + c^2 \approx 1$.

Following the procedure discussed for EDA complexes in section 2.3.1, the variational principle can be applied to the simplified exciplex wavefunction given by eq 2.30

and the exciplex energy and coefficients can then be calculated. Such a treatment is instructive since the variation in observable exciplex properties (exciplex dipole moment and exciplex energy) can be correlated to the interaction between the $|A^{\cdot-}D^+\rangle$ and $|^*AD\rangle$ configurations. In the EDA complex variational treatment we were able to assume the interaction between the no-bond and dative configurations was weakly perturbed; however, for exciplexes this assumption can not be applied since the $|A^{\cdot-}D^+\rangle$ and $|^*AD\rangle$ configurations may be degenerate in energy [71,72]. The full expression derived from expansion of the secular determinant must be used.

$$E_{EX} = \frac{\langle \Psi_{EX} | H | \Psi_{EX} \rangle}{\langle \Psi_{EX} | \Psi_{EX} \rangle} \quad (2.32)$$

$$= \frac{a^2 E_{CT} + 2acH + c^2 E_{LE}}{a^2 + 2acS + c^2}$$

where	$E_{CT} = \langle A^{\cdot-}D^+ H A^{\cdot-}D^+ \rangle$	Charge transfer configuration energy.
	$E_{LE} = \langle ^*AD H ^*AD \rangle$	Locally excited configuration energy.
	$H = \langle A^{\cdot-}D^+ H ^*AD \rangle$	Configuration mixing integral; H_{rp} .
	$S = \langle A^{\cdot-}D^+ ^*AD \rangle$	Configuration overlap.

Weller's group has empirically determined the charge transfer configuration integral to be [34,63,73]

$$E_{CT} = E_{ox}(D) - E_{red}(A) + 0.15 \text{ eV} \quad (2.33)$$

The locally excited configuration integral can be approximated by [72]

$$\langle {}^*A|D|H|{}^*A\rangle \cong \langle {}^*A|H|{}^*A\rangle = E_S \quad (2.34)$$

where E_S is the experimental singlet excited state energy of *A . The integral $\langle A^*D^+|H|{}^*A\rangle$ represents the additional stabilization energy gain through the resonance between the charge transfer and locally excited configurations. Using Mulliken's approximation for two-electron integrals, Beens and Weller derived a simple expression for this integral [71c,d,72].

$$\langle A^*D^+|H|{}^*A\rangle = -S(\Gamma_D + E_S) \quad (2.35)$$

$$\text{where } \Gamma_D \approx -20 \text{ eV} + IP_D$$

Applying the variational principle we find [61]

$$a(E_{CT} - E_{EX}) + c(H - E_{EX}S) = 0 \quad (2.36a)$$

$$a(H - E_{EX}S) + c(E_{LE} - E_{EX}) = 0 \quad (2.36b)$$

and for a nontrivial solution

$$\begin{vmatrix} (E_{CT} - E_{EX}) & (H - E_{EX}S) \\ (H - E_{EX}S) & (E_{LE} - E_{EX}) \end{vmatrix} = 0 \quad (2.37)$$

The expansion of the secular determinant eq 2.37 and subsequent rearrangement gives

$$(1 - S^2) E_{EX}^2 + (2HS - E_{LE} - E_{CT}) E_{EX} + (E_{LE}E_{CT} - H^2) = 0 \quad (2.38)$$

Equation 2.38 is a quadratic equation whose two solutions are

$$E_{EX} = \frac{-B \pm \sqrt{D}}{2A} \quad (2.39)$$

where

$$A = (1 - S^2)$$

$$B = 2HS - E_{EL} - E_{CT}$$

$$C = E_{LE}E_{CT} - H^2$$

$$D = B^2 - 4AC$$

The ratio of the coefficients is given from eq 2.36a

$$c/a = (E_{CT} - E_{EX}) / (H - E_{EX}S) \quad \text{if } E_{CT} < E_{LE} \quad (2.40a)$$

$$= (E_{LE} - E_{EX}) / (H - E_{EX}S) \quad \text{if } E_{LE} < E_{CT} \quad (2.40b)$$

The equations above are expressed in terms of the reactant properties. This does not impede any application of these equations since the interaction between the donor and acceptor is weak due to the small overlap integral S (less than 0.06 [71c,d,72]) hence the donor's and acceptor's properties are weakly perturbed. This is advantageous since only the overlap integral S is unknown but redox potentials, ionisation potentials and singlet energies are readily available or easily determined.

To get an impression on how the overlap integral and energy gap affects the exciplex's nature, let us consider two hypothetical situations where we have a singlet excited acceptor ($E_S = 3.0$ eV) and a series of electron donors (IP = 8.5 eV) that may form exciplexes of the description provided by eq 2.30. From eqs 2.32 to 2.40, we can illustrate the variation in the calculated exciplex dipole moment, μ_{ex} , and stabilization energy U_{Stab} gained by the $|A^-D^+\rangle \leftrightarrow |^*AD\rangle$ resonance. We will assume values for S of 0.03 and zero with a maximum dipole moment of 13 D for this illustration. Note that a S value of 0.03 represents a weak interaction (i.e., $S = \langle A^-D^+ | ^*AD \rangle \propto \langle A^-D^+ | H | ^*AD \rangle$) between the donor and acceptor (i.e., adiabatic), which is typical for exciplexes, and a S value of zero

represents no interaction (i.e., nonadiabatic). Figure 2.6 shows the variation in the exciplex dipole moment and the stabilization energy as a function of the HOMO-HOMO energy gap, which is determined by the difference $E_{CT} - E_{LE}$.

The calculation shown by Figure 2.6 demonstrates a number of features. Firstly, as expected the strongest $|A^{\cdot}D^{\cdot+}\rangle \leftrightarrow |^*AD\rangle$ resonance interaction occurs when the HOMO energy levels are degenerate ($E_{CT} - E_{LE} = 0$) and falls off to zero as the HOMO energy gap becomes larger. Note that for the region where $E_{CT} - E_{LE} > 0$ the exciplex gains some stabilization energy from this resonance interaction, hence a weakly polar exciplex is enthalpically favored relative to the singlet excited acceptor *A . Secondly, the exciplex dipole moment follows a sigmoidal curve. Thirdly, the resonance interaction becomes negligible at $E_{CT} - E_{LE}$ differences around 1.5 eV. In contrast, with a zero overlap integral there is absolutely no stabilization energy gained and a full electron is transferred to the singlet excited acceptor if its HOMO energy level lies below that of the donor's; a contact radical ion pair (CRIP) is formed.

2.4 Solvatochromism and Exciplex Dipolar Character

The term solvatochromism is generally used to describe UV-Vis absorption band shifts as a function of the medium's polarity [74-76]. A blue-shift (hypsochromic) with increasing medium polarity is usually called negative solvatochromism; a red-shift (bathochromic) is termed positive solvatochromism. Solvatochromism is frequently used to describe shifts in luminescence spectra with the medium's polarity.

The solvent effect on UV-Vis and fluorescence spectra provides information regarding the nature of the ground and excited configurations; that is, the difference between the ground (μ_g) and excited state dipole moments (μ_e) [74-76]. In general, if the excited state is more polar than the ground state ($\mu_e > \mu_g$) positive solvatochromism is observed as the medium polarity increases; negative solvatochromism is observed if the

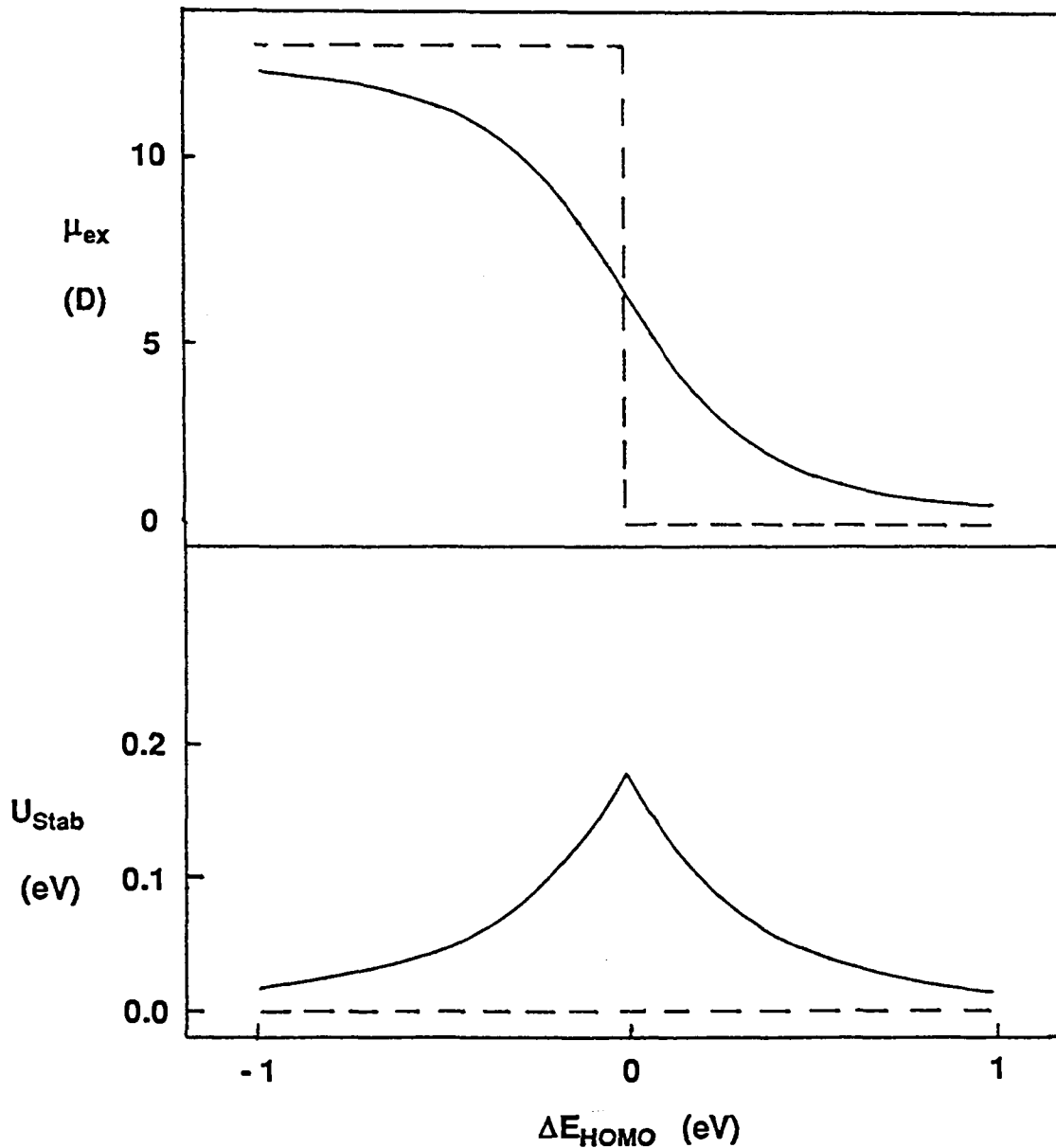


Figure 2.6: Simulated Exciplex Dipole Moment and Resonance Interaction Energy of a Hypothetical Exciplex with a Wavefunction Described by $\Psi_{\text{EX}} = a |A^{\cdot}D^{\cdot+}\rangle + b |^{\cdot}AD\rangle$. The Calculation Assumed a Configuration Overlap of 0.03, an Acceptor Singlet Energy of 3.0 eV, a Constant Donor IP of 8.5 eV and a Maximum Exciplex Dipole Moment of 13 D.

ground state dipole moment is larger than the excited state ($\mu_g > \mu_e$) [74-76]. This behavior is rationalized by the difference in stabilization energies, which is proportional to the solute's dipole moment [74-76] (Figure 2.7).

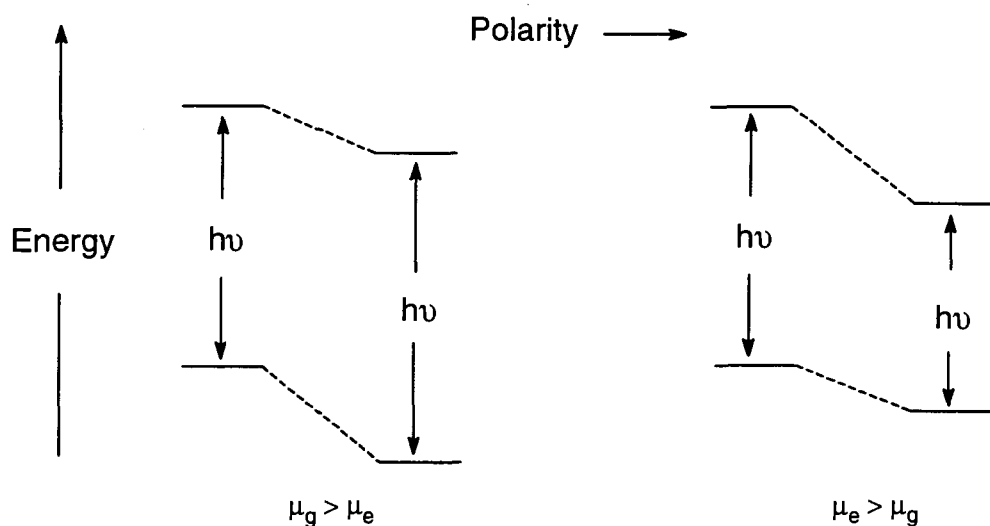
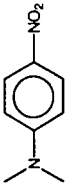
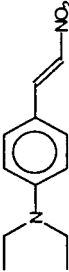
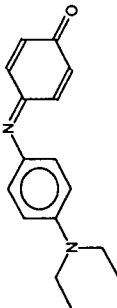
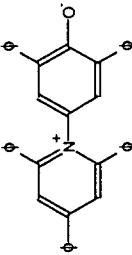
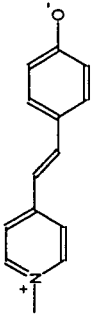


Figure 2.7: Schematic Representation of the Relative Change in the Excited and Ground Energy Levels as a Function of their Dipole Moments.

Examples of positive and negative solvatochromic compounds are given in Table 2.1, where the correlation between the solvatochromic shift direction and difference in ground and excited state dipole moments is apparent. Table 2.1 entry number 4 is the betaine used by Dimroth and Reichardt for their empirical polarity scale (E_T) [74].

We are interested in experimentally determining the interaction between the donor D and acceptor A, by developing an equation to access the CT character. Typically, the excited state dipole moment of a molecule is determined by the Lippert-Mataga equation where both the UV-Vis absorption and fluorescence maxima (Stokes' shift) are required for analysis [74,76]. However, an exciplex has no detectable EDA complex absorption band. Therefore, we need an equation that exploits solely the fluorescence emission maximum.

Table 2.1: Selected Solvatochromic Dyes and Their Properties^a

ID	Solvatochromism	Compound	μ_g (D)	μ_e (D)	λ_{max} (nm)		$\Delta\lambda$ (nm)
					Nonpolar ^b	Polar ^b	
1	Positive		5.1	12.9	365 (Cyclohexane)	430 (Water)	65
2	Positive		7.8	18	400 (Cyclohexane)	470 (1:9 EtOH:H ₂ O)	70
3	Positive		5.7	7.5-9.0	552 (Cyclohexane)	668 (Water)	116
4	Negative		14.7	6.0	810 (Diphenyl ether)	453 (Water)	-357
5	Negative		26.1	--	620 (Chloroform)	442 (Water)	-178

^a Adapted from reference 74. ^b λ_{max} obtained in the solvent within closed parentheses.

Beens et al. have derived such an equation [71b,77]. However, they neglected the contribution of the permanent dipole moments of the donor and acceptor since these were considered negligible and cancelled by an opposing dispersion term. In this study the β -diketonatoboron complexes are known to have significant dipole moments ($\mu_g = 5\text{-}7$ D, Table 1.1), which is up to one half of that typically found for exciplexes (12-14 D) [54]; therefore, the potential complex's dipole moment contribution to the observed exciplex dipole moment must be clarified.

Contemporary treatments of solvatochromism usually derive a solvatochromic relationship by either the reversible-work approach [78-80], which is derived from Marcus' theory of electron transfer, or the reaction-field approach, which has been promoted by Ooshika, Lippert, McRae, Liptay and others [74,81-86]. Both approaches give nearly identical relationships under the same simplifying assumptions, that is, Onsager's theory of dielectrics [79,80,87]. The formalism of van der Zwan and Hynes (the reversible-work approach) [79] is particularly convenient and we will adopt this formalism to derive an equation to evaluate an exciplex's dipole moment from its emission solvatochromism (this formalism was originally formulated for time-dependent fluorescence studies). The discussion below is for a single molecular entity (solute) but the derivation will be extended later to exciplex emission solvatochromism.

The van der Zwan and Hynes (ZH) approach is based on a form of Marcus' electron transfer theory [40,78, 79]. Figure 2.8 shows a free energy diagram (Helmholtz) of the ground and excited states of the solute vs. the solvation coordinate. The points from A to D in Figure 2.8 represent the solvent's equilibrium free energies (points A and C) and the solvent's non-equilibrium free energies (points B and D); note that there are equivalent statements: a relaxed (A and C) and a non-relaxed (B and D) solvent shell. The arrows represent the absorption (A to B) and relaxed fluorescence (C to D) processes. However, fluorescence can occur from any point between B and C (which occurs if the solute's lifetime is similar to that of the solvent's characteristic relaxation time) to any position

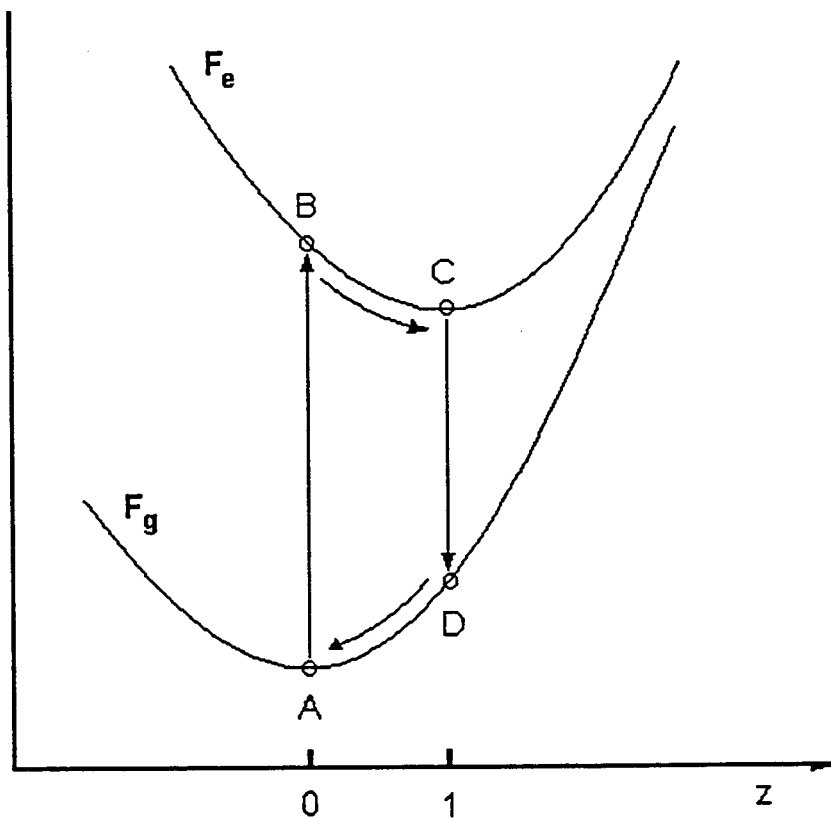


Figure 2.8: The Ground and Excited State Non-equilibrium Free Energies (F_g and F_e , Respectively) vs. the Solvation Coordinate (z). The Absorption (\uparrow) and Relaxed Emission (\downarrow) Processes are Shown. Adapted from Reference 79.

between A and D. Fortunately, most emitting species usually emit with a relaxed solvent shell (point C) [79,80]. The energy difference from C to D is given by eq 2.41.

$$h\nu_F = \Delta U = F_e^{\text{eq}} - F_g(t) \quad (2.41)$$

Note that eq 2.41 relates the energy of the solute / solvent (ΔU) with the Helmholtz free energy. This is possible since the entropy of the system is assumed to remain unchanged in a Franck-Condon transition [40].

The first term in eq 2.41, F_e^{eq} , is composed of two components (eq 2.42) which represent the gas phase energy and the work in bringing the solute from the gas phase into a dielectric medium.

$$F_e^{\text{eq}} = U_e^{\circ} - \frac{1}{2} (B_{\text{op}} + B_{\text{or}}) \mu_e^2 \quad (2.42)$$

U_e° represents the energy of the solute in its excited state in the gas phase and μ_e is the solute's excited state dipole moment. The second term, $\frac{1}{2} (B_{\text{op}} + B_{\text{or}}) \mu_e^2$, is the equilibrium solvation energy according to linear response theory. Using the Onsager model $B_{\text{op}} + B_{\text{or}}$ are [79]

$$B_{\text{op}} = (2 / \rho^3) [(n^2 - 1) / (2n^2 + 1)] \quad (2.43a)$$

$$B_{\text{or}} = (2 / \rho^3) [(\epsilon - 1) / (2\epsilon + 1) - (n^2 - 1) / (2n^2 + 1)] \quad (2.43b)$$

In eqs 2.43 ρ , ϵ and n represent the solvent cavity radius, solvent's bulk dielectric constant and refractive index, respectively. Equations 2.43a and 2.43b are the familiar parameters for the response of the solvent's valence electrons (B_{op}) and dipole (induced or permanent; B_{or}) to the solute's electrical field.

The second term in eq 2.41, $F_g(t)$, represents the non-equilibrium free energy of the ground state solute. In analogy to eq 2.42, $F_g(t)$ can be described by

$$F_g(t) = U_g^{\circ} - \frac{1}{2} (B_{op} + B_{or}) \mu_g^2 - F_g^{\text{neq}} [\mu_g - \mu(t)]^2 \quad (2.44a)$$

where U_g° is the ground state solute's energy in the ground state, μ_g is the solute's ground state dipole moment and $\mu(t)$ is the effective dipole moment ($\mu(t)$ is that which would be in equilibrium with the instantaneous nonequilibrium orientation at time t). ZH identifies $\mu(t)$ as μ_e (i.e., the solvent shell structure is identical at points C and D in Figure 2.7) and $F_g^{\text{neq}} = \frac{1}{2} B_{or}$. Therefore

$$F_g(t) = U_g^{\circ} - \frac{1}{2} (B_{op} + B_{or}) \mu_g^2 - \frac{1}{2} B_{or} [\mu_g - \mu_e]^2 \quad (2.44b)$$

Equations 2.44b and 2.42 allow us to derive a solvatochromic equation for the emission process via eq 2.41.

$$h\nu_F = h\nu_F^{\circ} - \frac{1}{2} (B_{op} + B_{or}) \mu_e^2 + \frac{1}{2} (B_{op} + B_{or}) \mu_g^2 - \frac{1}{2} B_{or} (\mu_g - \mu_e)^2 \quad (2.45)$$

$h\nu_F^{\circ}$ represents the difference in the solute's ground and excited state energies ($U_e^{\circ} - U_g^{\circ}$) in the gas phase. By expanding $(\mu_g - \mu_e)^2$ and substituting in eqs 2.43, it can be shown that eq 2.44 reduces to a more familiar emission solvatochromic expression (eq 2.46) [80].

$$h\nu_F = h\nu_F^{\circ} + (1 / \rho^3) \{ -2\mu_e \cdot (\mu_e - \mu_g) F_1 - (\mu_e^2 - \mu_g^2) F_2 \} \quad (2.46)$$

$$F_1 = (\epsilon - 1) / (2\epsilon + 1) - (n^2 - 1) / (2n^2 + 1)$$

$$F_2 = (n^2 - 1) / (2n^2 + 1)$$

The first term on the right hand side of eq 2.46 represents the reorientation of the surrounding solvent molecules and the second term represents the solvent polarizability. In nonpolar solvents the F_1 term is nearly zero since $\epsilon \cong n^2$. Equation 2.46 is almost exactly the same as that derived by Liptay and others [81-87] by the reaction-field approach except for a missing dispersion term, which is usually neglected for studies in polar solvents. The coupling between the solute's excited state and ground dipole moments is shown by the dot product $\mu_e \cdot (\mu_e - \mu_g)$; $\mu_e \cdot (\mu_e - \mu_g) = \mu_e^2 - \mu_e \mu_g \cos \phi$ where ϕ is the angle between the ground and excited state dipole moments. It is clear that this coupling could be negligible due to the angular relationship between μ_e and μ_g ; i.e., if $\phi = 90^\circ$.

An equivalent equation (eq 2.47) can be derived for the absorption process represented by points A to B in Figure 2.8.

$$h\nu_{Abs} = h\nu_{Abs}^0 + (1 / \rho^3) \{ -2\mu_g \cdot (\mu_g - \mu_e) F_1 - (\mu_g^2 - \mu_e^2) F_2 \} \quad (2.47)$$

$$F_1 = (\epsilon-1) / (2\epsilon + 1) - (n^2 - 1) / (2n^2 + 1)$$

$$F_2 = (n^2 - 1) / (2n^2 + 1)$$

The difference between eqs 2.46 and 2.47, $h\nu_{Abs} - h\nu_F$, can be shown to give the Lippert-Mataga equation (eq 2.48) [74,76]

$$h\nu_{Abs} - h\nu_F = \Delta h\nu + (2 / \rho^3) (\mu_e - \mu_g)^2 F_1 \quad (2.48)$$

where $\Delta h\nu = h\nu_{Abs}^0 - h\nu_F^0$.

The original purpose in deriving an emission solvatochromic equation was to assess the effect of the permanent ground state dipole moment(s) with respect to evaluation of the charge transfer character due to donor-acceptor interactions. At this point it is necessary to discuss the Franck-Condon ground state of the exciplex. Upon emission of a photon the donor and acceptor have no opportunity to change their relative

orientations. This ground state complex may be either repulsive or attractive depending on whether or not the Franck-Condon donor-acceptor orientation corresponds to that of the EDA complex (if one exists). The total dipole moment of the Franck-Condon ground state complex will be a sum of the permanent dipole moments and the induced dipole from the interaction between the donor and acceptor; this total dipole moment is represented by μ_g . For DBMBF₂ / substituted benzene exciplexes, it is a good assumption that DBMBF₂'s large dipole moment (Table 2.1) is the major contribution in the Franck-Condon ground state μ_g and that μ_g lies in the molecular plane. This assumption has a distinct advantage as will be demonstrated below.

The dipole moment μ_e in eq 2.46 is a vectorial sum of the dipole moment resulting from charge transfer between the donor and acceptor (μ_{ex}) and the permanent dipole moments μ_g (eq 2.49).

$$\mu_e = \mu_{ex} + \mu_g \quad (2.49)$$

If electron transfer neutralizes μ_g then $\mu_e = \mu_{ex}$. Substituting eq 2.49 into eq 2.46 we find

$$h\nu_F = h\nu_F^0 + (1 / \rho^3) \{ -2\mu_{ex} \bullet (\mu_{ex} - \mu_g) F_1 + (\mu_{ex}^2 + 2 \mu_{ex} \bullet \mu_g) F_2 \} \quad (2.50)$$

Equation 2.50 is rather complicated and difficult to utilize experimentally, however, the directional nature of μ_{ex} and μ_g allow further simplification. Permanent dipole moments are in the molecular plane whereas donor-acceptor charge transfer interactions are oriented perpendicular [50,51] to the molecular plane (Figure 2.9); an exception would be twisted intramolecular charge transfer where both μ_{ex} and μ_g are parallel [88]. Note that Figure 2.10 is an ideal situation where the orientation may very well be off centered hence μ_{ex} and μ_g will no longer be orthogonal. Assuming the ideal case and recalling that dot products of orthogonal vectors are zero, all dot products in eq 2.50 vanish; i.e., $\mu_{ex} \bullet \mu_g = \text{zero}$.

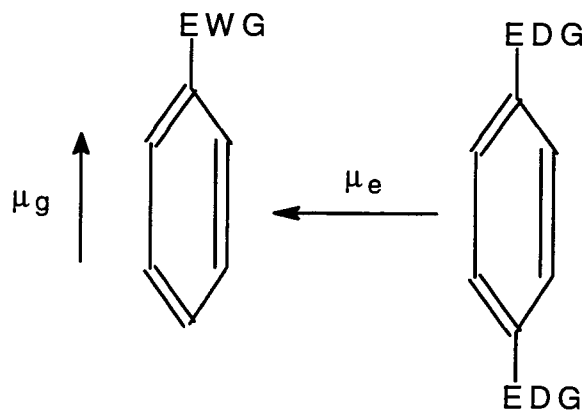


Figure 2.9 : Illustration of the Ideal Relative Orientation of the Ground and Charge Transfer Dipole Moments of Two π Systems. EWG and EDG Represent Electron Withdrawing and Donating Groups, Respectively.

Equation 2.50 therefore simplifies to eq 2.51.

$$h\nu_F = h\nu_F^0 - (2 / \rho^3) \mu_{ex}^2 F_3 \quad (2.51)$$

$$F_3 = (\epsilon - 1) / (2\epsilon + 1) - (n^2 - 1) / (4n^2 + 2)$$

Equation 2.51 should be applicable for non-orthogonal systems where the angle between μ_e and μ_g is less than 20° . Note that F_3 is similar but not identical to F_1 , wherein the polarization term is reduced by one half. An equivalent equation to that of eq 2.51 was derived earlier by Beens et al. [77] via Liptay's reaction-field theory (eq 2.52).

$$\begin{aligned} h\nu_F &= h\nu_F^0 - (2 / \rho^3) \mu_e^2 F_3 \\ &= h\nu_F^0 - (2 / \rho^3) (\mu_{ex} + \mu_g)^2 F_3 \end{aligned} \quad (2.52)$$

Comparison of eqs 2.51 and 2.52 shows that they only differ in the dipole moment term: μ_e and μ_{ex} where eq 2.52 suggests that the experimentally determined μ_e contains a contribution due to μ_g . The analysis above shows that the assumption that of a negligible μ_g is unnecessary and that the exciplex emission solvatochromism is directly related to the square of the extent of charge transfer (μ_{ex}) between the donor and acceptor without any interference from μ_g .

The dispersion term may be simply described by eq 2.53 [71b,77]

$$\text{Dispersion} = (2hcD / \rho^3) (n^2 - 1 / n^2 + 1) \quad (2.53)$$

where D is a term describing the dependence of the position of the absorption band on the dispersion interactions between the solute and solvent molecules. Since D is usually greater than zero the dispersion term results in a red spectral shift. Basu showed that D is a function of the solute's transition dipole moment, M_{if} , and the difference in the excited and ground state polarizability tensors, α , as shown by eq 2.54 [85,89].

$$D \propto |M_{if}|^2 + \xi (\alpha_e - \alpha_g) \quad (2.54)$$

The subscripts e and g represent the excited and ground states, respectively, and ξ is the average excitation energy of the solvent. Equation 2.54 is an approximation since dispersion interactions are not two body forces but are nearly additive [85,86]. The dispersion term may become important for easily polarizable solvent molecules where the solvent's contribution appears in eq 2.53 as the function $(n^2 - 1 / n^2 + 1)$; i.e., solvents with large n. Therefore, the dispersion contribution, which is difficult to quantitatively measure since D is not known, can be neglected if the experimental solvent series has similar refractive indices. This reduces the dispersion term to a constant thus D can be collected with the constant gas phase emission term $h\nu_F^0$.

The discussion above points out that the application of solvatochromic analysis is rather precarious. Simple equations like eq 2.52 or the Lippert-Mataga equation (eq 2.48) have held a great fascination in the literature, but they are not generally useful for theoretical analysis [85]. To illustrate this, the derivation of eq 2.52 was dependent on the assumptions listed in Table 2.2, some of which were stated previously.

All is not lost, however. Equation 2.52 can yield a physical meaning if we differentiate solvents into classes where correlations between theory and empirical scales can be sought.

Empirical solvent polarity scales, such as Taft's π^* scale [74, 90], are more faithful in manifesting the microscopic solvent polarity, at a deeper level, than theoretical polarity scales (i.e., F_3), especially since dispersion interactions can be accounted for. For example, cyclohexane and benzene would be considered to be similar in their polarity based on the F_3 theoretical polarity scale (cf. $F_3 = 0.101$ for cyclohexane, 0.116 for benzene, 0.254 for chloroform and 0.405 for water) whereas on the Taft π^* empirical polarity scale benzene is significantly more polar than cyclohexane and as polar as chloroform (cf. $\pi^* = 0.00$ for cyclohexane, 0.59 for benzene, 0.58 for chloroform and 1.09 for water [90]). The theoretical scale fails to account for the degree of polarizability of the benzene π orbitals whereas empirical scales do [74,90]. Unfortunately, empirical polarity scales are not tractable for quantitative evaluation of dipole moments from spectroscopic data.

For a meaningful dipole moment to be determined by solvatochromic analysis, such as eq 2.52, the solvent series must be chosen with respect to the following. Firstly, the dispersion term (point 7 in Table 2.2) influence can be minimized by using solvents with similar refractive indices such that the $(n^2 - 1 / n^2 + 1)$ term in eq 2.53 becomes relatively constant; this immediately eliminates the aromatic solvents due to their large refractive indices. Secondly, solvents suspected to be involved in specific interactions (point 2 in Table 2.2), such as hydrogen bonding or charge transfer interactions, must be excluded;

Table 2.2: Common assumptions applied in deriving solvatochromic equations

Point	Assumption
1	non-polarizable dipole
2	no specific solvent / solute interactions (hydrogen bonding and charge transfer interactions)
3	spherical solvent cavity
4	dipole's center of gravity at the origin of the solvent cavity
5	linear response theory
6	solvent can be treated as an isotropic dielectric continuum
7	neglect of dispersion interactions

this immediately eliminates alcohols (hydrogen bonding) and aromatics as potential solvents (charge transfer [91]). Chlorinated solvents must be eliminated if the excited solute is an electron donor due to charge transfer reactions (point 2 in Table 2.2); chlorinated solvents are good electron acceptors [92]. Thirdly, the ability of the theoretical polarity parameter F_3 to provide a measure of the microscopic solvent polarity should be demonstrated by a linear relationship between F_3 and an empirical polarity scale. A collection of solvents that obey the above conditions can be termed 'ideal' solvents. Having established a set of 'ideal' solvents, the subsequent solvatochromic analysis should extract physically meaningful dipole moment(s).

As a final note, the above discussion can be used in a reversed sense. Suppose we wished to demonstrate a specific interaction of solvent A with the solute. By plotting the experimental parameter (absorption peak, emission maximum, etc.) vs. a theoretical polarity scale, using a set of 'ideal' solvents and solvent A, specific interactions will be immediately noticeable if solvent A's point deviates from the 'ideal' solvent line. In addition, the deviation distance will be a rough measure of the specific interaction energy [93].

2.5 Polarographic and Excited State Energy Levels

Excited state energies, both the singlet (E_S) and triplet (E_T) states, have been known to be correlated to the redox properties of the molecule in question [94,95]. This is due to the fact that the difference between the oxidation and reduction ($E_{ox} - E_{red}$) potentials and the singlet or triplet energies all involve the HOMO and LUMO energy levels. It is generally found that there are good linear relationships between redox ($E_{ox} - E_{red}$) and excitation energies (E_S and E_T) [94,95]. For example, benzenoid alternant hydrocarbons have been shown to obey eq 2.55 if the redox potentials are reversible [58].

$$E_{ox} - E_{red} = E_S + \text{constant} \quad (2.55)$$

Note that the implicit assumption in eq 2.55 is that the redox potentials are reversible (i.e., thermodynamic values).

The relationship between $E_{\text{ox}} - E_{\text{red}}$ and E_{S} or E_{T} will be derived below. The relationship between the HOMO (ϵ_{ho}) and LUMO (ϵ_{lu}) energy levels with respect to spectroscopic and electrochemical energies is schematically shown in Figure 2.10. From Figure 2.10 the electrochemical potentials are related to ϵ_{ho} and ϵ_{lu} by [49,54,94,95]

$$E_{\text{ox}} = -\epsilon_{\text{ho}} + \Delta G_{\text{solv}}^{+} + E_{\text{Ref}} \quad (2.56a)$$

$$E_{\text{red}} = -\epsilon_{\text{lu}} - \Delta G_{\text{solv}}^{-} + E_{\text{Ref}} \quad (2.56b)$$

Note that eq 2.56 is a disguised form of eq 2.8 where Koopman's theorem [96] was applied. E_{ref} is the potential of the reference electrode on an absolute scale for which the SCE reference electrode E_{Ref} is - 4.40 eV [94c]. Equation 2.56 shows that the energy of the HOMO and LUMO levels are directly related to their respective redox potentials. Since $\Delta G_{\text{solv}}^{+}$ and $\Delta G_{\text{solv}}^{-}$ do not vary significantly between structurally different compounds, $\Delta E_{\text{ox}} \approx \Delta \epsilon_{\text{ho}}$ and $\Delta E_{\text{red}} \approx \Delta \epsilon_{\text{lu}}$. Similarly for the singlet and triplet energies.

$$E_{\text{S}} = \epsilon_{\text{lu}} - \epsilon_{\text{ho}} - J + 2K \quad (2.57a)$$

$$E_{\text{T}} = \epsilon_{\text{lu}} - \epsilon_{\text{ho}} - J \quad (2.57b)$$

J is the Coulomb integral and K is the exchange integral. Both integrals measure electron repulsion where J is the classic electrostatic repulsion of two charge distributions [72]. The integral K is a measure of the degree to which the electron in the HOMO and the electron in the LUMO come in to each other's way [72]; this provides a sense of the relative orbital orientation between the LUMO and the HOMO [36,97]. J is greater than or equal to K where K is greater than or equal to zero; i.e., $J \geq K \geq 0$ [97]. From eq 2.56 the difference in redox potentials is given by

$$E_{\text{ox}} - E_{\text{red}} = \varepsilon_{\text{lu}} - \varepsilon_{\text{ho}} - \Delta G_{\text{solv}}^+ - \Delta G_{\text{solv}}^- \quad (2.58)$$

Rearranging terms gives ($\Delta\Delta G_{\text{solv}} = \Delta G_{\text{solv}}^+ + \Delta G_{\text{solv}}^-$)

$$\varepsilon_{\text{lu}} - \varepsilon_{\text{ho}} = E_{\text{ox}} - E_{\text{red}} + \Delta\Delta G_{\text{solv}} \quad (2.59)$$

Substituting eq 2.59 into eq 2.57 gives eq 2.60.

$$E_{\text{S}} = E_{\text{ox}} - E_{\text{red}} + \Delta\Delta G_{\text{solv}} - J + 2K \quad (2.60a)$$

$$E_{\text{T}} = E_{\text{ox}} - E_{\text{red}} + \Delta\Delta G_{\text{solv}} - J \quad (2.60b)$$

Equation 2.60 predicts a linear relationship of E_{S} (or E_{T}) with $E_{\text{ox}} - E_{\text{red}}$ with unity slope, which is shown by eq 2.55. Interestingly, for plots of eq 2.60a the y-intercept is usually near zero which suggests that $\Delta\Delta G_{\text{solv}} + 2K$ is nearly the same as J [94]. The corresponding plots of eq 2.60b have been shown to be linear as well, however, the y-intercept is negative which is in accord with eq 2.60b ($J > \Delta\Delta G_{\text{solv}}$) [94]. Plots of eq 2.60 have been found to be linear with either unity or less than unity slope [95]. Less than unity slopes can be rationalized to be a result of using irreversible electrochemical potentials [95] or a systematic variation in J and K .

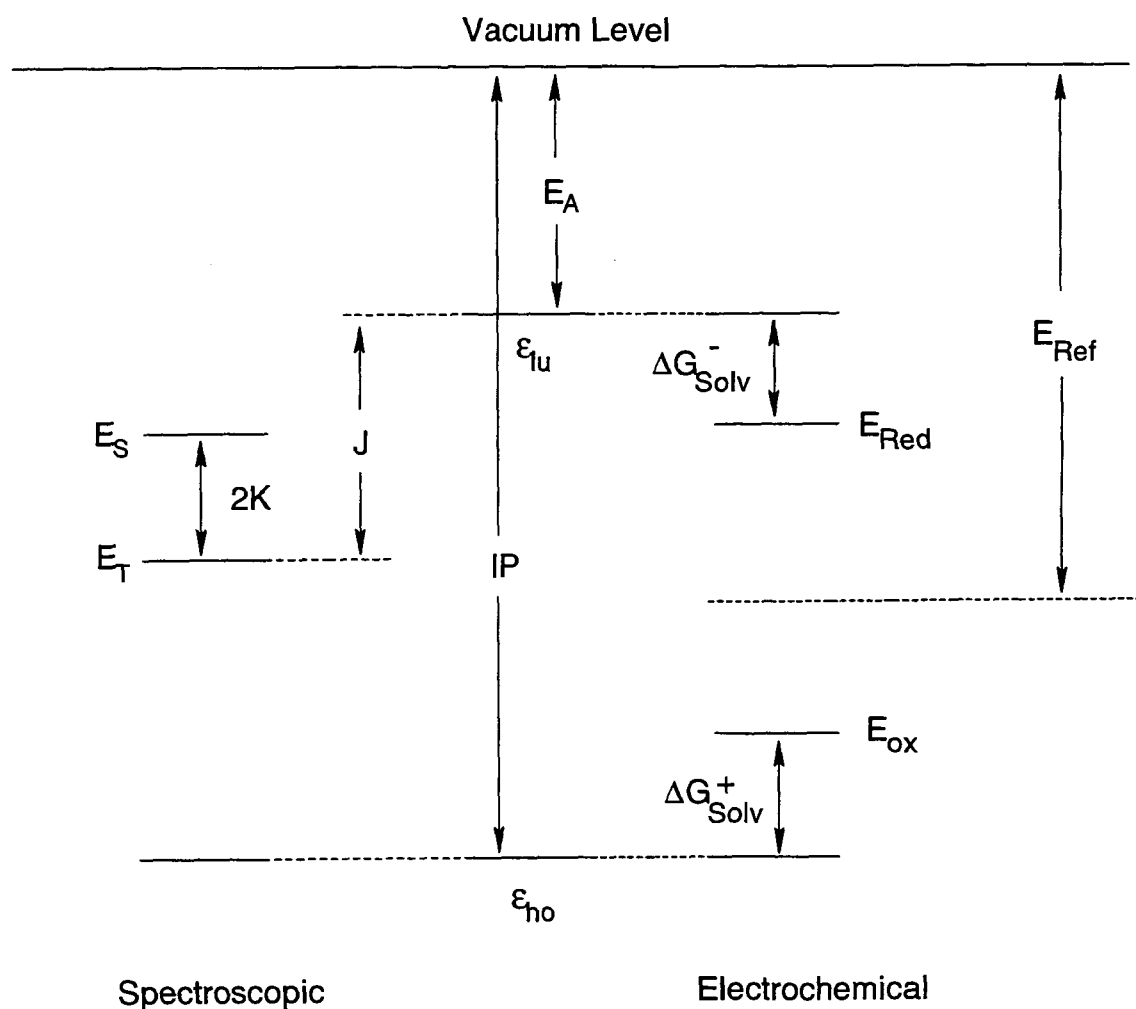


Figure 2.10: Relationship of Molecular Orbitals with Electrochemical and Spectroscopic Properties where the Energy Level Ordering has been Exaggerated. Adapted from Loufty and Loufty [95].

CHAPTER THREE

SPECTROSCOPIC AND REDOX PROPERTIES OF β -DIKETONATOBORON COMPLEXES

3.1 Introduction

Redox potentials (oxidation and reduction), UV-Vis absorption (λ_{max} and molar extinction coefficient) and luminescence (emission profiles, quantum yields and excited state lifetimes) properties are the basic 'ingredients' in the investigation of photochemical reactions. These quantities are useful in establishing the experimental conditions or reaction feasibility. Redox potentials are useful in determining the feasibility of either EDA and exciplex formation in nonpolar solvents or electron transfer reactions in polar solvents; for example, the free energy for a PET reaction can be calculated from eq 2.9 (Chapter 2.1.2) if the redox potentials are known. UV-Vis absorption and fluorescence spectra help the experimentalist to determine a suitable 'excitation window' and the quenching mechanism.

The basic photochemical parameters of β -diketonatoboron complexes [9,10,14,98-101] are not well represented in the literature. Luminescence studies have only been recently initiated and some of the reported findings are questionable; for example, the reported AABF₂ fluorescence ($\lambda_{\text{max}} \approx 420$ nm) at high AABF₂ concentrations [100b], which was suggested to be excimer emission [36], was determined to be due to an impurity. In this section, UV-Vis and luminescence spectroscopic data are reported for selected new and known β -diketonatoboron complexes to gain basic and reliable information.

3.2 UV-Visible Absorption- Results and Discussion

The observed UV-Vis absorption maxima (λ_{max}) and molar extinction coefficients (ϵ_{max}) of various β -diketonatoboron complexes (see Scheme 1.1 for abbreviations) are listed in Table 3.1.

Unlike the tautomerization of simple ketones, where the percentage enol tautomer is negligible, the *cis*-enol tautomer of β -diketone percentage is significant and may be the dominant tautomer in solution [102]. Hydrogen bonding is the major factor for the relative stability of the *cis*-enol tautomer where the enol hydrogen is involved in a hydrogen bond with the other carbonyl that forms a six member ring structure [102c,d]. It is known that *cis*-enol β -diketones have C_s symmetry where the barrier for proton transfer between the oxygens is amounting 4 to 5 kcal / mol [102c,d].

The *cis*-enol is readily identified by UV-Vis spectroscopy since the conjugated enone backbone absorbs more strongly at longer wavelengths (a $\pi \rightarrow \pi^*$ transition) than the keto tautomer (an $n \rightarrow \pi^*$ transition) [103]. The equilibrium constant for the *cis*-enol / keto tautomerization depends on the β -diketone, solvent and concentration [102]. For example, acetylacetone (AAH) *cis*-enol tautomer percentage in cyclohexane and acetonitrile is 97.0% and 52.9% [102a], respectively; in acetonitrile this percentage increases with increasing mole fraction of AAH to a limiting value of 79.6 % (i.e., the percentage of *cis*-enol AAH in neat AAH) [102a]. Therefore, the reported ϵ_{max} for the β -diketones in Table 3.1 are for the *cis*-enol tautomers but smaller than the true ϵ_{max} due to significant concentrations of the keto form. The reported ϵ_{max} are adjusted in accordance to their percentages in solution using the reported values in the literature; the corrected values are shown in parentheses (Table 3.1).

For conjugated enones the $n \rightarrow \pi^*$ transition is the lowest energy transition (e.g., mesityl oxide in 95% ethanol shows the $n \rightarrow \pi^*$ transition at λ_{max} ca. 310 nm and the $\pi \rightarrow \pi^*$ transition at λ_{max} ca. 240 nm [104]). For simple β -diketones like AAH and benzoylacetone (BAH) (Table 3.1), the $n \rightarrow \pi^*$ and $\pi \rightarrow \pi^*$ transitions are blue- and red-shifted, respectively, relative to conjugated enones. The red-shift of the $\pi \rightarrow \pi^*$ is due to

increased delocalization [2a] whereas the blue shift of the $n \rightarrow \pi^*$ transition can be rationalized to be due to intramolecular hydrogen bonding in analogy to hydrogen-bonding solvent effects on conjugated enones [104]. These opposing shifts result in the $n \rightarrow \pi^*$ transition becoming submerged under the more intense $\pi \rightarrow \pi^*$ transition. However, it's believed that the lowest singlet state of these β -diketones is the n, π^* state since no fluorescence can be detected at 77 K [103e,105]. For dibenzoylmethane (DBMH), the increase in conjugation lowers the energy of both the $\pi \rightarrow \pi^*$ and $n \rightarrow \pi^*$ transitions, but the change in the former is more marked since conjugation does not significantly affect the non-bonding orbitals due to spacial orientation. As a result, there is a switch in the energy ordering of the n, π^* and π, π^* states where the latter comprises the lowest singlet state in DMBH [105]. Because n, π^* states favor $S_1 \rightarrow T_1$ intersystem crossing [69], the switch in energy ordering provides a rationale for the appearance of singlet excited DBMH fluorescence emission in glassy matrix at 77 K whereas AAH and BAH show no fluorescence [105]. At room temperature, DBMH shows no fluorescence due to the dominant *cis* to *trans*-enol photoisomerization reaction [103a-d].

Unlike β -diketones, β -diketonatoboron complexes are locked into a ring structure as indicated by NMR spectroscopy (i.e., only one species is detected). The absorption profile is perturbed upon exchanging the enol hydrogen for a BF_2 moiety and a modest enhancement in the ϵ_{max} and a red-shift in the λ_{max} is observed. In addition, there is a minor influence on the overall absorption profile. The large extinction coefficients, positive solvatochromism and the observation of vibrational structure in some cases are supportive of a $\pi \rightarrow \pi^*$ transition within the chelated ligand. Relative to the parent *cis*-enol β -diketone, the shift of principal $\pi \rightarrow \pi^*$ absorption band to lower energies is a manifestation of a decreasing HOMO-LUMO energy gap. A plot of λ_{max} of the complexes vs. λ_{max} the *cis*-enol parent β -diketone is shown in Figure 3.1; the reasonable linear plots in Figure 3.1 are suggestive that β -diketonatoboron complexes and their parent β -diketones UV -Vis absorption bands are derived from similar $\pi \rightarrow \pi^*$ transitions. The red-shifted absorption

maxima, relative to the parent *cis*-enol tautomer β -diketones suggests a chelated structure as shown in Scheme 1.1. Within a series of β -diketonate ligands, AA to DBM, the λ_{max} shows a bathochromic shift of 80 nm that is attributed to the increase in conjugation by replacing a methyl with a phenyl substituent. Because of the increasing conjugation, ϵ_{max} more than doubles by exchanging the AA for the DBM β -diketonate ligand. With the same β -diketonate ligand, the ϵ_{max} shows little effect but a bathochromic shift is observed with respect to the counter ligand where λ_{max} increases (Table 3.1) in the following order: $\text{BF}_2 \approx \text{BN} \leq \text{BC} < \text{BM} < \text{BO}$.

The AABF_2 analogs (AABF_2 , ACHBF_2 , D-t- BBF_2 and Me- AABF_2) show interesting features. The absorption λ_{max} is not significantly affected by exchanging the methyl for *t*-butyl groups, however, replacing the ligand's methine hydrogen with an alkyl group results in a ca. 20 nm bathochromic shift. Clearly the electronic structure is affected by methine substitution.

The dihydroxynaphthalene derivatives, such as DBMBN, show similar absorption profiles with respect to the other β -diketonatoboron complexes except for a relatively low intensity absorption band partially obscured by the more intense principal absorption band (Figure 3.3). Repeated recrystallization did not remove this color, hence this band must be a characteristic of the complex. This band is responsible for the color of these complexes where, for example, the crystals of AABF_2 and DBMBF_2 is colorless and yellow, respectively, whereas AABN and DBMBN are yellow and ruby red in color, respectively. This band is not characteristic of either the β -diketonate or dihydroxynaphthalene ligands. This absorption may be due to charge transfer from the dihydroxynaphthalene ligand (electron donor) to the β -diketonate ligand (electron acceptor). With the limited number of complexes prepared we can not exclusively demonstrate this charge transfer band.

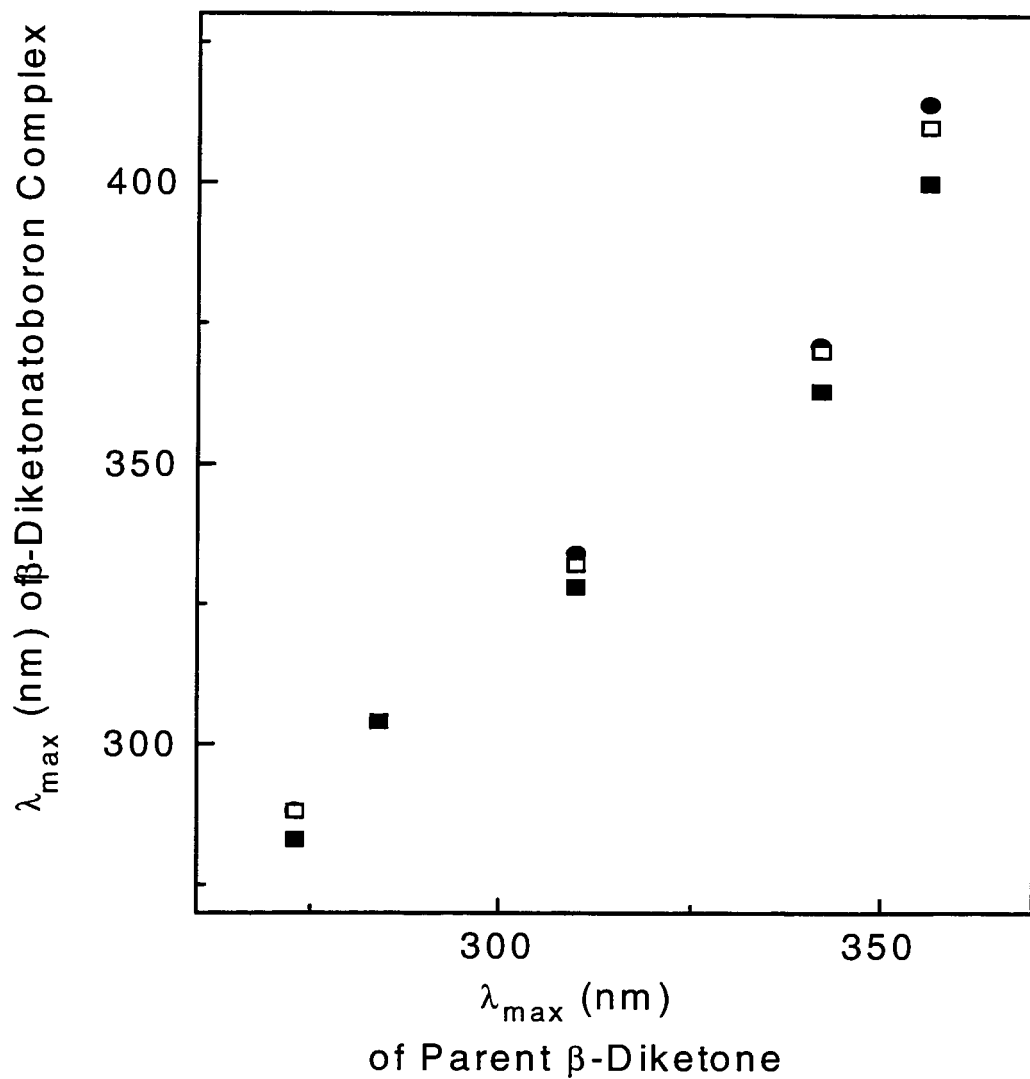


Figure 3.1: Relationship between λ_{\max} of Various β -Diketoneboron Complexes [(■) BF₂; (□) BM; (●) BO] and the λ_{\max} of their Parent β -Diketones in Acetonitrile.

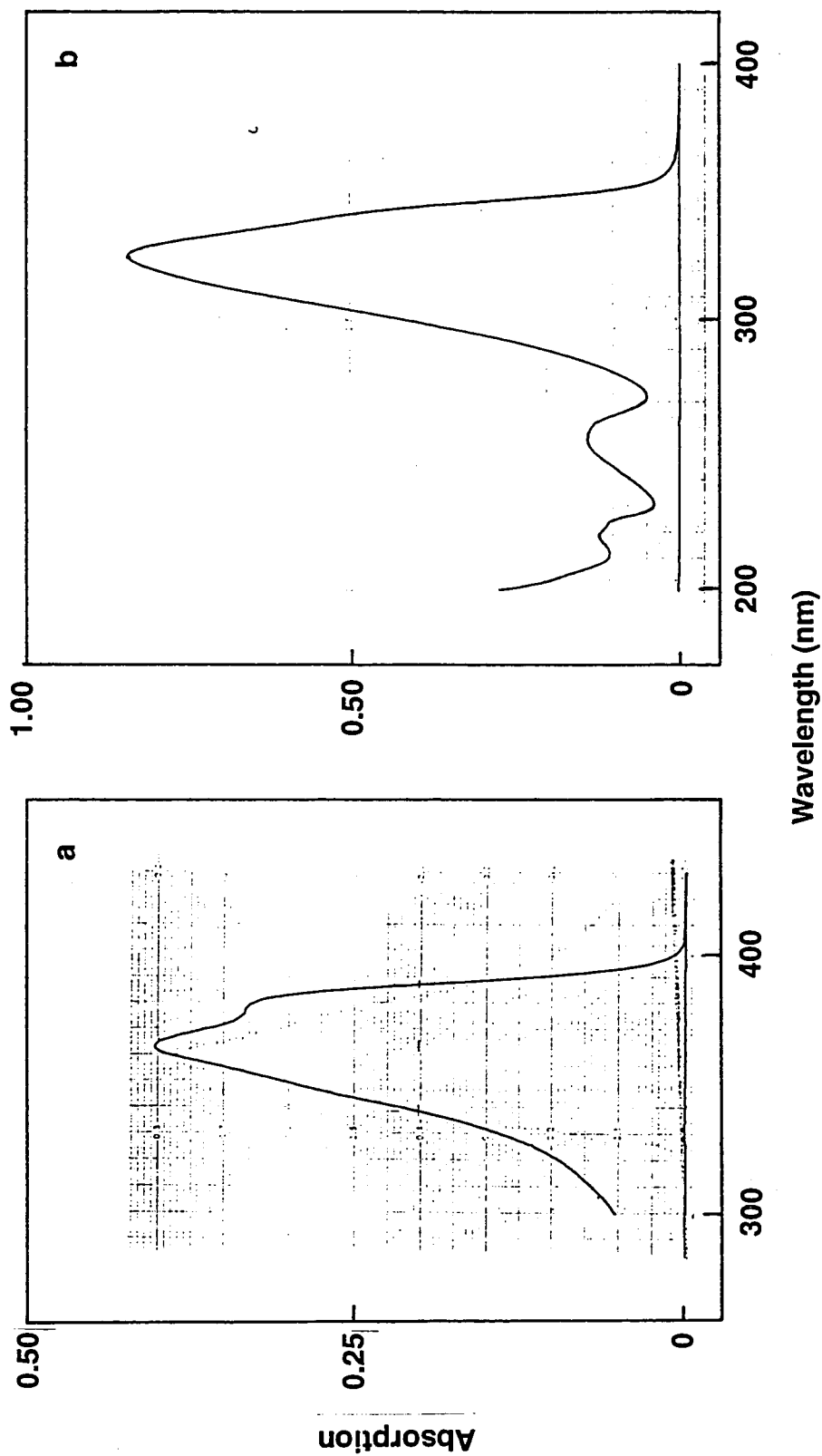


Figure 3.2: The UV - Vis Absorption Spectra of Some β - Diketonatoboron Complexes in Acetonitrile; (a) DBMBF₂ (1.05×10^{-5} M); (b) BABF₂ (3.14×10^{-5} M).

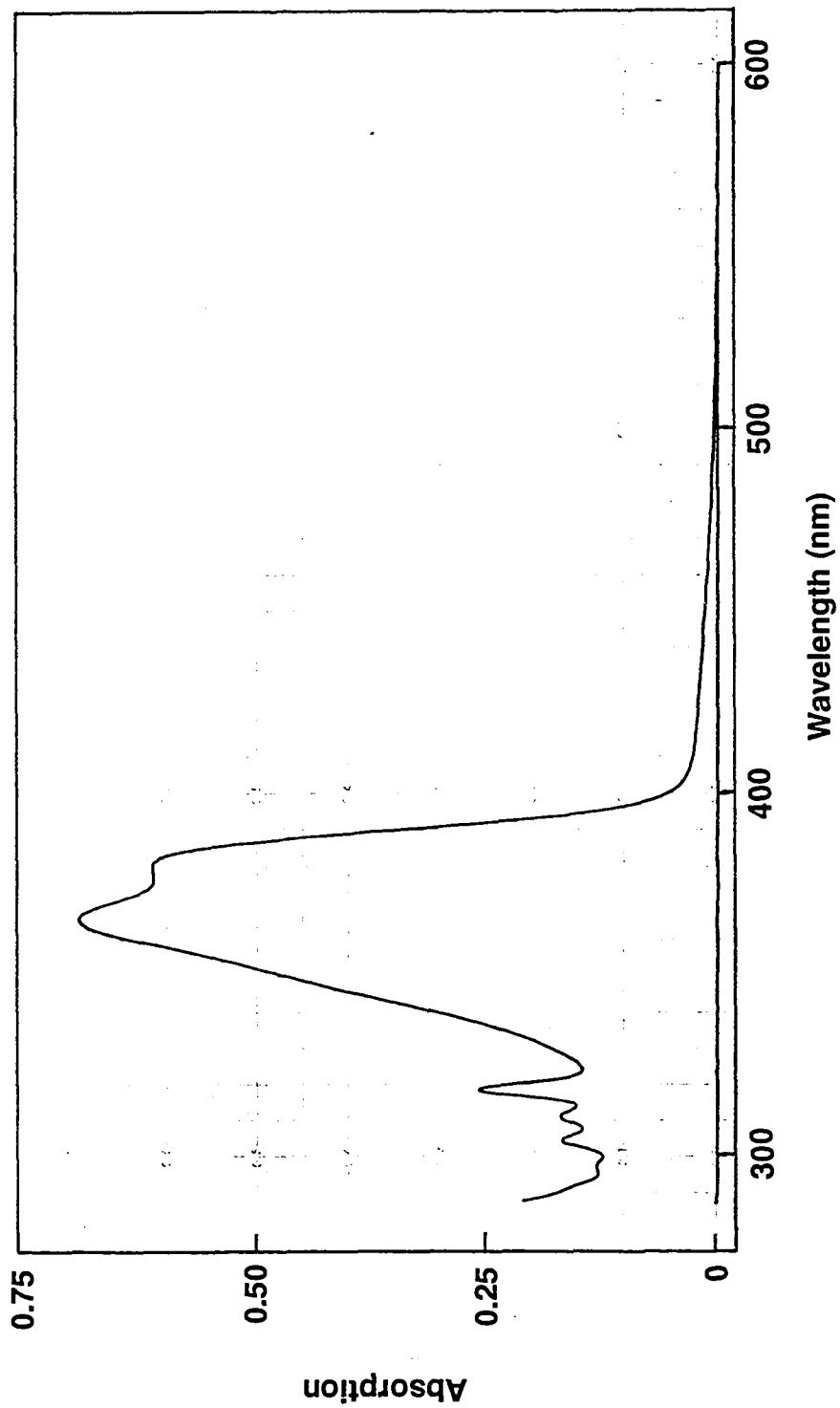


Figure 3.3: UV - Vis Absorption Spectrum of DBMBN (1.75×10^{-5} M) in Acetonitrile. Note the Weak Absorption Band at Beyond the Principle Absorption Band (cf. Figure 3.2a).

Table 3.1: UV-Vis Spectroscopic Data for the Principal Absorption Bands of Some β -Diketonatoboron Complexes and the Parent β -Diketones

Compound	Solvent	λ_{\max} (nm)	$\log \epsilon_{\max}$	Compound	Solvent	λ_{\max} (nm)	$\log \epsilon_{\max}$
DBMBF ₂	CH ₃ CN	363	4.61	BABO	CHCl ₃	334	4.25
	CH ₂ Cl ₂	364	4.55	AABO	CHCl ₃	288	4.09
	C ₆ H ₁₂	359	4.53	DBMBM	CH ₃ CN	370	4.57
MBDBF ₂	CH ₃ CN	400	4.82	MBDBM	CH ₃ CN	410	4.82
	DCM	401	4.78	BABM	CH ₃ CN	332 ^c	4.43 ^c
	C ₆ H ₁₂	392	4.72	AABM	CH ₃ CN	288 ^c	4.15 ^c
BABF ₂	CH ₃ CN	328	4.43	DBMBC	CH ₃ CN	368 ^c	4.62 ^c
AABF ₂	CH ₃ CN	283	4.13	MBDBC	CH ₃ CN	401 ^c	4.72 ^c
	CHCl ₃	285	4.24	BABC	CH ₃ CN	334 ^c	4.28 ^c
ACHBF ₂	CH ₃ CN	304 ^b	4.15 ^b	AABC	CH ₃ CN	287 ^c	4.13 ^c
D-t-BBF ₂	CH ₃ CN	284	4.09	DBMBN	DCE ^a	363	4.60
Me-AABF ₂	CH ₃ CN	3.02	4.20	MBDBN	DCE ^a	406 ^c	4.66 ^c
DBMBO	CH ₃ CN	371	4.60	BABN	DCE ^a	331 ^c	4.35 ^c
MBDBO	CH ₃ CN	414	4.80	AABN	DCE ^a	282	4.19

Table 3.1 (Continued)

Compound	Solvent	λ_{\max} (nm)	$\log \epsilon_{\max}$	Compound	Solvent	λ_{\max} (nm)	$\log \epsilon_{\max}$
DBMH	CH ₃ CN	342	4.38 (4.44) ^d	AAH	CH ₃ CN	273	3.83 (4.11) ^d
	C ₆ H ₁₂	338	4.39 (4.40) ^d		CHCl ₃	275	3.93 (4.01) ^d
MBDH	CH ₃ CN	356	4.51 ^e		C ₆ H ₁₂	273	4.03 (4.04) ^d
	C ₆ H ₁₂	350	4.51 ^e	ACHH	CH ₃ CN	284	3.91 ^e
BAH	CH ₃ CN	310	4.14 (4.21) ^d				
	C ₆ H ₁₂	305	4.26 (4.27) ^d				

^a DCE = 1,2-Dichloroethane. ^b Ouyang, X. M.Sc. Thesis, Simon Fraser University, October 1991. ^c Y.-H. Zhang, Unpublished results. ^d Corrected for the percentage of *cis*-enol tautomer [102] by dividing the experimental ϵ_{\max} by this percentage. ^e Percentage in acetonitrile of *cis*-enol tautomer unknown.

3.3 Luminescence

3.3.1 Introduction

One of the most important factors determining the luminescence behavior is the nature of the lowest lying singlet state. Since $\pi \rightarrow \pi^*$ transitions are usually characterized by high molar absorptivities [104] (hence fast radiative rate constants; $k_f \propto \epsilon_{\max}$ [69]), efficient fluorescence is frequently observed if the nature of the lowest lying state is π, π^* [69]. In contrast, if the lowest lying state is of n, π^* nature the fluorescence yield is very weak at best [69]. This is due to the low rate of fluorescence (due to a low degree of overlap between the n and π^* orbitals where k_f is proportional to the transition dipole moment, which is proportional to the orbital overlap) and a fast singlet to triplet state intersystem crossing rate. Strong phosphorescence is often a manifestation of a lowest n, π^* singlet state [69].

Another important factor determining luminescent behavior is the rigidity of the molecular frame [69,106-108]. It is generally observed that flexible molecules have short lifetimes (less than one nanosecond) and low fluorescence yields where the acquired energy from absorbing a photon is dissipated into heat energy by way of stretching and / or twisting motion(s). *Cis*-enol β -diketones and some transition metal β -diketonates are known to undergo *cis*- to *trans*-enol photoisomerization [103]. This isomerization reaction is the major excited state radiationless decay route.

From the study of β -diketones as chelating reagents for analytical analysis is a well documented area in chemistry [106], e.g., DBMH β -diketone is a useful analytical reagent for the fluorimetric determination of boron [106,107]. In forming a complex, the nonbonding electrons become associated with boron and their energy level is lowered [106]. As a result the $n \rightarrow \pi^*$ transition energy increases. The effect of complex formation may reverse the nature of the lowest singlet excited state from n, π^* to π, π^* ; the complex may

exhibit strong fluorescence whereas the ligand is usually weakly fluorescent [106,107]. Complex formation apparently inhibits the *cis*- to *trans*-enol photoisomerization reaction as well where this large amplitude motion is the major radiationless decay route for β -diketones [103].

Although β -diketonatoboron complex luminescence has been known for probably thirty years, only recently has there been an interest in systematically studying the luminescence of such molecules [14,98-101]. However, during the present study, and related work by Chow's group, it was discovered that many of the reported luminescent properties may be due to impurities. For example, Karasev and Korotkikh reported AABF₂ has an emission with a $\lambda_{\text{max}} \cong 530$ nm [100b] whereas Cheng found λ_{max} near 420 nm at high AABF₂ concentrations [36]. In this study, after repeated recrystallizations, AABF₂ shows no detectable emission, neither fluorescence nor phosphorescence. A number of other observations by Karasev and Korotkikh are also suspect. In the study by Ilge et al., they report the fluorescence quantum yields (Φ_F) ($= k_f / (k_f + k_{nr})$ under the assumption that the fluorescent species is produced with unit efficiency by photon absorption) fluorescence lifetimes and luminescence emission excitation wavelength dependence of a series of β -diketonatoboron complexes [14f]. Some of the reported values by Ilge et al. have been found to be incorrect [14f]. For example, Ilge et al. [14f] report that DBMBF₂'s fluorescence quantum yield is 0.8 in acetonitrile whereas in this study a fluorescence quantum yield near 0.1 was determined (the reported fluorescence yield for DBMBF₂ may be a typographic error, i.e., $\Phi_F = 0.08$). The disparities found in the literature prompted a re-investigation of the fluorescence and phosphorescence properties of various β -diketonatoboron complexes and the results are reported here.

3.3.2 Results and Discussion

3.3.2.1 General

β -Diketonatoboron complex fluorescence quantum yields and singlet excited state lifetimes are summarized in Table 3.2 and the singlet / triplet state energies are listed in Table 3.3.

β -Diketonatoboron complex fluorescence intensity is strongly dependent on the extent of conjugation as shown in Table 3.2. With acetylacetone as a ligand, fluorescence is either undetectable (AABF₂) or barely detectable (AABM and AABO). Exchanging AA for BA resulted in an enhanced fluorescence yield. Further substitution, BA to DBM, results in a dramatic jump in the fluorescence yield where the fluorescence quantum yield becomes as large as 0.8 (DBMBAc, Table 3.2) in acetonitrile. For those complexes that showed emission, the Stokes loss was small (about 1000 cm⁻¹) and the fluorescence was structured with DBM and MBD as ligands (for AA and BA as ligands, the large slit width, 15-20 nm, used to detect their weak fluorescence effectively smoothes out any structured emission).

Figure 3.4 shows the fluorescence excitation and emission (corrected) of DBMBX₂ (X = F, oxalyl and malonyl). The similarity between the excitation and UV-Vis absorption spectra (cf. Figure 3.2) demonstrates that the fluorescence emission originates from the lowest spectroscopic singlet state of DBMBX₂. Similar correspondence of excitation and UV-Vis absorption spectra were observed with other fluorescent complexes.

Berlman [108] has illustrated that information regarding the degree of ground and excited state molecular flexibility (or rigidity) can be gained from spectroscopic data (absorption and fluorescence) where a planar molecular frame (i.e., rigidity) is manifested by a structured spectroscopic profile; non-planar (flexible) frame is manifested by a featureless profile. A rigid ground state is correlated with a structured absorption band. A rigid excited state is correlated with a fluorescence profile that shows distinct vibrational structure; anthracene again is a good example where the fluorescence profile resembles the mirror image of its absorption. In contrast, non-rigid systems will be correlated with

Table 3.2: Fluorescence Lifetimes and Quantum Yields of Emission of Various β -
Diketonatoboron Complexes Under Argon at 23 ± 1 °C

Compound	Solvent	Φ_F	τ (ns)	Compound	Solvent	Φ_F	τ (ns)
AABF ₂	CH ₃ CN	ND	--	DBMBO	CH ₃ CN	0.41	1.35
ACHBF ₂	CH ₃ CN	< 0.01	< 0.3	MBDBO	CH ₃ CN	--	1.78
D-t-BBF ₂	CH ₃ CN	ND	--	AABM	CH ₃ CN	< 10 ⁻⁴	--
BABF ₂	CH ₃ CN	0.007	< 0.3	BABM	CH ₃ CN	< 10 ⁻³	--
DBMBF ₂	CH ₃ CN	0.092	0.28	DBMBM	CH ₃ CN	0.32	0.86
	CH ₂ Cl ₂	0.17	--	MBDBM	CH ₃ CN	--	2.14
	CHCl ₃	0.20	0.60 ^a	DBMBAc	CH ₃ CN	0.8 ^b	1.5 ^b
	CCl ₄	0.15	0.22 ^b	AAH	CH ₃ CN	ND	--
	C ₆ H ₁₂	0.045	0.23	ACHH	CH ₃ CN	ND	--
MBDBF ₂	CH ₃ CN	0.43	2.01	BAH	CH ₃ CN	ND	--
AABO	CH ₃ CN	< 10 ⁻⁴	--	DBMH	CH ₃ CN	ND ^c	--
BABO	CH ₃ CN	< 10 ⁻³	--	MBDH	CH ₃ CN	< 0.01 ^c	--

^a Reference [109]. ^b Reference [14f]. ^c Strong fluorescence in methylcyclohexane glass at 77 K.

Table 3.3: The Lowest Spectroscopic Singlet and Triplet Energies for Various β -Diketonatoboron Complexes

Compound	E_s (eV) ^a	Solvent	E_T (eV)	Solvent ^c
AABF ₂	4.12 ^{abs}	CH ₃ CN	ND ^b	MeC ₆ H ₁₁
ACHBF ₂	3.80	CH ₃ CN	2.89	MeC ₆ H ₁₁
D-t-DBF ₂	4.10 ^{abs}	CH ₃ CN	3.18	MeC ₆ H ₁₁
BABF ₂	3.54	CH ₃ CN	2.79	MeC ₆ H ₁₁
DBMBF ₂	3.19; 3.24	CH ₃ CN; C ₆ H ₁₂	2.69	MeC ₆ H ₁₁
MBDBF ₂	2.98;	CH ₃ CN; C ₆ H ₁₂	2.44	MeC ₆ H ₁₁
AABO	4.04 ^{abs}	CH ₃ CN	ND	MeC ₆ H ₁₁
BABO	3.46	CH ₃ CN	2.73	MeC ₆ H ₁₁
DBMBO	3.11	CH ₃ CN	ND	MeC ₆ H ₁₁
MBDBO	2.85	CH ₃ CN	2.39	MeC ₆ H ₁₁
AABM	4.04 ^{abs}	CH ₃ CN	3.25	MeC ₆ H ₁₁
BABM	3.47	CH ₃ CN	2.70	MeC ₆ H ₁₁
DBMBM	3.13	CH ₃ CN	2.62	MeC ₆ H ₁₁
MBDBM	2.85	CH ₃ CN	2.30	MeC ₆ H ₁₁
AAH	4.25 ^{abs}	CH ₃ CN	3.24 ^{c,d}	n-C ₅ H ₁₂
BAH ^{c,e}	3.54 ^{abs}	MeOH : EtOH (1:3)	2.64	MeC ₆ H ₁₁ : Et ₂ O (1:1)
DBMH ^c	3.23	MeC ₆ H ₁₁	2.58	MeC ₆ H ₁₁
MBDH ^c	3.16	MeC ₆ H ₁₁	2.57	MeC ₆ H ₁₁

^a Obtained from the crossover between absorption / excitation and fluorescence spectra.

In the absence of fluorescence, the singlet energy was estimated from the onset of the UV-Vis absorption and denoted by the superscript abs. ^b ND = No detectable emission. ^c

Obtained at 77 K. ^d Buono-Core, G., Unpublished results. ^e Reference [105].

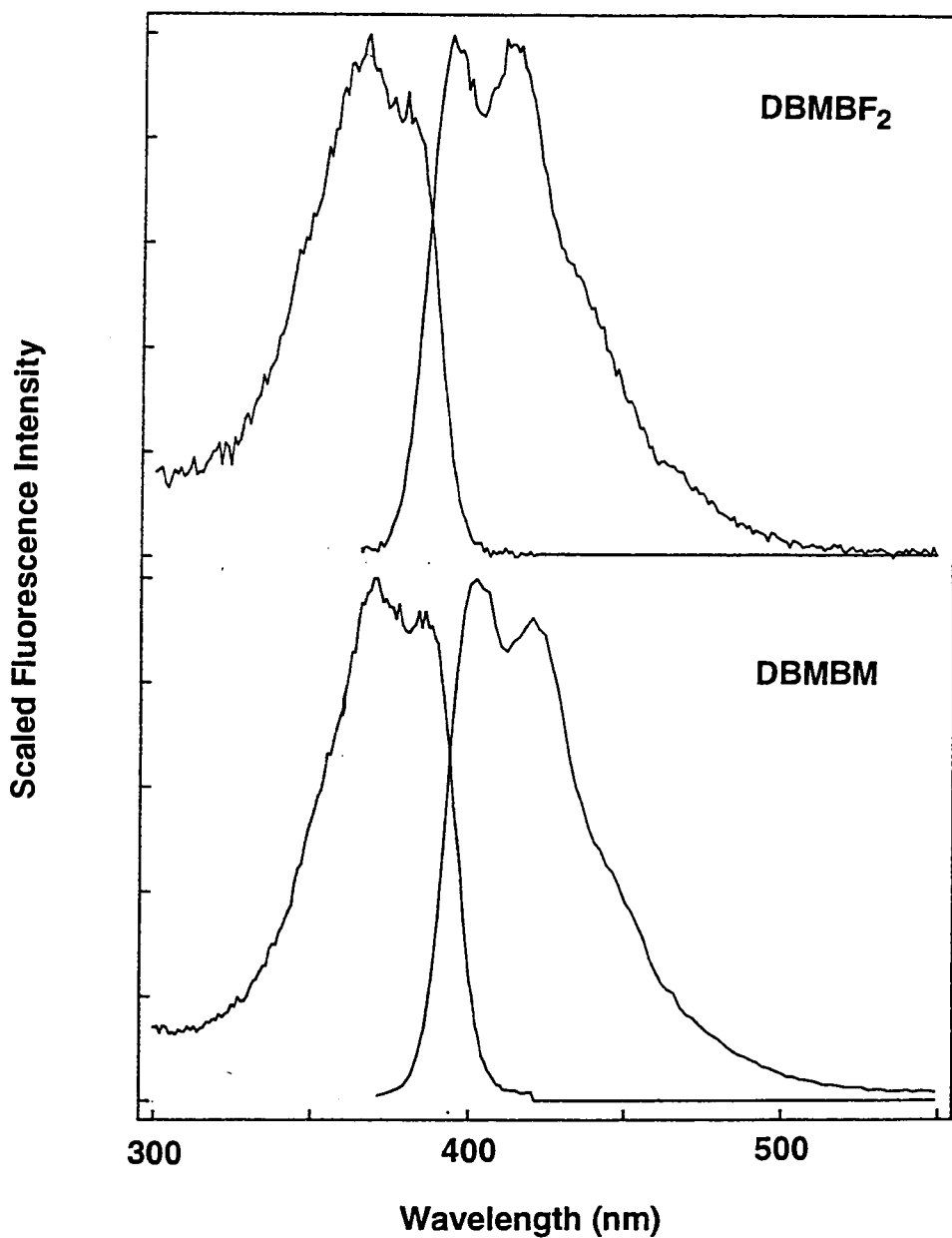


Figure 3.4: Fluorescence Excitation and Emission Spectra (Corrected and Normalized) of DBMBF₂ (8.0×10^{-7} M) and DBMBM (5.0×10^{-7} M) in Acetonitrile Under Argon. For Excitation Spectra λ_{mon} was 440 nm and for Emission Spectra λ_{ex} was 365 nm. The Excitation and Emission Slit Widths were 2 and 4 nm, Respectively.

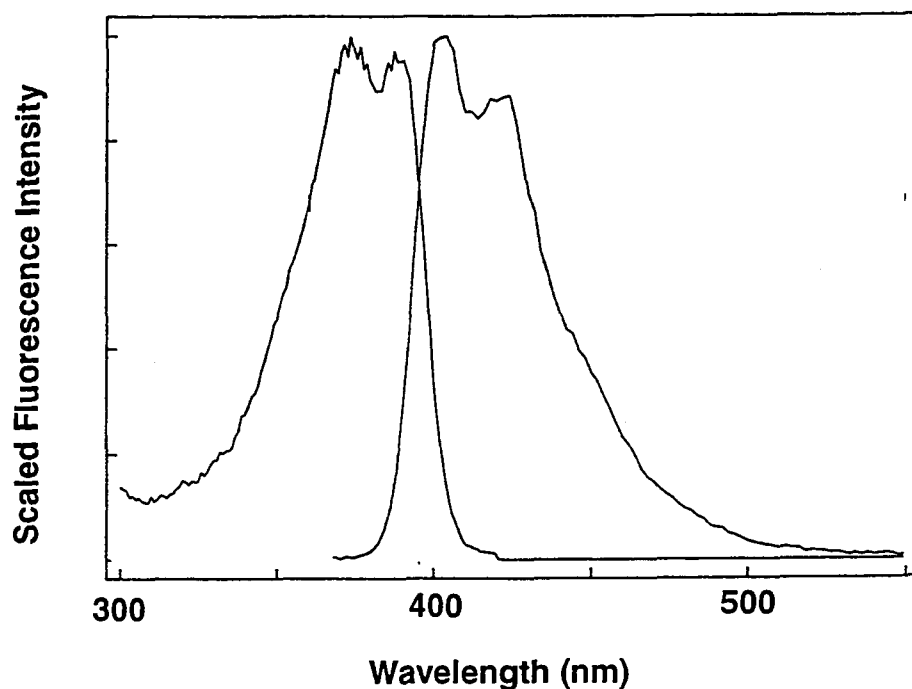


Figure 3.4 (Continued): Fluorescence Excitation and Emission Spectra (Corrected and Normalized) DBMBO (4.0×10^{-7} M) in Acetonitrile under Argon

broad and structureless spectroscopic profiles [108]. Because of molecular rigidity in the ground and excited states, the Stokes loss, which is defined as the energy difference (in cm^{-1}) between the singlet energy and the fluorescence ν_{max} , is small (a few hundred cm^{-1}) and that the fluorescence profile is reasonable mirror image of the absorption profile.

Inspection of Figure 3.4 shows that DBMBF_2 displays all the features of a rigid ground and excited state as discussed above; other complexes with the DBM or MBD as ligands display similar features. In a glassy matrix at 77 K, the fluorescence yield increases dramatically except for complexes with the AA ligand. For the complexes with the DBM and MBD ligands the fluorescence yield in glassy matrix at 77 K is near unity where $\Phi_F = 0.9$ for DBMBF_2 [99] (Figure 3.5); complexes with BA ligand the fluorescence

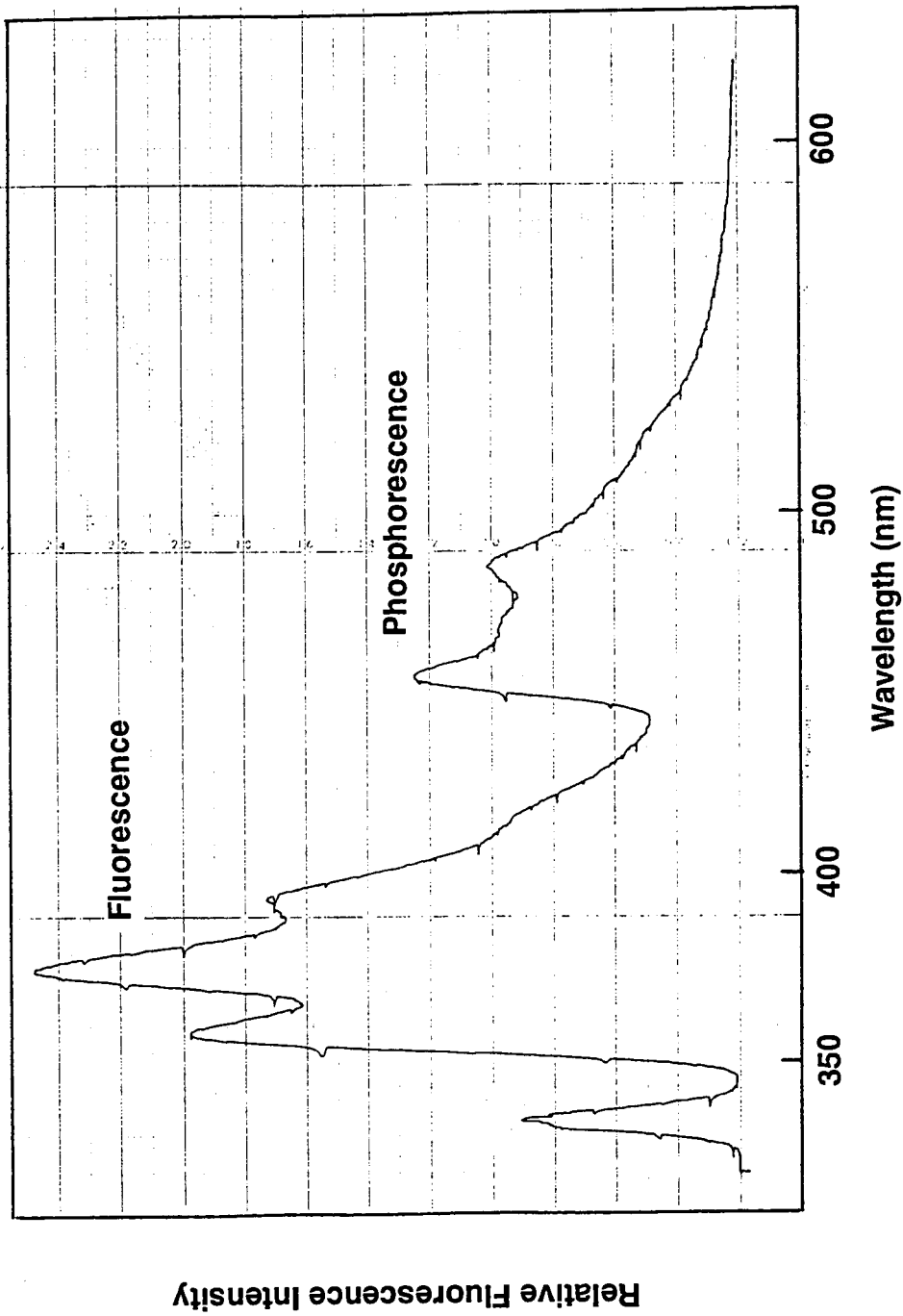


Figure 3.5: Total Emission Spectra (Uncorrected) of Some β -Diketoneboron Complexes in Methylcyclohexane Glass at 77 K. BABF₂ (2.8×10^{-4} M). Note that BABF₂ also shows Phosphorescence Emission. The Peak Near 335 nm is the Rayleigh Band.

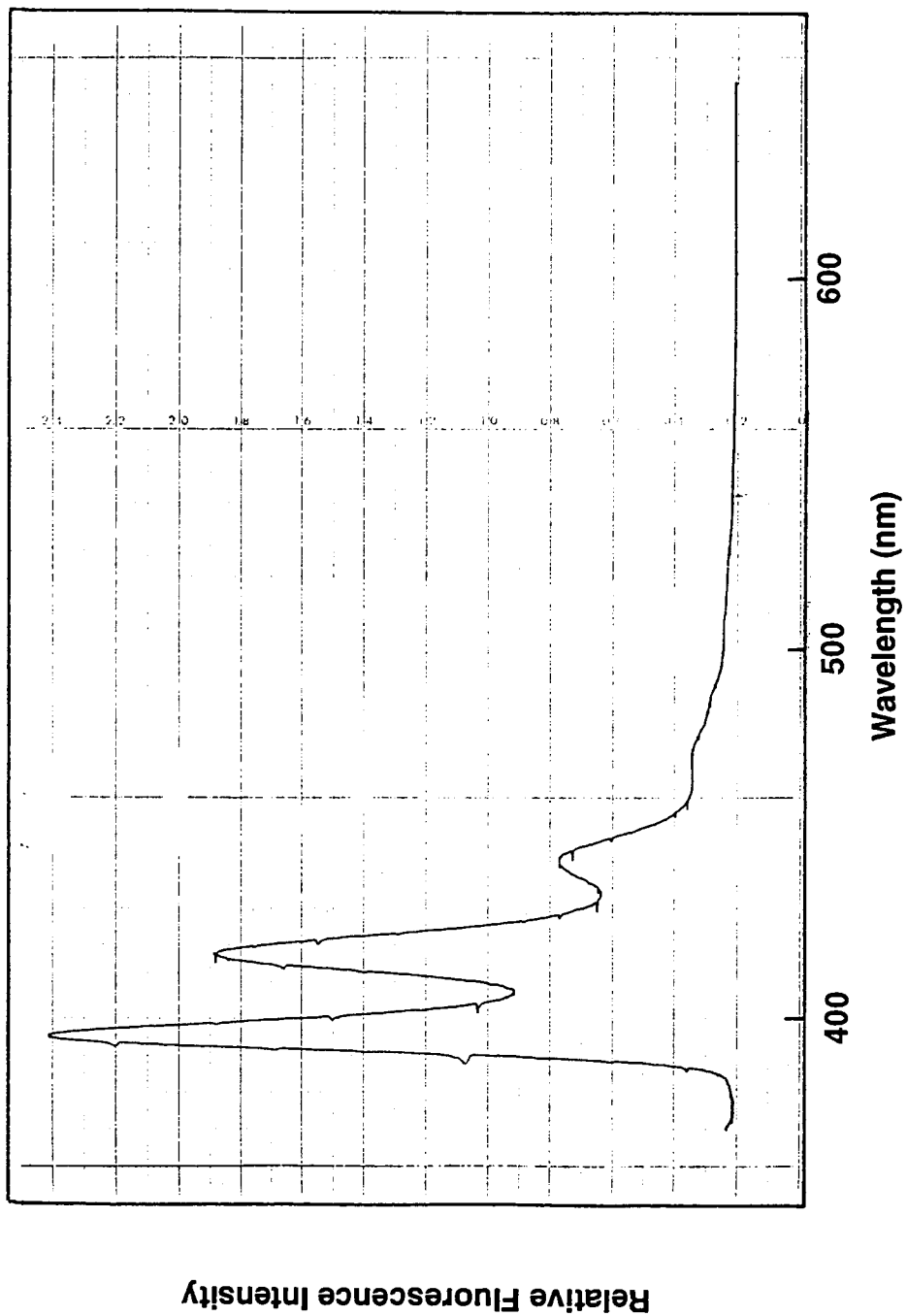


Figure 3.5 (Continued): DBMBF₂ (9.6×10^{-6} M). Phosphorescence of DBMBF₂ is Overwhelmed by its Fluorescence.

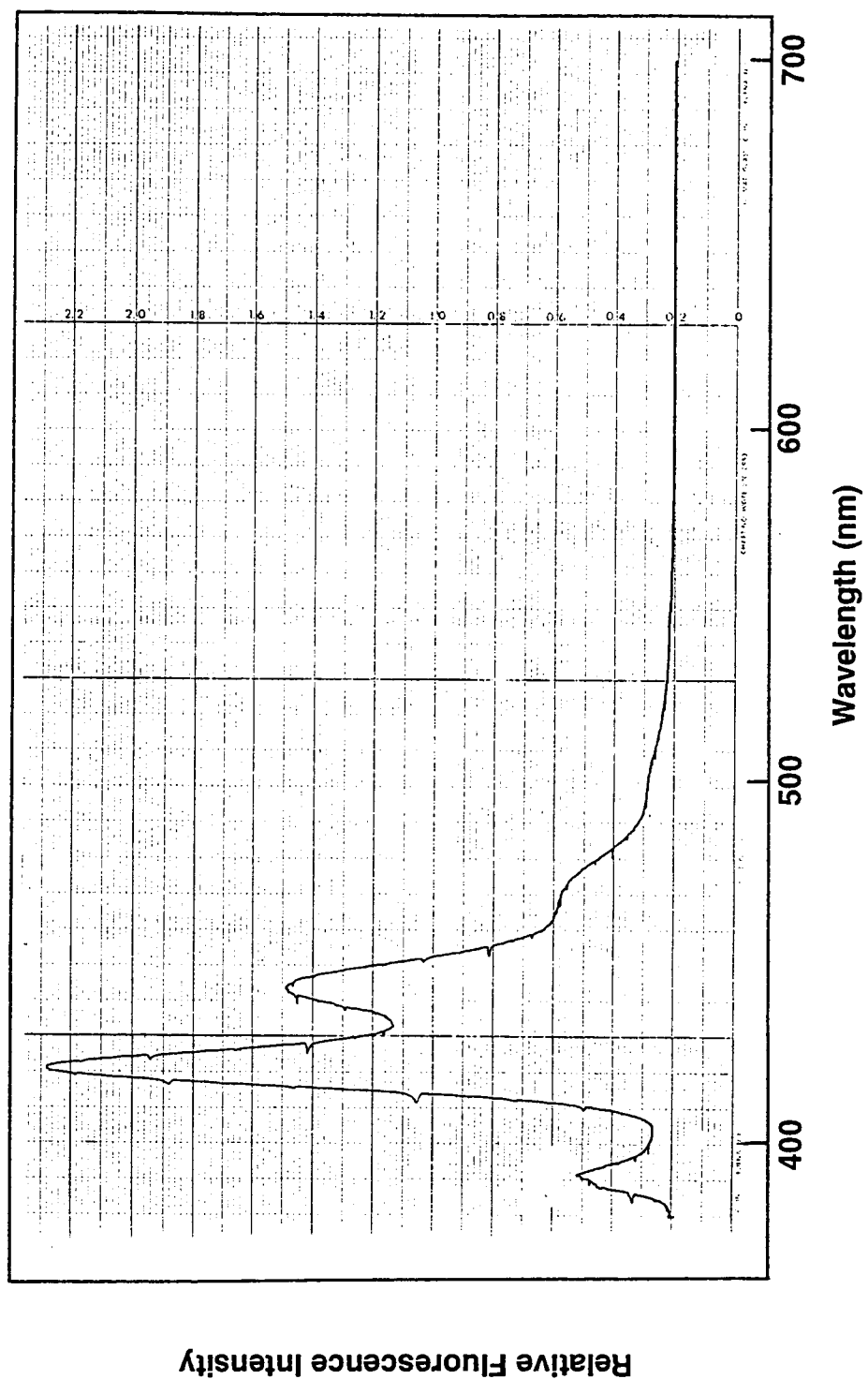


Figure 3.5 (Continued): MBDBF₂ (9 x 10⁻⁶ M). The Peak Near 390 nm is the Rayleigh Band.

yield increases by approximately one order of magnitude. BABF₂ (ca. 10⁻⁵ M) shows similar characteristics only in glassy methylcyclohexane at 77 K (environmental rigidity); at room temperature the absorption and fluorescence bands are structureless, which is potentially due to the large slit widths used, but the Stokes loss is small. AABF₂ does not show detectable fluorescence and phosphorescence at room temperature and in glassy methylcyclohexane at 77 K. AABM does show very weak structureless emission at room temperature, however, the large slit widths would erase any fine structure. In addition, due to the high concentrations required to observe AABM's emission (ca. 10⁻³ M) secondary inner filter effects severely distort the blue edge of the fluorescence bands, hence producing an artificially large Stokes' loss. The structureless absorption for these complexes, based on Berlman's empirical correlation, suggests that the ground state is non-planar but the excited state is planar. The more rigid ACHBF₂, which has a stronger fluorescence yield, shows structureless absorption and emission with a Stokes loss ca. four times larger than that found for the DBM complexes. This suggests that both the excited and ground states are non-planar. The complexes with the catechol and dihydroxynaphthalene ligands showed similar attributes except the fluorescence yield from the β-diketonate ligand is significantly reduced and no detectable fluorescence can be observed with AA and BA as ligands.

Table 3.3 demonstrates that the E_S energies of various complexes, with respect to their parent *cis*-enol β-diketones, are lower in energy by ca. 0.1 eV; the lowest spectroscopic triplet energy difference ranges from 0 to 0.1 eV. The change in the singlet energies follows the change in the UV-Vis absorption λ_{max} with respect to the counter ligand; i.e., λ_{max} increases in the following order: BF₂ > BM > BO. This is not unexpected since UV-Vis absorption is used to determine the singlet energy and a shift in the singlet energy should correspond to a shift in λ_{max}.

3.3.2.2 Nature of the Singlet and Triplet States

Recently, DBMBF₂'s fluorescence yield dependence on solvent viscosity and temperature was fitted to Kramers' model of large amplitude motion; i.e., an isomerization reaction [109]. The fit to Kramers' model was poor and it was concluded that the isomerization reaction exhibits non-Kramers behavior. It was suggested that the independent torsional motion of the phenyl rings dissipates the excitation energy. However, potential molecular flexibility as an excitation energy sink is not consistent with the rigid structure inferred from the absorption and emission bands and a small Stokes loss for DBMBF₂. Torsional motion can not rationalize the nearly one order in magnitude increase in the fluorescence yield for the complexes with the same dibenzoylmethane (DBM) ligand (cf. DBMBF₂ and DBMBAc in Table 3.2); i.e., the phenyl torsional motion is not expected to be significantly affected by the ligand substitution of fluoride for oxalyl acid. In addition, phenyl torsional motion is absent in the AA ligand complexes, hence their dominant radiationless process is obviously due to another factor(s). It is unknown whether β -diketonatoboron complexes also undergo *cis* to *trans* photoisomerization, presumably, the boron-oxygen bond prevents isomerization as indicated by the enhancement in fluorescence yield vs. their parent β -diketones.

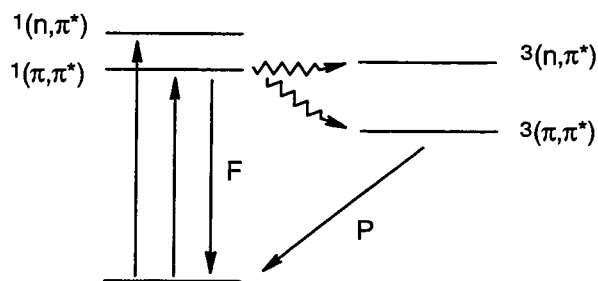
To rationalize the variation in Φ_F , the change in the intersystem crossing rate constant (a radiationless process) from the lowest spectroscopic singlet to the lowest spectroscopic triplet level can be attributed to the change in the lowest singlet-triplet energy gap. However, this is not a viable since the DBM ligand complexes have the smallest singlet-triplet energy gaps; due to the energy gap law these complexes should have the largest intersystem crossing rate but the opposite is observed [86]. In analogy to the n, π^* / π, π^* order switching for the *cis*-enol tautomer of β -diketones, a similar switch can be rationalized for β -diketonatoboron complexes. For complexes with BA, DBM and MBD ligand, the lowest singlet state is of π, π^* nature; this assignment is consistent with the observations of radiative rate constants of the order of 10^8 s^{-1} ($k_f = \Phi_F / \tau$), relatively large singlet-triplet energy difference ($\Delta E_{ST} > 10 \text{ kcal / mol}$), and vibrational structure on the

absorption and fluorescence spectra. Therefore, the n,π^* state should lie higher in energy. For boron acetylacetonate complexes, the singlet state nature can not be assigned beyond reasonable doubt; it is assumed that the lowest singlet state is n,π^* .

The triplet states of *cis*-enol BAH and DBMH β -diketones have been identified as mostly π,π^* in nature since the phosphorescence lifetimes are of the order of seconds and are affected by the external heavy atom effect [105] whereas n,π^* states typically have lifetimes of the order of milliseconds and are insensitive to external heavy atom effects [69]. For BABF₂ and DBMBF₂ the triplet lifetime is approximately 1 second [100b], hence the triplet state is mostly π,π^* in character. For the corresponding BA and DBM boron complex analogs, their phosphorescence profile (i.e., overall shape and vibronic spacing) and triplet energy are nearly identical to that of their BF₂ β -diketone analogs. This suggests that these complexes have spectroscopic triplet state of π,π^* nature as well. The above discussion suggests a relative energy ordering of the singlet and triplet states as shown in Scheme 3.2.

For the DBM ligand complexes, as the singlet energy, E_S (Table 3.3), decreases there is a corresponding increase in both the fluorescence yield and lifetime (Table 3.3). Since the radiative rate constant can be shown to be relatively constant (i.e., $k_f = \Phi_F / \tau \approx 3.3 \times 10^8 \text{ s}^{-1}$), the change in Φ_F or τ is essentially due to a change in the radiationless rate constant for these complexes; k_{nr} ($k_{nr} = \tau^{-1} - k_f$) changes by more than one order in magnitude from DBMBF₂ to DBMBAc. The simultaneous lowering of the singlet energy and the significant decrease in k_{nr} is indicative of the presence of a 'dark' triplet state (higher in energy than the spectroscopic triplet state, e.g., the n,π^* triplet state in Scheme 3.2); i.e., El Sayed rules[69]. On the basis of Scheme 3.2 it can be surmised that the n,π^* triplet state is near the π,π^* singlet state where a small energy gap between the singlet and triplet state facilitates intersystem crossing, hence a smaller fluorescence yield can be expected [69]. For the DBM β -diketonate complexes, exchanging fluoride for the oxalyli ligand decreases the spectroscopic singlet energy whereas the n,π^* triplet state should be

Scheme 3.2



relatively unaffected. The change in the $\Delta E_{ST}(\pi, \pi^* - n, \pi^*)$ energy gap is deduced to be the major influence on the observed fluorescence yield. This is consistent with the observed relative phosphorescence intensity of $BF_2 > BM > BO$ where DBMBO phosphorescence was not detected.

Another way to affect π, π^* and n, π^* state energy levels is solvent polarity. Because a π, π^* state has a more dipolar character than the n, π^* state, the π, π^* state is more sensitive to changes in solvent polarity [74,86]. Shifting from nonpolar to polar solvents can switch the energy between the π, π^* and n, π^* states or increase their energy gap. If Scheme 3.2 is a realistic description of the energy ordering for $DBMBF_2$ then an increase in solvent polarity is expected to increase the $\Delta E_{ST}(\pi, \pi^* - n, \pi^*)$ energy difference, hence decrease the radiationless decay rate constant. From Table 3.2, the radiationless decay rate constant is indeed affected by solvent polarity; cf. $4.2 \times 10^9 \text{ s}^{-1}$ in cyclohexane with $1.3 \times 10^9 \text{ s}^{-1}$ in chloroform.

Clearly for β -diketonatoboron complexes with the DBM β -diketonate ligand Scheme 3.2 is satisfactory rationalized by the variance in the energy ordering of the π, π^* and n, π^* states.

3.4 Redox Potentials of β -Diketonatoboron Complexes

3.4.1 Introduction [110]

The electrochemical behavior of substrates can be investigated by cyclic voltammetry (CV), which is one of the more popular electrochemical techniques. In this technique the potential of the electrode is varied linearly with a saw tooth wave from an initial potential to a final potential and back to the initial potential. Considering a reversible redox couple, during the initial potential rise, the electrode potential reaches the vicinity of a vacant (occupied) molecular orbital of the electroactive species and electron transfer from the electrode to (from) the electroactive species occurs; a current is measured. The admixture of the increasing electrochemical rate constant (proportional to the increasing potential) and decreasing electroactive species concentration leads to a current maximum. When the potential is reversed, the reduced (oxidized) electroactive species is oxidized (reduced) and a second maximum is observed. This process is illustrated in Figure 3.6. For an irreversible redox couple, the first current maximum is observed, however, the reverse current maximum may be absent.

Oxidation and reduction potentials are important parameters in evaluating the feasibility of either electron transfer reactions or donor-acceptor interactions (cf. Chapter Two). Unfortunately, the literature only reports reduction potentials of nine β -diketonatoboron complexes in monoglyme [10], most of which are not useful in this study.

3.4.2 Results and Discussion

3.4.2.1 Changes on Complexation

The oxidation and reduction potentials of various β -diketonatoboron complexes,

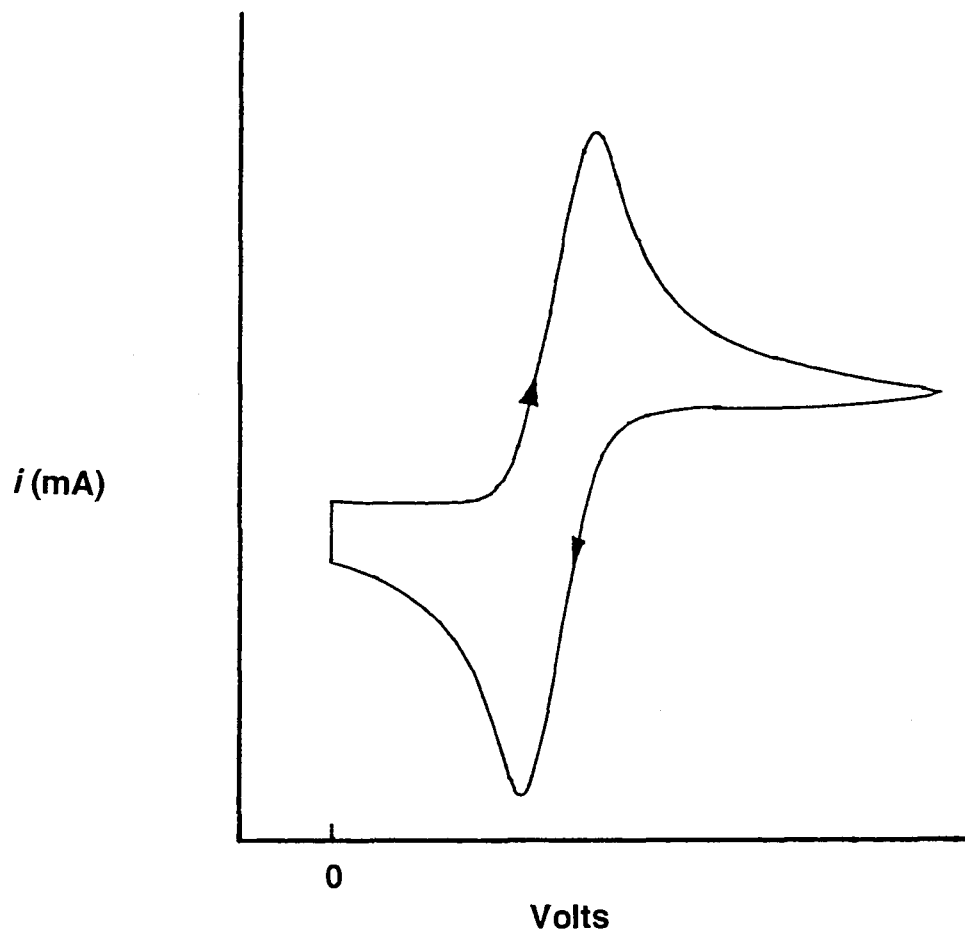


Figure 3.6: Illustration of a Cyclic Voltammogram for a Reversible Redox Couple.

and their corresponding parent β -diketones, are listed in Table 3.4. The electrochemical behavior is expected to be simpler than the metal β -diketone complexes since we need not consider the redox properties of the central metal atom. Most of the redox potentials measured were irreversible; i.e., only the forward current peak is observed. For the values in Table 3.4 marked with an asterisk (*), the forward and reverse current peaks were observed, however, the forward and reverse current peak difference increases with increasing scan rate (the peak difference at a low scan rate was nearly 60 mV). This observation suggests quasi-reversible behavior [110].

Table 3.4: Redox Potentials of Some Boron Complexes in Acetonitrile ^a

Compound	E _{ox} (V)	- E _{red} (V)	Compound	E _{ox} (V)	- E _{red} (V)
DBMBF ₂	2.45	0.91*	DBMBN	1.18	0.81*
BABF ₂	2.53	1.13	BABN	1.20	1.01
MBDBF ₂	1.96	1.01*	AABN	1.20	1.36
AABF ₂	2.88	1.48	MBDBN	1.11	0.91
Me-AABF ₂	2.34	1.48	DBMBM	2.43	0.70
ACHBF ₂	2.30	1.50	BABM	2.50	0.88
D-t-BBF ₂	2.80	1.50*	AABM	2.81	1.23
DBMBO	2.43	0.64	MBDBM	1.98	0.83
BABO	2.60	0.80	DBMH	est. 1.6 ^c	1.38 ^d
AABO	2.90	0.89 ^b	BAH	est. 1.8 ^c	1.54 ^d
MBDBO	1.97	0.78	AAH	2.25	1.78
DBMBC	1.05	0.85*			
BABC	1.07	1.06	2,3-DMN	1.39	
AABC	1.10	1.42	o-DMB	1.45	
MBDBC	1.10	0.94			

^a Obtained at ambient temperature under nitrogen with 0.1 M TEAP vs. the SCE reference electrode; scan rate 100 mV / sec. Errors \pm 0.05 Volts. ^b E_{red} believed to be closer to 1.15 V, see text. ^c Estimated from eq 2.60a where $\Delta\Delta G_{\text{solv-J}} + 2K$ (0.22 V) was calculated from the AAH values. ^d Buchta, R.C.; Evans, D.H. *Anal. Chem.* **1968**, *40*, 2181. * Quasi-reversible cyclic voltammograms.

Relative to their parent β -diketone in Table 3.4, the β -diketonatoboron complexes are more difficult to oxidize by a 0.6-0.8 V but are better electron acceptors by 0.3-0.5 V. This is consistent with literature depiction of these complexes where the chelated β -diketone contains a positive charge as shown in Scheme 1.1 and corroborated by the reported dipole moments of some of these complexes (Table 1.1). The interesting feature displayed by the potentials in Table 3.4, ignoring the catechol or dihydroxynaphthalene derivations for the moment, is that for complexes with the same β -diketone ligand the oxidation potentials are invariant with respect to the ligand; i.e., DBMBF₂, DBMBO and DBMBM have the same E_{ox} of ca. 2.44 V within experimental error (± 0.05 V). However, the ligand has a definite effect on the reduction potentials where the oxaly ligand has the largest influence with respect to the unchelated β -diketone. The decrease in the oxidation and reduction potentials within the AA-BA-DBM series reflects the HOMO and LUMO energy separation decrease with increasing conjugation, which is consistent with the observation that λ_{max} shifts to lower energies. Since the ligands are believed to be effectively electronically isolated from the β -diketone moiety, that is, no conjugation, the change in reduction potentials by exchanging fluorine with the other oxygen containing ligands is believed to be inductive. The trend in reduction potentials, however, is opposite from that expected from the inductive strength; for example, the strongest electronegative element fluorine does not induce a stronger electron acceptor.

For complexes containing the catechol or dihydroxynaphthalene moiety, the oxidation potentials are relatively invariant with respect to the β -diketone and are significantly smaller than expected. This is attributed to the more easily oxidizable catechol and dihydroxynaphthalene moiety, this is partially supported by small variations in E_{ox} and similar oxidation potentials of the corresponding methyl ethers (Table 3.4). The expected β -diketone oxidation peaks are observed if the voltage sweep is extended over a larger range; e.g., DBMBN shows three anodic peaks, two from 1.12 to 1.4 V and 2.45 V, the

latter of which correlates with the anodic peak for the DBM moiety found for other complexes.

The irreversible redox potentials observed for most compounds in Table 3.4 are probably due to an irreversible reaction step after electron transfer to (from) the electrode that depletes the resulting oxidized (reduced) species' concentration before reduction (oxidization) by the reverse wave can occur. The electrochemical behavior of β -diketonatoboron complexes were not investigated beyond determination of the peak potentials, hence it is tentatively assumed a EC reaction mechanism for these complexes (E = electron transfer; C = homogeneous chemical reaction) which results in the irreversible CV. A EC reaction is supported by the observation that the potential peak is a function of the scan rate, which is predicted for EC reactions [110]. In addition, an increase in the conjugation (cf. AABF₂ and DBMBF₂ Table 3.4) results in a quasi-reversible reduction potential. This can be rationalized to be due to the stabilization of the anion radical by resonance thus the anion can be oxidized back to the reactant.

3.4.2.2 Relationship to Electronic Structure: Acetylacetone β -Diketonatoboron Complexes

The acetylacetone β -diketonatoboron complexes may have either a C_{2v} or C_s symmetry. For a qualitative discussion of substituent effects on redox potentials, a simple Hückel description of the β -diketone fragment π system will suffice. Using C_{2v} symmetry for the β -diketone fragment Belford, Martell and Calvin [3] have calculated the coefficients, energies and electron densities for five lowest energy molecular orbitals obtained from a Hückel LCAO-MO treatment. The pertinent results of this calculation are shown in Figure 3.7. The calculations show that the methine carbon's coefficient is zero in the LUMO, which is expected based on symmetry considerations, but significant in the HOMO. The

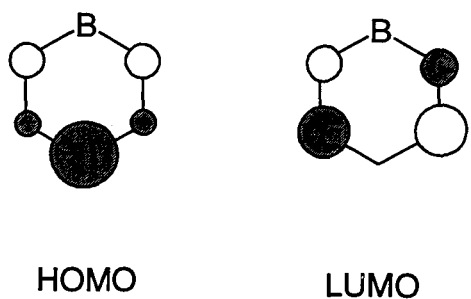


Figure 3.7: Hückel LCAO-MO Description of the Acetylacetonone β -Diketone Fragment. The Size of the Orbital Indicates the Relative Magnitude of the Coefficient.

zero coefficient of the methine in the LUMO immediately suggests that substitution at this position may result in negligible change in the reduction potential. In fact, this is observed where Me-AABF₂, ACHBF₂ and AABF₂ all have identical - E_{red} within experimental error. However, the non-zero HOMO methine coefficient accounts for the greater ease of oxidation of Me-AABF₂ and ACHBF₂ relative to D-t-BBF₂ and AABF₂. The lack of an effect for methine substitution on the E_{red} suggests a symmetrical structure for those complexes with the AA ligand.

3.4.2.3 Relationship with Excitation Energies

The relationship between excited state energies and redox potentials were examined in Chapter 2.5 where the following relationships were derived:

$$E_S = E_{ox} - E_{red} + \Delta\Delta G_{solv} - J + 2K \quad (2.60a)$$

$$E_T = E_{ox} - E_{red} + \Delta\Delta G_{solv} - J \quad (2.60b)$$

Equation 2.60 allows experimental evaluation of the exchange integral, K , and variations in the Coulomb integral, J . Plots of eq 2.60 is shown in Figure 3.8 using the values in Tables 3.3 and 3.4. The triplet state energies are nicely correlated with the difference in the corresponding redox potentials, however, the slope is less than unity (slope ≈ 0.5).

The triplet energy vs. $E_{\text{ox}} - E_{\text{red}}$ shows a reasonably smooth correlation, which indicates that kinetic influence on the redox potentials is relatively unimportant for those complexes where E_{T} could be determined. Since the J and K integrals and $\Delta\Delta G_{\text{solv}}$ should be relatively constant for eq 2.60 to show a linear relationship with unity slope, the less than unity slope can be simply rationalized on the basis that the extent of conjugation increases from right to left in Figure 3.8. Hence the integrals J and K are continuously changing; variation in $\Delta\Delta G_{\text{solv}}$ is typically less than 0.2 eV and apparently random regardless of the molecular structure [111]. In contrast, the singlet energies show large scatter, especially for those that their E_{T} values could not be determined. The scatter is believed to be due to kinetic effects on the redox values where kinetic effects can shift the thermodynamic redox potential several hundreds of millivolts [110]. This is partially collaborated by the observation that for those complexes displaying a smooth E_{T} vs. $E_{\text{ox}} - E_{\text{red}}$ correlation also display a reasonably smooth E_{S} vs. $E_{\text{ox}} - E_{\text{red}}$ (solid squares in Figure 3.10) One particular data point is worth mentioning; AABO (Figure 3.8) shows a large deviation of about 400 mV. Inspection of the redox values in Table 3.4 indicates that AABO's reduction potential falls out of correlation, that is, AABO's E_{red} is significantly closer to DBMBO and BABO than observed for the other complex series. In fact, the other β -diketonatoboron series show a consistent difference of 0.35 ± 0.02 V between those with the AA ligand vs. those with the BA ligand. Therefore on the basis of the consistency of the redox data set in Table 3.4, AABO's E_{red} is believed to be systematically shifted by 0.26 V ($E_{\text{red}} = -1.15$ V vs. SCE). Use of this value moves the point for AABO (Figure 3.8) on to the E_{S} vs. $E_{\text{ox}} - E_{\text{red}}$ correlation line.

The correlation lines in Figure 3.8 approach each other with decreasing redox

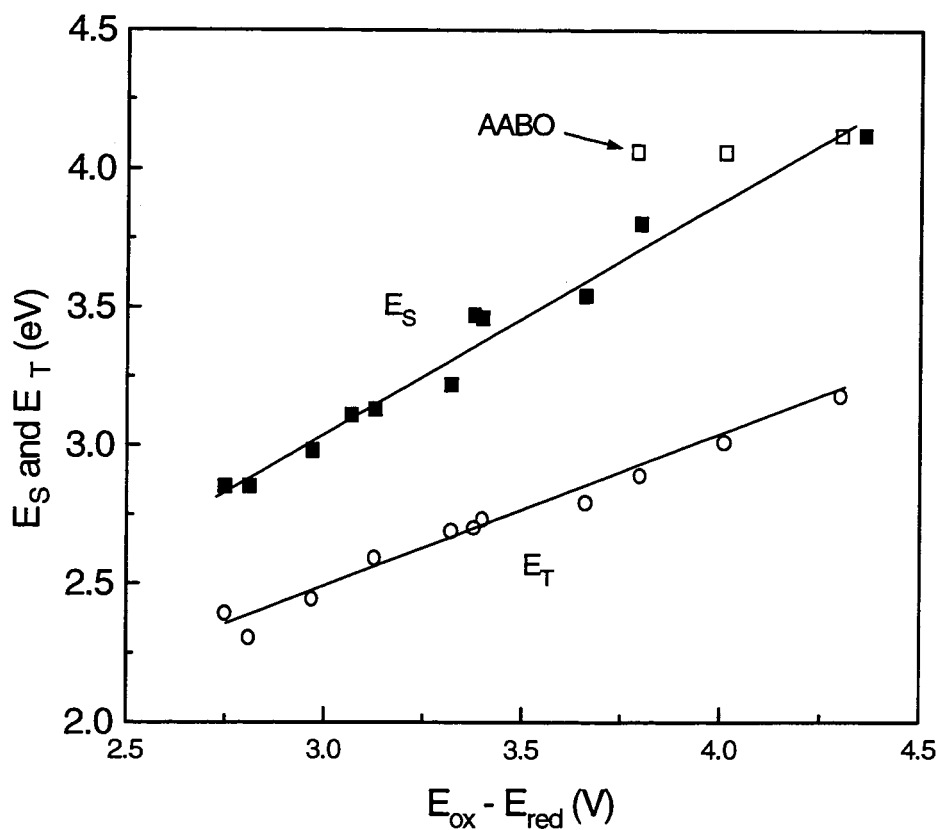


Figure 3.8: Relationship Between the Singlet and Triplet Energies (Table 3.3) and the Redox Potentials (Table 3.4) of Various β -Diketoneboron Complexes. The Open Squares Represent those Complexes where the E_S was Estimated from their UV-Vis Absorption.

potential. This is a manifestation of a decreasing K according to eqs 2.60; i.e., $E_S - E_T = 2K$. This indicates that the extent of delocalization is increasing [72,97] and indicative of increased conjugation with methyl to phenyl substitution on the β -diketonate ring.

3.5 Conclusions

The most important findings gained from the results in this chapter are i) the change in redox potentials of the β -diketonatoboron complexes relative to their parent β -diketones and the ii) the planarity or near planarity of the π system. For the former point, β -diketonatoboron complexes become relatively good electron acceptors. As for example, DBMBF₂'s reduction potential is the same as that found for a commonly used electron acceptor 9,10-dicyanoanthracene (- 0.89 V vs. SCE [47]). For the latter point, the planar ground and excited states are a characteristic feature of EDA complexes and exciplexes, which is due to optimal orbital interaction between the donor and acceptor.

CHAPTER FOUR

ELECTRON DONOR-ACCEPTOR COMPLEXES

4.1 Introduction

DBMBF₂ is known to form EDA complexes with electron rich olefins in acetonitrile. However, these complexes are weak as implied from their small equilibrium association constants (K_a) of less than 0.5 M⁻¹ [36]. Unfortunately, the charge transfer (CT) band of DBMBF₂ / olefin EDA complexes in the 300 to 450 nm region was obscured by the more intense DBMBF₂ absorption band ($\lambda_{max} = 363$ nm, Table 3.1). An EDA complex formed between DBMBF₂ and benzene has been proposed [112], however, no direct evidence was presented. In this chapter, the DBMBF₂ / benzene EDA complexes will be characterized.

4.2 Results and Discussion

Addition of DBMBF₂ solution (9 mM, acetonitrile) to a concentrated solution of benzenes (0.1 to 0.3 M, acetonitrile), both of which are colorless solutions, results in a distinct yellow colored solution. UV spectroscopy showed a new absorption band, only partially resolved from DBMBF₂'s local $\pi \rightarrow \pi^*$ absorption band, where this new absorption band increased with increasing arene concentration. This new absorption was uncharacteristic of either DBMBF₂ or arene absorption bands hence ascribed to a charge transfer (CT) band. With better electron donors, this CT band extended further into the visible region; weak donors like toluene did not show a significant CT band. Using benzene, toluene and p-xylene as solvents, DBMBF₂'s UV absorption band was found to be identical in overall absorption profile but slightly red-shifted from that of DBMBF₂ absorption in cyclohexane and blue-shifted with respect to DBMBF₂ absorption in acetonitrile; these

results are consistent with solvent effects on $\pi \rightarrow \pi^*$ absorption bands: positive solvatochromism.

These results suggests that the DBMBF₂ - arene system may form EDA complexes in acetonitrile with the stronger electron donating arenes. For those donors where the CT band was sufficiently resolved from the intense DBMBF₂ absorption (Figure 4.1), their association equilibrium constants (K_a) were obtained from the standard Benesi-Hildebrand analysis (eq 4.1) [55,59] under the experimental condition that the benzene concentration [D] was greater than [DBMBF₂]; [DBMBF₂] = 0.009 M and [D] \geq 0.05 M. The solution concentrations were adjusted, whenever possible, to yield an absorbance between 0.2 and 0.8.

$$[\text{DBMBF}_2] / \text{Abs.} = (K_a \epsilon_{\text{DA}} [\text{D}])^{-1} + \epsilon_{\text{DA}}^{-1} \quad (4.1)$$

where $K_a = \text{y-intercept/slope}$

Here ϵ_{DA} is the molar absorption coefficient at the monitoring wavelengths (430 and 450 nm, except for p-xylene where only the 430 nm monitor was possible) and the reported K_a values are the average K_a obtained at these wavelengths. Examples of the Benesi-Hildebrand plots obtained in acetonitrile are shown in Figure 4.2 for p-xylene, durene and PMB as donors. The saturation range, that is, the percentage of DBMBF₂ in EDA complex, was calculated from the determined K_a . The results are summarized in Table 4.1.

The strength of ground state association was determined according to a method described by Tamres [113]. The change in the absorption (monitored at 430 nm) of a mixture of DBMBF₂ (typically 0.009 M) and benzene (typically between 0.1 to 0.3 M) in acetonitrile was followed as a function of temperature. The slope of a plot of $\ln \Delta \text{Abs.}$ vs. $1/T$ gives the enthalpy of ground state complex formation (ΔH_a) according to eq 4.2.

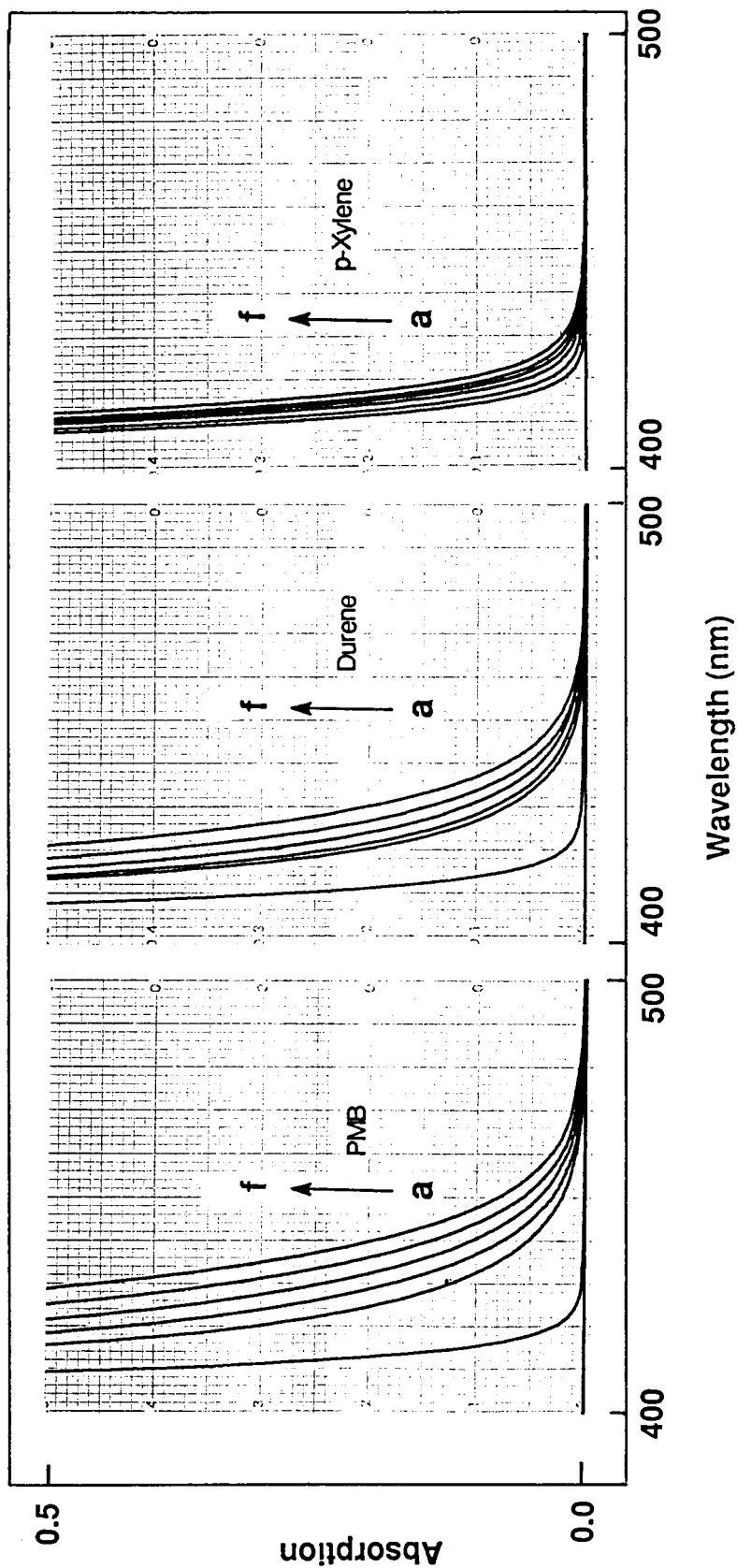


Figure 4.1: EDA Complex UV-Vis Absorption Bands Observed Between DBMBF₂ (0.009 M) and Benzenes in Acetonitrile; benzenes are PMB (a: 0 M; b: 0.06 M; c: 0.08 M; d: 0.11 M; e: 0.15 M; f: 0.20 M), Durene (a: 0 M; b: 0.11 M; c: 0.12 M; d: 0.16 M; e: 0.22 M; f: 0.31 M), and p-Xylene (a: 0 M; b: 0.08 M; c: 0.19 M; d: 0.32 M; e: 0.46 M; f: 0.63 M).

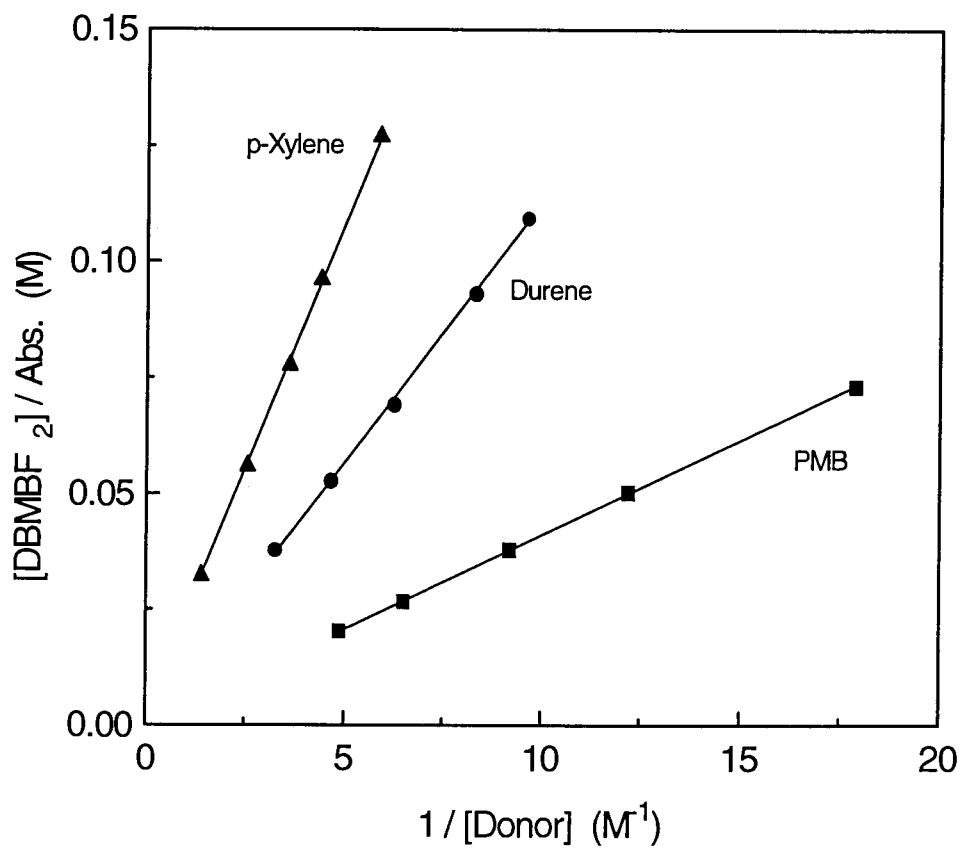


Figure 4.2: Benesi-Hildebrand plots for DBMBF₂ / benzene EDA Complexes in Acetonitrile at Ambient Temperature (cf. Figure 4.1).

Table 4.1: DBMBF₂ - Benzene EDA Complex Emission Maximum, Formation Enthalpies and Association Equilibrium Constants in Cyclohexane and Acetonitrile

Benzene	IP (eV)	Cyclohexane			Acetonitrile		
		$-\Delta H_a$ (kcal/mol)	ν_{\max} (cm ⁻¹)	$-\Delta H_a$ (kcal/mol)	K_a (M ⁻¹)	Saturation	ν_{\max} (cm ⁻¹)
HMB	7.85	3.5 ± 1.0	18,800 ± 100	2.9 ± 0.3	--	--	15,800 ± 100
PMB	7.92	2.5 ± 1.0	19,900 ± 100	2.6 ± 0.3	0.12 ± 0.03	0.01 - 0.02	16,400 ± 100
Durene	8.05	2.0 ± 1.0	20,200 ± 100	2.3 ± 0.2	0.14 ± 0.03	0.01 - 0.04	16,700 ± 100
1,2,3,5-TMB	8.06	--	20,500 ± 100	2.2 ± 0.2	0.11 ± 0.03	0.01 - 0.04	17,000 ± 100
1,2,3,4 -TMB	8.14	--	20,800 ± 100	2.0 ± 0.2	0.09 ± 0.02	0.01 - 0.04	--
1,2,4-TMB	8.27	--	--	1.7 ± 0.2	0.10 ± 0.03	0.01 - 0.06	17,700 ± 100
Mesitylene	8.42	--	21,800 ± 100	1.4 ± 0.1	0.10 ± 0.03	0.02 - 0.07	--
p-Xylene	8.44	--	22,100 ± 100	1.1 ± 0.1	0.07 ± 0.02	0.01 - 0.04	18,400 ± 100
m-Xylene	8.56	--	22,500 ± 100	0.9 ± 0.12	--	--	18,700 ± 100
o-Xylene	8.56	--	22,600 ± 100	0.80 ± 0.12	--	--	--
Toluene	8.82	--	23,200 ± 100	0.30 ± 0.12	--	--	21,300 ± 200

$$\ln \Delta \text{Abs.} = -\Delta H_a / RT + \text{constant} \quad (4.2)$$

This method eliminates the need to know precise donor and acceptor concentrations and only a single solution composition mixture is required. In addition, corrections for the change in solvent density with temperature (i.e., benzene concentration decreases with increasing temperature) are applied. Typical plots obtained by eq 4.2 are shown in Figure 4.3 for p-xylene, durene and PMB as donors and the results are summarized in Table 4.1. Some values in cyclohexane were also determined where the CT absorption band was sufficiently strong; unfortunately DBMBF₂'s solubility in cyclohexane is less than 10⁻⁴ M thus making it impossible to determine K_a since the EDA complex's absorption band is too weak.

Two types of ground state complexes may exist in solution, an EDA complex and a contact complex [50,113]. A contact complex is characterized by a weak and unresolved UV-Vis absorption band appearing at the low energy side of the longest wavelength absorption of the donor or acceptor and a binding smaller than the available thermal energy. Conversely, an EDA complex typically has a well resolved CT absorption band and a binding energy greater than thermal energy [113]. However, the dividing line between these two complexes is unclear. Tamres has suggested a criteria to characterize EDA complexes and contact complexes on the basis of their binding energies and association constants [113]: EDA complexes are defined by a binding energy greater than or equal to 1 kcal / mol, which is a slight excess of the available thermal energy at ambient temperatures (0.6 kcal / mol at 296 K) and K_a values greater than or equal to 0.1 M⁻¹. This classification scheme is adopted here for lack of anything better. However, this complex classification is not infallible since EDA complex formation can be spontaneous but favorable enthalpically due to a favourable entropic term [114].

In Table 4.1, it is clear that as the electron donating ability of the benzene increases the EDA complex stability increases, as measured by - ΔH_a, as expected; i.e., as the dative

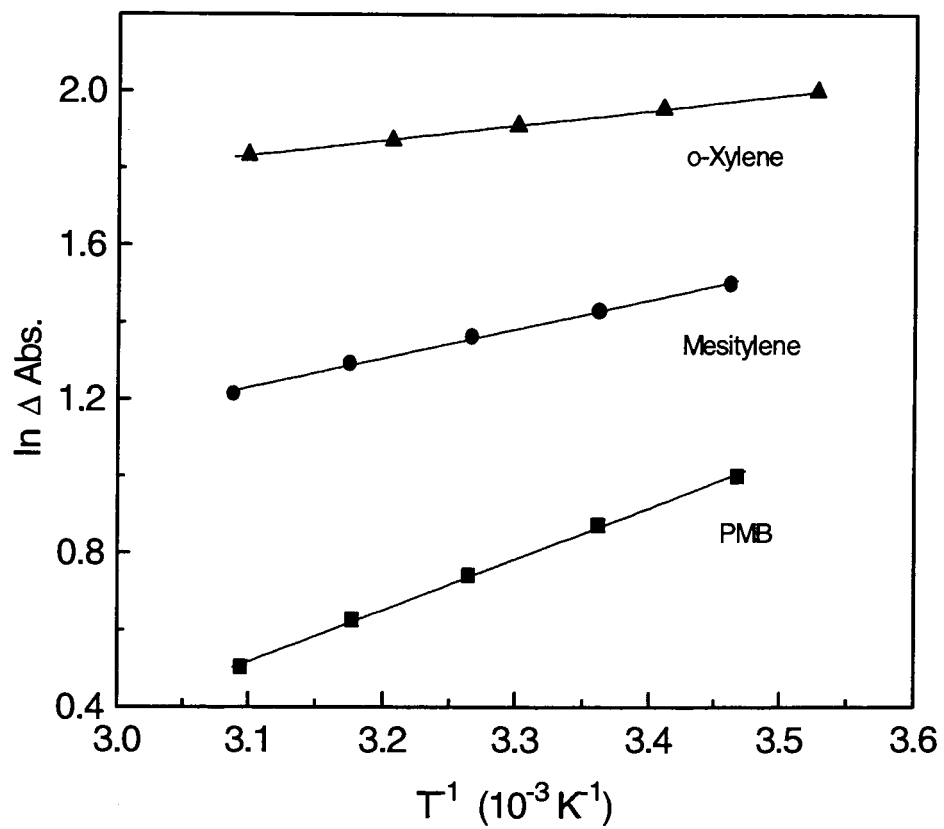


Figure 4.3: Ground State Association Enthalpic Plots (eq 4.2) Monitored at 420 nm.

Concentrations : [DBMBF₂] = 9 mM; [o-Xylene] = 0.248 M; [Mesitylene] = 0.389 M; [PMB] = 0.259 M.

and no-bond configurations' energy levels approach each other hence interaction between them becomes stronger. In acetonitrile, mesitylene and the better electron donating benzenes are classified as EDA complexes on the basis that their binding energies and K_a values are greater than one kcal / mol and 0.1 M^{-1} , respectively. The xylenes are borderline cases where the experimental errors do not allow definitive classification of the interaction, but toluene is a definite contact complex. Based on the trend in Table 4.1, benzene and the other weak electron donating benzenes are liable to be contact complexes as well.

The strongest interaction is between HMB and DBMBF_2 , where the donor-acceptor bond is - 2.9 kcal / mol. In relation to the strength of covalent bonds (ethane's C — C bond strength is 88 kcal / mol) the observed enthalpies indicate that the contribution of the dative configuration is small; i.e., $a^2 \ll e^2$. This can be further demonstrated as follows: following the discussion in Chapter Two, weak donor-acceptor interaction may show a linear plot of $-\Delta H_a$ vs. the IP of the donor (eq 2.27).

$$-\Delta H_a = \pm (a^2 / e^2) \text{ IP} + \text{constant} \quad (2.27)$$

The plot of $-\Delta H_a$ (in eV units) vs. IP, where the values for $-\Delta H_a$ in Table 4.1 were converted into eV units, shown in Figure 4.4, is indeed linear with a slope of - 0.12. The slope can be taken as a qualitative measure of the ratio a^2 / e^2 but it is expected that it will increase with increasing donor strength [50,51,114]; this ratio represents some sort of average for the donor series. In addition, Marks and Drago [115] argue that derivations such as those in Chapter Two, which lead to eq 2.27, do not account for the fact that there are two electrons involved in the process hence a factor of 2 should appear in eq 2.27. Therefore, the observed slope is suggested to be $-2a^2 / e^2$. Regardless of the actual value, the slope of - 0.12 suggests that $e > a$, which is consistent with the small binding energies observed.

It is quite common to find a linear relationship between the donor's IP and the complex's free energy of formation ($\ln K_a$) [62]. The values in Table 4.1 appear to have a correlation with donor's IP but no clear trend is observed. It must be emphasized that the use of the Benesi-Hildebrand equation (eq 4.1) is not trivial as one might initially expect. It has been shown that reported values of K_a for the same EDA complex varies drastically from one group to another (however, the product $K_a \epsilon_{DA}$ does not vary beyond experimental error) [116] and a number of explanations have been offered [50,51,59,116-119]. In this study there are three potential causes for the scatter in the K_a data in Table 4.1. Firstly, the monitoring wavelength was not at the EDA complex's UV-Vis λ_{max} due to poorly resolved DBMBF₂ and EDA complex absorption bands. The monitoring wavelength for Benesi-Hildebrand analysis (eq 4.1) was at the sloping edge of the EDA complex absorption band, hence a small error in the λ_{mon} will result in a significant error in ΔAbs . Secondly, Person [117] and Deranleau [118] have discussed that the most accurate K_a and ϵ_{DA} are obtained when the saturation range lies between 20 and 80 percent. This is due to the fact that equations like eq 4.1 can only determine one parameter independently; i.e., for eq. 4.1 a systematic error in ϵ_{DA} imparts a systematic error in K_a . Saturation values below 20 percent will also show linear Benesi-Hildebrand plots. However, the y-intercept will be closer to the origin than the true y-intercept. This results in a larger ϵ_{DA} ($\epsilon_{DA} = 1 / y\text{-intercept}$) hence a smaller K_a . The saturation range in Table 4.1 for the DBMBF₂ / benzene EDA complexes is estimated to be less than 10 percent. Therefore, the reported K_a values Table 4.1 may contain a substantial systematic error. They're suspected to be smaller than the true values. The graphical method of Seal et al., which independently determines K_a and ϵ_{DA} , did not result in any improvement. Thirdly, Orgel and Mulliken [50] have pointed out that linear Benesi-Hildebrand plots do not demonstrate a 1:1 complex since the coexistence of 1:1 complex plus contact complexes also give linear Benesi-Hildebrand plots [50]. Furthermore, the coexistence of a 1:1 complex plus contact complexes results in an over estimation of ϵ_{DA} hence an under estimation of K_a .

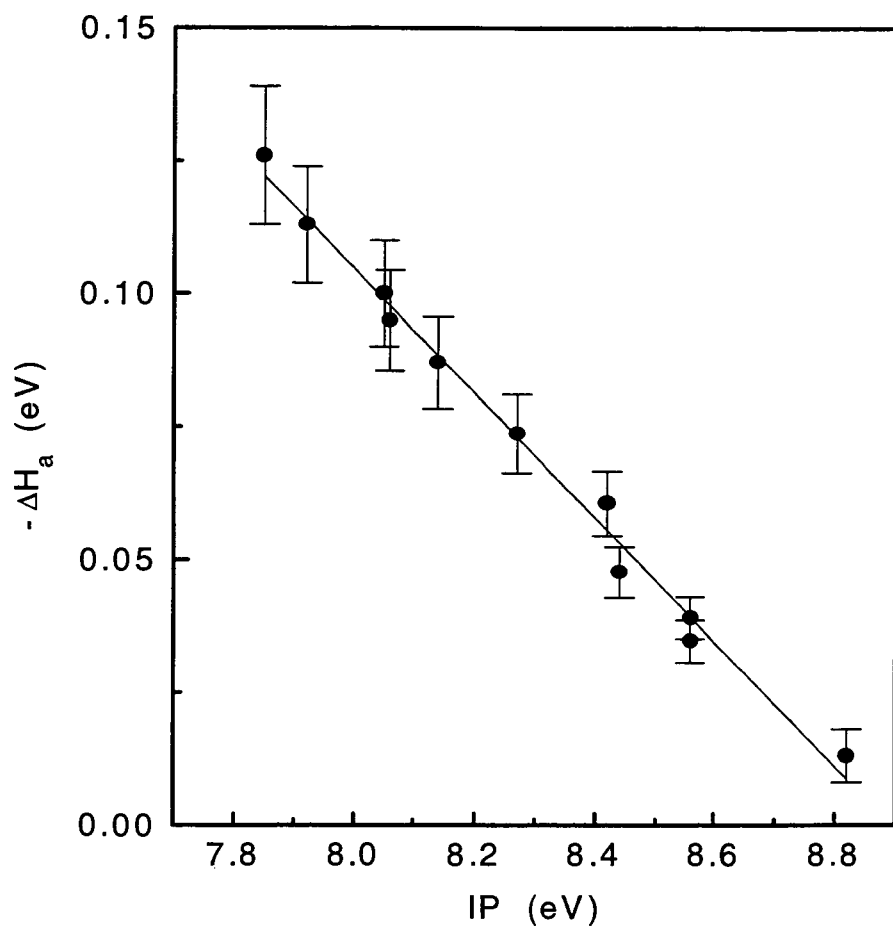


Figure 4.4: Correlation of DBMBF₂ / benzene EDA Complex Formation Enthalpy (in eV units) in Acetonitrile vs. Donor's IP.

[50]. Therefore, the K_a values listed in Table 4.1 should be viewed as order of magnitude estimates.

Very few excited EDA complexes are known to fluoresce in solution at room temperature [50,51]; typically, the fluorescence is extremely weak and its detection requires extra attention to solvent and reactant purification. For the DBMBF₂ / benzene system, the EDA charge transfer bands were irradiated at 400 nm (negligible DBMBF₂ absorption) and a structureless emission was observed (Figures 4.5 and 4.6) in both cyclohexane and acetonitrile where the latter was extremely weak. Emission could not be detected with the weak electron donating benzenes (e.g., benzene) due to insignificant CT band absorption at 400 nm; i.e., DBMBF₂ emission was stronger. The observed emission ν_{\max} are reported in Table 4.1. Comparison of the ν_{\max} in Table 4.1 shows a positive solvatochromism of approximately 3500 cm⁻¹. One can conclude that the excited EDA complex has i) a larger dipole moment (Figure 2.7) and ii) the large solvatochromic shift of 3500 cm⁻¹ (cf. Table 2.2) is indicative of a significant excited state dipole moment. Both conclusions are in accordance with Mulliken's theory [50,51].

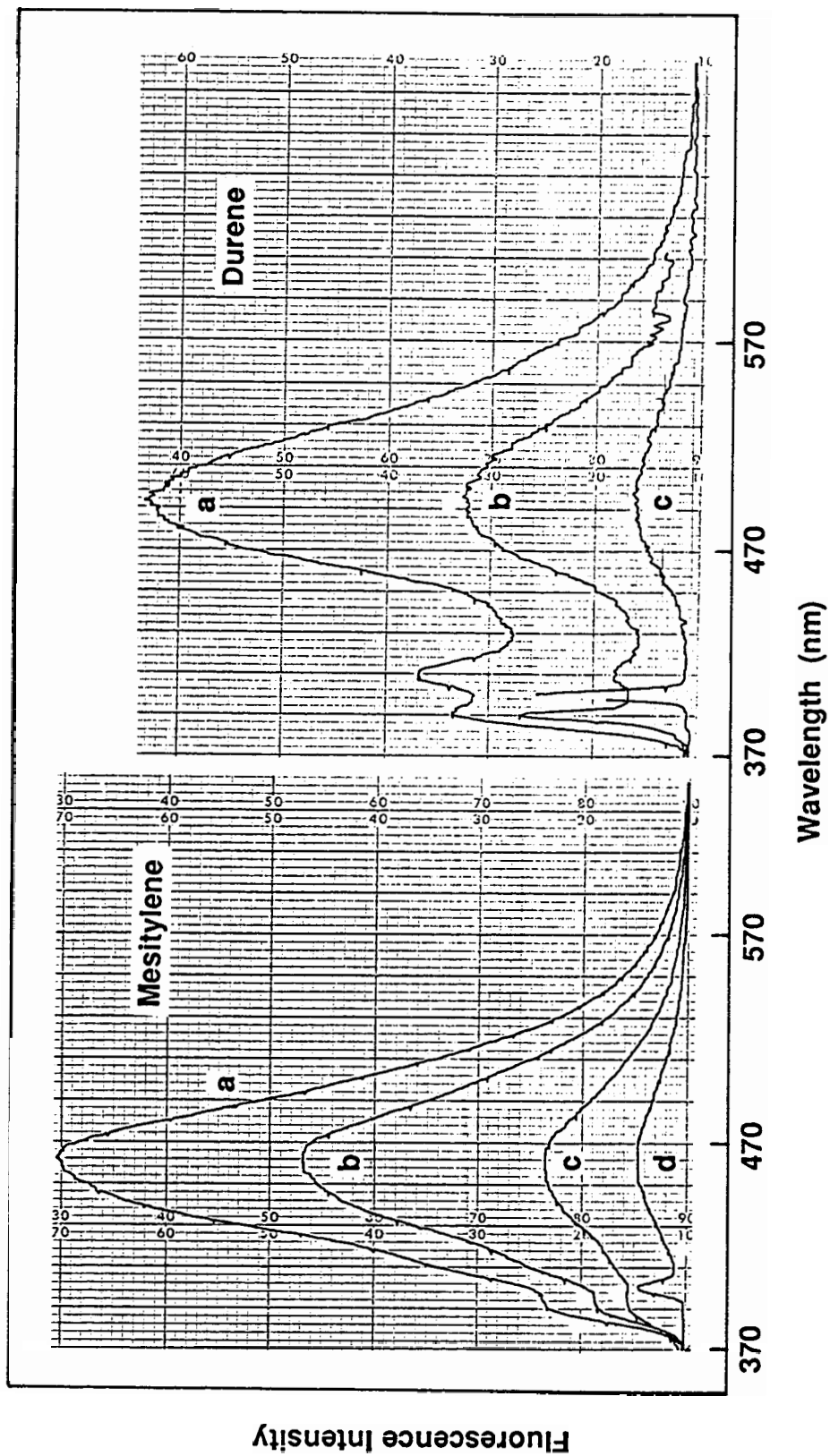


Figure 4.4: Examples of Excited EDA Complex Emission in Cyclohexane. [DBMBF₂] = 1.1 x 10⁻⁵ M. [Durene] = 0.134 M; Excitation Wavelengths: (a) 365 nm; (b) 390 nm; (c) 400 nm. [Mesitylene] = 0.204 M; Excitation Wavelengths: (a) 365 nm; (b) 350 nm; (c) 390 nm; (d) 400 nm.

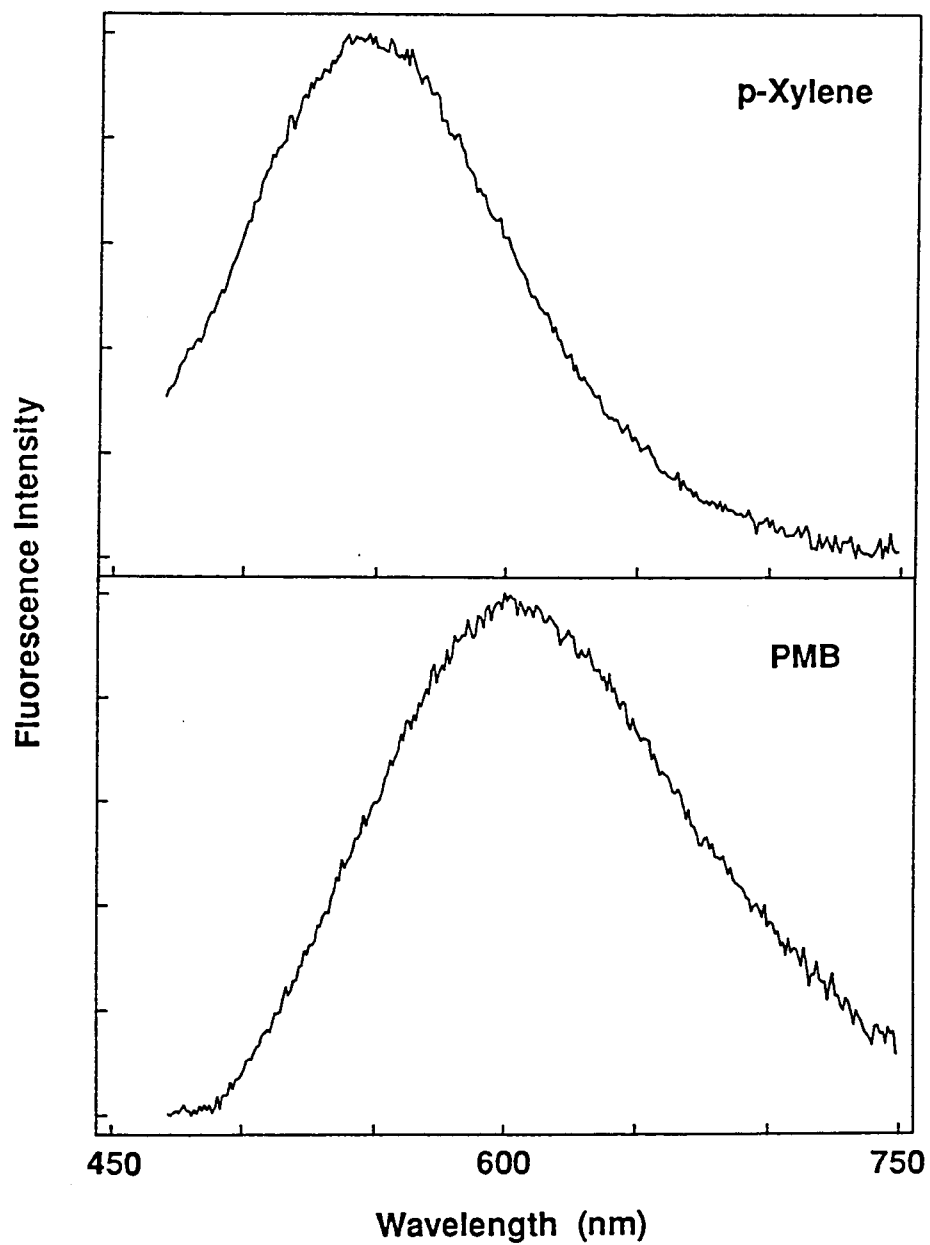


Figure 4.5: Examples of Excited EDA Complex Emission in Acetonitrile where $[\text{DBMBF}_2] = 9 \text{ mM}$ and $\lambda_{\text{ex}} = 400 \text{ nm}$. $[\text{p-Xylene}] = 0.298 \text{ M}$. $[\text{PMB}] = 0.254 \text{ M}$.

CHAPTER FIVE

GENERAL MECHANISTIC OVERVIEW

5.1 Introduction

A molecule in its excited state may either degrade or transfer the energy (gained by photon absorption) through several processes, namely luminescence, radiationless decay and bimolecular interaction with another ground state molecule [69]. For the latter process, this interaction is called quenching and the excitation energy is either transferred to the quencher, shared between them or the quencher assists the excited state species in dissipating the excitation energy by a radiationless process.

The analysis of a new system, which undergoes bimolecular quenching with an added quencher, requires establishment of the mechanism, where a complete photochemical mechanism includes knowledge of [69]

- all significant intermediates,
- rate constants (kinetics),
- forces responsible for interconverting species (thermodynamics).

Photochemical mechanistic investigation begins with a working set, and by a process of elimination the investigation arrives at a provisional mechanism. The standard photochemical mechanistic set commonly encountered is shown in Table 5.1 along with the associated characteristics; in some cases a common quencher affiliated with a particular process is listed [65,69].

The interpretation of fluorescence quenching kinetics is largely based on the Law of Mass Action: the rate is proportional to the reactant's concentrations, raised to the power

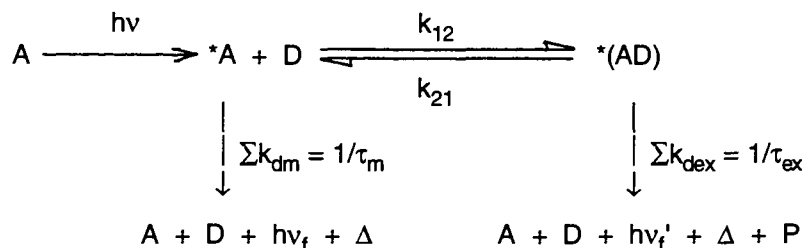
Table 5.1: Bimolecular Quenching Processes

	Process	Characteristics	Quencher
I	Paramagnetic	Unpaired electrons	O ₂ , NO
II	External Heavy Atom Effect	Large spin-orbit coupling constant	RX, φX, Xe
III	Energy Transfer:	Overlap of luminescence and absorption bands.	
	- Collisional	- Energy acceptor's excited state energy smaller than donor's	
	- Coulombic/Trivial	- strong absorption band	
IV	Charge Transfer	Planar and unhindered aromatic π systems	
	- Exciplex		
	- Excimer		PAH ^a
V	Electron Transfer	Strong oxidizing/reducing agents in their excited states (cf. Chapter Two)	

^a PAH = Polyaromatic hydrocarbons.

of their stoichiometric coefficients, and independent of other concentrations and reactions [120]. Due to the very dilute ^{*}A concentrations the [^{*}A] in the rate of fluorescence quenching is expected to be first order. Experimentally, fluorescence quenching kinetics are typically performed under steady state conditions (usually termed photostationary conditions) where the reactant is pumped to its excited state with a constant intensity light source. As an example, the simplest fluorescence quenching reaction involving a singlet excited ^{*}A, a ground state quencher D and a reaction intermediate ^{*}(AD) (exciplex) is shown in Scheme 5.1.

Scheme 5.1



Σk_{dm} (reciprocal of the lifetime τ_m) and Σk_{dex} (reciprocal of the lifetime τ_{ex}) are the rate constants for the decay of *A and its exciplex, respectively. $h\nu_f$, Δ and P represent light emission, radiationless decay (as heat gained by the surroundings) and reactions product(s), respectively. Under photostationary condition, it can be shown that the ratio of the steady state concentrations ($[{}^*A]^0$ and $[{}^*A]$), which equal the ratio of fluorescence intensities (I^0 and I), in the absence and presence of D (respectively) is given by eq 5.1 [65,69]

$$I^0 / I = [{}^*A]^0 / [{}^*A] = 1 + k_{obs}\tau_m [D] \quad (5.1)$$

$$\text{where } k_{obs} = k_{12} / (1 + k_{21}\tau_{ex})$$

This equation is called the Stern-Volmer equation. Knowledge of the excited state *A concentration is not required, however, use of eq 5.1 requires a constant $[A]$ concentration such that the number of promoted A molecules remains constant.

This section will be concerned only with the determination of the fluorescence quenching mechanism of singlet excited DBMBF₂ by benzenes in nonpolar (cyclohexane and carbon tetrachloride) and weakly polar (chloroform and dichloromethane) solvents; i.e.,

ascertain the significant intermediates. The kinetics (rate constants) and thermodynamics will be investigated, in cyclohexane and acetonitrile, in the following chapters.

5.2 Results and Discussion

5.2.1 Reaction Intermediate

DBMBF₂'s fluorescence is efficiently quenched by added benzenes and olefins in either degassed nonpolar (e.g., cyclohexane) or polar (e.g., acetonitrile) solvents (Figure 5.1). In nonpolar and weakly polar solvents, the fluorescence quenching of singlet excited DBMBF₂ by benzenes shows the emergence of a red-shifted structureless emission; it has been reported that fluorescence quenching by olefins in acetonitrile do not show any hint of a red-shifted emission [36]. In addition, the maximum of this emission shifts to longer wavelengths with decreasing benzene IP and the emission intensity decreases rapidly with increasing solvent polarity; the weak electron donating benzenes (chlorobenzene to cyanobenzene) were weakly solvent dependent. The observation of a new emission band is indicative of a metastable intermediate, whose lifetime is long enough to emit a photon of light.

The observed new emission was dependent on donor concentration and an isoemissive point was observed (Figure 5.1). In analogy to isobestic points in UV-Vis spectroscopy, an isoemissive point shows that the new emission is kinetically derived from the fluorescence quenching of ^{*}A by added D [121,122]. In cases where DBMBF₂'s fluorescence and the new emission bands were well resolved, the excitation spectra were nearly identical regardless of the monitoring wavelength ($\lambda_{\text{mon}} = 410 \text{ nm}$ for DBMBF₂ and 550 nm for the new emission), which suggests that the new emission is not entirely due to the light absorption by a EDA complex (Figure 5.2). Therefore, the observations can be tentatively described by the following equation.

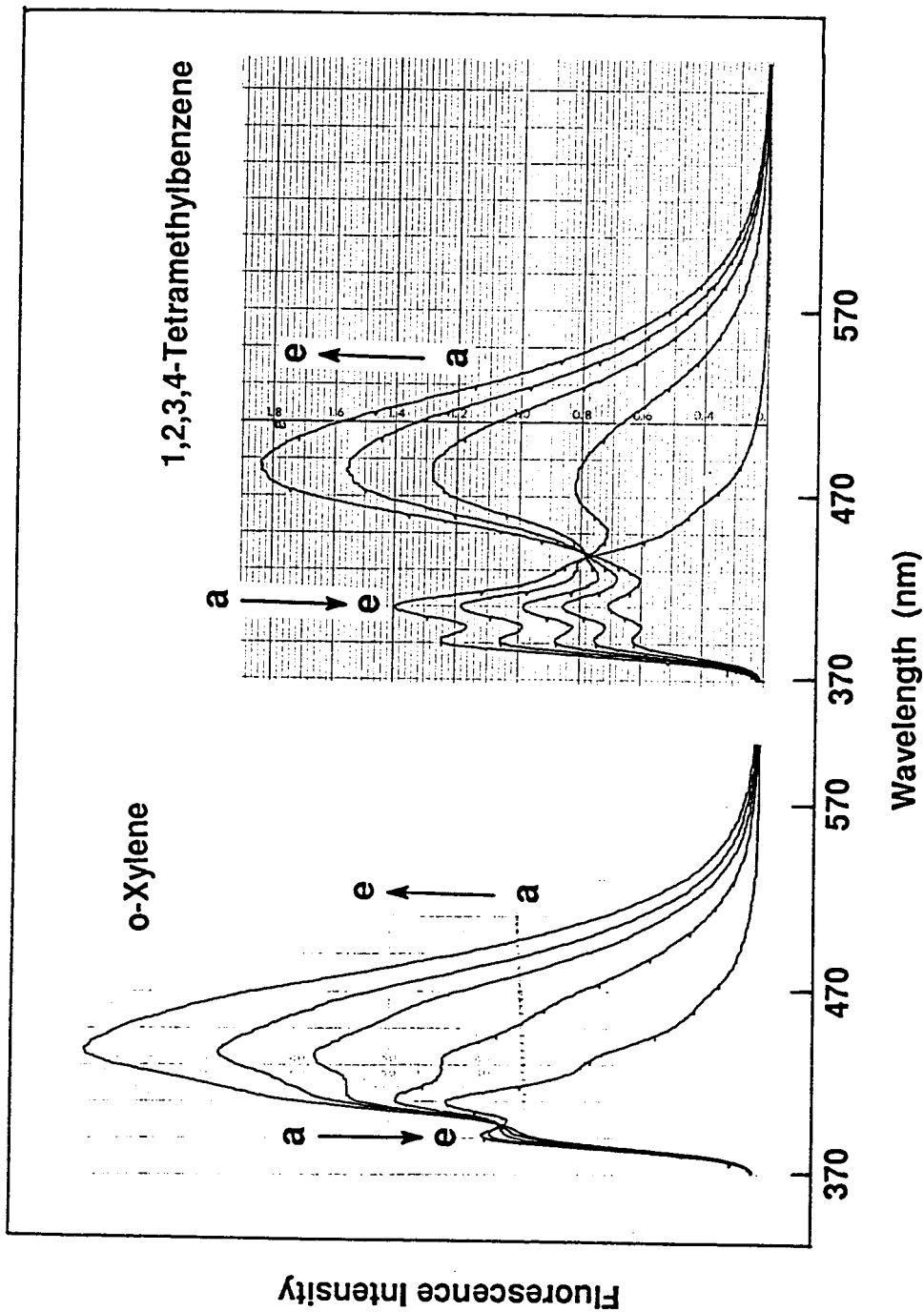


Figure 5.1: Fluorescence (uncorrected, $\lambda_{\text{ex}} = 365 \text{ nm}$) Quenching of Singlet Excited DBMBF₂ ($1 \times 10^{-5} \text{ M}$) by Benzenes in Cyclohexane. A: o-Xylene; (a) 0 M; (b) 0.05 M; (c) 0.11 M; (d) 0.15 M; (e) 0.21 M. B: 1,2,3,4-Tetramethylbenzene; (a) 0 M; (b) 0.04 M; (c) 0.09 M; (d) 0.13 M; (e) 0.20 M.

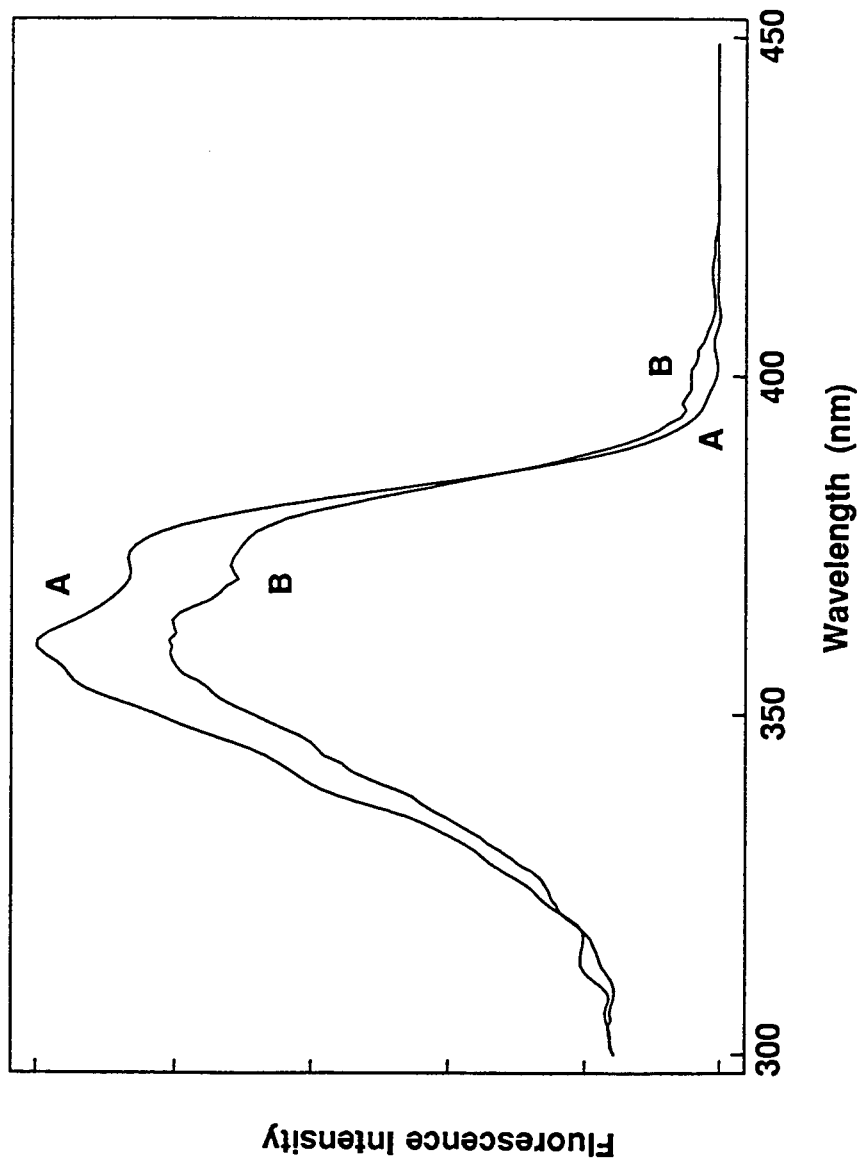
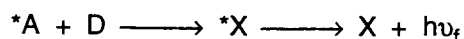


Figure 5.2: Fluorescence Excitation Spectra of the DBMBF₂ (1×10^{-5} M) / Durene (0.153 M) System. A: Excitation Spectrum Monitored at DBMBF₂ (410 nm); B: Excitation Spectrum Monitored at the Exciplex (550 nm).



The intermediate, *X, can be identified by a process of elimination of a number of established fluorescence quenching processes as illustrated below:

	Scheme	Process(es)
1	$*A + D \longrightarrow *A^3 + D \longrightarrow A + D + \text{Phosphorescence from A}$	I - V
2	$*A + D \longrightarrow A + *D \longrightarrow A + D + \text{Fluorescence from D}$	III
3	$*A + D \longrightarrow *(AD) \longrightarrow A + D + \text{Exciplex Fluorescence}$	IV

All the processes in Table 5.1 are known to evenly populate the triplet state of either the donor or acceptor [38,54,63,65,69,71,72], however, this scheme can be eliminated on the basis that DBMBF₂'s phosphorescence (Table 3.3) and methyl substituted benzene fluorescence [123,124] occur in a different spectral region from that observed. In addition, their emission is known to have some vibrational structure whereas the observed intermediate emission is structureless. For 2 energy transfer is not energetically feasible from singlet excited DBMBF₂ to benzene since DBMBF₂ has a smaller singlet energy ($E_S = 3.19$ eV, Table 3.3) than the quenchers (alkyl benzenes range from 4.42 to 4.77 eV and chlorobenzene, methyl benzoate and cyanobenzene have values of 4.55, 4.42 and 4.51, respectively [123]). In addition, the alkyl benzene fluorescence occurs in the 300 to 400 nm region whereas the observed emission begins at 400 nm. For the remaining scheme, 3, exciplex fluorescence is characterized by a dependence on the donor's IP and sensitivity to solvent polarity [65,66,69,71]. These features agree with most of the quenchers used except for the weaker electron donating benzenes (see Chapter Six). However, the

weaker electron donors fit scheme **3** better than **1** or **2**. It is concluded that the intermediate *X is probably an exciplex of undefined nature and stoichiometry.

In Chapter Four, it was discovered that DBMBF₂ forms EDA complexes with benzenes in acetonitrile and cyclohexane. Since the excited state of DBMBF₂ / substituted benzene EDA complexes have been shown to be emissive at room temperature and that the DBMBF₂ / substituted benzene EDA complex absorption lies underneath the principal absorption band of DBMBF₂ the question arises whether the EDA complex is connected to the exciplex. For example, it has been shown that for the 1,2,4,5-tetracyanobenzene (TCB) / substituted benzene system, the same emissive excited state species can be achieved by exciting either TCB or its EDA complex UV-Vis absorption bands [125]. At excitation wavelengths greater than 400 nm, where DBMBF₂ absorption is negligible, the EDA complex is promoted to its excited state. As shown in Chapter Four, the resulting emission was observed with most DBMBF₂ - benzene mixtures except for poor electron donating benzenes like benzene (due to negligible EDA absorption band). These emissions were identical with respect to the emission λ_{max} and overall emission profile (Figure 4.4). The same emission characteristics regardless of the excited state generation process strongly indicates that the excited EDA complex and exciplex are one and the same. This result is interesting on the basis that the experimental requirements for defining an exciplex (Chapter 2.3.2) specifically state the absence of a EDA complex. The question arises should the exciplex definition be modified or not; this question will be partially answered in Chapter Seven.

5.2.2 Reaction Order

5.2.2.1 Stoichiometric Expressions

For EDA complexes the stoichiometry is usually determined from Job's method of variations, where the EDA absorption intensity is plotted as a function of the donor and acceptor mole fractions; such a plot will show a volcano-type curve where the maximum is correlated with the EDA complex stoichiometry [126]. Similar plots for exciplexes are not possible since the fluorophor's concentration must be held constant (very dilute concentrations) since the fluorescence intensity of the fluorophor and exciplex are related to the rate of light absorption by the fluorophor's ground state and proportional to the fluorophor's concentration in the dilute range. Another method is needed.

Determining the exciplex stoichiometry, that is, a 1:1 or 1:2 complex, is achieved by following the variation in fluorophor's and complex's emission intensity as a function of quencher's concentration only. On the basis of Scheme 5.1 it can be shown that, under photostationary conditions, the ratio of the exciplex and DBMBF₂'s fluorescence quantum yields is given by eq 5.2 (cf. Chapter Seven) [65,127,128].

$$\ln(I_{\text{ex}} / I_{\text{A}}) = \ln[D] + \text{Constant} \quad (5.2)$$

I_{ex} and I_{A} represent the exciplex and DBMBF₂ fluorescence intensities, respectively. Equation 5.2 provides a measure of the exciplex stoichiometry by a plot of $\ln(I_{\text{ex}} / I_{\text{A}})$ vs. $\ln[D]$, where the slope directly determines the stoichiometry; i.e., reaction order with respect to D. The complication of the exciplex being quenched by another ground state D, ${}^*(\text{AD}) + \text{D} \rightarrow {}^*(\text{ADD})$, will be manifested by a downward curvature of a plot of eq 5.2 [127]; this assumes that either the triplex, ${}^*(\text{ADD})$, is nonemissive or its emission is well resolved from that of the exciplex. Typically, this complication is usually evident only at large D concentrations.

It is known that at higher donor concentrations termolecular reactions are possible [128]; i.e., a triplex; ${}^*\text{A} + 2\text{D} \rightarrow {}^*(\text{ADD})$, formation. For a termolecular reaction, ${}^*\text{A} + 2\text{D} \rightarrow$ triplex, eq 5.2 is modified to eq 5.3

$$\ln (I_{\text{trp}} / I_{\text{A}}) = 2 \ln [D] + \text{constant} \quad (5.3)$$

where I_{trp} represents the triplex fluorescence intensity. Higher order reactions may be manifested by a slope of two or more.

5.2.2.2 DBMBF₂ / Substituted Benzene Complex Stoichiometry

The fluorescence quenching spectra discussed above, such as Figure 5.1, contain information regarding the DBMBF₂ / substituted benzene exciplex stoichiometry. Figure 5.3 shows typical plots of eq 5.2 for the fluorescence quenching of singlet excited DBMBF₂ by substituted benzenes in cyclohexane. The stoichiometry for these exciplexes was determined for most of the donors in cyclohexane but only for a chosen few in the medium polarity solvents. In acetonitrile, only those that showed strong exciplex emission were evaluated.

As shown in Figure 5.3, plots of eq 5.2 had unity slopes within experimental error, hence demonstrating that the observed emission is due to a 1:1 stoichiometric exciplex. Downward (exciplex quenching by another ground state D) or upward curvature (higher order reaction) was not detectable in any of the plots where the quencher concentration ranged as high as 1 M. Plots with unity slopes were obtained regardless of the donor. The exciplexes with tert-butyl substituted benzene donors were not analyzed due to the fact that they are structurally similar. It is improbable that these donors would show a drastic variation in exciplex stoichiometry; it is expected, however, that these donors would be unlikely to form higher order complexes due to steric effects.

The results above indicate that higher order complexes can be neglected for D concentrations less than or equal to 1 M and that the fluorescence quenching of singlet

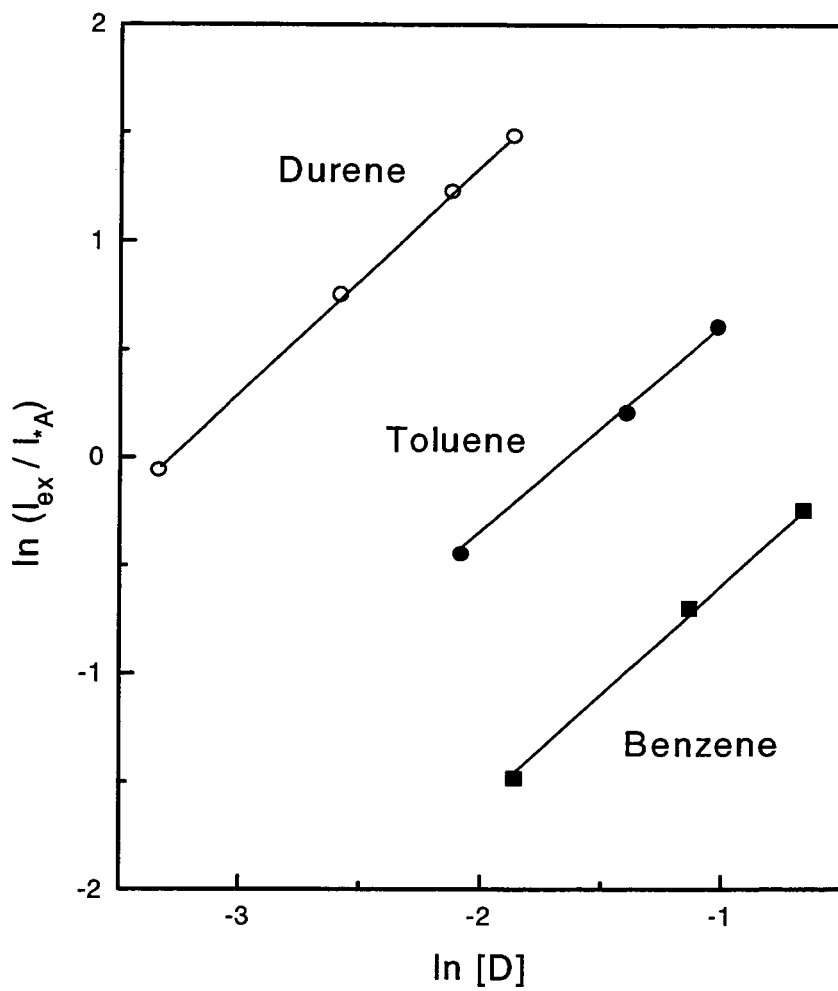


Figure 5.3: DBMBF₂ (1×10^{-5} M) - Benzene Exciplex Stoichiometric Plots in Cyclohexane.

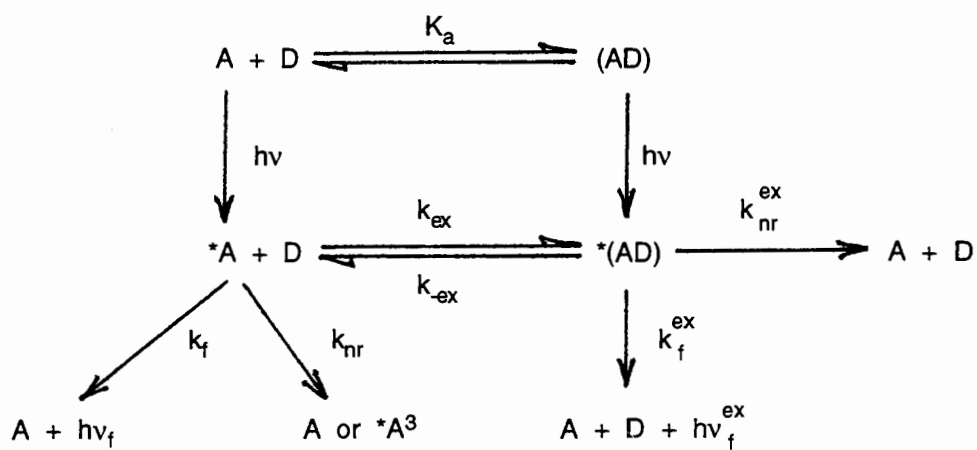
Plots of $\ln(I_{\text{ex}} / I_A)$ vs. $\ln[D]$ (eq 5.2).

excited DBMBF₂ by benzenes is second order order (first order in [*A] and [D]) as depicted in Scheme 5.1.

5.2.3 Reaction Scheme

Scheme 5.2 represents the interpretation of the observations for the DBMBF₂ (A) and substituted benzene (D) system, where the radiative and radiationless processes for singlet excited DBMBF₂ (*A) and its exciplex [* (AD)] are shown. Most of the processes in Scheme 5.2 will be examined in the following chapters; EDA complex formation was discussed earlier in Chapter Four and the decay processes of *A were discussed in Chapter Three. For the remaining processes, the nature the exciplex will be examined in Chapter Six. Chapter Seven discusses the binding energies in cyclohexane and Chapter Eight discusses the kinetics and free energies of formation. Chapter Nine shows the correlations between exciplex character on the exciplex's radiative and radiationless rates. Chapter Ten shows the influence of solvent polarity on the fluorescence quenching mechanism.

Scheme 5.2: Fluorescence Quenching Mechanism of Singlet Excited DBMBF₂ by Substituted Benzenes.



CHAPTER SIX

THE NATURE OF THE EXCIPLEX

6.1 Introduction

Chapter Five emphasized the photochemical mechanism of singlet excited DBMBF₂ with substituted benzenes where the fluorescence quenching of DBMBF₂ results in exciplex formation. The observation of a reaction intermediate allows access in examining the fluorescence quenching driving force and the intermediate's nature.

For the DBMBF₂ / substituted benzene exciplexes, the use of methyl substituted benzenes, with the exception of methyl benzoate and cyanobenzene, avoided significant changes in electronic, structural and steric factors while still covering a useful oxidation range. Therefore, the observed properties may be related to electronic factors. In addition, the sterically hindered alkyl-substituted benzenes retained similar electronic factors as their methyl counterparts but the geometrical factors could be explored.

6.2 Results and Discussion

6.2.1 DBMBF₂ / Substituted Benzene Exciplex Dipolar Character

Exciplexes formed between singlet excited DBMBF₂ and ground state substituted benzenes were shown in Chapter Five to have significant fluorescence intensities. This is fortunate because a strong intensity facilitates more accurate solvatochromic analysis where a significant part of the error results in the uncertainty in λ_{max} . The exciplex fluorescence maximum showed positive solvatochromism. However, the solvatochromism was clearly stronger for the benzenes with lower ionization potentials.

For example, DBMBF₂ / benzene exciplex showed a small solvatochromism whereas the DBMBF₂ / HMB exciplex showed significantly larger solvatochromism (Table 6.1). On the basis of Chapter 2.4 these observations are indicative that the exciplex charge transfer character is a function of the benzene's electron donating ability.

The fluorescence maximum in cyclohexane provides preliminary information regarding the exciplex CT nature. Weller and co-workers have established that plots of the exciplex emission maxima against the donor-acceptor's redox values in nonpolar solvents such as n-hexane provide a qualitative measure of the extent of the exciplex's charge transfer [54,69,73]. They were able to demonstrate that the contact radical ion pair's (CRIP) emission maximum obeys eq 6.1b. Furthermore, it was observed that for excited EDA complexes and exciplexes the observed $h\nu_{\max}$ was larger (eq 6.1a) and smaller (eq 6.1c) than that calculated by eq 6.1b, respectively.

$$\text{Excited EDA Complex} \quad h\nu_{\max} > E_{\text{ox}} - E_{\text{red}} - 0.15 \quad (6.1a)$$

$$\text{CRIP} \quad h\nu_{\max} = E_{\text{ox}} - E_{\text{red}} - 0.15 \quad (6.1b)$$

$$\text{Exciplex} \quad h\nu_{\max} < E_{\text{ox}} - E_{\text{red}} - 0.15 \quad (6.1c)$$

Equation 6.1b is an amended form of eq 2.28 where U_{Stab} is zero and the remaining terms, are empirically determined to be 0.15 eV [73]. Equation 6.1c is a manifestation of the stabilization acquired from $|A^+D^- \rangle \leftrightarrow |A^*D \rangle$ resonance, U_{Stab} , and eq 6.1a is a manifestation of EDA complex destabilizing the excited state (cf. eq 2.23). Weller has shown that eq 6.1b is accurate to within ± 0.10 eV for a variety of donor-acceptor pairs where the majority of the error was proposed to be due to the uncertainty in the redox values obtained from different sources [73]. The use of these equations requires that the observed complex emission $h\nu_{\max}$ be from a 1:1 complex, or exciplex, since higher order complexes will obey a different relationship [129]; DBMBF₂ / substituted complex emission has been identified as being due to an exciplex (cf. Chapter 5).

Table 6.1: DBMBF₂ / Benzene Exciplex Emission Maxima in Various Solvents

Donor	Exciplex Emission ν_{\max} (10^3 cm^{-1}) ^a				
	CH ^b	CT	CF	DCM	AN
	0.101 ^c	0.119	0.254	0.318	0.393
Cyanobenzene	24.0				24.0
Methyl benzoate	24.2		24.1	24.0	24.0
Benzene	24.2		24.0	23.9	23.9
Chlorobenzene	24.3		23.8	23.8	23.6
Toluene	23.3		22.2	21.8	21.5
o-Xylene	22.6	22.5	21.7	20.9	E ^d
m-Xylene	22.5	22.3	21.2	20.8	E
p-Xylene	22.3	21.9	20.8	20.3	NE
Mesitylene	21.8	21.5	20.7	20.2	E
1,2,4-TMB	21.3	21.0	19.9	19.3	NE
1,2,3,4-TMB	20.9	20.5	19.5	18.6	NE
1,2,3,5-TMB	20.5	20.1	19.0	18.2	NE
Durene	20.5	20.1	19.1	18.1	NE
PMB	19.9	19.6	18.3	17.6	NE
HMB	18.7	18.4	17.1	NE	NE

Table 6.1 (Continued)

Donor	Exciplex Emission ν_{\max} (10^3 cm^{-1})				
	CH ^b	CT	CF	DCM	AN
	0.101 ^c	0.119	0.254	0.318	0.393
t-Butylbenzene	23.3		22.2	21.8	21.5
p-t-Butyltoluene	22.3	21.8	20.8	20.1	NE
5-t-Butyl-m-xylene	21.8	21.5	20.8	20.1	NE
4-t-Butyl-o-xylene	21.3	21.1	20.0	19.3	NE
5-t-Butyl-1,2,3-TMB	20.8	20.6	19.4	18.7	NE
Biphenyl	21.9	21.5	20.0	19.4	NE

^a Error $\pm 100 \text{ cm}^{-1}$. ^b Solvents : CH = cyclohexane; CT = carbon tetrachloride; CF = Chloroform; DCM = dichloromethane; AN = CH_3CN . ^c Theoretical polarity of the corresponding solvent according to eq 2.51 (F_3) ^d E = Exciplex emission detected; NE = No detectable exciplex emission.

For DBMBF₂ / substituted benzene exciplexes in cyclohexane, a plot of $h\nu_{\max}$ vs. $E_{\text{ox}} - E_{\text{red}}$ is shown in Figure 6.1 where the solid line is calculated from eq 6.1b. Figure 6.1 clearly shows that for the good electron donors, such as PMB, the observed exciplex fluorescence maxima follow eq 6.1b to within 0.05 eV. This demonstrates that these exciplexes have predominately CT character; therefore, the electronic coupling must be small. The exciplex dipole moments are therefore expected to be significantly greater than 10 D, whereas typical high CT exciplexes fall in the 12 to 14 D range [54,71]. For the electron donors xylenes to toluene, the observed exciplex maxima fall below the calculated CRIP line, hence these exciplexes are suspected to have diluted CT character according to eq 6.1c. Exciplexes with chlorobenzene to cyanobenzene electron donors are apparently independent of the redox potentials as suggested by the absence of a correlation with $E_{\text{ox}} - E_{\text{red}}$. The lack of any correlation with donor-acceptor redox potential is indicative of a nonpolar exciplex where a locally excited configuration(s) dominates the exciplex's nature (eq 2.29). It should be noted that the use of eqs 6.1 to evaluate the change in exciplex character for an electron donor series is only applicable in nonpolar solvents like cyclohexane, where the solvent influence on λ_{\max} is minimal (cf. eq 2.51).

In Figure 6.1, the singlet energy of DBMBF₂ in cyclohexane is represented by the horizontal line. The observed exciplex fluorescence maxima approach the E_S line monotonically then turn and run parallel to it. Following Chapter 2.3.2 the dilution of CT character for the exciplexes in the turning and parallel regions is due to the mixing of the locally excited configuration $|^*AD\rangle$ with the $|A^*D^+\rangle$ configuration since their energies are similar. Figure 6.1 and the discussion above are informative and purely qualitative, but indicative of what to expect from a more quantitative analysis.

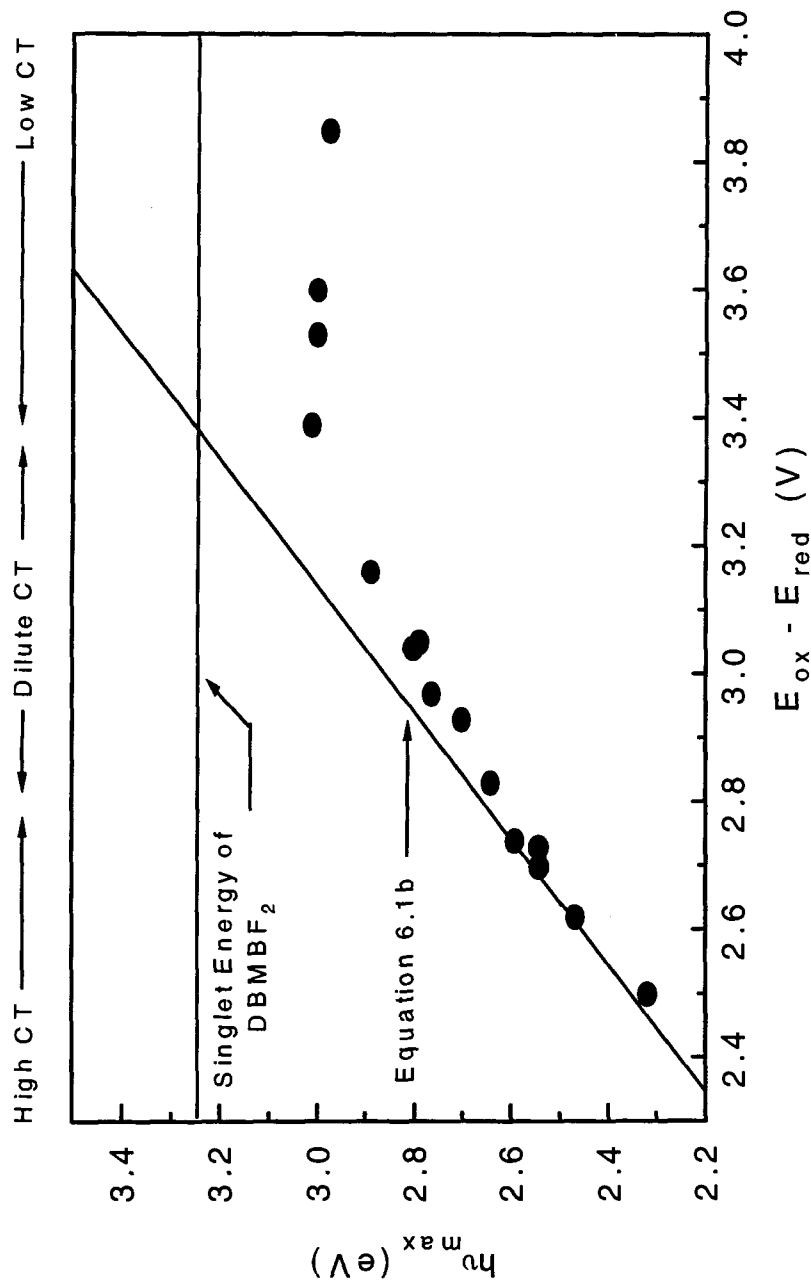


Figure 6.1: A Plot of the DBMBF₂ / Substituted Benzene Exciplex Fluorescence Maximum in Cyclohexane ($h\nu_{max}$) Against the Difference in the Redox Potentials of the Donor (E_{ox}) and Acceptor (E_{red}); E_{ox} values for Table 6.2. The Inclined Solid Line was Calculated According to eq 6.1b. The Horizontal Solid Line Represents the Singlet Energy of DBMBF₂ in Cyclohexane ($E_S = 3.24$ eV, Table 3.3).

The stronger electron donors in Table 6.1 are known to form EDA complexes (Chapter Four) in solution with DBMBF₂. Therefore, the corresponding exciplex emission would be expected to follow eq 6.1a and not 6.1b as observed (Figure 6.1); i.e., $h\nu_{\max}$ should be larger than the 0.10 eV error range. This failure suggests that the exciplex's Franck-Condon ground state donor-acceptor orientation is different from that of the corresponding EDA complex. This proposal will be further examined in Chapter Seven.

6.2.2 Solvatochromic Analysis

As discussed in Chapter Two, solvatochromic measurements require careful analysis in order to obtain a quantitative measure of the exciplex dipole moment. It was found that cyclohexane, carbon tetrachloride, chloroform, dichloromethane and acetonitrile give a linear plot of $F_3 = (\epsilon - 1) / (2\epsilon + 1) - (n^2 - 1) / (4n^2 + 2)$ against Dimroth and Reichardt's empirical polarity scale (E_N^T) [74] as shown in Figure 6.2. In addition, the refractive indices (relative dispersion interaction strength) are similar (1.42-1.44 [30a]), except for acetonitrile (1.3416 [30a]), thereby minimizing the influence of dispersion interactions. A more polar solvent than dichloromethane was necessary for the weakly solvatochromic exciplexes but a suitable solvent with a refractive index greater than 1.4 was not available; since acetonitrile is correlated with the other chosen solvents in Figure 6.2, it is assumed that the dispersion effects are somehow accounted for.

The slope, $2\mu_{\text{ex}} / \rho^3$, was evaluated from the exciplex emission solvatochromatic shift from eq 2.51 using the values in Table 6.1. In eq 2.51, the symbols are those described in Chapter 2.4. A representative plot of eq 6.1, using the corresponding values in Table 6.1, is shown by Figure 6.3. The quoted errors are standard deviations.

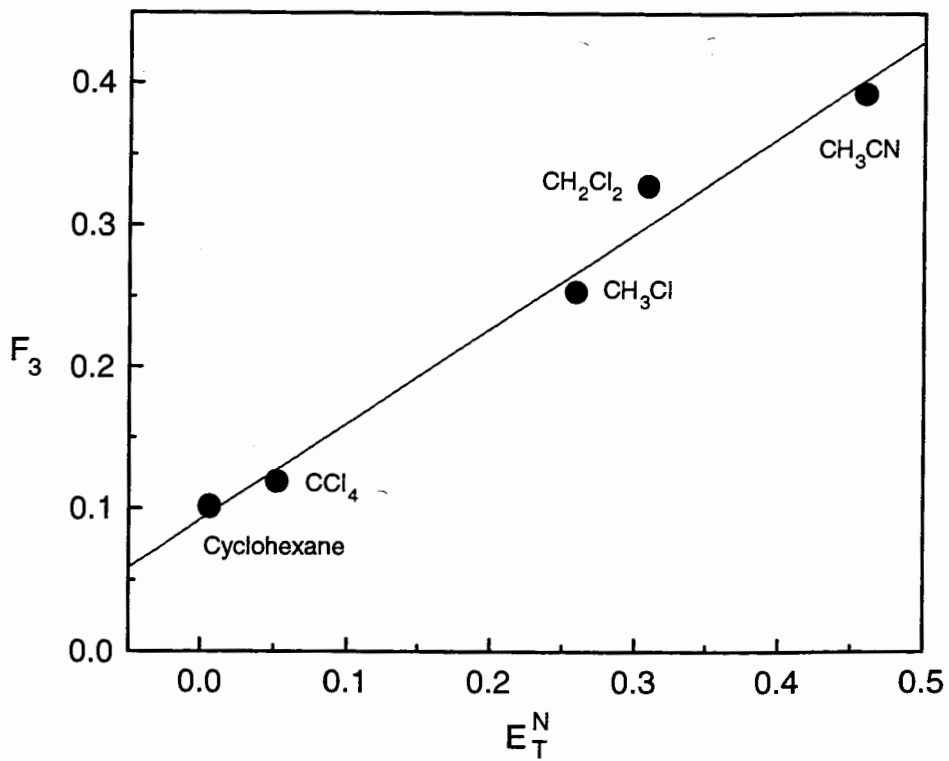


Figure 6.2: Plot of the Theoretical (F_3 , eq 2.11) Against Dimroth and Reichardt's Empirical Polarity Scale (E_T^N). The Solid Line is the Best Fit Through the 'Ideal' Solvents.

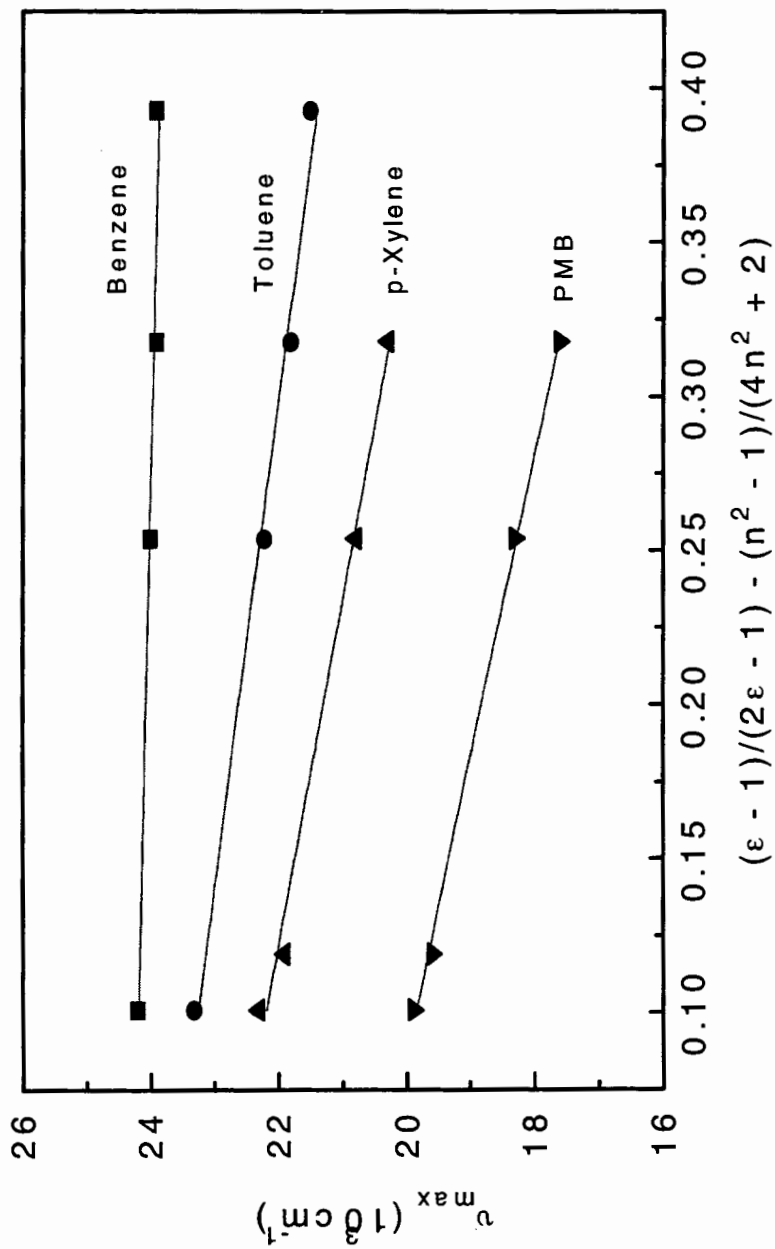


Figure 6.3: Representative Solvatochromic Plots (eq 2.51) for the DBMBF₂ / Substituted Benzene Exciplex Fluorescence with PMB, p-Xylene, Toluene and Benzene as Electron Donors.

$$h\nu_F = h\nu_F^0 - (2 / \rho^3) \mu_{ex}^2 F_3 \quad (2.51)$$

$$F_3 = (\epsilon - 1) / (2\epsilon + 1) - (n^2 - 1) / (4n^2 + 2)$$

To compute the exciplex dipole moment knowledge of the cavity radius, ρ , is necessary. Suppan has demonstrated that ρ can be reasonably estimated from the solute's molecular volume, V_M [130]. For exciplexes, the sum of the donor's and acceptor's ground state V_M are used in order to estimate ρ . Molecular volumes are readily calculated for liquids if the density is known. However, many of the benzene donors and DBMBF₂ are solids. This problem was circumvented by calculating the van der Waal's volume (V_{VDW}), using Edward's van der Waal increments [131], and enlarging this volume by 75 percent; the 75 percent factor was obtained from comparisons of V_M and V_{VDW} for those benzenes that are liquids at room temperature. The calculated V_M gave ρ values ranging around 5.5 Å (Table 6.2), which is a typical radius quoted for other exciplex systems. The values for ρ are assumed to be solvent independent in the absence of specific interactions (strong intermolecular interactions either contract or expand the solvent cavity [132]). Using the calculated ρ and the slope obtained by solvatochromic plots (Table 6.2) the exciplex μ_{ex} can be calculated easily from

$$\mu_{ex} = [(\text{slope} \times \rho^3) / (2 \times 5020.2)]^{1/2} \quad (6.2)$$

where the factor 5020.2 converts the terms under the square root to D. The calculated μ_{ex} values are reported in Table 6.2.

Inspection of Table 6.2 shows that the calculated DBMBF₂ / substituted benzene exciplex dipole moments (μ_{ex}) are sensitive to the electron donor's oxidation potential, from excimer-like (low μ_{ex}) to essentially CRIP like (13.3 D), over a narrow IP range of 1.7 eV. Comparison of the exciplex dipole moments in Table 6.2 and Figure 6.1 shows that

Table 6.2: DBMBF₂ / Benzene Exciplex Dipolar Nature

Donor	E _{ox} (V) ^a	IP (eV) ^a	Slope (cm ⁻¹) ^b	ρ (Å) ^c	μ _{ex} (D)	μ _{ex} ⁰ (D) ^d	% CT
Cyanobenzene	2.94 ^e	9.70	(-350 ± 350)	5.14	1.5 ± 1.5	1.1 ± 1.1	0 ~ 16
Methyl benzoate	2.69 ^e	9.34	-700 ± 200	5.14	3.0 ± 0.5	2.3 ± 0.4	17 ± 3
Benzene	2.62	9.23	-1100 ± 400	5.04	3.7 ± 0.7	2.9 ± 0.7	21 ± 5
Chlorobenzene	2.48 ^e	9.07	-2300 ± 400	5.12	5.5 ± 0.5	4.2 ± 0.5	30 ± 4
Toluene	2.25	8.82	-6300 ± 500	5.13	9.2 ± 0.4	7.1 ± 0.4	51 ± 3
o-Xylene	2.13	8.56	-7400 ± 900	5.21	10.2 ± 0.6	f	74 ± 4
m-Xylene	2.14	8.56	-7900 ± 300	5.21	10.5 ± 0.3	f	76 ± 2
p-Xylene	2.06	8.44	-8800 ± 700	5.21	11.1 ± 0.5	f	80 ± 4
Mesitylene	2.02	8.42	-6900 ± 500	5.29	10.1 ± 0.4	f	73 ± 3
1,2,4-TMB	1.92	8.27	-8900 ± 400	5.29	11.5 ± 0.3	f	83 ± 2
1,2,3,4-TMB	1.82	8.14	-9700 ± 1000	5.38	12.2 ± 0.6	f	88 ± 4

Table 6.2 (Continued)

Donor	E_{ox} (V) ^a	IP (eV) ^a	Slope (cm^{-1}) ^b	ρ (\AA) ^c	μ_{ex} (D)	μ_{ex}° (D) ^d	% CT
1,2,3,5-TMB	1.83	8.06	-9,900 \pm 800	5.38	12.4 \pm 0.5	f	90 \pm 4
Durene	1.79	8.05	-10,100 \pm 1200	5.38	12.5 \pm 0.7	f	91 \pm 5
PMB	1.71	7.92	-10,300 \pm 300	5.46	12.9 \pm 0.3	f	94 \pm 2
HMB	1.59	7.85	-10,200 \pm 700	5.54	13.3 \pm 0.5	f	96 \pm 4
t-Butylbenzene	2.21	--	-6,300 \pm 500	5.38	9.9 \pm 0.4	7.6 \pm 0.4	62 \pm 3
p-t-Butyltoluene	2.06	--	-9,300 \pm 1000	5.46	12.3 \pm 0.7	f	89 \pm 5
5-t-Butyl-m-xylene	2.02	--	-7,100 \pm 800	5.54	10.9 \pm 0.6	f	79 \pm 4
4-t-Butyl-o-xylene	1.92	--	-8,900 \pm 400	5.54	12.3 \pm 0.3	f	89 \pm 2
5-t-Butyl-1,2,3-TMB	1.83	--	-9,500 \pm 300	5.61	12.9 \pm 0.3	f	94 \pm 2
Biphenyl	--	--	-11,300 \pm 600	5.38	13.3 \pm 0.4	f	96 \pm 3

^a Schlessener, C.J.; Amatore, C.; Kochi, J.K. *J. Phys. Chem.* **1986**, *90*, 3747. ^b Determined from Plots of eq 2.51 (Figure 6.3) and

Errors are One Standard Deviation. ^c Calculated from the Sum of DBMBF₂ and Donor's Molecular Volume (See Text). ^d Estimated

Gas Phase Dipole Moment. ^e This Work. ^f See μ_{ex} Column.

when the $h\nu_{\max}$ is near the calculated line for a CRIP, the μ_{ex} is relatively large. In addition, the larger difference between the observed $h\nu_{\max}$ and that calculated from eq 6.1b is correlated with a smaller exciplex dipole moment.

The exciplex dipole moment for the DBMBF₂ / cyanobenzene exciplex could not be determined by solvatochromic methods due to the exciplex emission insensitivity with respect to solvent polarity. This insensitivity does indicate that this exciplex's dipole moment is small. An estimate of the μ_{ex} range is possible: the error in determining λ_{\max} is ± 2 nm, which represents an error of ± 100 cm⁻¹ for a ν_{\max} of about 24,000 cm⁻¹. Therefore, the emission maximum can be as large as 24,100 cm⁻¹ in cyclohexane and as small as 23,900 cm⁻¹ in acetonitrile; this gives a slope of - 700 cm⁻¹ according to eq 2.51, which represents the maximum possible $2 \mu_{\text{ex}} / \rho^3$, but the actual value must lie within the range from zero to - 700 cm⁻¹. Therefore, the DBMBF₂ / cyanobenzene exciplex is assigned a dipole moment of 1.5 ± 1.5 D.

6.2.3 Solvent Effect on Exciplex CT Character

The solvatochromic model in Chapter Two was derived on the basis of a non-polarizable dipole, which is a good assumption for contact radical ion pairs. For exciplexes with medium and low charge transfer character, this assumption is most certainly unrealistic. Less than full charge transfer exciplexes should be polarized by the solvent, due to the reaction field set up by the solvent that opposes the electrical field generated by the exciplex's dipole moment. Such polarization by the reaction field has been experimentally demonstrated for exciplexes [133] and leads to an enlargement of the exciplex dipole moment. For benzene donors such as benzene and toluene, we expect their exciplex dipole moments with DBMBF₂ to be solvent dependent, it follows that their μ_{ex} values (Table 6.2) are mean values.

On the basis of electrostatics, the gas phase exciplex dipole (μ_{ex}°) is related to the dipole in solution by

$$\mu_{\text{ex}} = \mu_{\text{ex}}^{\circ} / (1 - f\alpha_{\text{ex}}) \quad (6.3)$$

where α_{ex} is given by

$$\alpha_{\text{ex}} = \rho^3 (D_{\text{in}} - 1) / (D_{\text{in}} + 2) \quad (6.4)$$

μ_{ex}° represents the exciplex dipole moment in the gas phase and $f = \rho^3 (\epsilon - 1 / 2\epsilon + 1)$. The expression for α_{ex} represents the isotropic polarizability of the exciplex where D_{in} is the dielectric constant inside the solvent cavity. For contact radical ion pairs it is usually assumed that they are non-polarizable hence $D_{\text{in}} \approx 1$ and $\alpha_{\text{ex}} \approx 0$; therefore, the original solvatochromic expression is valid. Brunshwig et al. have argued that for polarizable systems the D_{in} should be approximately $n^2 (\cong 2)$ on the basis that the reorientation of the solute's dipole is damped but the valence electrons will be capable of following (polarization) the change in electric potential field [80]. Substituting n^2 for D_{in} into eqs 6.3 and 6.4 we obtain eq 6.5 after some rearranging.

$$\mu_{\text{ex}} = \mu_{\text{ex}}^{\circ} \frac{(2\epsilon + 1)(n^2 + 2)}{(2\epsilon + n^2) \cdot 3} = \mu_{\text{ex}}^{\circ} \phi(\epsilon, n^2) \quad (6.5)$$

This is the same result obtained by Böttcher in his discussion on the reaction field of a polarizable dipole [75]. In eq 6.5, the polarization term, $\phi(\epsilon, n^2)$, will be always greater than one; eq 6.5 predicts that the solvent will induce a 10 to 30 percent enlargement of the exciplex dipole moment. This is in agreement with that found by Baumann and co-workers [133]. Substituting eq 6.5 into 2.11 gives

$$h\nu_F = h\nu_F^{\circ} - (2 / \rho^3) (\mu_{\text{ex}}^{\circ})^2 F_4 \quad (6.5b)$$

$$F_4 = \frac{(2\varepsilon + 1)^2 (n^2 + 2)^2}{9 (2\varepsilon + n^2)^2} \left[\frac{(\varepsilon - 1)}{(2\varepsilon + 1)} - \frac{(n^2 - 1)}{(4n^2 + 2)} \right]$$

Plotting F_4 against F_3 (not shown) for the solvents used in this study gives a rather good linear relationship with a slope of 1.68. This indicates that the observed mean μ_{ex}^2 values is 68 percent larger than $(\mu_{\text{ex}}^{\circ})^2$, thus μ_{ex}° can be calculated. The estimate of μ_{ex}° better reflects the donor-acceptor interaction. The solvent influence on μ_{ex} will be further examined in Chapter Nine.

6.2.4 Exciplex Wavefunction and Frontier Orbitals

As discussed in Chapter Two, the relationship between exciplex μ_{ex} and the donor's electron donating ability can be discerned from a plot of μ_{ex}° vs. the HOMO gap (Figure 6.4), which is represented by the difference in the ionization potential (IP); for the stronger electron donors the μ_{ex} values are used. This figure shows a sigmoidal curve where μ_{ex}° asymptotically approaches a maximum value of 13.8 ± 0.5 D. This value represents the μ_{ex}° for a DBMBF₂ / benzene CRIP. The dashed curve is the best fit through the data points that illustrate the sigmoidal relationship (vide infra). The DBMBF₂ / substituted benzene exciplex μ_{ex}° trend in Figure 6.4 resembles the sigmoidal curve in Figure 2.6 (Chapter 2.3.2) where a hypothetical exciplex CT character was simulated by modulating the HOMO energy gap. This similarity is due to the fact that the HOMO levels of benzene donors lie above (HMB, IP = 7.85 eV) and below (cyanobenzene, IP = 9.70 eV) relative to DBMBF₂'s (est. IP of 9.0 eV; E_{ox} is approximately that of chlorobenzene). This is illustrated in Figure 6.5 where the redox potentials were used to give a relative ordering of the HOMO energy levels where a and d represent the MOs of the acceptor and donor, respectively; the (') represents the LUMO. This figure displays three situations

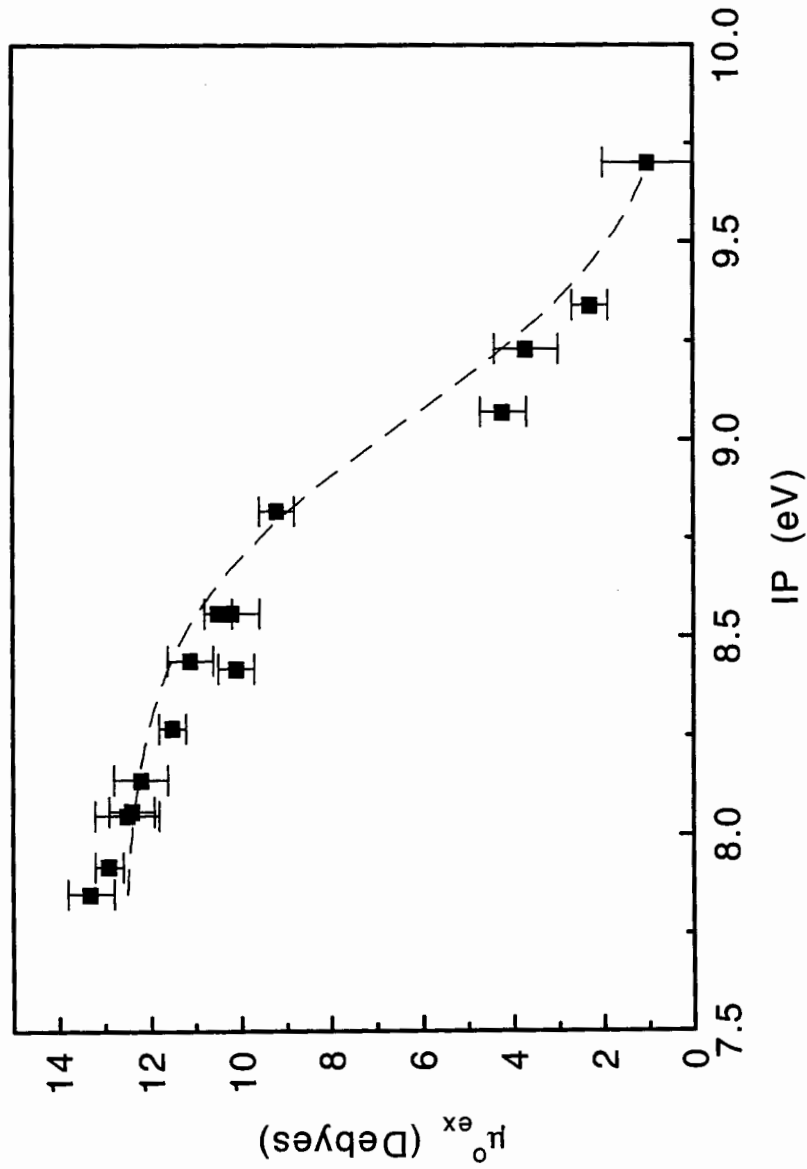


Figure 6.4: Relationship Between the Observed and Estimated Gas Phase Exciplex Dipole Moment and the Donor's Ionization Potential. The Dashed Line Represents the Best Fit of Equations 2.36 and 2.37 with an Overlap Integral Value of 0.037.

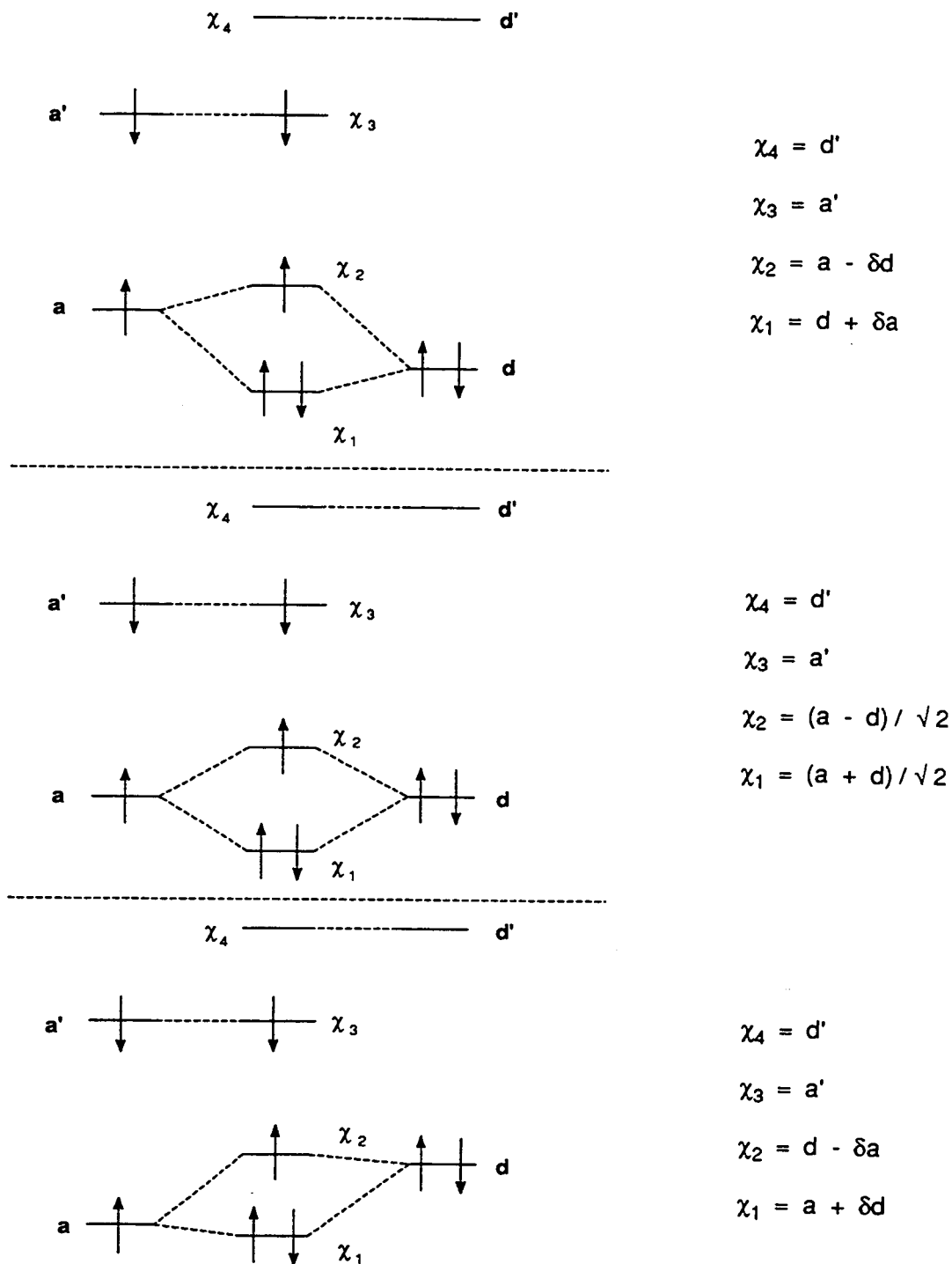


Figure 6.4: Frontier Orbital Interpretation of Variable Exciplex Dipolar Character. The Acceptor MO's are Denoted by **a** and the Donor by **b** where the Prime (') Denotes the LUMO.

where the HOMO of the electron donor is below, equal to and higher than DBMBF₂'s HOMO. The HOMO-HOMO interaction (LUMO-LUMO interactions are ignored (vide infra)) results in two new supermolecular orbitals and establishes a weak donor-acceptor bond; the new MOs, χ_1 and χ_2 , are defined on the right-hand side of Figure 6.5 in terms of a and d MOs. In the situation where the donor's HOMO lies below that of DBMBF₂ (Figure 6.5I), χ_1 is mostly characterized by d with a perturbational contribution from a; small amount of electron density is polarized towards the acceptor (small μ_{ex}^0). Figure 6.5II shows the isoelectronic case where the three electrons in χ_1 and χ_2 are shared equally between the donor and acceptor, the exciplex dipole moment is expected to be one half of that for complete electron transfer. Figure 6.5III shows the situation where electron donation is an exothermic process and χ_1 is mostly characterized by a whereas χ_2 is mostly characterized by d. The net result is nearly complete electron transfer and a large exciplex dipole moment is expected. Examples for each of these cases would be DBMBF₂ / HMB (Figure 6.5III), DBMBF₂ / chlorobenzene (Figure 6.5II) and DBMBF₂ / cyanobenzene (Figure 6.5I).

As a first order approximation, the minimum DBMBF₂ / benzene exciplex wavefunction basis set can be described by

$$\Psi_{\text{EX}} = a |A^*D^+\rangle + c |A^*D\rangle \quad (2.30)$$

LUMO-LUMO interaction, hence the $|A^*D^+\rangle$ and $|A^*D\rangle$ terms, is neglected (vide infra). In Chapter Two the calculation of U_{Stab} indicated that for the interaction of two configurations is negligible if their energy difference is greater than 1 eV. Based on this and that the closest approach of DBMBF₂'s and benzene donor's LUMO is at best 1.4 V (for benzenes, $E_{\text{red}} = -2.3 - 2.6$ V, and DBMBF₂, $E_{\text{red}} = -0.91$ V, Table 3.4), the LUMO-LUMO interaction is negligible. In addition, the HOMO-HOMO interaction becomes weak at an energy gap of 0.8 V (DBMBF₂ / HMB exciplex), which is nearly one half the the smallest LUMO energy

gap (vide supra). The $|A^+D^- \rangle$ and $|A^*D \rangle$ terms are finite, however, their presence can not be probed by solvatochromic methods. The contribution of the no-bond configuration $|AD \rangle$ is also believed to be negligible on the basis that eq 6.1b is satisfied.

A clear test of the simple exciplex wavefunction shown by eq 2.30 can be illustrated if the equations developed in Chapter Two (eqs 2.31 to 2.40) can be fitted to the observed exciplex dipole moments (Table 6.2). The solid line in Figure 6.4 represents the best weighted fit to the observed μ_{ex}^o , with a S of 0.037 (see experimental), where the μ_{ex}^o 's around IP of 9.0 eV were given more weight since these values are the most sensitive to HOMO gap variations. This value for S represents an averaged value. The fit is surprisingly good using a fixed overlap. Therefore, the exciplex wavefunction given by eq 2.30 qualitatively fits the observed data (vide supra). Alternatively, the same equations can be fitted to the observed exciplex dipole moments in Figure 6.4, where the overlap integral S is used as a fitting parameter.

There are notable deviations in Figure 6.4. The DBMBF₂ / mesitylene exciplex μ_{ex} is well below the dashed line. The smaller μ_{ex}^o value for this exciplex indicates an increased $|A^+D^+ \rangle \leftrightarrow |^*AD \rangle$ interaction than indicated for a S of 0.037. The μ_{ex}^o for the DBMBF₂ / HMB exciplex is larger, hence S may be smaller than 0.037 in this case. This is reasonable since HMB is the most sterically hindered benzene of the methyl alkyl benzenes (if one varies the S fitting parameter, the calculated and observed μ_{ex}^o are in agreement with S = 0.022). The averaged value for S is quite reasonable for exciplexes. If there were a mismatch of the interacting orbitals and nodes, the overlap integral S would be small; i.e., for structurally dissimilar donor and acceptor. For comparison, Beens and Weller have calculated values for S ranging from 0.014 for the aniline / anthracene exciplex (dissimilar) to 0.046 for the naphthalene / 2-cyanonaphthalene exciplex (similar) [71d]. The averaged S value of 0.037 implies reasonable orbital matching between the HOMOs of DBMBF₂ and the benzene donors.

The comparison of the exciplex $h\nu_{\max}$ for hindered and unhindered benzenes as donors shows little variation in all the solvents used, hence the slopes determined by the solvatochromic equation 2.51 will be the same. The difference in the computed exciplex dipole moment is a result of the differences in the solvent cavity radius upon replacement of a methyl for a t-butyl substituent. This coincidence suggests that the procedure used in estimating the cavity radius artificially changes the exciplex dipole moment. However, the work of Suppan [130] and evidence discussed later in Chapter Nine provide a clear indication that the observed dipole moments are reasonable estimates of the extent of charge transfer for the exciplexes with hindered benzenes as donors. The larger exciplex dipole moments observed with hindered benzene donors are attributed to steric hindrance. The reduction in the orbital overlap reduces the $|A^+D^- \rangle \leftrightarrow |A^*D \rangle$ resonance and results in a larger dipole moment (cf. Figure 2.6). This is consistent with the estimate of S for the DBMBF₂ / HMB exciplex of 0.022. This exciplex is the most hindered of the methyl benzene donor exciplexes and thus has a much smaller S value than the average $S = 0.037$.

6.2.5 β -Diketonatoboron Complex and Exciplex CT Character

The exciplex dipolar character between singlet excited DBMBF₂ and substituted benzenes has been shown above to be dependent on the donor's electron donation ability. In this section, the donor is held constant and the electron acceptor is varied in an effort to evaluate the role of the electron acceptor.

p-Xylene was used as the electron donor in the search for exciplex emission with other β -diketonatoboron complexes. p-Xylene was chosen because that it gives a polar exciplex with DBMBF₂ that contains a significant locally excited configuration contribution and because it is a liquid at room temperature. The latter point is important since exciplexes with acetylacetonatoboron complexes are weakly fluorescent, hence p-xylene

was used as a solvent to maximize exciplex fluorescence intensity. In addition, β -diketonatoboron complex fluorescence is assumed to be completely quenched. Table 6.3 lists the observed exciplex emission maxima.

The observed exciplex emission maxima are plotted against the difference in the redox values (Table 3.4) according to eq 6.6, Figure 6.5 [54,71b-d].

$$h\nu_{\max} = m (E_{\text{ox}} - E_{\text{red}}) + \text{Constant} \quad (6.6)$$

Note that equation 6.6 is the generic form of eq 6.1b. Figure 6.5 shows that the β -diketonatoboron complexes fall into three groups based on the identity of the β -diketonate ligand. The apparent independent slopes are also listed in Table 6.3.

Weller's group and others have indicated that the slopes of plots such as shown in Figure 6.5 can be interpreted as the fraction of charge transfer within the exciplex [54,71b-d]. This interpretation is consistent with Figure 6.1 and the earlier discussion in Chapter 6.2.1. However, it is clear that this interpretation requires the charge transfer contribution within the exciplex to be similar otherwise the slope should be continually changing (cf. Figure 6.1). For example, the DBM β -diketonate / *p*-xylene exciplexes are expected to have similar charge transfer character based on their nearly identical HOMO energy levels (Table 3.4). To check this interpretation of the slope, m , of eq 6.6, comparison with experimental exciplex dipole moments of one of the donor-acceptor pairs in each group is necessary. The dipole moment of the exciplex formed with DBMBF₂ as acceptor was evaluated above (Table 6.2) and those for BABF₂ and AABF₂ as electron acceptors are evaluated in Table 6.4.

The reasonable agreement between $\mu_{\text{ex}} / 13.8 \text{ D}$ and the slope m (Table 6.5) provides support for the interpretation of m representing the degree of exciplex charge transfer character. A reasonable agreement between $\mu_{\text{ex}} / 13.8 \text{ D}$ and the slope m was expected since the cavity radius, ρ , variation with different electron acceptor molecular

Table 6.3: β -Diketonatoboron / p-Xylene Exciplex Fluorescence Maximum in neat p-

Xylene

Compound	$E_{\text{ox}} - E_{\text{red}}^{\text{a}}$ (Volts)	$h\nu_{\text{max}}$ (eV)	Eq 6.6 slope ^b
AABF ₂	3.54	2.89	
AABM	3.29	2.58	1.15 ± 0.10
AABO	3.21	2.52	
BABF ₂	3.19	2.70	
BABM	2.95	2.53	0.74 ± 0.10
BABO	2.86	2.47	
DBMBF ₂	2.97	2.64	
DBMBM	2.76	2.47	0.77 ± 0.10
DBMBO	2.70	2.43	

^a E_{red} from Table 3.4 and E_{ox} of p-Xylene (2.06 V vs.

SCE) from Schlesener, C.J.; Amatore, C.; Kochi, J.K. *J. Phys.*

Chem. **1986**, *90*, 3747. It is assumed that the redox difference

determined in acetonitrile is the same in any other solvent. ^b

Error in slope m is one standard deviation.

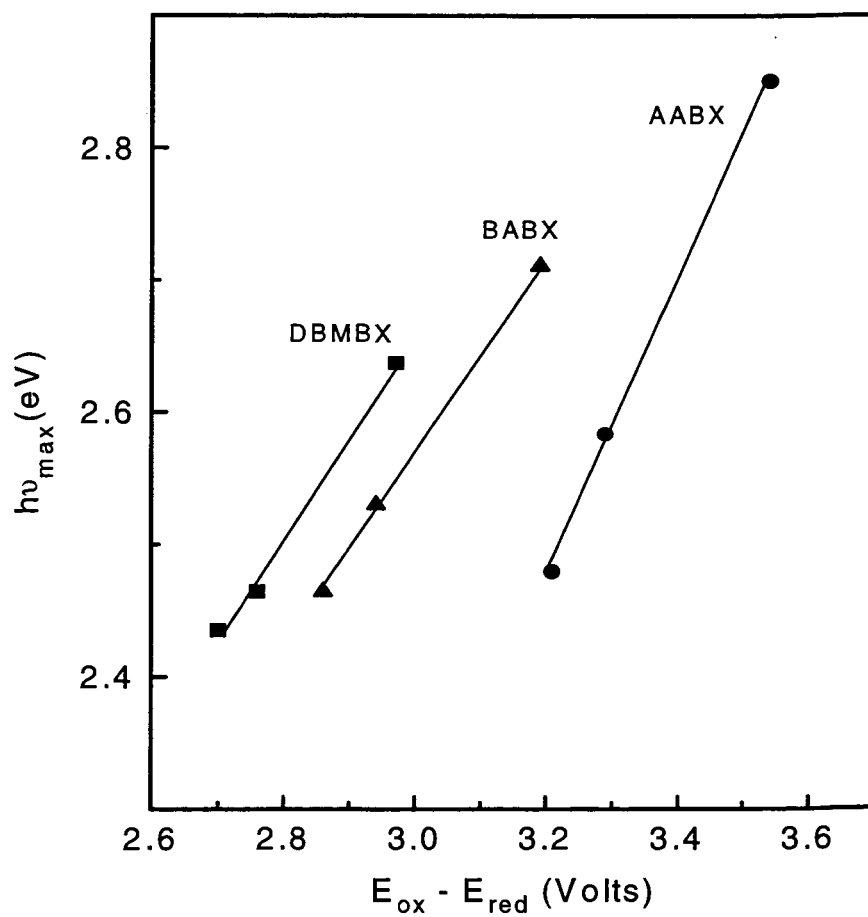


Figure 6.6: Correlation of Exciplex Fluorescence Maximum with Redox Potentials in p-Xylene. X Represents F, Oxalyl and Manonyl Ligands. Data from Table 6.3.

volumes also affects the exciplex emission maximum (cf. eq 2.51). However, correction for ρ does not change the conclusion, hence this correction was not applied to the experimental $h\nu_{\max}$.

This agreement between $\mu_{\text{ex}} / 13.8 \text{ D}$ and the slope m is a consequence of the HOMO (E_{ox} potentials) remaining constant regardless of the counter ligand (e.g., fluoride vs. oxaly); cf. Figure 6.4). The increase in exciplex charge transfer character from DBM to AA β -diketonate ligand can be rationalized as a result of the increase in the HOMO-HOMO energy gap (0.39 V for the DBMBF₂ / p-xylene pair and 0.82 V for the AABF₂ / p-xylene pair) that reduces the extent of $|A^*D^+\rangle \leftrightarrow |^*AD\rangle$ electronic mixing. The similar HOMO-HOMO energy values for DBMBF₂ / p-xylene and BABF₂ / p-xylene exciplexes are manifested by similar μ_{ex} values.

6.2.6 Final Comments

Unfortunately, the results in this chapter do not provide information on the orientation of the donor over the acceptor's π system. If DBMBF₂ / olefin exciplexes exist, the 2+2 photocycloaddition products obtained from the reaction between singlet excited DBMBF₂ and olefin [32] infers the donor lies near the chelated ring. The relative orientation of donor and acceptor can be demonstrated intramolecularly: the donor can be attached to one of DBMBF₂'s phenyl rings by an alkyl chain that imposes geometrical restrictions on the donor relative orientation. For example, a three carbon alkyl chain restricts the interaction between the donor and DBMBF₂'s phenyl ring. Similar exciplex emission from the intra- and intermolecular exciplexes supports the notion that the donor-acceptor orientation is similar. Therefore, the intermolecular exciplexes the donor-acceptor orientation can be proposed.

Table 6.4: DBMBF₂, BABF₂ and AABF₂ / p-Xylene Exciplex Emission Maxima in Various Solvents: Influence of Acceptor^a

Acceptor	Exciplex Emission ν_{\max} (10^3 cm^{-1})				Slope (cm^{-1})	μ_{ex} (D) ^b
	CH	CT	CF	DCM		
	0.101 ^c	0.119	0.254	0.318		
DBMBF ₂	22.3	21.9	20.8	20.3	-8800 ± 700	11.1 ± 0.5
BABF ₂	23.3	22.9	21.4	20.8	-11300 ± 900	11.6 ± 0.5
AABF ₂	25.0	24.6	22.4	NE	-16700 ± 1000	12.8 ± 0.8

^a See comments of Table 6.1 for symbol definitions. ^b ρ values with each acceptor are: DBMBF₂ ($\rho = 5.21 \text{ \AA}$); BABF₂ ($\rho = 4.93 \text{ \AA}$); AABF₂ ($\rho = 4.61 \text{ \AA}$).

Table 6.4: Comparison of Exciplex Charge Transfer Fraction Obtained from Solvatochromic Analysis and the Slope in Figure 6.5

BF ₂ Complex	$\mu_{\text{ex}} / 13.8 \text{ D}$	m (eq 6.6)
DBMBF ₂	0.80 ± 0.08	0.77 ± 0.10
BABF ₂	0.84 ± 0.08	0.74 ± 0.10
AABF ₂	0.93 ± 0.06	1.15 ± 0.10

CHAPTER SEVEN

EXCIPLEX BINDING ENERGY IN CYCLOHEXANE

7.1 Introduction and Mathematical Formulae

7.1.1 General

In Chapter Six it was stated that the degree of exciplex emission red-shift from singlet excited DBMBF₂ fluorescence is dependent on the donor's electron donating ability (Figure 6.1). However, the exciplex emission maximum is also dependent on other factors. This is illustrated by the energy cycle shown in Figure 7.1 where the separated ground state donor and acceptor molecules serve as an energy reference point [65,70]. The donor-acceptor system is prepared with an initial energy content of E_S ; i.e., the singlet energy of either the donor or acceptor. Exciplex formation releases part of this energy ($-\Delta H_{ex}$) to the environment thus the internal energy of the exciplex becomes

$$E_{EX} = E_S - \Delta H_{ex} \quad (7.1)$$

relative to the separated ground state donor and acceptor. After radiative or radiationless decay the Franck-Condon ground state complex may have either a positive (repulsive) or negative (attractive) energy content (R_E). The energy cycle is quantified by eq 7.2.

$$E_S = |\Delta H_{ex}| + h\nu_{max} + R_E \quad (7.2)$$

From eqs 7.1 and 7.2 it can be shown that the exciplex binding and emission energies are related by

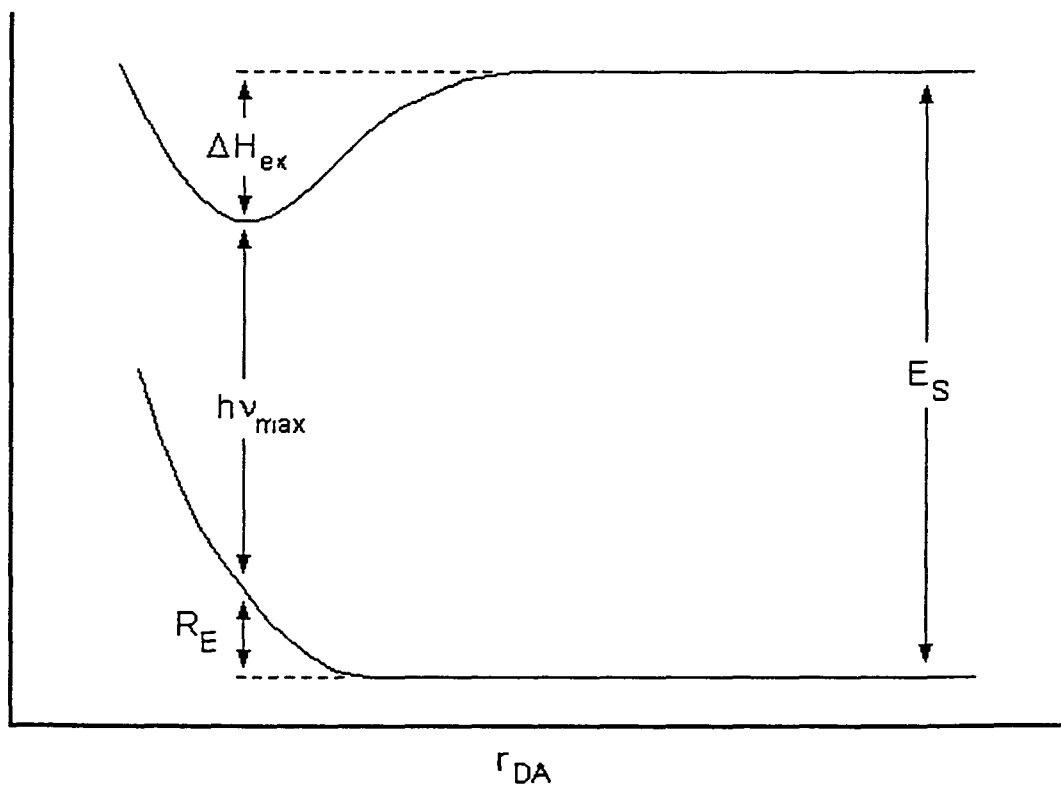


Figure 7.1: Potential Energy Scheme for Excited State Complexes (Exciplexes and Excimers) as a Function of Donor - Acceptor Distance.

$$E_{EX} = E_S - |\Delta H_{ex}| = hv_{max} + R_E \quad (7.3)$$

For a number of highly polar exciplex systems Weller's group has determined R_E to be approximately constant with a value of 0.28 ± 0.10 eV in n-hexane [54,66,70,71,73,134]. Therefore, semiquantitatively the exciplex emission maximum (hv_{max}) provides information regarding the exciplex's binding energy (ΔH_{ex}) for a set of structurally similar donor-acceptor systems in a single solvent (i.e., comparisons can not be done between solvents due to solvatochromic effects) if the Franck-Condon ground state energy, R_E , is assumed.

Since the pioneering work of Weller's group [38,54,64,70,71,73,77], Mataga's group [66,135] and others [136], charge transfer interactions have been considered the dominant driving force for exciplex formation where the exciplex energy is closely related to the redox potentials by the semi-empirical relationship shown below [54,70,71,73].

$$\begin{aligned}
 E_{EX} &= E_{CRIP} + \text{Perturbation Term} \\
 &= \underbrace{E_{ox} - E_{red} + 0.15 \text{ eV}}_{E_{CRIP}} + \underbrace{(U_{Dest} - U_{Stab})}_{\text{Perturbation Term}} \quad (7.4)
 \end{aligned}$$

The symbols in eq 7.4 are those discussed in Chapter Two and the constant 0.15 eV was determined empirically. Implicit in eq 7.4 is that steric effects are relatively constant regardless of the donor and acceptor and that charge transfer is the dominant interaction between the donor and acceptor [54,70]. The perturbing term encompasses the destabilization from interaction with the ground state surface (U_{Dest}) and stabilization from interactions with a locally excited configuration (U_{Stab}). Comparison of eqs 7.3 and 7.4 shows that the relationship between exciplex emission and redox values is [54,70,71,73]

$$hv_{max} = E_{ox} - E_{red} + U_{Dest} - U_{Stab} - R_E + 0.15 \text{ eV} \quad (7.5)$$

Equation 7.5 is the basis for eq 6.1 discussed in Chapter Six

In this work, the degree of the exciplex emission red-shift is correlated to the electron donating ability of the benzene donor (Chapter Six). For electron-poor benzenes as donors the unresolved (or poorly resolved) DBMBF₂ and exciplex emission (Figure 5.1a) suggests a small binding energy. For the more electron-rich benzenes as donors (Figure 5.1b), the resolved DBMBF₂ / exciplex emissions suggest a stronger binding energy. In addition, this trend in exciplex binding energies with the position of the exciplex emission is correlated with the exciplex charge transfer character. The variable charge transfer character of DBMBF₂ / substituted benzene exciplexes provides an opportunity to investigate the driving forces for exciplex formation.

7.1.2 Formulae for the Determination of Exciplex Binding Energies

Scheme 5.2 provides the nucleus of the method that can be used to determine the exciplex binding energy under steady state conditions (usually termed photostationary condition [65]); i.e., the sample was under constant illumination, hence the singlet excited DBMBF₂ concentration is independent of time. The photostationary condition is valid only if no significant photoreaction(s) occur during the experiment where the DBMBF₂ or donor concentrations become depleted. On the basis of Scheme 5.2 under photostationary conditions it can be shown that the ratio of the exciplex and DBMBF₂'s fluorescence quantum yields is given by eq 7.6 [65,134,137].

$$I_{\text{ex}} / I_{\text{A}} \propto \Phi_{\text{ex}} / \Phi_{\text{A}} = (k_{\text{f}}^{\text{ex}} / k_{\text{f}}) \{k_{\text{ex}} / (k_{\text{-ex}} + k_{\text{f}}^{\text{ex}} + k_{\text{nr}}^{\text{ex}})\} [\text{D}] \quad (7.6)$$

I_{ex} (Φ_{ex}) and I_{A} (Φ_{A}) represent the exciplex and DBMBF₂ fluorescence intensities (quantum yields), respectively. The rate constants shown are those described in Scheme 5.2. Note that eq 7.6 is the basis for eq 5.1 used to determine exciplex stoichiometry.

The binding energy of an exciplex formed between singlet excited DBMBF₂ and the electron donor can be determined using eq 7.6 under the conditions that the exciplex is fluorescent and the reaction is reversible. If the exciplex dissociation rate constant is significantly larger than the exciplex decay rate constants, $k_{-ex} \gg k_f^{ex} + k_{nr}^{ex}$, exciplex formation is said to be reversible [65,134,137]. Under this condition eq 7.3 is reduced to a more simplified form as shown by eqs 7.7 and eq 7.8.

$$\begin{aligned} I_{ex} / I_{\cdot A} &\propto \Phi_{ex} / \Phi_{\cdot A} = (k_f^{ex} / k_f) (k_{ex} / k_{-ex}) [D] \\ &= (k_f^{ex} / k_f) \exp(-\Delta G_{ex} / RT) [D] \end{aligned} \quad (7.7)$$

$$\ln (I_{ex} / I_{\cdot A}[D]) = -\Delta H_{ex} / RT + \text{Constant} \quad (7.8)$$

The underlining assumption for eqs 7.7 and 7.8 is that the fluorescence rate constants of DBMBF₂ and its exciplex (k_f and k_f^{ex} , respectively) are temperature independent; for other exciplex systems k_f^{ex} has been found to have at best a weak temperature dependence that can be neglected over a temperature range of 50 °C [138].

Plots of eq 7.8 [$\ln (I_{ex} / I_{\cdot A}[D])$ vs. $1 / T$] show three distinctive regions as demonstrated in Figure 7.2 [65,134]. Region A corresponds to the reversible exciplex formation condition, $k_{-ex} \gg k_f^{ex} + k_{nr}^{ex}$, where the slope is proportional to $-\Delta H_{ex} / R$. Region B corresponds to an intermediate region where $k_{-ex} \approx k_f^{ex} + k_{nr}^{ex}$. Region C corresponds to the irreversible exciplex formation, $k_{-ex} \ll k_f^{ex} + k_{nr}^{ex}$, where eq 7.8 is not followed and the slope is proportional to the activation energy for viscous flow of the solvent [65,137].

Typically, plots of eq 7.8 that show region A behavior have been presented as evidence for reversible exciplex formation [65,134]. However, Selinger and co-workers [137] have argued that region A behavior can be achieved under the conditions that k_{-ex} is not significantly larger than $k_f^{ex} + k_{nr}^{ex}$ and that the calculated absolute enthalpy value will

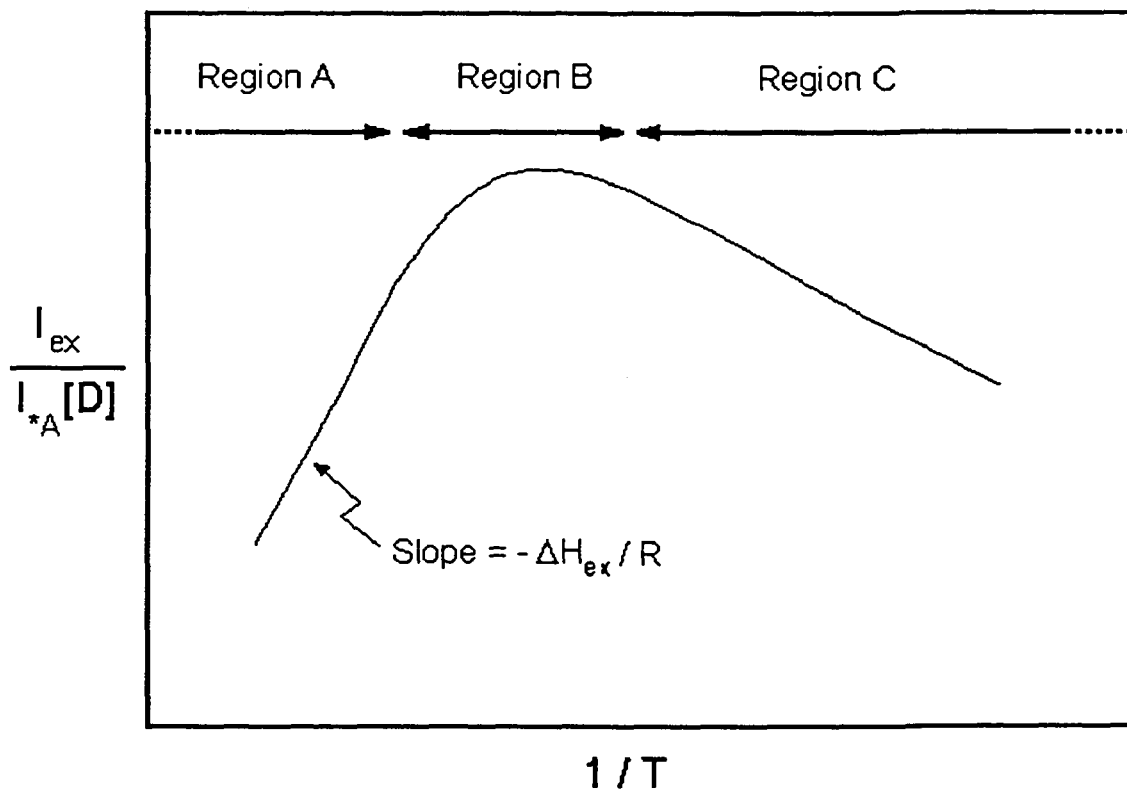


Figure 7.2: Illustration of the Change in the Exciplex / *A Fluorescence Intensities for an Exciplex Passing from a Reversible to an Irreversible Reaction.

be smaller than the 'true' value. Selinger and co-workers have suggested that perturbing the steady state concentration [*AD] with a small addition of another quencher Q can demonstrate reversibility. This perturbing quencher is usually molecular oxygen. For reversible exciplex formation, the exciplex dissociation rate constant is usually very large ($k_{-ex} > 10^9 \text{ s}^{-1}$) and typically dominates the other exciplex decay processes ($k_f^{ex} + k_{nr}^{ex}$). The addition of a small amount of oxygen (i.e., aerated solution where $[O_2]$ is typically 10^{-3} M) will increase the overall exciplex decay rate by $10^7 - 10^8 \text{ s}^{-1}$ ($= k_{diff}[O_2]$) hence the steady state *AD concentration will not be significantly perturbed. The effect of oxygen to perturb the steady state *AD concentration can be shown to be quantified by eq 7.9 [139].

$$\left(\frac{I_{ex}^o}{I_{ex}} \right) / \left(\frac{I_{A}^o}{I_{A}} \right) = 1 + k_{diff} \tau_{ex}^* [O_2] \quad (7.9)$$

where $\tau_{ex}^* = (k_{-ex} + k_f^{ex} + k_{nr}^{ex})^{-1}$

The fluorescence intensities, I_{ex} and I_A , are those described above where the superscript 'o' represents the fluorescence intensity in the absence of oxygen. The ratio I_{ex}^o / I_{ex} represents the effect of oxygen on the steady state [*AD] where the I_A^o / I_A ratio removes the influence of oxygen quenching on *A . From eq 7.9 we will have two ideal situations

$$\begin{aligned} \left(\frac{I_{ex}^o}{I_{ex}} \right) / \left(\frac{I_A^o}{I_A} \right) &= 1 && \text{if } k_{-ex} \gg k_f^{ex} + k_{nr}^{ex} \\ \left(\frac{I_{ex}^o}{I_{ex}} \right) / \left(\frac{I_A^o}{I_A} \right) &> 1 && \text{if } k_{-ex} \ll k_f^{ex} + k_{nr}^{ex} \end{aligned}$$

Therefore, simultaneous observation of a plot of eq 7.8 corresponding to region A (Figure 7.2) and $(I_{ex}^o / I_{ex}) / (I_A^o / I_A) = 1$ persuasively suggests reversible exciplex formation [140].

7.2 Results and Discussion

7.2.1 Exciplex Binding Energy

The enthalpy of DBMBF₂ / substituted benzene exciplex formation was evaluated by monitoring the variation with temperature of the exciplex / DBMBF₂ fluorescence intensity ratio, monitored at 550 and 390 nm, respectively, according to eq 7.8. An illustrative example of the change in fluorescence intensities with temperature is shown in Figure 7.3. From such spectra, plots based on eq 7.8 were constructed. Representative examples are shown in Figure 7.4 where the three regions discussed in the introduction are illustrated; i.e., the reversible, intermediate and irreversible regions (cf. Figure 7.2). Figure 7.4a represents the reversible ($k_{\text{ex}} \gg k_f^{\text{ex}} + k_{\text{nr}}^{\text{ex}}$) case where the slope is positive. Figure 7.4b and 7.4c represent the intermediate case ($k_{\text{ex}} \approx k_f^{\text{ex}} + k_{\text{nr}}^{\text{ex}}$) and Figure 7.4d represents the irreversible case ($k_{\text{ex}} \ll k_f^{\text{ex}} + k_{\text{nr}}^{\text{ex}}$).

The suggestion of Cohen and Selinger [137] was adopted to confirm that k_{ex} was indeed significantly larger than $k_f^{\text{ex}} + k_{\text{nr}}^{\text{ex}}$; i.e., the oxygen test. The oxygen test (Table 7.1) is listed as positive (+) if $(I_{\text{ex}}^0 / I_{\text{ex}}) / (I_{\text{A}}^0 / I_{\text{A}}) = 1$ otherwise negative (-) if there was a detectable effect on this ratio (eq 7.9); in addition, the observed ratio (see experimental),

$$(I_{\text{ex}}^0 / I_{\text{ex}}) / (I_{\text{A}}^0 / I_{\text{A}}),$$

at room temperature is listed. The DBMBF₂ / p-xylene exciplex shows a linear plot of $\ln(I_{\text{ex}} / I_{\text{A}}[D])$ vs. $1/T$ over a 20 degree range (40-60 °C); however, the oxygen test performed at 45 °C indicated the condition $k_{\text{ex}} \gg k_f^{\text{ex}} + k_{\text{nr}}^{\text{ex}}$ was nearly reached (oxygen had a minute effect on the ratio of ratios). The reported value of 5.1 kcal / mol for the DBMBF₂ / p-xylene is believed to be a good estimate. The interaction between singlet excited DBMBF₂ with benzene to xylenes is fairly weak but significantly larger than the available thermal energy at room temperature (0.6 kcal / mol at 298 K). This, together with the oxygen test remarks in Table 7.1, indicates that the dissociation rate constant, k_{ex} , can be

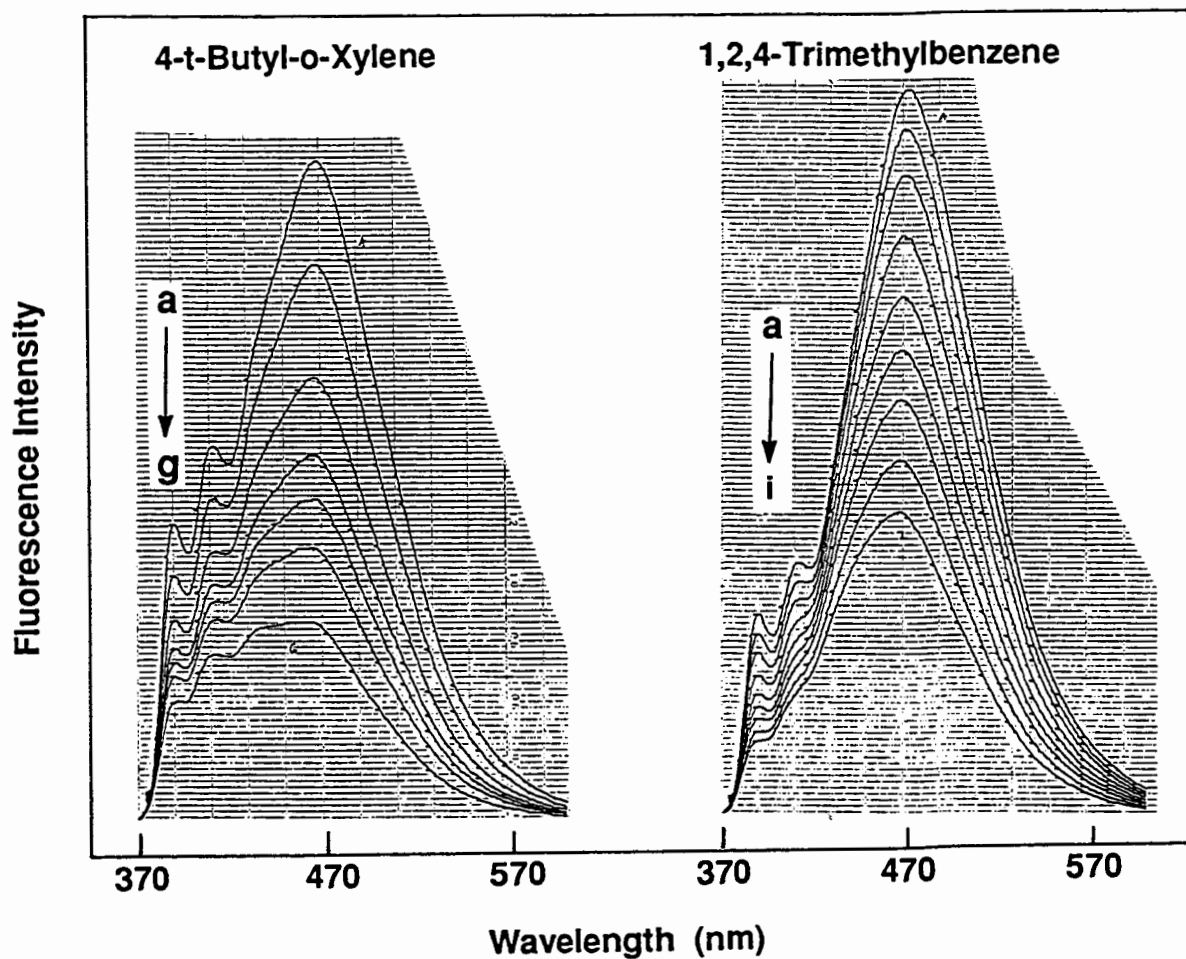


Figure 7.3: Variation in the Exciplex / DBMBF₂ (4.3×10^{-6} M) Fluorescence Intensities with Temperature in Cyclohexane Under Argon. Donors: 4 - t - Butyl - o - xylene (0.18 M) {Temperatures (°C) : (a) 14.5, (b) 21.6, (c) 29.1, (d) 35.6, (e) 40.1, (f) 46.3 and (g) 54.9}; 1,2,4 - Trimethylbenzene (0.18 M) {Temperatures (°C) : (a) 13.3, (b) 17.7, (c) 22.0, (d) 29.0, (e) 35.8, (f) 41.5, (g) 46.4, (h) 53.5 and (i) 59.8}.

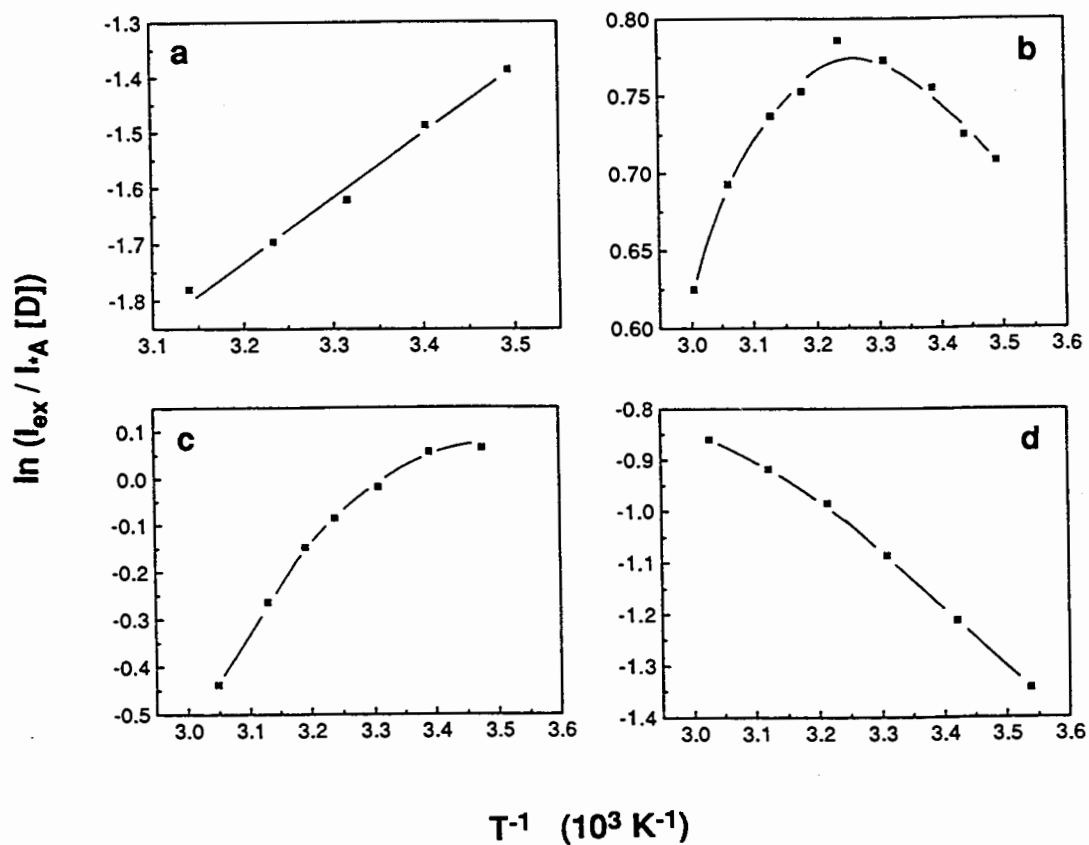


Figure 7.4: Variation of the Exciplex / DBMBF₂ Fluorescence Intensities with Temperature (eq 7.3). Donors: *t*-Butylbenzene (a); 1,2,4-Trimethylbenzene (b); 5-*t*-Butyl-*o*-Xylene (c); HMB (d). Note that the Three Regions (Reversible, Intermediate and Irreversible) are Displayed.

Table 7.1: DBMBF₂ - Benzene Exciplex Enthalpies of Formation in Cyclohexane

Benzene	$-\Delta H_{\text{ex}}$ (kcal/mol)	Remarks	O ₂ Test	≥ 41 °C	$-\Delta H_{\text{ex}} + R_E$ (kcal/mol)	R_E (kcal/mol)	$\Sigma \nu_C$
			R. T.	Ratio			
Cyanobenzene	(0.8) ^j	b	+	1.00 ^h	6.1 ± 0.2	(5.3) ^j	0.75
Methyl benzoate	(0.2)	b	+	1.00	6.4 ± 0.2	(6.0)	1.14
Benzene	2.5 ± 0.2 ^a	b	+	1.00	6.4 ± 0.2	3.9 ± 0.4	0
Toluene	3.2 ± 0.2	c	-	1.02	8.1 ± 0.2	4.9 ± 0.4	0.52
o-Xylene	4.4 ± 0.3	c	-	1.04	10.1 ± 0.2	5.7 ± 0.5	1.04
m-Xylene	4.5 ± 0.3	c	-	1.04	10.4 ± 0.2	5.9 ± 0.5	1.04
p-Xylene	≈ 5.1	c/d	-	1.06	11.0 ± 0.2	≈ 5.9	1.04
Mesitylene	(5.6)	d	-	1.05	12.4 ± 0.2	(6.8)	1.56
1,2,4-TMB	(7.0)	e	-	1.30	13.8 ± 0.2	(6.8)	1.56

Table 7.1 (Continued)

Benzene	$-\Delta H_{\text{ex}}$ (kcal/mol)	Remarks	O ₂ Test		$-\Delta H_{\text{ex}} + R_E$ (kcal/mol)	R_E (kcal/mol)	ΣV_C
			R.	T. $\geq 41^\circ\text{C}$			
Ratio							
1,2,3,4-TMB	(7.2)	f	-	1.35	15.0 ± 0.2	(7.8)	2.08
1,2,3,5-TMB	(7.5)	f	-	1.46	15.3 ± 0.2	(7.8)	2.08
Durene	(8.3)	g	-	1.56	16.1 ± 0.2	(7.8)	2.08
PMB	(9.1)	g	-	1.60	17.8 ± 0.2	(8.7)	2.60
HMB	(11.6)	g	-	1.66	21.3 ± 0.2	(9.7)	3.12
t-Butylbenzene	2.4 ± 0.2	b	+	1.00	8.1 ± 0.2	5.7 ± 0.4	1.24
4-t-Butyltoluene	3.7 ± 0.3	c	-	1.03	11.0 ± 0.2	7.3 ± 0.5	1.78
4-t-Butyl-o-xylene	(5.7)	c	-	1.07	13.8 ± 0.2	(8.1)	2.28
5-t-Butyl-m-xylene	4.3 ± 0.3	f	-	1.18	12.4 ± 0.2	8.1 ± 0.5	2.28

Table 7.1 (Continued)

Benzene	$-\Delta H_{\text{ex}}$ (kcal/mol)	Remarks	O ₂ Test		$-\Delta H_{\text{ex}} + R_E$ (kcal/mol)	R_E (kcal/mol)	ΣV_C
			R.	T. ≥ 41 °C			
Ratio							
5- <i>t</i> -Butyl-1,2,3-TMB	(5.9)	f	-	1.38	15.0 ± 0.2	(9.1)	2.80
Biphenyl	5.2 ± 0.3	c	-	+	12.2 ± 0.2	7.0 ± 0.5	1.66

^a Reported errors for $-\Delta H_{\text{ex}}$ are the standard deviation. Remarks; b: reversible at all temperatures (10 - 60 °C); c: reversible at elevated temperatures; d: almost reaches reversibility at elevated temperatures; e: irreversible at RT; intermediate region at elevated temperatures; f: irreversible, however, k_{ex} becomes significant at elevated temperatures; g: irreversible at all temperatures (10 - 60 °C). ^h Calculated from plots of eq 7.7 (see experimental). ⁱ Nearly reversible. ^j Values calculated by the aid of the correlation line in Figure 7.7 and column five.

expected to be large. This clearly follows from eq 7.9. The product $k_{\text{diff}} [\text{O}_2]$ in cyclohexane (aerated solution) is known to be $5.9 \times 10^7 \text{ s}^{-1}$ [141], which is the averaged value obtained from the quenching of aromatic hydrocarbon fluorescence by oxygen in cyclohexane. For the product $k_{\text{diff}} \tau_{\text{ex}}^* [\text{O}_2]$ to be at or nearly zero, $1/\tau_{\text{ex}}^*$ must be significantly greater than $k_{\text{diff}} [\text{O}_2]$; this requires a k_{ex} greater than 10^9 s^{-1} . This prediction will be assessed in Chapter Eight.

7.2.2 Steric Effects on the Ground and Excited State Surfaces

From Table 7.1 and eq 7.3 the Franck-Condon ground state energy, R_E , can be determined easily since both E_S and $h\nu_{\text{max}}$ are known (Tables 3.3 and 6.1, respectively). For those exciplexes where ΔH_{ex} could be experimentally evaluated, the Franck-Condon ground state energy was calculated and these values are listed in Table 7.1. The R_E ground state energy also contains a contribution due to the unrelaxed solvent shell (cf. Figure 2.8), a contribution that is unrecognized. R_E can be broken into two parts, the intrinsic contribution due to donor-acceptor interactions and the unrelaxed solvent shell energy.

$$R_E = R_E^{\circ} + \frac{1}{2} B_{\text{or}} (\mu_g - \mu_{\text{ex}})^2 \quad (7.10)$$

R_E° is the intrinsic donor-acceptor interaction energy and $\frac{1}{2} B_{\text{or}} (\mu_g - \mu_{\text{ex}})^2$ is the solvent shell contribution where the symbols are those described in Chapter 2.4. From nonpolar to polar solvents, for example from cyclohexane to acetonitrile, B_{or} ranges from 0.0004 to 0.3064. Therefore, the solvent contribution can be neglected in cyclohexane ($\frac{1}{2} B_{\text{or}} (\mu_g - \mu_{\text{ex}})^2 \approx 0$) and the R_E values in Table 7.1 are essentially free of solvent effects; note that $B_{\text{or}} (\propto (\epsilon - 1) / (2\epsilon + 1) - (n^2 - 1) / (2n^2 + 1))$ is nearly zero in nonpolar solvents because $\epsilon \cong n^2$.

The calculated R_E in Table 7.1 definitely shows an increasing trend with increasing steric bulk of the benzene ring substituent. To better quantify this trend, a plot of R_E vs. a steric parameter was constructed (Figure 7.5). The steric parameter of Charton (v_C) was chosen because this parameter is based on the intrinsic size of the substituent [142] and assumed to be additive. An excellent linear relationship is observed. The linearity of this plot indicates that steric effects are the dominating influence on the change in Franck-Condon ground state energy.

Using the correlation between R_E and v_C and the known sum of $\Delta H_{ex} + R_E$, Figure 7.5 can be exploited to calculate the $-\Delta H_{ex}$ for those exciplexes where $-\Delta H_{ex}$ was not experimentally accessible. The results of such a calculation are given in parentheses in Table 7.1 where the error is less than 1 kcal/mol. In addition, any systematic error in the experimental $-\Delta H_{ex}$ will, of course, exist in the estimated $-\Delta H_{ex}$ values. The calculated $-\Delta H_{ex}$ values for the stronger electron donating benzenes follow the trend expected (eq 7.4), that is, $-\Delta H_{ex}$ is a reasonable linear function of the donor-acceptor redox potentials, which was manifested in Figure 6.1 (cf. eq 7.3).

Steric effects within the exciplex are not directly given by the R_E values in Table 7.1. Because charge is transferred between the DBMBF₂ and benzene donor, changes in electronic as well as steric effects are possible with exchange of a methyl for a t-butyl substituent. Since the hindered exciplexes have larger exciplex dipole moments than their unhindered analogs (Table 6.2), steric effects must introduce a change in the electronic structure. Therefore, both electronic and steric effects occur upon changing a methyl for a t-butyl substituent for this system. However, it was noted earlier that the exciplex emission ν_{max} was independent of steric effects. Since the Franck-Condon ground state energy was affected by steric effects, the exciplex must be affected to the same degree if this emission maxima invariance were true. This can be shown by rearranging eq 7.10. If the sum $|\Delta H_{ex}| + R_E$ is to remain constant then any change in R_E is compensated by a similar change in $|\Delta H_{ex}|$; i.e., $\Delta\Delta H_{ex} = -\Delta R_E$.

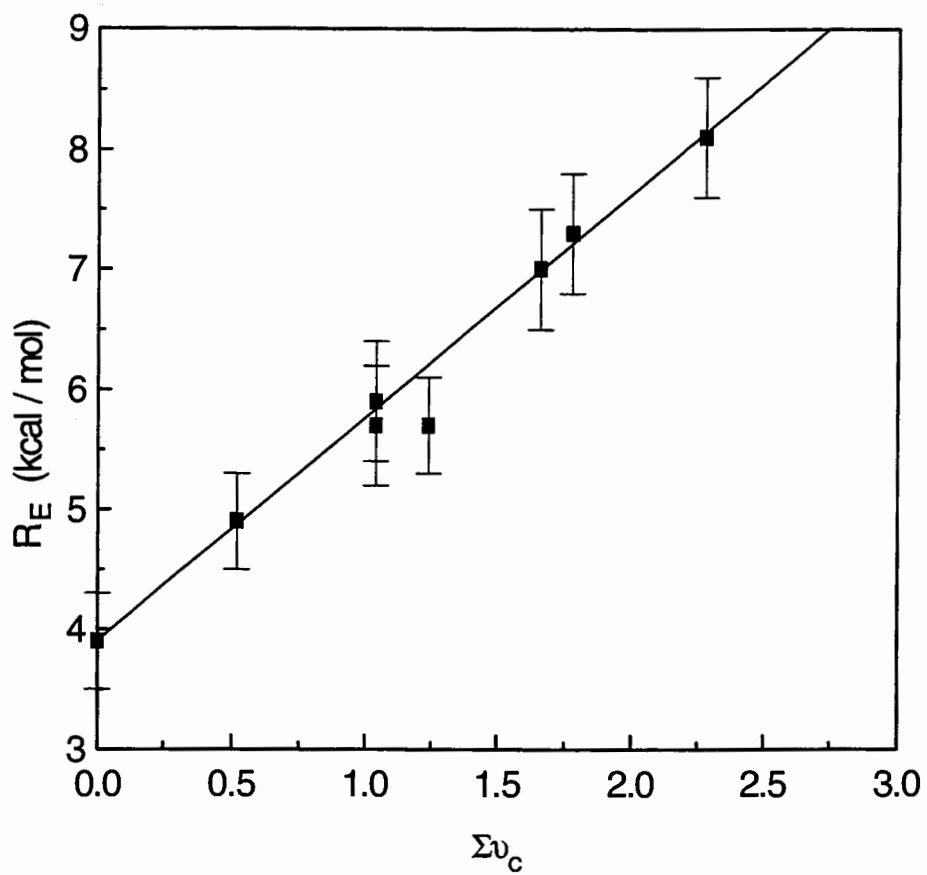


Figure 7.5: Correlation Between the Exciplex's Franck-Condon Ground State Complex Energy and Charton's Steric Parameter (ν_c).

$$E_S - hv_{\max} = |\Delta H_{\text{ex}}| + R_E = \text{Constant} \quad (7.11)$$

Assuming that the HOMO energy gap is similar between those exciplexes with the hindered and unhindered analogs, any observed changes in the exciplex properties can be assigned to changes in the overlap integral $S (= \langle A \cdot D^+ | I^* AD \rangle)$. In other words, exciplexes formed from singlet excited DBMBF₂ with p-xylene and p-t-butyltoluene have the same inherent binding energy, E_{CT} , but potentially different acquired stabilization from orbital interactions, U_{Stab} (eq 7.4). Therefore, changes in ΔH_{ex} are essentially a result of changes in S . Inspection of Table 7.1 shows that the unhindered benzenes have stronger binding energies of ca. 1.3 kcal/mol, which is ascribed to a reduction in S for the hindered benzenes. A smaller S is also reflected in a larger exciplex dipole as, indeed, was calculated for these donors (Table 6.2). A reduction in the overlap integral S suggests the more sterically hindered benzenes have difficulty in achieving the corresponding overlap obtained for the unhindered analogs.

In Chapter Four, it was shown that DBMBF₂ forms EDA complexes with benzenes in solution. Therefore, if the exciplex and EDA complex donor-acceptor orientations were identical, R_E should be a negative quantity. Since the observed R_E values are all positive (a repulsive ground state) the donor-acceptor orientation for the exciplex must be different from that of the EDA complexes (an attractive ground state). The consequences of a different ground and excited donor-acceptor orientation is that the excited state wavefunction for the excited EDA complex is no longer a valid description of the relaxed exciplex; i.e., the discussion of the EDA complex wavefunction in Chapter Two pointed out that the excited EDA complex Ψ_V is the Franck-Condon excited state. The promotion of the EDA complex to its 'relaxed' excited state has been shown to be that of the exciplex due to identical fluorescence bands (Chapter Four and Five). In addition, the different donor-acceptor orientation for the exciplex vs. the excited EDA complex probably significantly reduces the mixing between the exciplex wavefunction with the no-bond

configuration IAD) due to a reduced orbital overlap integral, which is indicated by the agreement between $h\nu_{\max}$ and eq 6.1b and not with eq 6.1a.

To reconcile the above findings, as the DBMBF₂ / benzene EDA complex is promoted to its Franck-Condon excited state by light absorption, the complex undergoes reorientation to the more relaxed exciplex arrangement, which is apparently more energetically favored. Consideration of the interacting molecular orbitals of these two excited complexes shows that this is a natural consequence for these complexes. It was concluded earlier that DBMBF₂ / substituted benzene exciplexes are stabilized by HOMO-HOMO interactions whereas EDA complexes are known to be stabilized by HOMO-LUMO interactions. As a consequence of the LUMO of DBMBF₂ having one more node than the HOMO, to achieve optimum orbital overlap the excited EDA complex must have a different orientation than the exciplex hence a different electronic interaction. For other donor-acceptor systems this difference in complex orientation may be a general pattern. For instance, 1,4-dicyanonaphthalene/alkylbenzene [143] and tetracyanobenzene/alkylbenzene [144] complexes have been proposed to have different excited EDA and exciplex donor-acceptor orientations.

As a final note, we can answer the question posed in Chapter Five: "should the definition of an exciplex be changed to reflect that both a EDA complex and an exciplex can exist for the same donor-acceptor pair ?" The answer, unfortunately, depends on how strict a definition is required or even necessary. The important point is that exciplex formation does not preclude EDA complex formation.

7.2.3 Stabilization of Weak CT Exciplexes

Charge transfer interactions are a central theme in the description of exciplexes, as is evident in eq 7.4, hence the exciplex dipole moment is usually large. The DBMBF₂/benzene system shows variable charge transfer character where low CT

exciplexes have a reasonable binding energy (cf. benzene as a donor in Table 7.1). For EDA complexes discussed in Chapter Two, there is agreement in the literature that the majority of the complex's binding energy comes from the no-bond (IAD) configuration rather than the charge transfer configuration [50-52,57,58]. Therefore, it is unclear whether the locally excited configuration I^*AD has any contribution to the exciplex's binding energy. If the locally excited configuration has a net stabilization, it must be a result of an imbalance between the intermolecular interaction (i.e., electrostatic, polarization and exchange interactions [142]); i.e., treating the intermolecular interactions of weak CT exciplexes on the same basis as EDA complexes [50,57,58]. For example, where Sol represents the solvent and \cdots represents intermolecular interaction, reaction of one $A\cdots Sol$ and one $D\cdots Sol$ is replaced by one $A\cdots D$ and one $Sol\cdots Sol$. The energies may only approximately cancel and small $-\Delta H_{ex}$ values are sufficient for exciplex formation (Table 7.1).

In Chapter Two the exciplex energy can be calculated from the quadratic equation

$$(1 - S^2) E_{EX}^2 + (2HS - E_{LE} - E_{CT}) E_{EX} + (E_{LE}E_{CT} - H^2) = 0 \quad (2.38)$$

For illustration purposes we will assume that $E_{CT} \neq E_{LE}$. Since S is small (Chapter Six), that is, a weak interaction between the donor and acceptor, it can be shown that [50]

$$E_{EX} = E_{CT} - \frac{(H - E_{CT}S)^2}{E_{CT} - E_{LE}} \quad \text{if } E_{CT} < E_{LE} \quad (7.12a)$$

$$E_{EX} = E_{LE} - \frac{(H - E_{LE}S)^2}{E_{LE} - E_{CT}} \quad \text{if } E_{LE} < E_{CT} \quad (7.12b)$$

where eqs 7.12a and 7.12b were derived under the conditions that $a \gg c$ and $c \gg a$, respectively. Equation 7.12a is identical to eq 7.4 where

$$U_{\text{Stab}} = \frac{(H - E_{\text{CT}}S)^2}{E_{\text{CT}} - E_{\text{LE}}}$$

Equation 7.12 illustrates that the binding energy of an exciplex has an intrinsic part (E_{CT} or E_{LE}) and a perturbing part (U_{Stab}). Therefore, an exciplex may gain additional stabilization through frontier orbital interaction as long as the energy gap $E_{\text{CT}} - E_{\text{LE}}$ is not large. Since the integral H can be related to the overlap integral S under various approximations [50,58], the value of U_{Stab} is strongly dependent on S : $U_{\text{Stab}} \propto S^2$.

Substitution of eq 7.12 into eq 7.3 and rearrangement gives

$$h\nu_{\text{max}} = E_{\text{CT}} - U_{\text{Stab}} - R_{\text{E}} \quad \text{if } E_{\text{CT}} < E_{\text{LE}} \quad (7.13a)$$

$$h\nu_{\text{max}} = E_{\text{LE}} - U_{\text{Stab}} - R_{\text{E}} \quad \text{if } E_{\text{LE}} < E_{\text{CT}} \quad (7.13b)$$

Equations 7.13a and 7.13b are collaborated by Figure 6.1 where 7.13a predicts a linear relationship between $h\nu_{\text{max}}$ and the redox potentials and 7.13b predicts $h\nu_{\text{max}}$ to be relatively constant.

For the weak electron donors, according to eq 7.12b, any stabilization energy is acquired through E_{LE} and U_{Stab} where the latter is dependent on the energy difference $E_{\text{LE}} - E_{\text{CT}}$. The trend in Table 7.1, as the extent of charge transfer within the exciplex decreases, shows that the binding energy appears to be approaching zero; for methyl benzoate and cyanobenzene as donors the calculation of ΔH_{ex} is believed to provide reasonable estimates. It appears that the stabilization energy of weak CT exciplexes is entirely through the U_{Stab} term under the assumption that the interaction between *A and D (excluding charge transfer interaction) results in negligible stabilization in solution. The

conclusion that $\langle {}^*AD | H | {}^*AD \rangle \equiv \langle {}^*A | H | {}^*A \rangle$ is crucial in the calculation of the exciplex radiative rate constant on a theoretical basis (Chapter Nine).

CHAPTER EIGHT

KINETIC AND THERMODYNAMIC PARAMETERS OF DBMBF₂ / BENZENE

EXCIPLEXES IN CYCLOHEXANE

8.1 Introduction and Mathematical Models

The photochemical mechanism, exciplex nature and exciplex binding energy have been evaluated in the preceding chapters. As part of the complete photochemical mechanism, the kinetics and thermodynamic properties will be discussed here. In evaluating the kinetics of fluorescence quenching by added quencher the experimenter has two options: i) steady state methods [145] and ii) time-resolved methods [146]. Steady state fluorescence quenching is the most common technique in examining excited state interactions and kinetics. The advantage of this technique is that the experiments are relatively straightforward to perform. Unfortunately, this technique can not easily allow access to all the rate constants. For example, steady state fluorescence quenching kinetic studies generally use the Stern-Volmer equation (eq 8.1a)

$$I^0 / I = 1 + k_{\text{obs}}\tau_m[D] \quad (8.1a)$$

where, for the system of interest here, the observed fluorescence quenching rate constant is a collection of the rate constants for exciplex formation, dissociation and decay.

$$k_{\text{obs}} = k_{\text{ex}} / (1 + k_{-\text{ex}}\tau_{\text{ex}}) \quad (8.1b)$$

The separation of the individual rate constants contained within k_{obs} by steady state methods is difficult at best. On the other hand, time-resolved fluorimetry can be used to separate all the rate constants [138,146] and will be discussed below.

In this chapter time-resolved fluorimetry will be used to examine the fluorescence quenching of singlet excited DBMBF₂ by benzenes in cyclohexane. Time-resolved fluorimetry uses a pulsing light source that pumps a fraction of the ground state DBMBF₂ into its singlet excited state. From Scheme 5.1, the change in *A and *AD concentration with respect to time is given by eq 8.2 [146].

$$d[*A] / dt = I_a + k_{-ex}[*AD] - \{k_{ex}[D] + k_f + k_{nr}\} [*A] \quad (8.2a)$$

$$d[*AD] / dt = k_{ex}[D] - \{k_{-ex} + k_f^{ex} + k_{nr}^{ex}\} [*AD] \quad (8.2b)$$

I_a represents the lamp flash, which will have its own temporal profile. Assuming that I_a is an ideal light pulse (with an infinitely narrow width) these simultaneous linear differential equations can be solved by eigenvalue methods using exponential trial functions [147,148].

The resulting temporal concentrations for *A and *AD are given by

$$[*A] = c_1 \exp(-\lambda_1 t) + c_2 \exp(-\lambda_2 t) \quad (8.3a)$$

$$[*AD] = c_3 \{ \exp(-\lambda_1 t) - \exp(-\lambda_2 t) \} \quad (8.3b)$$

where $\lambda_1 = \frac{1}{2} [X + Y + \{(X - Y)^2 + 4k_{ex}k_{-ex}[D]\}^{1/2}] \quad (8.3c)$

$$\lambda_2 = \frac{1}{2} [X + Y - \{(X - Y)^2 + 4k_{ex}k_{-ex}[D]\}^{1/2}] \quad (8.3d)$$

$$X = k_{ex}[D] + k_f + k_{nr} = k_{ex}[D] + (\tau_m)^{-1}$$

$$Y = k_{-ex} + k_f^{ex} + k_{nr}^{ex} = k_{-ex} + (\tau_{ex})^{-1}$$

λ_1 and λ_2 are called characteristic values. Under irreversible conditions (k_{-ex} is negligible) these values are equal to the reciprocal of the *A and *AD lifetimes, respectively.

Measurement of these characteristic values at various donor concentrations allows evaluation of most of the process rate constants shown in Scheme 5.1 where the following relationships are useful [138,146,148].

$$\lambda_1 + \lambda_2 = k_{\text{ex}}[D] + k_{-\text{ex}} + (\tau_m)^{-1} + (\tau_{\text{ex}})^{-1} \quad (8.4a)$$

$$\lambda_1\lambda_2 = (\tau_m)^{-1}\{k_{-\text{ex}} + (\tau_{\text{ex}})^{-1}\} + k_{\text{ex}}[D](\tau_{\text{ex}})^{-1} \quad (8.4b)$$

By plotting $\lambda_1 + \lambda_2$ and $\lambda_1\lambda_2$ vs. $[D]$, k_{ex} , $k_{-\text{ex}}$, and $(\tau_{\text{ex}})^{-1}$ can be evaluated where τ_m (lifetime of *A in the absence of D) is known. However, if one of the characteristic values is too small to measure with accuracy, the remaining λ value can be numerically fitted to eq 8.3d to extract the same rate constants [138d]. Note that the exciplex lifetime τ_{ex} is different from that discussed in Chapter Seven (τ_{ex}^*) where the latter contains the reverse reaction rate constant ($k_{-\text{ex}}$) and the former does not; this was done for mathematical convenience.

8.2 Results and Discussion

8.2.1 Exciplex Process Rate Constants in Cyclohexane

Lifetime measurements were determined on a Photon Technology International LS-1 lifetime system using the time-correlated single photon counting method [148]. The system was made available by the courtesy of Professor P. Wan (Department of Chemistry, University of Victoria). Excitation was either at a λ_{ex} of 358 or 365 nm (UV-Vis λ_{max} of DBMBF₂) and the fluorescence signal was monitored at $\lambda_{\text{mon}} \geq 550$ nm (negligible DBMBF₂ fluorescence), except where noted, and 390 nm for DBMBF₂'s fluorescence decay. In some cases the excitation wavelength was set at 400 nm to pump the EDA complex into its excited state and monitor its decay. The deconvolution of two lamp profiles (FWHM typically 1.8 to 2.0 ns) gave a lifetime of 0.10 ns, which represents the

lower detection limit of the LS-1 under the experimental conditions; this lower detection limit is consistent with the work of Cramer and Spears [149], where they suggested a detection limit of 1 / 15 th of the lamp's FWHM. The system was tested for short lifetime capabilities by measuring DBMBF₂'s lifetime in acetonitrile; singlet excited state DBMBF₂ lifetime was recently measured on a picosecond time-resolved system to be 0.295 ns [109]. A lifetime of 0.28 ns was obtained on the LS-1 hence this luminescence system can be used to measure lifetimes at least as short as 0.2-0.3 ns (see experimental). The DBMBF₂ lifetime in cyclohexane was found to be 0.23 ns.

Due to the short DBMBF₂ lifetime in the presence of donor (< 0.2 ns), only the DBMBF₂ / benzene exciplex characteristic values in the presence of various concentrations of donors could be measured with confidence. The fluorescence decay was fitted with single and biexponential functions of the form shown by eq 8.3. The criteria for the goodness of fit was judged by four statistical tests provided by the LS-1 software: chi squared, residuals, autocorrelation and Durbin-Watson parameters. A good fit to the experimental curve is demonstrated by a chi squared less than 1.3, random residuals and autocorrelation and a Durbin-Watson parameter of 1.7 or better [148]. All the lifetimes measured, except for a few, displayed good fits with a single exponential function based on the above criteria. This indicated that biexponential and multiexponential fitting can not be statistically justified [148]. Table 8.1 summarizes the results obtained in cyclohexane.

For benzenes that showed irreversible exciplex formation with singlet excited DBMBF₂ (Table 7.2) at room temperature, their fluorescence decay curves were single exponential (Figure 8.1a). In addition, the exponential decay was invariant with the donor concentration, which indicated no exciplex quenching step [147,148]; i.e., $^*(AD) + D \rightarrow A + 2D$. The lifetime obtained from these decay curves is equal to τ_{ex} .

Table 8.1: Observed DBMBF₂ / Benzenes Exciplex Lifetimes, τ_{obs} ($1/\lambda_2$), in Oxygen Free Cyclohexane at 23 °C.

Benzene	[D] (M)	λ_{ex} (nm)	λ_{mon} (nm)	τ_{obs} (ns)	Benzene	[D] (M)	λ_{ex} (nm)	λ_{mon} (nm)	τ_{obs} (ns)
HMB	0.011	358	550	25.4	1,2,3,5-TMB	0.053	365	550	19.6
	0.034	358	550	25.2		0.141	365	550	19.4
	0.089	358	550	24.7		0.141	400	550	19.0
PMB	0.089	400	550	24.2	1,2,3,4-TMB	0.024	358	550	16.0
	0.026	365	550	24.3		0.049	358	550	15.8
	0.054	365	550	24.4		0.099	358	550	16.0
Durene	0.114	365	550	24.3	1,2,4-TMB	0.099	400	550	15.9
	0.114	400	550	24.2		0.080	365	550	13.4
	0.026	358	550	23.1		(7.40)	365	550	17.4
	0.052	358	550	22.5		0.039	365	550	7.4
	0.113	358	550	23.0		0.090	365	550	7.5
	0.052	400	550	22.6	0.182	365	550	7.9	

Table 8.1 (Continued)

Benzene	[D] (M)	λ_{ex} (nm)	λ_{mon} (nm)	τ_{obs} (ns)	Benzene	[D] (M)	λ_{ex} (nm)	λ_{mon} (nm)	τ_{obs} (ns)
Mesitylene	0.182	400	550	8.0	p-Xylene	3.994	365	550	9.4
	0.345	365	550	8.1		5.896	365	550	10.9
	0.510	365	550	8.3		(8.16)	365	550	13.1
	1.065	365	550	8.7		0.043	365	550	3.0
	2.213	365	550	9.3		0.101	365	550	3.3
p-Xylene	4.925	365	550	10.7	m-Xylene	0.195	365	550	3.5
	(7.19)	365	550	11.7		0.346	365	550	3.7
	0.046	365	550	5.8		0.456	365	550	3.9
	0.117	365	550	6.1		2.072	365	550	6.0
	0.230	365	550	6.6		4.314	365	550	6.7
m-Xylene	0.395	365	550	7.0	m-Xylene	5.896	365	550	7.2
	0.506	365	550	7.5		(8.17)	365	550	7.8
	1.917	365	550	9.0					

Table 8.1 (Continued)

Benzene	[D]	λ_{ex}	λ_{mon}	τ_{obs}	Benzene	[D]	λ_{ex}	λ_{mon}	τ_{obs}
	(M)	(nm)	(nm)	(ns)		(M)	(nm)	(nm)	(ns)
o-Xylene	0.046	365	550	3.0	Toluene	1.335	365	550	1.8
	0.097	365	550	3.2		2.887	365	550	2.5
	0.225	365	550	3.6		5.709	365	550	3.2
	0.317	365	550	3.8		(9.14)	365	550	3.7
Toluene	0.366	365	550	3.9	Benzene	0.346	365	550	0.35
	1.631	365	550	5.3		0.602	365	550	0.40
	4.465	365	550	6.4		0.994	365	550	0.52
	(8.19)	365	550	8.0		1.410	365	550	0.63
	0.273	365	550	1.0		1.824	365	550	0.71
	0.716	365	550	1.3		(11.2)	365	550	2.1

Table 8.1 (Continued)

Benzene	[D] (M)	λ_{ex} (nm)	λ_{mon} (nm)	τ_{obs} (ns)	Benzene	[D] (M)	λ_{ex} (nm)	λ_{mon} (nm)	τ_{obs} (ns)
5-t-Butyl-1,2,3 -	0.085	365	550	13.8	p-t-Butyltoluene	0.078	365	550	2.6
TMB	0.184	365	550	13.8		0.232	365	550	3.0
	0.325	365	550	14.0		0.625	365	550	3.6
4-t-Butyl-o-	0.041	365	550	11.0		1.34	365	550	4.4
xylene	(5.34)	365	550	19.3		2.39	365	550	5.2
5-t-Butyl-m -	0.40	365	550	5.8		3.56	365	550	5.9
xylene	0.081	365	550	6.0		(5.75)	365	550	6.9
	0.118	365	550	6.1	tBB	0.290	365	440	0.47
	0.118	400	550	5.9		0.564	365	440	0.55
	0.192	365	550	6.2		0.763	365	440	0.65
	0.343	365	550	6.4		1.063	365	440	0.82
	(5.35)	365	550	8.9		1.979	365	440	1.03

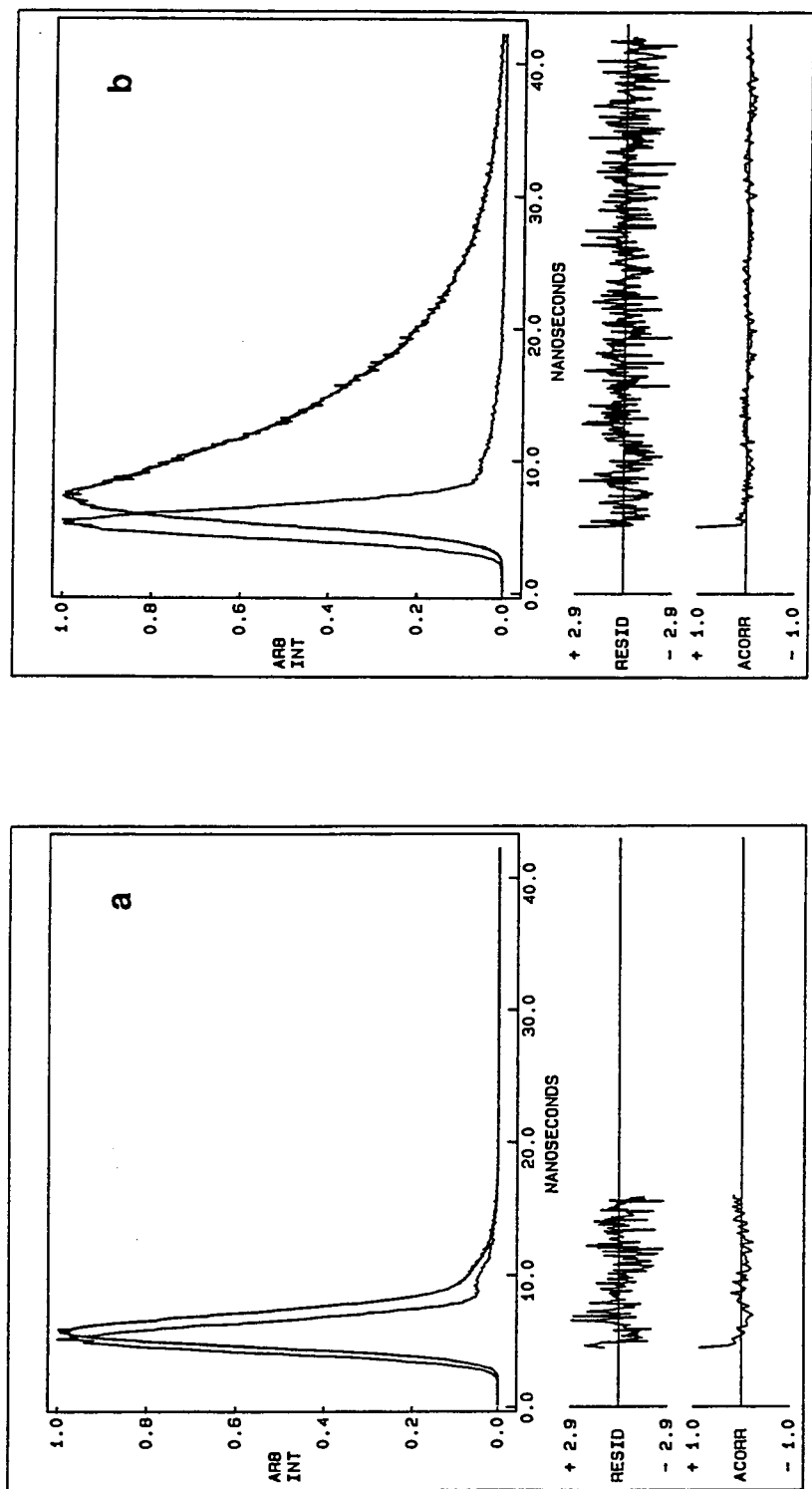


Figure 8.1: Fluorescence Decay Examples of DBMBF₂ / Benzene Exciplexes in Degassed Cyclohexane (296 K). Donors: (a) Benzene (1.8 M); (b) p-Xylene (0.23 M). The First Symmetrical Peak is the Lamp Profile. The Residuals (RESID) and the Autocorrelation (ACORR) are shown below the Fluorescence Decay Trace.

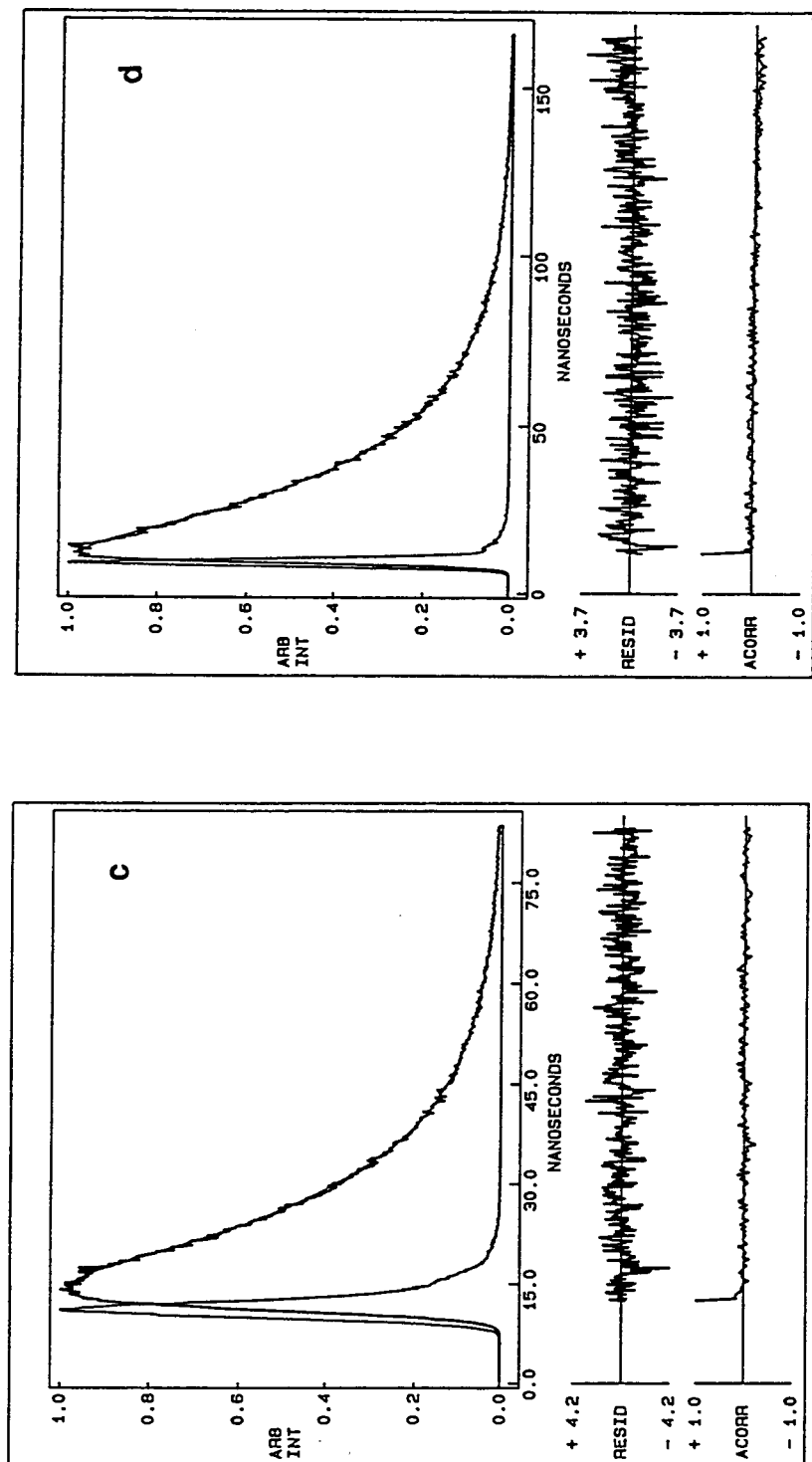


Figure 8.1 (Continued): Donors: (c) 1,2,4 - Trimethylbenzene (0.08 M); (d) PMB (0.11 M).

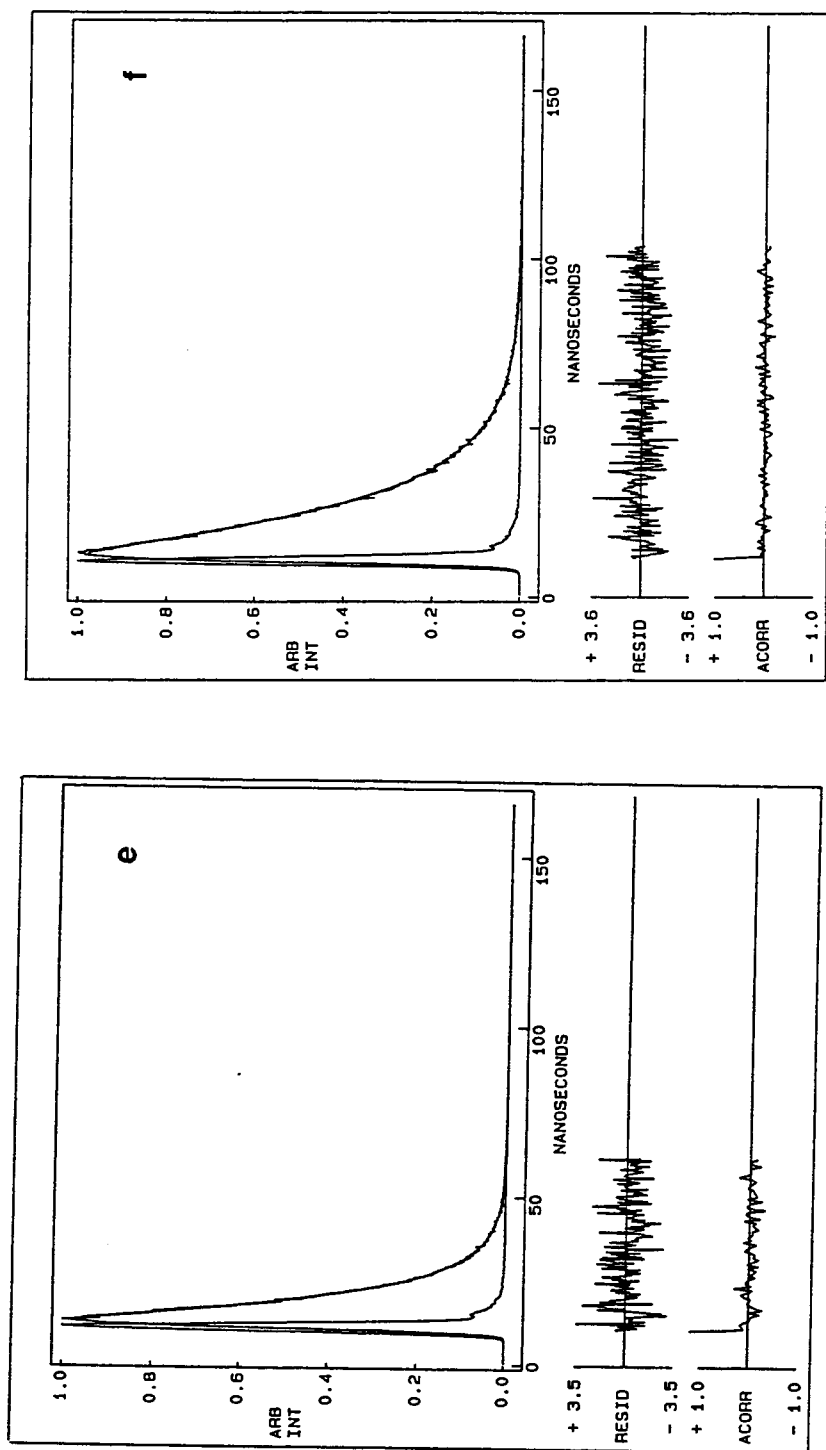


Figure 8.1 (Continued): Donors: (e) p-t-Butyltoluene (neat); (f) 5-t-Butyl-1,2,3-Trimethylbenzene (0.085 M).

For exciplexes that fall into the intermediate region, $k_{\text{ex}} \approx k_{\text{f}}^{\text{ex}} + k_{\text{nr}}^{\text{ex}}$, the exciplex decay could be fitted adequately to a single exponential (Figure 8.1b). A satisfactory biexponential fit of the form given by eq 8.3b indicates a short grow in lifetime. However, the characteristic value of this grow in exponential (λ_2) could not be analyzed with confidence since the signal growth, where the majority of the λ_1 information is contained, is known to be distorted by the PMT tube [148,150]. In addition, the biexponential fit was not statistically better than a single exponent fit in most cases. The exciplex decay lifetime, λ_2 , was unaffected by fitting either exponential or biexponential functions. DBMBF₂'s fluorescence decay (monitored at 390 nm) showed biexponential behavior but it was not clear whether this was due to true biexponential decay behavior as predicted by eq 8.3a or to contributions from exciplex emission (it is known that the exciplex has non-negligible emission intensity at 390 nm) (cf. Figure 5.1). Therefore, the biexponential behavior for DBMBF₂'s fluorescence decay could not be experimentally established. The apparent exciplex lifetimes were found to be strongly dependent on the donor concentration, which is attributed to the partial reversibility as suggested by eq 8.3d and consistent with the heats of exciplex formation determined in Chapter Seven.

The DBMBF₂-benzene exciplex was determined in Chapter Seven (Table 7.1) to be fully reversible at room temperature. Under this condition, the lifetime measured at either DBMBF₂ or exciplex monitoring wavelengths should be identical according to eq 8.5 [151].

$$\tau_{\text{obs}} = \{\tau_{\text{m}} + \tau_{\text{ex}} K_{\text{SV}}[\text{Benzene}]\} / 1 + K_{\text{SV}}[\text{Benzene}] \quad (8.5)$$

This reveals that the observed apparent lifetime should be wavelength invariant as was found to be true. The apparent lifetime was the same at 550 (exciplex emission), 440 (exciplex plus DBMBF₂ emission) and 390 nm (DBMBF₂ emission) monitoring wavelengths. This confirms the earlier conclusion in Chapter Seven that the DBMBF₂ /

benzene exciplex is reversibly formed at room temperature. Identical results were found for the DBMBF₂ / t-butylbenzene exciplex.

The rate constants for exciplex formation and decay were determined by numerical fitting of the observed apparent lifetimes (for [D] < 2 M) to the function

$$1 / \tau_{\text{obs}} = \lambda_2 = \frac{1}{2} [k_{\text{ex}}[D] + (\tau_m)^{-1} + k_{-\text{ex}} + (\tau_{\text{ex}})^{-1} - \{(k_{\text{ex}}[D] + (\tau_m)^{-1} - k_{-\text{ex}} - (\tau_{\text{ex}})^{-1})^2 + 4k_{\text{ex}}k_{-\text{ex}}[D]\}^{1/2}] \quad (8.6)$$

using the Origin MicroCal scientific spreadsheet (Version 3.0). DBMBF₂'s lifetime, τ_m , is known to be 0.23 ns (Table 3.2) hence this parameter was used in the fitting to reduce the number of unknown parameters to three: k_{ex} , $k_{-\text{ex}}$ and τ_{ex} . The initial estimate for k_{ex} was $7.5 \times 10^9 \text{ M}^{-1}\text{s}^{-1}$ (diffusion control rate constant in cyclohexane) [123] and the sum $k_{-\text{ex}} + (\tau_{\text{ex}})^{-1}$ was obtained from extrapolation to infinite dilution (eq 8.7).

$$\lim_{[D] \rightarrow 0 \text{ M}} \lambda_2 = k_{-\text{ex}} + (\tau_{\text{ex}})^{-1} \quad (8.7)$$

Only the data at donor concentrations less than 2 M were used in the fitting. The results are listed in Table 8.2 and examples of the quality of fit are demonstrated in Figure 8.2.

Since the diffusion control rate constant in cyclohexane is known to be about $7.5 \times 10^9 \text{ M}^{-1}\text{s}^{-1}$ in cyclohexane [123], Table 8.2 shows that k_{ex} reaches the diffusion limit for xylenes and mesitylene; for the better electron donors (that formed irreversible exciplexes with DBMBF₂) their k_{ex} values are expected to be diffusion controlled as well. Both the rate constants for exciplex dissociation, $k_{-\text{ex}}$, and exciplex decay, $1 / \tau_{\text{ex}}$, decrease with respect to decreasing IP of the donor. However, the exciplex dissociation rate constant decreases faster than the exciplex decay. The trend for $k_{-\text{ex}}$ is consistent with the observation that the observed exciplex binding energies (Table 7.2) increase with the better

Table 8.2: Evaluated Rate Constants of some DBMBF₂ / Substituted Benzene Exciplexes in Degassed

Cyclohexane (296 K)

Benzene	k_{ex} (10 ⁹ M ⁻¹ s ⁻¹)	$k_{\text{-ex}}$ (10 ⁸ s ⁻¹)	K_{ex} (M ⁻¹)	$(\tau_{\text{ex}})^{-1}$ (10 ⁸ s ⁻¹)	$(\tau_{\text{ex}})^{-1}$ (10 ⁸ s ⁻¹) ^b
Benzene	4.5 ± 0.5	43 ± 4	1.1 ± 0.2	3.3 ± 0.3	4.8 ± 0.5
Toluene	5.0 ± 0.5	11 ± 1	4.5 ± 0.6	1.8 ± 0.2	2.7 ± 0.3
o-Xylene	7.0 ± 0.5	2.1 ± 0.2	33 ± 5	1.3 ± 0.1	1.3 ± 0.1
m-Xylene	7.5 ± 0.5	2.5 ± 0.3	30 ± 4	1.1 ± 0.1	1.3 ± 0.1
p-Xylene	8.0 ± 0.5	0.85 ± 0.09	94 ± 13	0.93 ± 0.09	0.76 ± 0.08
Mesitylene	8.0 ± 0.5	0.35 ± 0.04	230 ± 30	1.0 ₅ ± 0.1	0.85 ± 0.09
t-Butylbenzene	4.5 ± 0.5	27 ± 3	1.7 ± 0.2	0.27 ± 0.03	--
p-t-Butyltoluene	8.0 ± 0.5	2.8 ± 0.3	29 ± 4	1.5 ± 0.2	1.4 ± 0.1
5-t-Butyl-m-Xylene	8.0 ± 0.5	0.50 ± 0.05	160 ± 20	1.3 ± 0.1	1.1 ± 0.1

a $K_{\text{ex}} = k_{\text{ex}} / k_{\text{-ex}}$ b τ_{ex} in aromatic solvent from Table 8.1.

electron donating potential; i.e., the activation barrier for dissociation increases. The reverse reaction rate constant (k_{-ex}) for the reversible exciplexes was qualitatively assessed from eq 7.9 to be greater than 10^9 s^{-1} ; this estimation is clearly confirmed in Table 8.2 for three of them. In addition, the more hindered benzenes (t-butyl substituted benzenes) showed smaller binding energies, which suggested a larger k_{-ex} value. This conclusion is confirmed by inspection of Table 8.2.

Figure 8.2 demonstrates the fitting of eq 8.3d to the observed exciplex lifetimes with p-Xylene and mesitylene as donors. The fit is very good for concentrations less than 2 M but the observed lifetimes deviate from the calculated line at larger concentrations. This was observed for most of the exciplexes except with toluene, m-xylene and o-xylene as donors (the reversible exciplexes are excluded as well since the concentration range was less than two molar). At such large concentrations the number of aromatic molecules around ground state or singlet excited DBMBF₂ should be weakly dependent on donor concentration [128] and the reverse reaction [$^*(AD) \rightarrow ^*A + D$] is nearly suppressed: eq 8.6c has a practical concentration range. Of the possibilities to explain this increase in τ_{ex} at high donor concentrations, formation of either nonemissive or emissive higher order complexes can be neglected; fluorescence quenching of the exciplex with a ground state donor (k_{qex}) to form a nonemissive triplex should be evident from a decrease, not an increase, in τ_{ex} ($1 / \tau_{ex} = k_f^{ex} + k_{nr}^{ex} + k_{qex}[D]$) [138d]. The formation of an emissive triplex, or higher order complex, can be neglected since single exponential fluorescence decay behavior was observed; i.e., the observed decay will be biexponential (sum of two or more exponentials) if an emissive triplex were formed [147]. An alternative proposal is that the change in solvent's composition, as the benzene concentration increases, affects the exciplex's decay rate constants and the reverse reaction k_{-ex} . From Table 8.2, this proposal is partially warranted by the comparison of the computed exciplex lifetime in cyclohexane (fifth column) to that observed in neat aromatic solvent (sixth column) where these two exciplex lifetimes are different in some cases. To illustrate the effect of

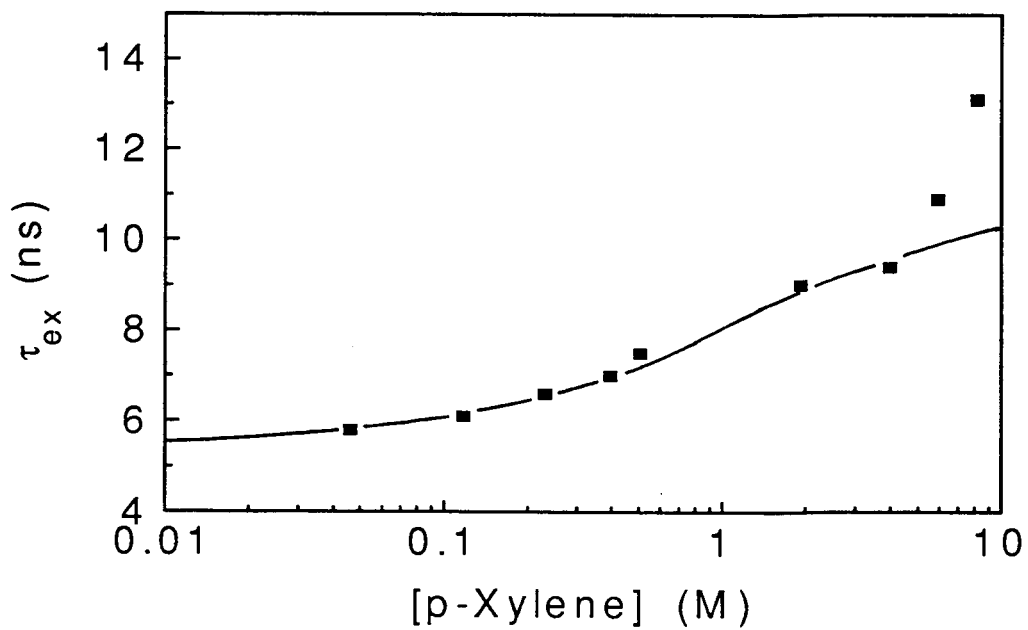
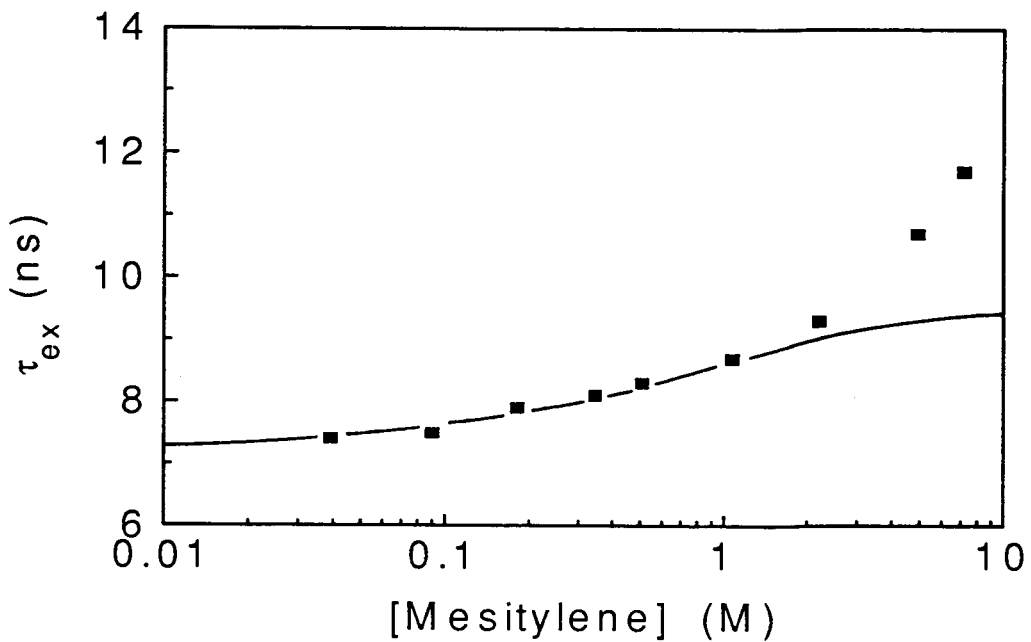


Figure 8.2: Typical Examples of the Fit of the Observed Exciplex Lifetimes as a Function of the Donor Concentration. The Solid Line Represents the Best Fit of Eq 8.6.

a change in τ_{ex} and k_{ex} , simulated plots of τ_{obs} vs. donor concentration are shown in Figure 8.3 and 8.4, respectively. These figures were constructed using eq 8.6 and rate constants similar to those experimentally found for the DBMBF₂ / p-xylene exciplex. It is evident from Figures 8.3 and 8.4 that changes in τ_{ex} and k_{ex} produces a sizable effect on τ_{obs} hence eq 8.6 is sensitive to changes in τ_{ex} and k_{ex} ; changes in k_{ex} produce a negligible effect. However, changes in τ_{ex} ($1 / \Sigma k_{\text{dex}}$) produce a more dramatic shift in τ_{obs} at large donor concentrations (Figure 8.3) whereas changes in k_{ex} produce the strongest effect at the lower concentration range.

For the stronger electron donors, such as PMB, exciplex formation is irreversible hence the exciplex lifetime, τ_{ex} , can be directly measured from the fluorescence decay [138,139,148]; however, due to irreversibility the dissociation rate constant is not experimentally accessible. From Table 8.2, the largest exciplex equilibrium constant, K_{ex} , is 230 M⁻¹ and we can expect that for the better electron donors a K_{ex} of the order 500 M⁻¹ or more hence k_{ex} is estimated to be less than $2 \times 10^7 \text{ s}^{-1}$. The exciplex formation rate constant is expected to be diffusion controlled ($k_{\text{ex}} \cong 7.5 \times 10^9 \text{ M}^{-1}\text{s}^{-1}$) on the basis i) that the better electron donors in Table 8.2 are at the diffusion limit and ii) that the binding energy is stronger for these donors (Table 7.1).

8.2.2. Exciplex and Excited EDA Complex

In Chapter Five, spectroscopic evidence was presented to show that the excited EDA complex and exciplex was one and the same; therefore, it is then expected that the lifetimes should be the same. For most of the stronger electron donating benzenes, where a significant EDA CT band exists, the emitting state was prepared by exciting DBMBF₂ (365 nm) and the CT band (400 nm) and the lifetimes were collected by the time-correlated single photon counting method. The results are listed in Table 8.3.

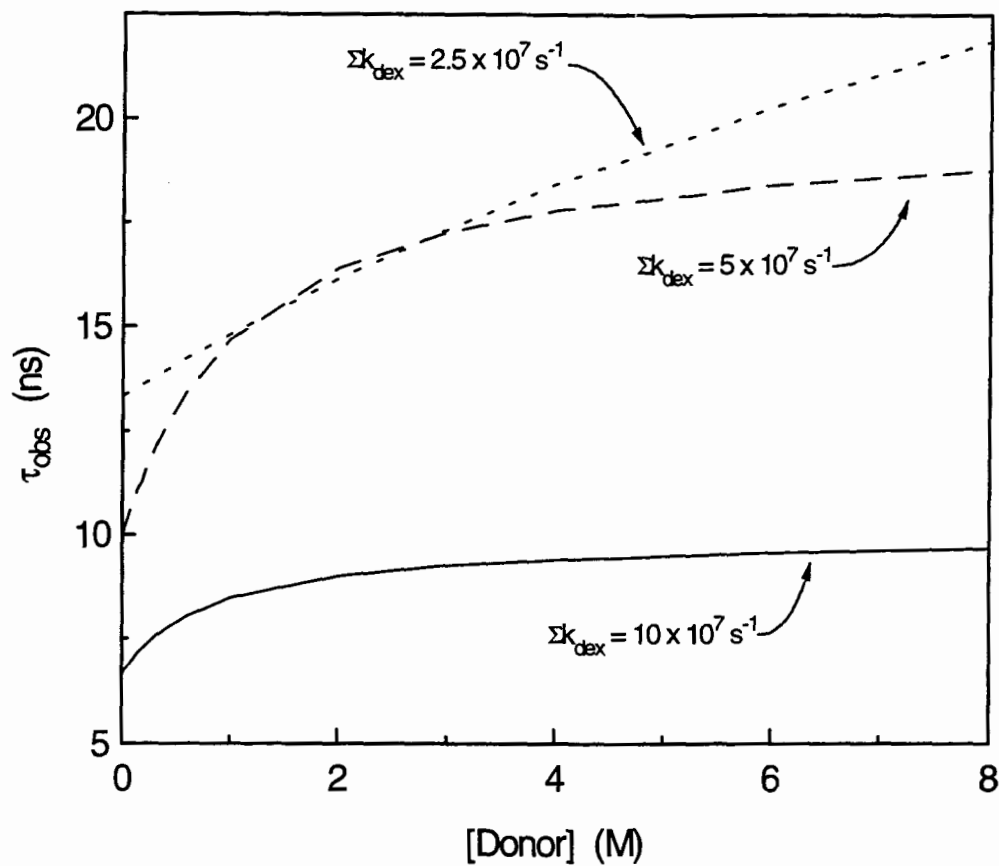


Figure 8.3: The Influence of the Exciplex's Decay Rate Constant (Σk_{dex}) on the Observed Exciplex Lifetime. The Lines were Calculated Using Eq 8.6 with the Following Parameters: $1/\tau_m = 4.3 \times 10^9 \text{ s}^{-1}$; $k_{\text{ex}} = 5 \times 10^7 \text{ s}^{-1}$; $k_{\text{ex}} = 7.5 \times 10^9 \text{ M}^{-1} \text{ s}^{-1}$.

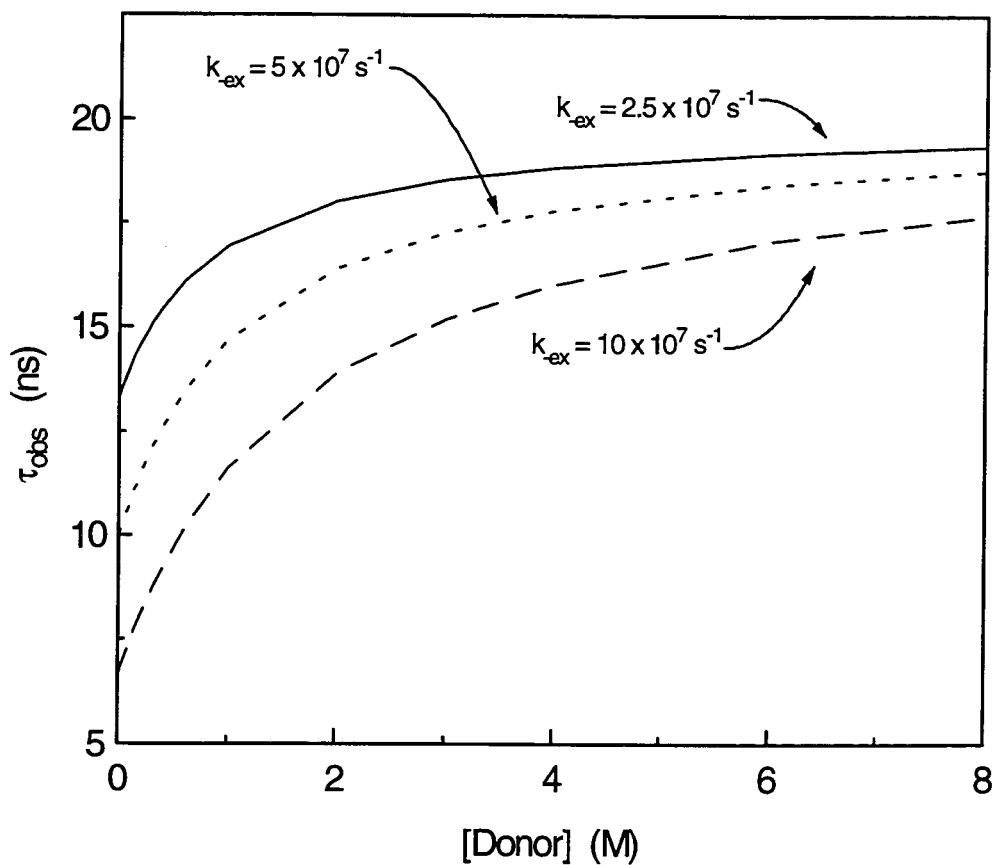


Figure 8.4: The Influence of the Exciplex's Decay Rate Constant (k_{ex}) on the Observed Exciplex Lifetime. The Lines were Calculated Using Eq 8.6 with the Following Parameters: $1/\tau_m = 4.3 \times 10^9 \text{ s}^{-1}$; $\Sigma k_{\text{dex}} = 5 \times 10^7 \text{ s}^{-1}$; $k_{\text{ex}} = 7.5 \times 10^9 \text{ M}^{-1} \text{ s}^{-1}$.

Table 8.3: Comparison of the Lifetimes of the DBMBF₂ / Benzene Exciplex and Excited EDA Complex in Argon Degassed Cyclohexane at 23 °C.

Donor	[Donor] (M)	τ_{obs} (ns) ^a	
		365 nm ^b	400 nm ^b
HMB	0.085	24.7	24.2
PMB	0.114	24.3	24.2
Durene	0.052	23.1	22.6
1,2,3,5-Tetramethylbenzene	0.141	19.4	19.0
1,2,3,4-Tetramethylbenzene	0.099	16.0	15.9
Mesitylene	0.182	7.9	8.0
5-t-Butyl-m-Xylene	0.118	6.1	5.9

^a Excitation wavelength. ^b Monitored at 550 nm.

The good agreement in Table 8.3 between the relaxed EDA complex and exciplex's lifetimes, together with the spectroscopic data in Chapter Five, are conclusive evidence that these two species are the same.

8.2.3. Thermodynamic Properties

The exciplex enthalpy of formation ($-\Delta H_{\text{ex}}$) was discussed in Chapter Seven where the binding energy was correlated with the degree of charge transfer within the exciplex. From the rate constants in Table 8.2, the free energy of exciplex formation in cyclohexane ($\Delta G_{\text{ex}} = -RT \ln(K_{\text{ex}})$) can be calculated. Since both $-\Delta G_{\text{ex}}$ and $-\Delta H_{\text{ex}}$ (Table 7.1) are now known, $-\Delta S_{\text{ex}}$ is readily calculated (Table 8.3). The results are listed in Table 8.4.

According to Weller [54,65,70,134,138d,154] the ΔH_{ex} and ΔG_{ex} are correlated to the donor and acceptor's redox potentials by

$$-\Delta H_{\text{ex}} = E_{\text{ox}} - E_{\text{red}} + U_{\text{Dest}} - U_{\text{Stab}} + 0.15 \text{ eV} - E_{\text{S}} \quad (8.8)$$

$$\begin{aligned} -\Delta G_{\text{ex}} &= -\Delta H_{\text{ex}} + T\Delta S_{\text{ex}} \\ &= E_{\text{ox}} - E_{\text{red}} + U_{\text{Dest}} - U_{\text{Stab}} + 0.38 \text{ eV} - E_{\text{S}} \end{aligned} \quad (8.9)$$

Equation 8.8 is obtained from a rearrangement of eqs 7.1 and 7.4 and eq 8.9 was derived from 8.8 on the assumption that $-\Delta S_{\text{ex}}$ has a constant value of 18 e.u. (0.23 eV) [54,70,134]. These equations predict that the exciplex binding energy becomes stronger and that the free energy becomes more spontaneous with decreasing oxidation potential (with a single acceptor the E_{red} is constant). Weller [54,70,134] was able to demonstrate that ΔG_{ex} and ΔH_{ex} are linear functions of $E_{\text{ox}} - E_{\text{red}}$ with unit slope for exciplexes with large dipole moments ($\mu_{\text{ex}} \geq 10$ Debyes). For DBMBF₂ / benzene exciplexes listed in Table 8.4, they are not expected to strictly follow eq 8.8 due to the curvature in Figure 6.1 (the exciplex emission energy and ΔH_{ex} are linearly related by eq 7.2) and that the exciplex

energy becomes invariant of the donor and acceptor's redox potentials (cf. Chapter Six and Seven). Because $\Delta H_{\text{ex}} \propto \Delta G_{\text{ex}}$, eq 8.9 is not expected to hold as well. As an indication of the inapplicability of eq 8.9 to estimate ΔG_{ex} , estimated values are shown in the ΔG_{ex} column of Table 8.4, the experimental ΔH_{ex} values and the assumed $\Delta S_{\text{ex}} = -18$ e.u. were used to calculate ΔG_{ex} . Note that using the experimental ΔH_{ex} values in this calculation allows inclusion of the $U_{\text{Dest}} - U_{\text{Stab}}$ terms, which are unknown. The calculated ΔG_{ex} suggests a non-spontaneous reaction in all but one case whereas the experimental values are all spontaneous. This poor prediction is the result of assigning a constant ΔS_{ex} of -18 e.u.

The assumption of Weller [54,70,134] that $-\Delta S_{\text{ex}}$ has the constant value of 18 e.u. is not borne out in this system (Table 8.4); this was also noted in other exciplex systems [138d,153,154] where a linear relationship between $-\Delta H_{\text{ex}}$ and $-\Delta S_{\text{ex}}$, with a positive slope, was observed (compensation rule [114]). For the methylbenzenes as electron donors, $-\Delta S_{\text{ex}}$ was a constant value ca. 8 e.u. whereas the exciplexes with hindered benzene donors hint of a linear relationship between $-\Delta H_{\text{ex}}$ and $-\Delta S_{\text{ex}}$ with a negative slope (opposite of the compensation rule).

The total change in entropy in forming an exciplex can be represented as a sum of three terms [114,152,153]:

$$\Delta S_{\text{ex}} = \Delta S_{\text{trans/rot}} + \Delta S_{\text{vib/int-rot}} + \Delta S_{\text{solvent}} \quad (8.10)$$

The first term is related to changes in the translational and rotational degrees of freedom whereas the second term is related to changes in the intramolecular degrees of freedom during complex formation (vibrational and internal rotational); i.e., the appearance of new vibrations due to the intramolecular bond. The contribution of the $\Delta S_{\text{trans/rot}}$ [114,152] is always negative, that is, a loss in the degrees of freedom, and reasonably constant (since $\Delta S_{\text{trans/rot}}$ is related to the movement of rigid bodies) for a set of structurally similar

Table 8.4: Thermodynamic Properties of Some DBMBF₂ / Benzene Exciplexes in Cyclohexane Under Argon.

Benzene	- ΔG _{ex}		- ΔH _{ex}	- ΔS _{ex}
	(kcal / mol)		(kcal / mol)	(e.u.)
	Obs.	Calc. ^a		
Benzene	0.06 ± 0.11	- 2.8	2.5 ± 0.2	8.2 ± 0.6
Toluene	0.89 ± 0.08	- 2.1	3.2 ± 0.2	7.8 ± 0.6
o-Xylene	2.07 ± 0.08	- 0.9	4.4 ± 0.3	7.9 ± 0.8
m-Xylene	2.01 ± 0.08	- 0.8	4.5 ± 0.3	8.4 ± 0.8
p-Xylene	2.69 ± 0.07	- 0.2	5.1 ± 0.5	8.1 ± 1.2
Mesitylene	3.22 ± 0.07	0.3	5.6 ± 0.5	8.0 ± 1.2
t-Butylbenzene	0.31 ± 0.07	- 2.9	2.4 ± 0.2	7.1 ± 0.6
p-t-Butyltoluene	1.99 ± 0.07	- 1.6	3.7 ± 0.3	5.8 ± 0.8
5-t-Butyl-m-xylene	3.01 ± 0.07	- 1.0	4.3 ± 0.3	4.4 ± 0.8

a Calculated from $\Delta G_{ex} = \Delta H_{ex} - T\Delta S_{ex}$ where $\Delta S_{ex} = - 18$ e.u.

compounds. The contribution of $\Delta S_{vib/int-rot}$ is usually positive. The $\Delta S_{solvent}$ contribution is may be either positive or negative depending on whether the solvent shells around the *A and D is more or less ordered than the solvent shell around the exciplex. The major contribution to this quantity has been suggested to be due to the vibrational modes of the donor-acceptor bond. Changes in ΔS_{ex} can be attributed to changes in $\Delta S_{vib/int-rot}$ [114]. For weak binding systems the donor-acceptor bond is expected to have a low vibrational frequency hence a significant positive contribution to $\Delta S_{vib/int-rot}$, in other words, as the binding energy decreases the $\Delta S_{vib/int-rot}$ contribution increases: the overall entropy of

exciplex formation may be related to the enthalpy of exciplex formation (compensation rule) [114,152]. It is known that EDA complexes [50,114,152], excimer [155] and exciplex systems [138d,153,154] follow the compensation rule hence it can be stated that the donor-acceptor bond is the major influence in changes in ΔS_{ex} . Since the compensation rule is based on solid statistical thermodynamic foundations [114,117] and has been experimentally established for EDA complexes [50,114,152], excimer [155] and exciplex systems [138d,153,154], correlation between ΔH_{ex} vs. ΔS_{ex} for exciplexes can be expected if the largest variation in ΔS_{ex} is due to changes in the intramolecular vibrational frequency. This influence on ΔS_{ex} can be illustrated by eq 8.11, which is derived from the simple harmonic oscillator partition function.

$$\bar{S}_{\text{vib}} = R \sum \left[\frac{hv}{k_B T (\exp(hv / k_B T) - 1)} - \ln (1 - \exp(- hv / k_B T)) \right] \quad (8.11)$$

Since the binding energy is proportional to the vibrational frequency of a simple harmonic oscillator, a small binding energy results in a small ν . As a result of smaller frequencies the ΔS_{vib} given by eq 8.11 becomes larger.

In Table 8.4 the methylbenzene donors show isoentropic behavior within experimental error. This behavior may represent that the change in degrees of freedom for the DBMBF₂ / substituted benzene exciplexes in cyclohexane is a manifestation of a balancing act between changes in the intramolecular bond frequency and another degree of freedom with different donors. In contrast, for the hindered benzene donors, ΔS_{ex} increases with decreasing ΔH_{ex} . This trend is opposite from that expected based on the compensation rule, suggesting that the intramolecular bond vibrational frequency contribution can no longer counterbalance the overall entropy. Two candidates appear to be contributors to ΔS_{ex} : the change in substituents and the change in exciplex charge transfer character. The fact that changing the substituent group affects ΔS_{ex} suggests that

the degrees of freedom can be associated with the vibrational / rotational degrees of freedom of the substituent. For the latter candidate, the percentage of charge transfer character within the exciplex is changing with different benzene donors, hence the solvent shell around the exciplex becomes more ordered and the removal / gain of electron density can lead to the weakening of a chemical bond.

Under the assumption that the observed ΔS_{ex} values in Table 8.4 are due to the substituent contribution to the $\Delta S_{\text{vib/int-rot}}$ term in eq 8.10, the sources for changes in entropy are the C — H and C — C vibrations and rotation of the substituent. Substituents are not electronically isolated from the benzene π system as manifested by the changes in IP (or E_{ox}) with the number of methyl substituents where Figure 8.5 illustrates the in phase π_{CH_3} mixing with the benzene π system that allows communication between the substituent and the benzene moiety [156]. Forming an exciplex with singlet excited DBMBF₂ results in electron density being removed from the benzene π system. The C — H periplanar bond is expected to be preferentially weakened due to donation of electron density into the benzene ring as a result of the benzene ring yielding electron density to singlet excited DBMBF₂. Therefore, the periplanar C — H vibrational frequency is expected to decrease thereby affecting the vibrational degrees of freedom and $\Delta S_{\text{vib/int-rot}}$. It is known that the involvement of the periplanar C — H bonds in exciplexes are manifested in their radiationless decay [157,158]. However, eq 8.11 predicts that the frequency required to produce a sizable change in ΔS_{ex} (eq 8.11) is less than 500 cm⁻¹ which is unlikely. The rotational degree of freedom of the substituent is another possible influence on ΔS_{ex} . However, the rotation of the substituent is more hindered in a complex, which produces a negative contribution on ΔS_{ex} [114].

Having excluded $\Delta S_{\text{trans/rot}}$ and $\Delta S_{\text{vib/int-rot}}$ as sources to rationalize the constant ΔS_{ex} , we are left with the contribution due to the solvent, $\Delta S_{\text{solvent}}$. It is clear that increasing a exciplex's dipole moment will result in a more ordered solvent shell. This has a net positive contribution to the ΔS_{ex} relative to an exciplex with a smaller dipole moment.

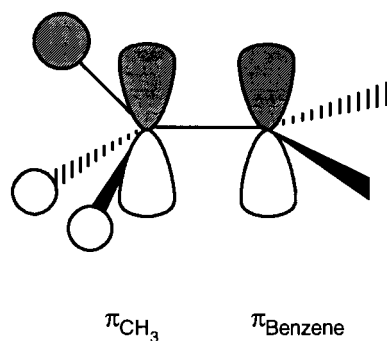


Figure 8.5: In Phase Mixing of the π_{CH_3} with the Benzene Ring π System; Only the Ipso Carbon π Orbital is Shown for Clarity.

For the benzene electron donors listed in Table 8.4, the corresponding exciplex with singlet excited DBMBF₂ has a significant change from 4 to 10 D (Table 6.2). The contribution of the exciplex dipole moment on the $\Delta S_{\text{solvent}}$ can be determined if the free energy, or work, of polarizing the solvent shell is known, hence the change in entropy can be calculated from $\partial \Delta G / \partial T = - \Delta S$. From Liptay's work [84], the work to polarize a medium is proportional to the square of the dipole immersed in the medium. Therefore we can expect $\Delta S_{\text{solvent}} \propto (\mu_{\text{ex}})^2$ assuming that the exciplex dipole moment is not temperature dependent: the increase in exciplex charge transfer results in a net positive contribution to ΔS_{ex} . The isotropic behaviour observed in Table 8.4 may be due to opposing contributions within ΔS_{ex} (i.e., $\Delta S_{\text{trans/rot}} + \Delta S_{\text{vib/int-rot}}$ vs. $\Delta S_{\text{solvent}}$).

CHAPTER NINE

EXCIPLEX RADIATIVE AND RADIATIONLESS PROCESSES IN CYCLOHEXANE

9.1 Introduction and Mathematical Models

9.1.1 General

Radiationless [159-171] and radiative [159,172-177] decay processes of electronically excited molecules have been extensively investigated. Theoretical expressions for the radiative rate constant are usually based on Einstein's derivation for the probability of spontaneous emission [159,172-177]. Experimental tests of these theoretical models have shown that they predict the radiative rate constant atleast within an order of magnitude. In numerous cases the agreement between theory and experiment is excellent [159,172-177]. However, for excited state molecular complexes the cooperative interaction between the donor and acceptor to either emit a photon or thermally degrade the excitation energy is not fully understood and only recently have serious attempts to characterize the radiative and radiationless processes in excited EDA complexes and exciplexes been undertaken [38,60,135a,163,164,178-181].

9.1.2 Emission Probability

The emission probability of an excited molecular complex has been proposed by Prochorow and Siegoczyński [179a] to be due to the extent of locally excited state contribution to the complex's wavefunction; i.e., the complex 'steals' its emission probability by coupling with $^1A^*$ or $^1D^*$. This proposal has gained acceptance in the literature [182,183]; however, there has been no rigorous test where the examples had essentially

complete charge transfer nature. The variable charge transfer exciplexes described in this thesis provide a better system to test this hypothesis.

To test the hypothesis of Prochorow and Siegoczyński we need some working relationships that are experimentally tractable. The Einstein probability per second, A , for spontaneous emission for nondegenerate states is given by eq 9.1 [72,135a,159,172]

$$A = (64\pi^4 / 3hc^3) n^3 \nu_{\max}^3 |M|^2 \quad (9.1)$$

where M is the transition dipole moment between the excited and ground state, n is the refractive index and the other symbols have their usual meaning. For an exciplex, the expression for the emission transition dipole moment is given by [71d,72,135a,184,185]

$$M = M_{\text{ex}} = \langle \Psi_{\text{EX}} | \Sigma \mathbf{r} | \text{AD} \rangle = a \langle \text{A}^* \text{D}^+ | \Sigma \mathbf{r} | \text{AD} \rangle + c \langle \text{A}^* \text{A} | \Sigma \mathbf{r} | \text{AD} \rangle \quad (9.2)$$

Since the operator \mathbf{r} is not a function of the spin coordinates, transition between states of different multiplicity is forbidden. The first integral $\langle \text{A}^* \text{D}^+ | \Sigma \mathbf{r} | \text{AD} \rangle$ has been shown by Mulliken [50] to be small and we will tentatively neglect this integral.

The second integral can be approximated by the local $\text{A}^* \text{A} \rightarrow \text{A}$ transition integral [71c,d], $\langle \text{A}^* \text{A} | \Sigma \mathbf{r} | \text{AD} \rangle \cong \langle \text{A}^* \text{A} | \Sigma \mathbf{r} | \text{A} \rangle$, where $\langle \text{A}^* \text{A} | \Sigma \mathbf{r} | \text{A} \rangle$ may be evaluated from experimental quantities; this approximation was found to be reasonable (cf. Chapter Six & Seven). Substituting eq 9.2 into eq 9.1 we find

$$A = (64\pi^4 / 3hc^3) n^3 \nu_{\max}^3 c^2 |\langle \text{A}^* \text{A} | \Sigma \mathbf{r} | \text{A} \rangle|^2 \quad (9.3)$$

This equation shows that the radiative probability of an excited molecular complex is mainly derived from the radiative probability of one of the complex partners. Therefore, eq 9.3 suggests two ways to improve a complex's emission probability: i) the $\text{A}^* \text{A} \rightarrow \text{A}$

should be fully allowed (i.e., maximize the $\langle *A | \Sigma \epsilon r | A \rangle$ integral) and ii) maximize the weight of this integral through the coefficient c.

The Einstein probability of spontaneous emission, A, is equal to the radiative rate constant (the reciprocal of the emissive lifetime) [69,159]; however, observed lifetimes contain two components, the radiative and radiationless rate constants hence separation of these two rate constants is necessary. To access the radiative and radiationless rate constants we will need the exciplex's fluorescence quantum yield, Φ_{ex}^{∞} , as defined by eq 9.4 [65].

$$\Phi_{ex}^{\infty} = k_f^{ex} / (k_f^{ex} + k_{nr}^{ex}) = k_f^{ex} \tau_{ex} \quad (9.4)$$

Experimentally, the exciplex's fluorescence quantum yield is concentration dependent as shown by eq 9.5 according to Scheme 5.1.

$$\Phi_{ex} = \frac{k_f^{ex} k_{ex} [D]}{(k_{-ex} + \Sigma k_{dex}) \{ \Sigma k_d + (k_{ex} \Sigma k_{dex} [D] / (k_{-ex} + \Sigma k_{dex})) \}} \quad (9.5)$$

$$\text{where } \Sigma k_d = k_f + k_{nr} \text{ and } \Sigma k_{dex} = k_f^{ex} + k_{nr}^{ex}$$

When $k_{ex} \Sigma k_{dex} [D] / (k_{-ex} + \Sigma k_{dex}) \gg \Sigma k_d$, eq 9.5 reduces to eq 9.4: $\Phi_{ex} \rightarrow k_f^{ex} \tau_{ex}$. This limit can not be reached experimentally for obvious reasons but an equation that can be used evaluate Φ_{ex}^{∞} is shown below.

$$(\Phi_F) / (\Phi_F^0) + (\Phi_{ex}) / (\Phi_{ex}^{\infty}) = 1 \quad (9.6)$$

Equation 9.6 follows from $(\Phi_F) / (\Phi_F^0) = 1 / (1 + p k_{ex} \tau_m [D])$, $(\Phi_{ex}) / (\Phi_{ex}^{\infty}) = p k_{ex} \tau_m [D] / (1 + p k_{ex} \tau_m [D])$ and $p = (k_{-ex} \tau_{ex} + 1)^{-1}$. If the exciplex is quenched by second molecule of

ground state D then eq 9.6 is invalid; the determination of the exciplex stoichiometry in Chapter Five showed no hint of this.

Once these quantum yields and lifetimes (see above) are known, the radiative radiationless rate constants for the exciplex can be evaluated.

$$k_f^{\text{ex}} = \Phi_{\text{ex}}^{\infty} / \tau_{\text{ex}} \quad \text{and} \quad k_{\text{nr}}^{\text{ex}} = (\tau_{\text{ex}})^{-1} - k_f^{\text{ex}} \quad (9.7)$$

9.1.2 Radiationless Probability

The radiationless processes for high charge transfer exciplexes and excited EDA complexes are the most understood of the molecular complexes and have been discussed by several authors on theoretical and experimental grounds [38,60,164,165,178,179]. The usual starting point for the description of radiationless processes, from an electronic state *i* to *f*, is the Fermi 'golden rule' [160-168,186], according to which the transition rate constant is proportional to the square of the matrix element between the two states, $\langle \Psi_i | V | \Psi_f \rangle$, where *V* is the appropriate perturbation causing the transition [168,186]. For internal conversion (i.e., between states of the same multiplicity) *V* is the nuclear kinetic operator and for intersystem crossing (i.e., between states of different multiplicity) *V* is the spin-orbit coupling or hyperfine coupling operator [71]. With a number of approximations, it can be shown that the radiationless rate constant of an excited state complex decreases exponentially with an increase in the energy gap between states *i* and *f*. This trend is typically termed the energy gap law [38,69,186].

A milestone treatment, and the most recent, is the work of Gould, Farid and Young for contact radical ion pairs (CRIP) [60]; i.e., weak electronic coupling. Gould and Farid have shown that the current theories of electron transfer, cast in the form of a golden rule expression, quantitatively predict the rate of back electron transfer, which is the dominant nonradiative rate for these complexes. The essential parameters are derived from the

CRIP's emission spectral profile [60,186]. The back electron transfer step can be regarded as internal conversion.

The work of Gould and Farid is a critical first step in quantifying the radiationless process. However, in general, the non-negligible electronic coupling common to most exciplexes invalidates the use of electron transfer theory as a theoretical basis. For the exciplexes in this study the $|A^{\cdot-}D^{\cdot+}\rangle \leftrightarrow |^*AD\rangle$ resonance interaction requires an entirely different approach. Because of this, highly to weakly polar exciplexes have received little attention regarding their radiationless processes.

As originally proposed by Zachariasse [178], high CT exciplexes belong to the 'strong coupling limit' in theories of radiationless processes. This was also recognized earlier by Siebrand [163] for excimers and Freed and Jortner [164] for excited EDA complexes. In the strong coupling limit, Englman and Jortner [165] derived an equation that follows the energy gap. Experimentally, it is found that the rate for internal conversion in excited EDA complexes is dependent on the coupling of the exciplex to one of its components [157,158], either A or D, and strongly depends on the exciplex's energy (i.e., follows the energy gap law) and charge transfer character. Isotopic substitution (C — H to C — D) reduces the radiationless rate constant as generally expected for internal conversion [157]. The rate for intersystem crossing is chiefly influenced by spin-orbit coupling and is insensitive to the exciplex energy [187,188]; heavy atom substitution leads to a large increase in the radiationless rate constant. It is generally observed that intersystem crossing from the singlet exciplex results in the formation of a triplet A or D [188]. In addition, it is believed that spin-orbit coupling is enhanced by charge transfer interactions [184,187]. The infrequent occurrence of a triplet exciplex has been rationalized to be due to the singlet-triplet coupling integral, $\langle ^1\Psi_{ex} | H_{SO} | ^3\Psi_{ex} \rangle$, is zero [157]. Another rationalization is that the triplet exciplex wavefunction is dominated by $|^3A^*D\rangle$ [72], hence observable properties of the triplet exciplex may be indistinguishable from that of $^3A^*$.

9.2 Results and Discussion

9.2.1 General

In nonpolar and weakly polar solvents the fluorescence quenching of singlet excited DBMBF₂ by substituted benzenes results in strong exciplex emission. The fluorescence intensity is strongest in nonpolar solvents, such as cyclohexane, and becomes weaker with increasing solvent polarity; in acetonitrile exciplex emission could only be observed for weak electron donating benzenes (cf. Table 6.1). The lifetimes for these exciplexes in cyclohexane were evaluated in Chapter Eight.

The exciplex fluorescence quantum yield ($\Phi_{\text{ex}}^{\infty}$) was measured for a selected group of benzene quenchers ranging from electron rich (HMB) to electron poor (benzene). The $\Phi_{\text{ex}}^{\infty}$ was calculated from integrated fluorescence spectra, in the presence and absence of donor, according to eq 9.9, which is based on eq 9.6.

$$\Phi_{\text{ex}}^{\infty} = \Phi_{\text{F}} (A_{\text{ex}} / A_{\text{A}}^{\circ} - A_{\text{A}}) \quad (9.9)$$

A_{ex} and A_{A} represents the exciplex and DBMBF₂'s integrated fluorescence intensity, respectively; A_{A}° is DBMBF₂'s fluorescence intensity in the absence of quencher. This in effect uses the unquenched DBMBF₂ fluorescence intensity as a secondary fluorescence quantum yield standard. Using the known value for Φ_{F} in cyclohexane of 0.045 (Table 3.2), $\Phi_{\text{ex}}^{\infty}$ was evaluated at several donor concentrations ($[D] < 1 \text{ M}$) and the mean values reported. The advantage of eq 9.9 is that the donor concentration need not be known; this equation has one disadvantage in that DBMBF₂ fluorescence intensity must be significantly quenched because the largest source of error occurs with the term $A_{\text{A}}^{\circ} - A_{\text{A}}$. Due to errors in A_{A}° and A_{A} , a small difference between A_{A}° and A_{A} will result in large errors in the calculated $\Phi_{\text{ex}}^{\infty}$. Typically, the fluorescence of singlet excited DBMBF₂ was quenched

more than 10 percent. Unfortunately, the electron poor benzenes do not quench DBMBF₂'s fluorescence significantly at concentrations less than 1 M hence the $\Phi_{\text{ex}}^{\infty}$ for the exciplexes with methyl benzoate and cyanobenzene as donors can not be obtained; their exciplex emission intensity was qualitatively larger than that for benzene as a donor.

The $\Phi_{\text{ex}}^{\infty}$ results are summarized in Table 9.1. Included in Table 9.1 are some exciplex's $\Phi_{\text{ex}}^{\infty}$ values obtained in neat aromatic solvent where it was assumed that all the singlet excited state DBMBF₂ was completely quenched; this is supported by no observable DBMBF₂ fluorescence. Therefore, $\Phi_{\text{ex}}^{\infty}$ in aromatic solvents was calculated by eq 3.2 using DBMBF₂ (cyclohexane) as a fluorescence quantum yield standard.

The effect of the charge transfer nature of DBMBF₂ / substituted exciplexes on the fluorescence quantum yield is quite dramatic as shown in Figure 9.1. Over a IP range of 1.4 eV the $\Phi_{\text{ex}}^{\infty}$ drops by one fifth from benzene to HMB as donors. This indicates that $\Phi_{\text{ex}}^{\infty}$ is a strong function of the charge transfer nature of these exciplexes. A similar trend was found by Davis et al. [184] for the 1,4-dicyanonaphthalene / benzene exciplexes in n-heptane. In their study the $\Phi_{\text{ex}}^{\infty}$ drops from 0.55 to 0.01 for the 1,4-dicyanonaphthalene / o-xylene to 1,4-dicyanonaphthalene / 1,2,4-trimethoxybenzene exciplexes, respectively. Using the lifetimes in Table 8.1 and 8.2 with the exciplex $\Phi_{\text{ex}}^{\infty}$ in Table 9.1, the radiative and radiationless rate constants for these exciplexes were calculated from eq 9.7 and listed in Table 9.2.

9.2.2 Exciplex Radiative Probability

In Table 9.2, the radiative rate constant, k_f^{ex} , clearly shows a dependence on the exciplex donor. This rate constant decreases by nearly two orders in magnitude from benzene to HMB. As shown in the introduction, the mathematical model for exciplex radiative probability indicates that the radiative rate constant for an exciplex is a function of the exciplex fluorescence maximum and the extent of charge transfer (by way of M_{ex}).

Table 9.1: DBMBF₂ - Benzene Exciplex Fluorescence Quantum Yields ($\Phi_{\text{ex}}^{\infty}$) in Argon
Purged Cyclohexane^a

Benzene	IP (eV)	$\Phi_{\text{ex}}^{\infty}$	Benzene	IP (eV)	$\Phi_{\text{ex}}^{\infty}$
	b			b	
HMB	7.85	0.11	o-Xylene	8.56	0.43
PMB	7.92	0.16			0.42 ^c
Durene	8.05	0.21	Toluene	8.82	0.51
1,2,3,5-TMB	8.06	0.22			0.52 ^c
1,2,3,4-TMB	8.14	0.27	Benzene	9.24	0.56
1,2,4-TMB	8.27	0.31			0.38 ^c
Mesitylene	8.42	0.41	t-Butylbenzene	--	0.30
		0.45 ^c	p-t-Butyltoluene	--	0.26
p-Xylene	8.44	0.39	5-t-Butyl-m-Xylene	--	0.28
		0.46 ^c	4-t-Butyl-o-Xylene	--	0.21
m-Xylene	8.56	0.40	5-t-Butyl-1,2,3-TMB	--	0.14

^a Absolute error $\pm 10\%$ and relative error $\pm 5\%$. ^b Ionisation potentials obtained from Schlesener, C.J.; Amatore, C.; Kochi, J.K. *J. Phys. Chem.* **1986**, *90*, 3747. ^c Value in aromatic solvent.

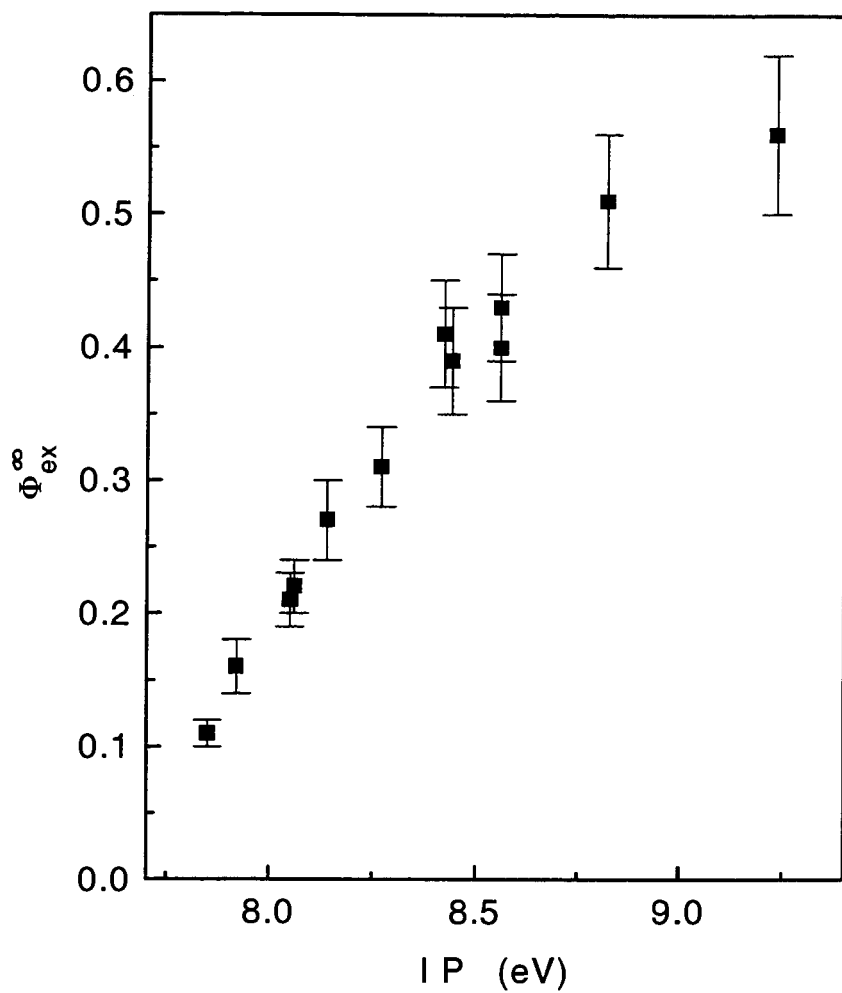


Figure 9.1: Plot of Φ_{ex}^{∞} vs. donor's IP.

Table 9.2: DBMBF₂ / Substituted Benzene Exciplex Radiative and Radiationless Rate Constants in Cyclohexane and Aromatic Solvents; Comparison of Observed and Calculated Radiative Rate Constants

Benzene	k _f ^{ex} (10 ⁶ s ⁻¹)			k _{nr} ^{ex} (10 ⁶ s ⁻¹)
	Obs.	Cal.		Obs.
		a	b	
HMB	4.3 ± 0.4	4 ± 4	--	35 ± 1
PMB	6.6 ± 0.7	7 ± 5	--	34 ± 1
Durene	9.2 ± 0.9	12 ± 5	--	36 ± 1
1,2,3,5-TMB	11 ± 1	13 ± 5	--	40 ± 1
1,2,3,4-TMB	17 ± 2	15 ± 5	--	46 ± 2
1,2,4-TMB	23 ± 2	23 ± 3	--	51 ± 2
Mesitylene	43 ± 6	39 ± 4	--	62 ± 12
	38 ± 4 ^c	--	--	47 ± 4 ^c
p-Xylene	36 ± 5	32 ± 6	48 ± 9	56 ± 10
	35 ± 4 ^c	--	--	41 ± 4 ^c
m-Xylene	44 ± 6	40 ± 3	56 ± 4	66 ± 12
o-Xylene	56 ± 8	43 ± 5	60 ± 7	74 ± 13
	53 ± 6 ^c	--	--	73 ± 6 ^c
Toluene	92 ± 13	59 ± 6	80 ± 8	88 ± 24
	140 ± 15 ^c	--	--	130 ± 15 ^c
Benzene	185 ± 30	150 ± 30	160 ± 30	150 ± 45
	180 ± 20 ^c	--	--	300 ± 20 ^c

Table 9.2 (Continued)

Benzene	k_f^{ex} (10^6 s^{-1})			$k_{\text{nr}}^{\text{ex}}$ (10^6 s^{-1})
	Obs.	Cal.		
		a	b	
t-Butylbenzene	81 ± 12	65 ± 8	73 ± 9	190 ± 18
p-t-Butyltoluene	39 ± 6	14 ± 10	--	110 ± 10
5-t-Butyl-m-xylene	35 ± 5	27 ± 3	--	91 ± 10
4-t-Butyl-o-xylene	19 ± 2	13 ± 2	--	72 ± 2
5-t-Butyl-1,2,3-TMB	10 ± 1	6 ± 3	--	62 ± 1

^a Calculated from eq 9.14 using c^2 obtained from the experimental degree of charge transfer (μ_{ex} in Table 6.2), ν_{max} obtained from Table 6.1, ν_{ave} of 24,100 cm^{-1} and a k_f of $2 \times 10^8 \text{ s}^{-1}$. ^b As in ^a except the solvent induced polarization of the exciplex is accounted for; the degree of solvent induced polarization is estimated to be 11.5% (cf. Chapter Six) and this value together with the gas phase μ_{ex}^0 (Table 6.2) was used to calculate c^2 . ^c Value in aromatic solvent.

However, it is not clear if only the change in the exciplex fluorescence maximum is responsible for the observed trend in k_f^{ex} ; i.e., the emission transition moment, M_{ex} , is constant. Equation 9.1 can be used to demonstrate this possibility where $A = k_f^{ex}$.

$$k_f^{ex} = (64\pi^4 / 3hc^3) n^3 v_{max}^3 |M_{ex}|^2 \quad (9.1)$$

Taking the natural log of eq 9.1 gives

$$\ln(k_f^{ex}) = 3 \ln(v_{max}) + \text{Constant} \quad (9.10)$$

Therefore, a plot of $\ln(k_f^{ex})$ vs. $\ln(v_{max})$ should be linear with a slope of three if and only if M_{ex} is constant. Using the values for v_{max} in Table 6.1 and k_f^{ex} given above, this plot is shown in Figure 9.2.

The curvature of the data points in Figure 9.2 clearly contradicts the suggestion that M_{ex} is constant. Therefore, to account for the curvature in Figure 9.2 M_{ex} must be changing with the change in exciplex charge transfer character. This variation in M_{ex} is obviously a smooth function due to the gradual change in the slope.

To confirm that M_{ex} is a function of the exciplex charge transfer character, k_f^{ex} was calculated according to

$$k_f^{ex} \cong (64\pi^4 / 3hc^3) n^3 v_{max}^3 b^2 | \langle *A | \Sigma \text{er} | A \rangle |^2 \quad (9.11)$$

where the assumption that $\langle *ADI \Sigma \text{er} | AD \rangle = \langle *A | \Sigma \text{er} | A \rangle$ was applied. However, this equation is not in a tractable form. Noting that the radiative rate constant for singlet excited DBMBF₂ in cyclohexane can be cast into a form similar to that shown above,

$$k_f = (64\pi^4 / 3hc^3) v_{ave}^3 n^3 | \langle *A | \Sigma \text{er} | A \rangle |^2 \quad (9.12)$$

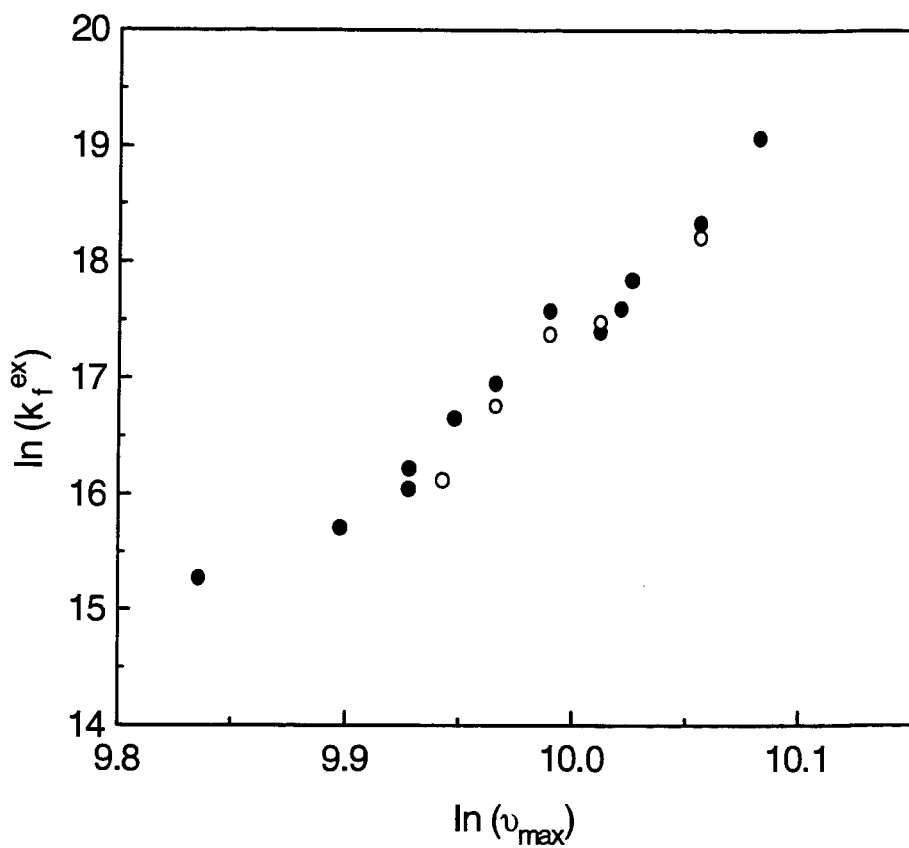


Figure 9.2: Relationship Between Exciplex Radiative Rate Constant and Emission Maximum in Cyclohexane. Methyl Benzenes (●) and t-Butyl Benzenes (○).

where ν_{ave} is the first moment of the fluorescence spectrum,

$$\nu_{ave} = \int \nu I(\nu) d\nu / \int I(\nu) d\nu \quad (9.13)$$

the exciplex radiative rate constant can be more compactly expressed in terms of DBMBF₂'s fluorescence k_f by substitution of eq 9.12 into 9.11.

$$k_f^{ex} \equiv c^2 (\nu_{max} / \nu_{ave})^3 k_f \quad (9.14)$$

All the quantities on the RHS of eq 9.14 are known experimental quantities where k_f (= 0.045 / 0.23 ns) = $2.0 \times 10^8 \text{ s}^{-1}$ (Table 3.2 and 3.3) and $\nu_{ave} = 24,100 \text{ cm}^{-1}$. The coefficient c and ν_{max} are obtained from Table 6.1. Using the appropriate values and eq 9.15, k_f^{ex} was calculated for the different electron donors and listed in Table 9.2.

Using the values in Table 9.2, a plot of the calculated and observed k_f^{ex} is shown in Figure 9.3 where the solid squares and open circles represent calculations based on the observed exciplex dipole moment; in effect we assume an unpolarizable exciplex dipole (cf. Chapter Six). The solid line represents unity slope. The calculated and observed k_f^{ex} are in excellent agreement for HMB to p-xylene as donors, which suggest that i) the exciplex emission probability is practically derived from DBMBF₂'s emission probability through the assumption $\langle {}^*AD | \Sigma \epsilon r | AD \rangle = \langle {}^*A | \Sigma \epsilon r | A \rangle$. Since the calculations are based on the simple exciplex wavefunction

$$\Psi_{EX} = a |A \cdot D^+ \rangle + c |{}^*AD \rangle \quad (2.30)$$

through the evaluation of the coefficient c , the agreement between the calculated and observed k_f^{ex} is in harmony with the earlier conclusion (Chapter Six) that eq 2.30 provides an adequate description of DBMBF₂ / benzene exciplexes.

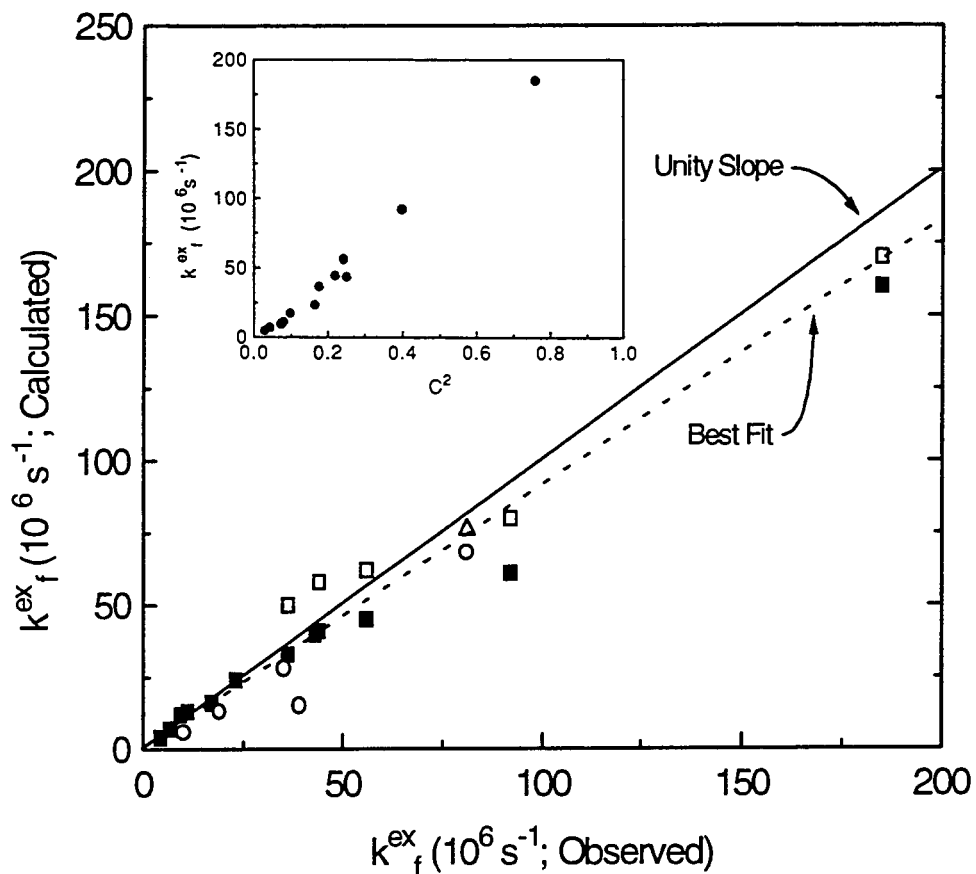


Figure 9.3: Correlation Between the Radiative Rate Constants for DBMBF₂ / Benzene Exciplexes in Cyclohexane Calculated from |*AD> Contribution to the Exciplex Wavefunction to that Observed. The Error Bars are not Shown for Clarity. The Inset Shows the Relationship of k_f^{ex} with Respect to c^2 . Symbols : (■) DBMBF₂ / Methyl Benzene Exciplexes; (□) DBMBF₂ / Methyl Benzene Exciplexes Corrected for Solvent Induced Polarization; (O) DBMBF₂ / t - Butyl Benzene Exciplexes; (Δ) DBMBF₂ / t - Butyl Benzene Exciplexes Corrected for Solvent Induced Polarization.

A closer examination of Figure 9.3 reveals that for o-xylene to benzene as donors the calculated and observed k_f^{ex} are quite different where value with toluene as a donor is outside the error limit; the downward trend appears to be real. One probable explanation for this trend is the difference in the degree of polarisation of these exciplex's dipole moments from one solvent to another. It would therefore be useful to estimate the polarization degree in cyclohexane and recalculate k_f^{ex} to see if the downward trend in Figure 9.3 can be accounted for. Based on eq 6.5 (for cyclohexane $\epsilon = 2.024$ and $n = 1.4235$ [30a]) cyclohexane is capable of increasing the exciplex's dipole moment by 11.5 % relative to the gas phase dipole moment. Using the estimated gas phase exciplex dipole moments in Table 6.2, k_f^{ex} was recalculated for exciplexes with p-xylene to benzene as donors and these results are represented as the open squares in Figure 9.3 (and listed in Table 9.2).

The polarisability correction for the exciplexes with p- and m-xylene as donors are too large, probably because these complexes are nearly full charge transfer in character. For o-xylene as a donor, this correction overestimates k_f^{ex} ; however, the corrected value is closer to the unity line than the uncorrected value. For benzene a small improvement is calculated. The largest change occurs for toluene as a donor where this correction leads to a definite improvement; calculated and observed k_f^{ex} now agree within experimental error. This improvement supports the earlier statements (Chapter Six) that the solvent may induce a larger dipole moment. However, the results above indicate that the degree of solvent enhancement of μ_{ex} becomes negligible for exciplexes that are practically CRIPs.

The smaller 'best fit' slope can be attributed to a systematic error in the calculation of k_f^{ex} by eq 9.14 in determining the values of v_{ave} and k_f . Another systematic error may exist in the solvent refractive index correction factor n^3 in eq 9.11. The work of Shibuya [189] has shown that the shape of the solute molecule affects the power of the solvent n correction term. For example, a large flat molecule, a long linear molecule (transition

dipole moment on the longitudinal axis) and a spherical molecule have correction factors of n , $n^{3.3}$ and $n^{2.7}$, respectively. Since the shape of DBMBF₂ is different from its exciplex, eq 9.14 may still contain a residual refractive index correction term, hence the data points in Figure 9.3 are not expected to fall on the unity slope line.

Exciplexes with hindered benzene donors are also in good agreement with the unity slope line, except for one point. This supports the estimation for the solvent cavity, ρ , from the calculation of the exciplex's molecular volume, V_M . It also suggests that the μ_{ex} for these exciplexes are not artificially larger due to this calculation (Chapter Six). The point for the DBMBF₂ / p-butyltoluene exciplex is of particular interest since this exciplex's k_f^{ex} is calculated to be one half the experimental value (Table 9.2). The large dipole moment for this exciplex (Table 6.2) suggests that polarization enhancement of the μ_{ex} is relatively unimportant. The experimental data for this exciplex (v_{max} , k_f^{ex} , Φ_{ex}^∞ and lifetime) not show any deviation from the observed trends. Unfortunately, this complex's k_f^{ex} remains an enigma. Using the observed k_f^{ex} and v_{max} (Table 6.1) for the DBMBF₂ / p-t-butylbenzene and eq 9.14, a c^2 of 0.24 is calculated for this exciplex or a dipole moment of 10.5 Debyes.

Figure 9.3 does indicate that the best fit line through the data points (dashed line) passes through or is near the origin. From the inset of Figure 9.3, the extrapolation ($c^2 \rightarrow$ zero or $a^2 \rightarrow$ unity) gives a k_f^{ex} of $1 \times 10^6 \text{ s}^{-1}$. This supports the conclusion that the contribution of the $\langle A^{\cdot}D^+ | \Sigma \text{er IAD} \rangle$ integral to k_f^{ex} is insignificant relative to $\langle ^*AD | \Sigma \text{er IAD} \rangle$ (eq 9.2). This result reaffirms the initial neglect of the $\langle A^{\cdot}D^+ | \Sigma \text{er IAD} \rangle$ integral, as suggested by Mulliken [50], for the DBMBF₂ / benzene exciplex system. The neglect of this integral has consequences. First, CRIPs are known to be at best weakly fluorescent [50,51,53,54,60,179], which is rationalized by assuming the c coefficient is too small. Second, if both complex partners have very weak emission probabilities their excited state complexes should have low emission yields. Note that these arguments require significant

radiationless rates; i.e., if k_{nr}^{ex} is practically zero then the magnitude of k_f^{ex} is irrelevant ($\Phi_{ex}^{\infty} = k_f^{ex} / (k_f^{ex} + k_{nr}^{ex}) \cong k_f^{ex} / k_f^{ex} = 1$).

The exciplex lifetime and fluorescence quantum yield were also evaluated in neat donor solvent. In Table 9.2 the radiative rate constants in cyclohexane and in neat donor solvents are the same within experimental error, except for toluene. Because of the demonstrated correlation of k_f^{ex} with the exciplex wavefunction (eq 2.27) in Figure 9.3, the similarity of k_f^{ex} indicates only a 1:1 stoichiometric exciplex in neat donor solvent. For toluene, the increase in k_f^{ex} is puzzling and may be evidence for a triplex and higher order complexes; however, it is not clear why toluene would form a triplex with singlet excited DBMBF₂ and benzene, p-xylene and mesitylene would not.

9.2.3 Exciplex Radiationless Probability

In the theory of radiationless transitions of Englman and Jortner [165] the strong coupling limit is described by a relatively large change in configuration that occurs as a result of the radiationless process. The change in configuration leads to an intersection of the initial (i) and final (f) potential surfaces (Figure 9.4a), which are assumed to be harmonic. For complexes this change in configuration is interpreted as a difference in the donor-acceptor orientation. Such a difference has been suggested for DBMBF₂ / benzene exciplexes in Chapter Seven. Furthermore, Zachariasse [178] and Gould et. al [60] have provided evidence for the strong coupling limit for highly polar exciplexes and excited EDA complexes, respectively. In addition, Zachariasse pointed out that if the initial state is of |A⁻D⁺) character and the final state is of |AD) the connection to Marcus' theory of electron transfer becomes obvious (cf. Figures 2.1 and 9.4a).

The weak coupling limit is described by a relatively small change in configuration, leads to the initial state being nestled within the final state potential surface (Figure 9.4b).

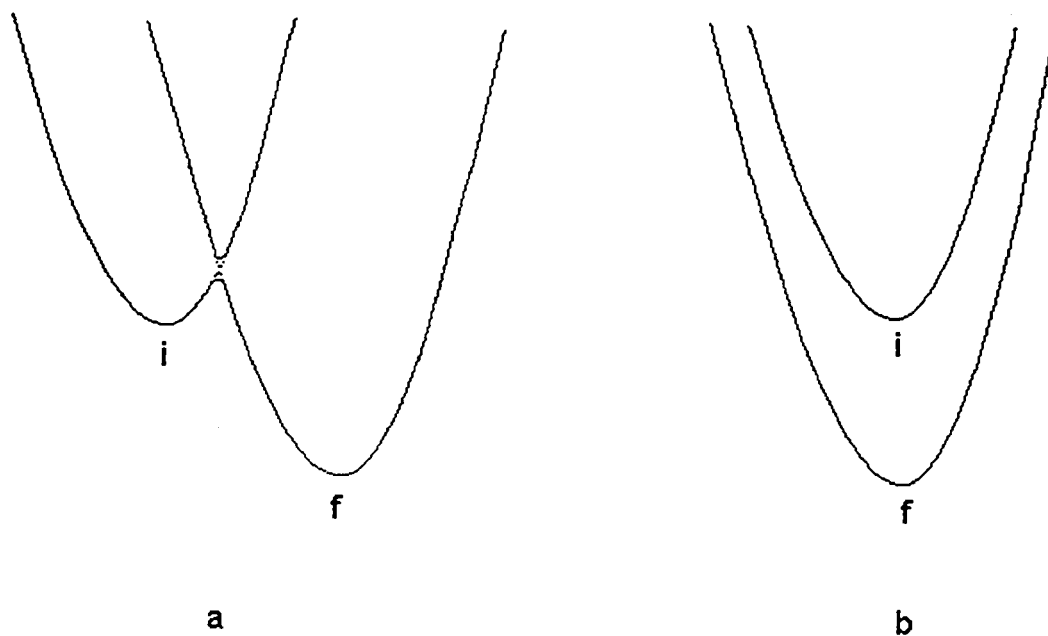


Figure 9.4: The Engleman-Jortner Pictorial Description of the Radiationless Process; The Strong (a) and Weak Coupling (b) Limits.

The weak coupling limit has found applicability in describing the radiationless processes of individual molecules [164,165].

The radiationless rate processes for excited complexes in solution generally follow the energy gap law [38,60,164,165,178,179]. The radiationless rate constant increases as the energy gap between the excited and ground state decreases; the energy gap is equated to $h\nu_{\max}$ [178]. For the DBMBF₂ / benzene system, inspection of Table 9.2 reveals that the change in the radiationless rate constant does not follow the energy gap law where $k_{\text{nr}}^{\text{ex}}$ increases with increasing $h\nu_{\max}$ (cf. Figure 7.4). This result was entirely unexpected. However, review of the literature revealed that this observation is not without precedent [179d,184]. This trend is believed to be reliable since increasing the exciplex fluorescence

quantum yield by 50%, which is significantly larger than the estimated experimental error, does not change this trend in k_{nr}^{ex} .

Unlike the work of Lim et. al [157] and Deperaińska et. al [158] the exciplexes in this study display a wide range of CT character that gradually shifts from the weak to the strong coupling limit (Figure 2b to 2a, respectively). For example, the highly polar DBMBF₂ / benzene exciplexes are expected to belong to the strong coupling limit [178] due to the difference in EDA and exciplex donor-acceptor orientation (Chapter Seven). Due to the domination of $|^*AD\rangle$ ($\approx |^*A\rangle$) within $^1\Psi_{ex}$, the weakly polar DBMBF₂ / benzene exciplexes are believed to be described by the weak coupling case. Therefore, the theory of Englman and Jortner [165] can not be applied to analyze the data in Table 9.2.

Lim et. al [157] and Deperaińska et. al [158] have shown that the radiationless decay of excited EDA complexes (methylbenzene donors) is sensitive to the H / D isotope effect. The C — H stretch serves as the energy accepting vibrational mode. Therefore they were able to conclude that internal conversion is the dominant radiationless mechanism for these complexes on the basis that intersystem crossing was not expected to display an isotope effect. Lim et al. [157] further demonstrated that only the substituent CH bonds are the most important accepting mode where the C — H stretching frequency was modified in the complex due to weakening of this bond by electron donation to the benzene ring (cf. Figure 8.5). For the DBMBF₂ / benzene exciplex system, the internal conversion radiationless mechanism does not appear to influence the radiationless decay since exchanging a methyl for a t-butyl substituent (a loss in energy accepting vibrational modes) does not reduce k_{nr}^{ex} but actually enhances k_{nr}^{ex} (Table 9.2).

Because the simple $^1\Psi_{EX}$ wavefunction, given by eq 2.30, was successful in correctly predicting k_f^{ex} by a semi-empirical treatment, we may be able to treat the radiationless rate constant, k_{nr}^{ex} , in a similar manner [184]. According to Fermi's Golden Rule [160], the radiationless rate constant is given by

$$k_{nr}^{ex} = (2\pi / h) \rho(E) |\langle {}^1\Psi_{EX} | V | \Psi_f \rangle|^2 \quad (9.15)$$

where $\rho(E)$ is the density of states of Ψ_f lying adjacent to ${}^1\Psi_{EX}$ with excess energy E above the origin of Ψ_f . Ψ_f is the final state, which is either (both) the triplet exciplex, (${}^3A^*D$), or (and) Franck-Condon ground state, (A^*D), and V is the appropriate operator. Using eq 2.30, eq 9.15 can be expanded to eq 9.16. k_{nr}^{ex} (CRIP) represents the hypothetical radiationless rate constant for a CRIP, (A^*D^+), k_{nr}^{ex} (LE) is the hypothetical radiationless rate constant of a nonpolar exciplex, A^*D , and k_{nr}^{ex} (CT) represents the cross term.

$$\begin{aligned} k_{nr}^{ex} &= (2\pi / h) \rho(E) |a \langle A^*D^+ | V | \Psi_f \rangle + c \langle {}^1A^*D | V | \Psi_f \rangle|^2 \\ &= (2\pi / h) \rho(E) \{a^2 \langle A^*D^+ | V | \Psi_f \rangle^2 + c^2 \langle {}^1A^*D | V | \Psi_f \rangle^2 \\ &\quad + 2ac \langle A^*D^+ | V | \Psi_f \rangle \langle {}^1A^*D | V | \Psi_f \rangle\} \\ &= a^2 k_{nr}^{ex} \text{ (CRIP)} + c^2 k_{nr}^{ex} \text{ (LE)} + 2ack_{nr}^{ex} \text{ (CT)} \end{aligned} \quad (9.16)$$

Equation 9.16 suggests that the observed k_{nr}^{ex} is the mixing of two processes, namely back electron transfer and an intrinsic radiationless process of DBMBF₂. Although k_{nr}^{ex} (LE) can be expected to be relatively constant, k_{nr}^{ex} (CRIP) is expected to follow Marcus' theory (exponential behavior) hence k_{nr}^{ex} may not be a simple function.

The next step is to identify the final state Ψ_f in which the process of elimination will be used to arrive at a consistent solution. First, since observed k_{nr}^{ex} tends to increase with decreasing charge transfer character (inset of Figure 9.3), the local excited configuration (${}^1A^*D$) is probably the major influence on the complex's radiationless process. Lim et. al [157] and Deperasińska et. al [158] have determined that the $\langle A^*D^+ | H_{SO} | {}^3A^*D \rangle$ integral is significantly larger than the $\langle {}^1A^*D | H_{SO} | {}^3A^*D \rangle$ integral hence k_{nr}^{ex} (CRIP) \gg k_{nr}^{ex} (LE). Therefore it is reasonable to expect that as the charge transfer character increases, the observed k_{nr}^{ex} should increase. In fact, the opposite is observed. Therefore, we can eliminate intersystem crossing as a radiationless process for DBMBF₂ / benzene

exciplexes. For the internal conversion process, the variance of the integrals $\langle A^*D^+IH_{1C}|AD \rangle$ and $\langle ^1A^*DIH_{1C}|AD \rangle$ is unknown. The former integral is known to follow an exponential function [60] whereas the latter is expected to be constant. This can be further expressed by plotting the observed k_{nr}^{ex} vs. c^2 (Figure 9.5). The positive linear slope is clearly indicative of the dominant influence of the $\langle ^1A^*DIH_{1C}|AD \rangle$ integral. Similar to the radiative rate constant, the exciplex 'steals' its radiationless probability from DBMBF₂ (eq 9.17). Least squares analysis gives a y-intercept of $28 \times 10^6 \text{ s}^{-1}$ and a k_{nr}^{ex} (LE) of $1.6 \times 10^8 \text{ s}^{-1}$.

$$k_{nr}^{ex} \propto c^2 k_{nr}^{ex} \text{ (LE)} \quad (9.17)$$

Included in Figure 9.5 are the results for exciplexes with hindered benzenes (open circles). According to the hypothesis that k_{nr}^{ex} is a manifestation of DBMBF₂'s radiationless decay, the slope of k_{nr}^{ex} vs. c^2 should be invariant of steric effects if and only if the integral $\langle ^1A^*DIH_{1C}|AD \rangle$ can be approximated by $\langle ^1A^*IH_{1C}|A \rangle$; the k_{nr}^{ex} (LE) is constant. Ignoring one point, the best parallel line (dashed line in Figure 9.5) appears to randomly pass through the open circles hence suggesting that $\langle ^1A^*DIH_{1C}|AD \rangle$ is indeed approximated by $\langle ^1A^*IH_{1C}|A \rangle$. For the discordant data point, the deviation can be rationalized on the basis of either a breakdown of this approximation or by assuming that the k_{nr}^{ex} (CRIP) term is becoming significant.

The observed trend in Figure 9.5 is a fortunate occurrence since the observed k_{nr}^{ex} is expected to increase with decreasing donor oxidization potential. This is due to the fact that k_{nr}^{ex} (CRIP) is expected to follow Marcus' theory [60]. For example, Davis et al. observed that, for 1,4-dicyanonaphthalene / benzene exciplexes, the observed k_{nr}^{ex} passes through a minimum [184].

Further studies are necessary to firmly establish the radiationless processes of DBMBF₂ / benzene exciplexes. Internal conversion can be demonstrated by the H / D isotope effect as shown by Lim et. al [157] and Deperaińska et. al [158] in their systems.

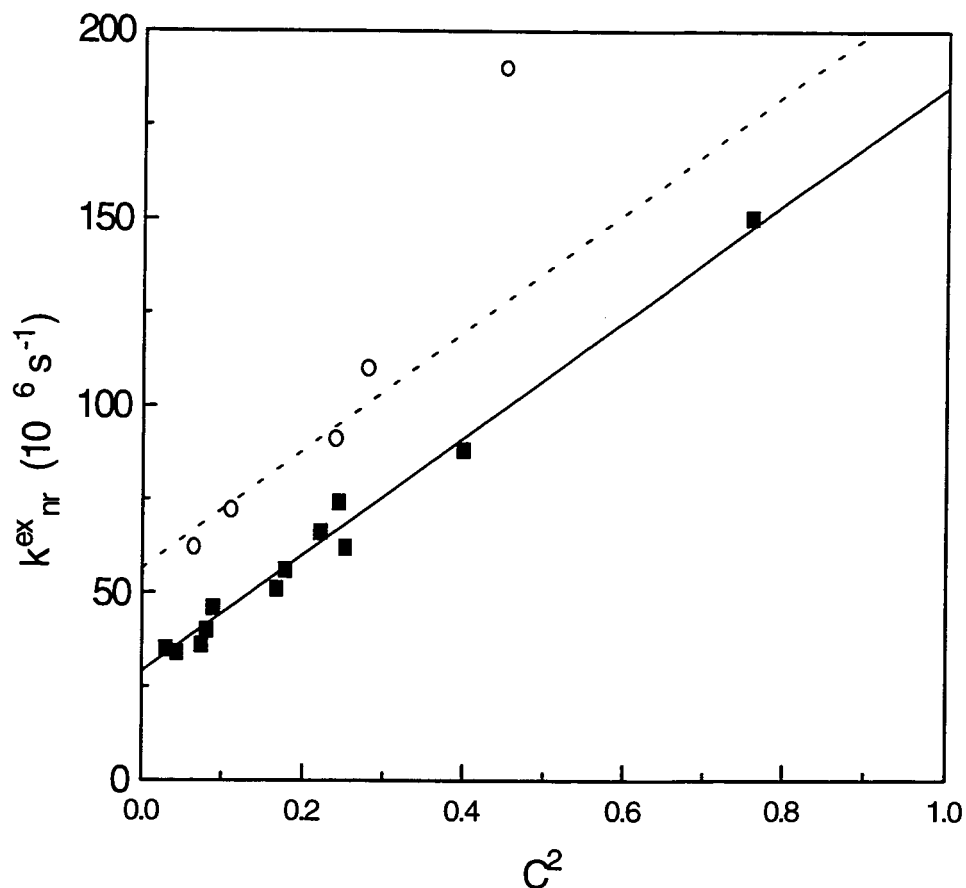


Figure 9.5: Relationship between DBMBF₂ / Benzene Exciplex Radiationless Rate Constant and Contribution of |*AD> to the Exciplex's Wavefunction. Closed Squares Represent Methylbenzene Donors and the Open Circles Represent Hindered Benzene Donors. The Coefficient c^2 was Obtained from Table 6.2 and k_{nr}^{ex} from Table 9.2. The Solid Line is the Best Fit Through the Closed Squares and the Dashed Line is Best Line Through the Open Circles that is Parallel to the Solid Line; the Last Point was Ignored.

Intersystem crossing can be demonstrated by flash photolysis where the change in the quantum yield of triplet state formation ($^3A^*$ or $^3D^*$) is indicative of the $^1(AD) \rightarrow ^3A^*$ ($^3D^*$) step [184,188].

CHAPTER TEN

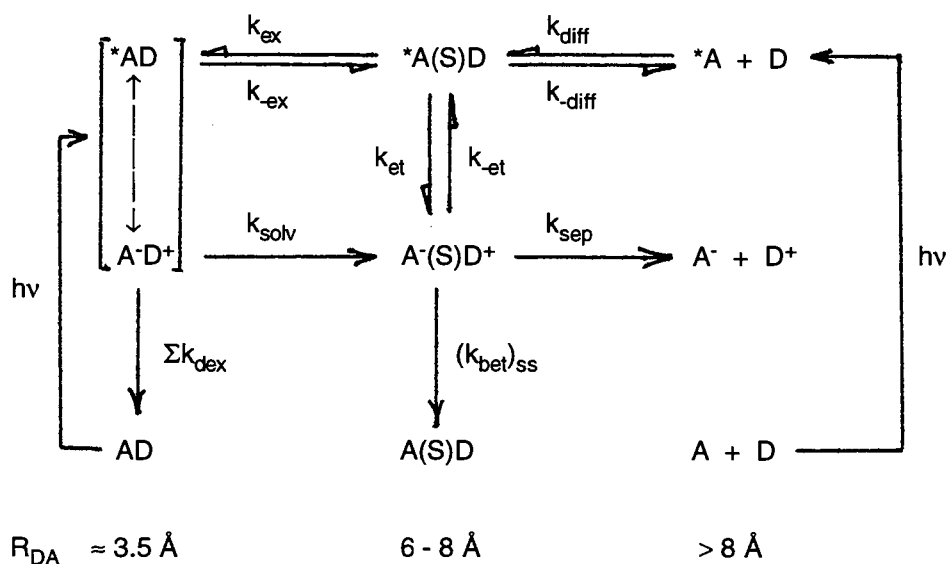
FLUORESCENCE QUENCHING DYNAMICS IN ACETONITRILE

10.1 Introduction

Photoinduced electron transfer reactions are usually performed in polar solvents to facilitate the formation of radical ions [46,53,54,63-66, 70,71,190]. Exciplexes, CRIPs or SSRIPs intermediates or a combination thereof have been proposed [38,45-47,54,63-66,71]. Despite the considerable body of experimental evidence concerning the nature and dynamics of these complexes, only recently have their roles been defined clearly and quantified [191-196]. In particular, in polar solvents there is considerable debate whether CRIP formation precedes by electron transfer [66,94] or electron transfer occurs while the donor and acceptor are in a loose configuration (i.e., Rehm-Weller mechanism) [53,54,63,64,70,71]. Recently, there has been mounting evidence for a dual dynamic pathway as shown in Scheme 10.1 (adapted from Gould et al. [191]) as originally proposed by Weller and co-workers for medium polarity solvents [63,70]. In Scheme 10.1 the horizontal distance represents the increasing separation of the donor and acceptor from left to right and changes in solvation. The vertical distance represents the increasing energy from the bottom up. For two aromatic π systems the smallest center-to-center distance, ca. 3.5 Å [63,70,191,195], is accomplished in a face-to-face orientation, which is represented by the exciplex $A\cdot D^+ \leftrightarrow {}^*AD$. The solvent separated radical ion pair, $A^-(S)D^+$ and encounter complexes, $A(S)D$ and ${}^*A(S)D$, have average center-to-center distances of 6 to 8 Å [63,70,191,195]. The larger distance reflects the dimensions of the solvent molecules. For a CRIP, unlike an exciplex, the electronic coupling is negligible such the donor-acceptor have no particular orientation and in a continuous state of motion. The

competition between the SSRIP and the exciplex in Scheme 10.1 depends on their respective driving forces and any activation barriers (i.e., potential kinetic controls [191]).

Scheme 10.1



It is conceivable that the exciplex resonance $A^-D^+ \leftrightarrow {}^*AD$ can be the contributing factor which allows the exciplex to gain a larger driving force with respect to the SSRIP [70].

According to Scheme 10.1, the efficiency for the formation of the free radical ions ($A^- + D^+$) is controlled by three intermediates: the encounter complex, $A(S)D$, the exciplex and the SSRIP, $A^-(S)D^+$. In each of these intermediates there is a competition between changes in the complex's solvation and an electron transfer reaction. For CRIPs and SSRIPs the electron transfer process has been extensively characterized. The effects of molecular dimension, molecular charge, isotopic substitution, separation distance, stoichiometry, solvent polarity, steric effects and external pressure have been reported [191]. However, the effects of significant electronic coupling between the donor and acceptor on the processes in Scheme 10.1 are not well understood. The variable DBMBF₂

/ substituted benzene exciplex charge transfer character provides an opportunity to look at this effect on the processes in Scheme 10.1.

This chapter focuses on the effect of variable exciplex charge transfer character on the fluorescence quenching mechanism in acetonitrile and its manifestation on the Rehm-Weller plot by focusing on the distance at which quenching occurs, R_{DA} . Using structurally similar electron donors allows the assumption of near uniform reorganization energy, λ . In Chapter Eight the kinetic rate constants were evaluated from the exciplex temporal profile in cyclohexane under the assumption that no electron transfer takes place. In acetonitrile, similar kinetic evaluations does not provide information on the partitioning at the encounter complex to the exciplex and SSRIP since this process runs consecutively with exciplex formation. Therefore, an alternative approach will be discussed.

10.2 Results and Discussion

10.2.1 Substituted Benzene Electron Donors

Singlet excited DBMBF₂ is efficiently quenched by the addition of substituted benzene. In some cases exciplex emission can be observed for those exciplexes with weaker charge transfer character. The quenching efficiency was determined by the Stern-Volmer equation (eq 10.1)

$$I^0 / I = 1 + K_{SV} [D] \quad (10.1)$$

$$\text{where } K_{SV} = k_{obs} \tau_m$$

I^0 and I represent DBMBF₂'s fluorescence intensity (monitored at 398 nm) in the absence and presence of quencher, respectively. K_{SV} is called the Stern-Volmer constant where k_{obs} and τ_m , are those described in Chapter Eight (eq 8.1). Plots of eq 10.1 (Figure 10.1)

are linear with intercepts of one for the weaker electron donors (cyanobenzene to toluene). However, for the stronger electron donors the Stern-Volmer plots show a distinct curvature which is more pronounced with increasing electron donation ability of the benzene. The Stern-Volmer constants for curved plots were evaluated from the limiting slope at infinite dilution (*vide infra*). The experimental Stern-Volmer constants are listed in Table 10.1. Using the DBMBF₂ lifetime determined in Chapter Three, the apparent bimolecular fluorescence quenching rate constants were calculated and listed in Table 10.1.

It is generally believed that for donor and acceptor systems which show highly polar exciplex character in nonpolar solvents, the fluorescence quenching mechanism in polar solutions by-passes the exciplex [71]; i.e., the efficiency for the electron transfer step A(S)D → A⁻(S)D⁺ is unity. Based on this mechanism, Rehm and Weller [197] derive a kinetic relationship for electron transfer within the encounter complex (eqs 10.2 and 10.3).

$$k_{\text{PET}} = \frac{k_{\text{diff}}}{1 + 0.25 [\exp(\Delta G_{\text{ET}}^{\circ} / RT) + \exp(\Delta G_{\text{ET}}^{\ddagger} / RT)]} \quad (10.2)$$

$$\Delta G_{\text{ET}}^{\ddagger} = [(\Delta G_{\text{ET}}^{\circ} / 2)^2 + (\Delta G_{\text{ET}}^{\ddagger}(0))^2]^{1/2} - (\Delta G_{\text{ET}}^{\circ} / 2) \quad (10.3)$$

$$\text{where } \Delta G_{\text{ET}}^{\ddagger}(0) = 2.4 \text{ kcal / mol}$$

This relationship can be used to demonstrate fluorescence quenching by electron transfer.

To illustrate the potential correlation of the k_{obs} with Rehm and Weller's model, the k_{PET} 's in Table 10.1 are plotted (as $\log k_{\text{PET}}$) against the free energy for electron transfer (Figure 10.2), which was calculated according to eq 2.7

$$\Delta G_{\text{ET}}^{\circ} = E_{\text{ox}} - E_{\text{red}} - C - E_{\text{S}} \quad (2.7)$$

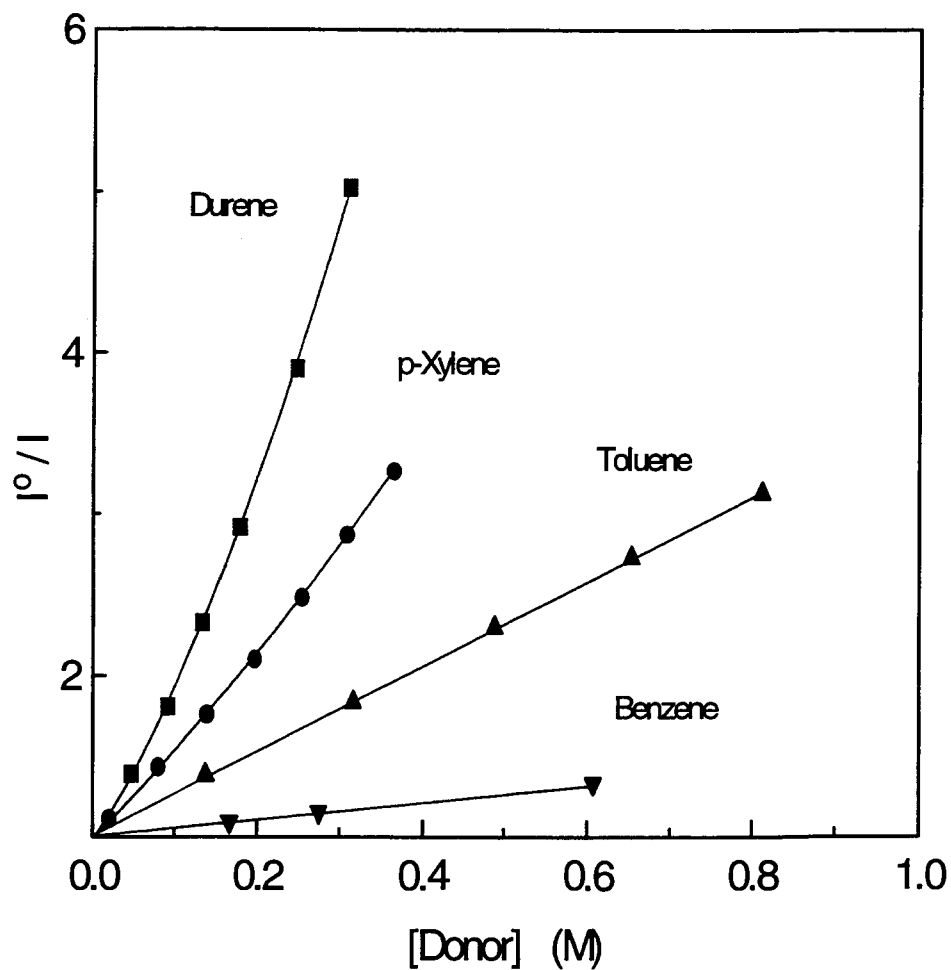


Figure 10.1: Plots of eq 10.1 (Stern-Volmer equation) for the Fluorescence Quenching of Singlet Excited DBMBF₂ by Benzenes in Aerated Acetonitrile. [DBMBF₂] = 2 × 10⁻⁶ M, λ_{ex} = 365 nm and slits 4 nm.

Table 10.1: Fluorescence Quenching Parameters of Singlet Excited DBMBF₂ by Benzenes in Areated Acetonitrile.

Benzene	E _{ox} (V vs. SCE)	ΔG _{ET} ^o (eV) ^a	K _{SV} (M ⁻¹)	k _{obs} (10 ⁹ M ⁻¹ s ⁻¹) ^b	D _{DA} (cm ² s) ^c	R _{VWD} (Å) ^d	R _{eff} (Å)	β ^e
HMB	1.59	-0.75	9.94	33.1	4.39	7.29	6.1 ± 0.9	0.76
PMB	1.71	-0.63	9.00	30.0	4.53	7.18	5.6 ± 0.8	0.62
Durene	1.79	-0.55	7.36	24.5	4.69	7.06	5.2 ± 0.8	0.51
1,2,3,5-TMB	1.83	-0.51	7.47	24.9	4.69	7.06	5.2 ± 0.8	0.51
1,2,3,4-TMB	1.82	-0.52	7.56	25.2	4.69	7.06	4.8 ± 0.7	0.41
1,2,4-Trimethylbenzene	1.92	-0.42	7.02	23.4	4.85	6.92	4.2 ± 0.6	0.24
Mesitylene	2.02	-0.32	5.81	19.4	4.85	6.92	3.8 ± 0.6	0.14
p-Xylene	2.06	-0.28	5.03	16.8	5.09	6.78	3.5 ± 0.5	0.05
m-Xylene	2.14	-0.20	4.03	13.4	5.09	6.78	3.3 ± 0.5	0
o-Xylene	2.13	-0.21	4.29	14.3	5.09	6.78	3.2 ± 0.5	0
Toluene	2.25	-0.09	2.65	8.83	5.23	--	--	--
Chlorobenzene	2.48	0.14	0.91	3.0	--	--	--	--

Table 10.1 (Continued)

Benzene	E_{ox} (V vs. SCE) ^a	$\Delta G_{\text{ET}}^{\circ}$ (eV) ^b	K_{SV} (M^{-1})	k_{obs} ($10^9 \text{M}^{-1}\text{s}^{-1}$) ^c	D_{DA} ($\text{cm}^2 \text{s}^{-1}$) ^d	R_{VWD} (\AA) ^e	R_{eff} (\AA)	β^f
Benzene	2.62	0.28	0.54	1.8	--	--	--	--
Methylbenzoate	2.69	0.35	0.53	1.8	--	--	--	--
Cyanobenzene	2.94	0.60	0.16	0.5	--	--	--	--
t-Butylbenzene	2.21	-0.13	1.22	4.1	4.70	--	--	--
4-t-Butyltoluene	(2.06)	-0.28	4.57	15.2	4.54	7.39	3.4 ± 0.5	0.08
5-t-Butyl-m-xylene	(2.02)	-0.32	5.05	16.8	4.39	7.49	3.8 ± 0.6	0.19
4-t-Butyl-o-xylene	(1.92)	-0.42	6.10	20.3	4.39	7.49	3.9 ± 0.6	0.35
5-t-Butyl-1,2,3-TMB	(1.83)	-0.51	6.94	23.1	4.26	7.59	5.1 ± 0.8	0.54
Biphenyl	1.96	-0.38	7.70	25.7	4.69	7.06	4.8 ± 0.8	0.41

^a Schlesener, C.J.; Amatore, C.; Kochi, J.K. *J. Phys. Chem.* **1986**, *90*, 3747; Ref. 191e. ^b Calculated from eq 2.7 using E_{red} of - 0.91 eV (Table 3.4), $E_{\text{S}} = 3.19$ eV (Table 3.3) and $C = 0.06$ eV [197]. ^c Calculated from $k_{\text{obs}} = K_{\text{SV}} / \tau_{\text{m}}$ where $\tau_{\text{m}} = 0.30$ ns (Table 3.2). ^d Calculated from eq 10.7. ^e Calculated from Edward's atomic increments [131]. ^f Calculated from eq 10.9a.

Table 10.2: Fluorescence Quenching Parameters of Singlet Excited DBMBO by Benzenes in Areated Acetonitrile.

Benzene	E_{ox} (V vs. SCE) ^a	ΔG_{ET}° (eV) ^a	K_{SV} (M^{-1})	k_{obs} ($10^9 M^{-1}s^{-1}$) ^a	D_{DA} ($cm^2 s^{-1}$) ^a	R_{VDW} (\AA) ^a	R_{eff} (\AA)	β^a
HMB	1.59	-0.94	35.1	26.0	4.39 ^b	7.29 ^b	6.3 ± 0.8	0.81
1,2,3,5-TMB	1.83	-0.70	30.6	22.7	4.69 ^b	7.06 ^b	5.3 ± 0.8	0.54
p-Xylene	2.06	-0.47	26.3	19.5	5.09 ^b	6.78 ^b	4.4 ± 0.8	0.30
Toluene	2.25	-0.28	19.8	14.7	5.23 ^b	6.66 ^b	3.3 ± 0.8	0
Chlorobenzene	2.48	-0.05	8.69	6.4	--	--	--	--
Benzene	2.62	0.09	4.53	3.6	--	--	--	--
Methyl benzoate	2.69	0.16	0.80	0.6	--	--	--	--
Cyanobenzene	2.94	0.41	~ 0.004	~ 0.003	--	--	--	--

^a See comments of Table 10.1. ^b Using the values for DBMBF₂ / Benzene excplexes.

with $C = 0.06$ eV [197] and $E_S = 3.19$ eV (Table 3.3). The k_{PET} from the theory of Rehm and Weller is shown by the solid line where the reorganization energy was that determined by Rehm and Weller (0.42 eV) [197] and k_{diff} was $3 \times 10^{10} \text{ M}^{-1}\text{s}^{-1}$ [123]. Cases where exciplex emission was observed are denoted by the open circles in Figure 10.2.

Figure 10.2 shows that the reaction between singlet excited DBMBF₂ (circles) and DBMBO (triangles) with benzenes reaches the diffusion limit with the xylenes as donors ($k_{diff} = 2 - 3 \times 10^{10} \text{ M}^{-1}\text{s}^{-1}$). The Rehm-Weller prediction is not fulfilled for the DBMBF₂ at $\Delta G_{ET}^{\circ} > 0$ eV whereas for the DBMBO system it shows reasonable agreement. At $\Delta G_{ET}^{\circ} < 0$ eV the apparent fair agreement between the calculated and observed k_{obs} 's is probably a result of masking by diffusion. Therefore, the Rehm-Weller PET mechanism does not effectively provide a rationale for the quenching of DBMBF₂'s fluorescence by benzenes.

In the $\Delta G_{ET}^{\circ} > 0$ eV region for the DBMBF₂ system, the k_{obs} deviate significantly from those calculated for PET. Obviously, the fluorescence quenching mechanism is not due to electron transfer. Because strong exciplex emission is observed for these benzene donors (comparable to that in cyclohexane) as shown in Table 10.3, the encounter complex must collapse to an exciplex with unit efficiency. In the $\Delta G_{ET}^{\circ} \leq 0$ eV region, exciplex emission is still observed, although weakly, up to mesitylene as an electron donor. No exciplex emission could be detected at stronger driving forces. This suggests that the encounter complex partitions between the exciplex and the SSRIP.

10.2.2 Exergonic Region

The pronounced curvature observed in the Stern-Volmer plots represents a more complex mechanism than irreversible fluorescence quenching of DBMBF₂ by benzenes. Such curvature is usually a manifestation of EDA complex formation and is termed static quenching [198]. This is a distinct possibility in this system since EDA complexes were characterized in Chapter Four. It can be shown [198] that eq 10.1 becomes eq 10.4.

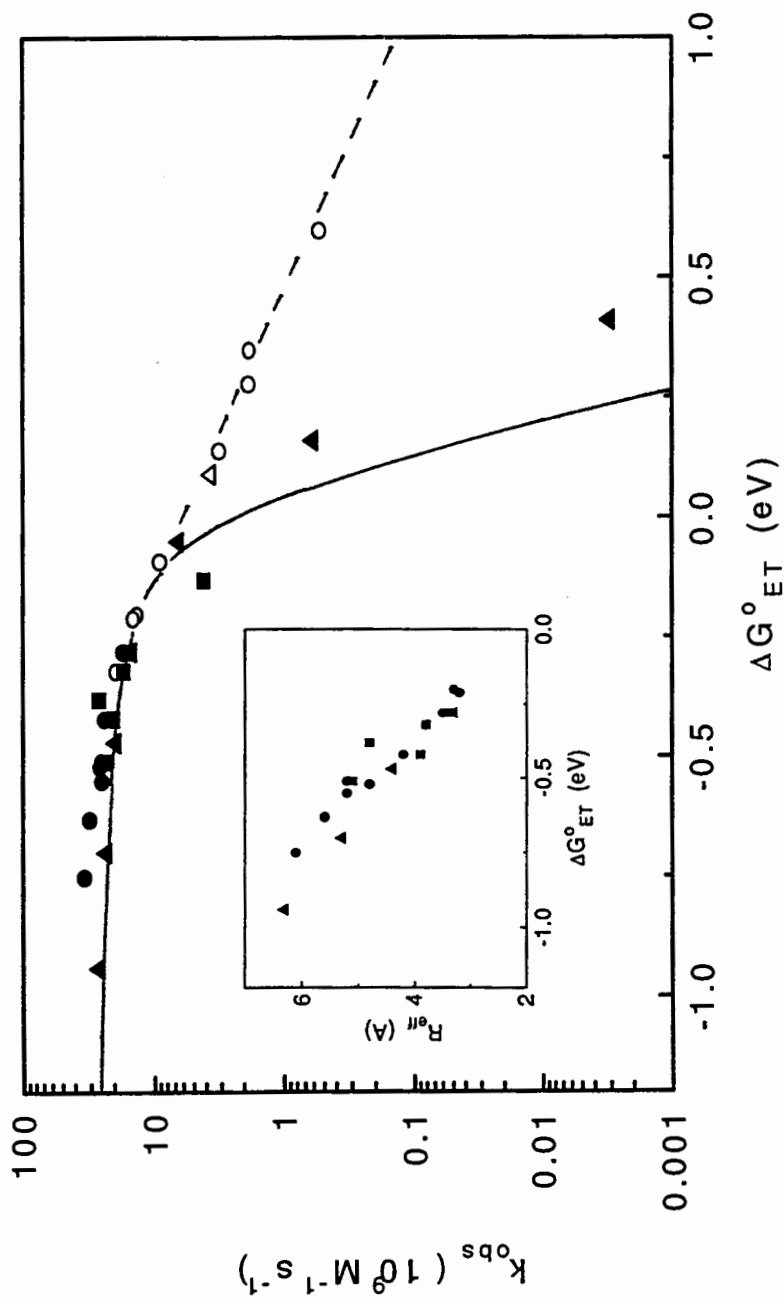


Figure 10.2: Semilog plot (Rehm-Weller plot) for the fluorescence quenching of singlet excited DBMBF₂ (circles; squares for hindered benzenes) and DBMBO (triangles) by benzenes in acetonitrile (aerated, 23 ± 2 °C). The solid line represents the calculated k_{obs} from the PET model of Rehm and Weller. The inset shows the change in the fluorescence quenching distance with electron transfer exothermicity. The presence of exciplex emission is denoted by open circles and triangles.

Table 10.3: Fluorescence Quantum Yields of DBMBF₂ / Benzene Exciplexes in Aerated Acetonitrile.

Benzene	$\Phi_{\text{ex}}^{\infty}$ ^a	$\Phi_{\text{ex}}^{\infty}$ Ratio ^b
Cyanobenzene	0.22	(0.3) ^c
Benzene	0.14	0.25
Toluene	0.03	0.06
o-Xylene	0.01	0.02
m-Xylene	0.01	0.03
p-Xylene	ND ^d	< 0.01
Mesitylene	0.005	0.01

^a Fluorescence for stronger electron donors beyond mesitylene could not be detected. ^b Represents the $\Phi_{\text{ex}}^{\infty}$ in acetonitrile divided by the $\Phi_{\text{ex}}^{\infty}$ found in cyclohexane (Table 9.1). ^c Estimated from Figure 9.1 where $\Phi_{\text{ex}}^{\infty}$ in cyclohexane (~ 0.7) was determined by extrapolation. ^d ND = not detected.

Equation 10.4 is a result of the fact that the quencher's spacial orientation around the fluorophor is not statistical and the EDA complex acts as a photon sink.

$$I^0 / I = (1 + K_a' [D])(1 + K_{SV} [D]) \quad (10.4)$$

$$1 + (K_a' + K_{SV})[D] + K_a' K_{SV}[D]^2$$

$$\text{where } K_a' = K_a (\epsilon_{AD} / \epsilon_A)$$

The K_a is the EDA complex association constant discussed in Chapter Four and ϵ_{AD} and ϵ_A represent the molar extinction coefficients of the EDA complex charge transfer band and

DBMBF₂, respectively, at λ_{exc} . Inspection of eq 10.4 shows that the non-linear behavior originates from the second order power term. Note that the limiting form of eq 10.4 reduces to eq 10.1 if the ratio $\epsilon_{AD} / \epsilon_A$ becomes negligible; this condition can be approached easily if the EDA absorption band lies under an intense local absorption band (i.e., ϵ_{AD} are usually about $3000 \text{ M}^{-1} \text{ cm}^{-1}$, less than 10% of DBMBF₂'s ϵ_A).

Assuming the unrealistic situation that $\epsilon_{AD} = \epsilon_A$ ($K_a' = K_a$) the determined K_a in Chapter Four are found to be too small to introduce any curvature in Stern-Volmer plots. For a K_a of 0.14 M^{-1} and a K_{SV} of 10 M^{-1} at a benzene concentration of 0.1 M results in a deviation from the linear Stern-Volmer slope ($K_a + K_{SV}$) of only one percent. A small variation of one percent is not easily discernible. The actual deviation from linearity is expected to be minute since $\epsilon_{AD} < \epsilon_A$. Therefore, it can be concluded that EDA complex formation is not responsible for the observed curvature in some of the Stern-Volmer plots.

Transient effects on fluorescence quenching reactions have been extensively studied and demonstrated to produce upward curvature in Stern-Volmer plots [199-205]. The requirements for observation of transient effects on Stern-Volmer plots are that the quenching reaction be diffusion controlled and that the excited state species' lifetime be short (less than 2 nanoseconds) [201a]. From Table 10.1, the observed fluorescence quenching rate constants are near to or greater than the 'ball park' diffusion rate constant in acetonitrile of $3.0 \times 10^{10} \text{ M}^{-1} \text{ s}^{-1}$ [123,141]. In addition, DBMBF₂'s lifetime is 0.28 ns (Table 3.2) which is a order of magnitude smaller than 2 nanoseconds. Therefore, the fluorescence quenching of singlet excited DBMBF₂ by good electron donating substituted benzenes may fulfill the criteria for observable transient effects. It is assumed that these conclusions are true for the DBMBO system as well.

The transient effect on fluorescence quenching kinetics allows access to the fluorescence quenching distance (R_{DA}), that is, the mean distance between singlet excited DBMBF₂ and benzene at which quenching will occur [199-205]. The Stern-Volmer

equation, modified to include the transient effect, is shown by eq 10.5, which is called the SCK equation in the literature [199, 200]

$$I^0 / I = (1 + 4\pi R_{\text{eff}} D_{\text{AD}} N_A' [D] \tau_m) Y^{-1} \exp(V[D]) \quad (10.5)$$

where

$$Y = 1 - (b / \sqrt{a}) \pi^{1/2} \exp(b^2 / a) \operatorname{erfc}(b / \sqrt{a})$$

$$a = (\tau_m)^{-1} + 4\pi R_{\text{eff}} D_{\text{AD}} [D]$$

$$b = 4\pi R_{\text{eff}}^2 D_{\text{AD}} [D] (\sqrt{\pi} D_{\text{AD}})^{-1}$$

$$V = (4\pi / 3) (R_{\text{eff}}^3 - R_{\text{VDW}}^3)$$

where $\exp(V[D])$, or Perrin's formulation [69], is a modification suggested by Andre et al. [201e]. D_{AD} , R_{VDW} and N_A' represent the sum of the donor and acceptor's diffusion coefficients ($D_{\text{AD}} = D_A + D_D$), R_{VDW} is the donor and acceptor's van der Waals' center-to-center distance and N_A' is Avogadro constant divided by 1000, respectively. R_{eff} is the effective fluorescence quenching distance. In the limit as $[D]$ approaches infinite dilution, eq 10.5 predicts a limiting slope of [206].

$$k_{\text{obs}} \tau_m = 4\pi R_{\text{eff}} D_{\text{AD}} N_A' [D] \tau_m \{1 + (R_{\text{eff}} / \sqrt{D_{\text{AD}} \tau_m})\} \quad (10.6)$$

Equation 10.6 justifies using the slope at infinite dilution to determine k_{obs} (vide supra).

Equations 10.5 and 10.6 show an interesting feature. The effective fluorescence quenching distance, R_{eff} , can be evaluated if D_{AD} and R_{VDW} are known. Since R_{eff} is correlated to the donor-acceptor separation during the quenching act [199] (vide infra), the magnitude of R_{eff} provides information on whether an exciplex or SSRIP (or both) is initially formed; i.e., $R_{\text{eff}} \approx R_{\text{AD}}$ in Scheme 10.1. This information represents the dynamic partitioning of the encounter complex, A(S)D, to the exciplex and SSRIP.

R_{VDW} was calculated from the method and values in Edward's paper [131]. Diffusion coefficients for benzene donors and DBMBF₂ were estimated from the data of Chan and Chan [207]; the same data are used for the DBMBO system where the difference in the calculated exciplex volume is negligible. Chan and Chan showed that for pseudo-planar solutes their diffusion coefficient is related to V_{VDW} by

$$1/D = mV_{VDW} + b \quad (10.7)$$

where the error in calculating D from this equation is estimated to be two percent.

Because R_{eff} is the only unknown in eq 10.5, R_{eff} was systematically varied until the best fit with the experimental data was achieved; the solid lines for durene and p-xylene donors in Figure 10.1 are typical examples. A 10% variation in either D_{AD} or R_{VDW} resulted in a calculated variation in R_{eff} of less than 15 percent.

The significance of R_{eff} relies on the condition that the reaction is diffusion controlled. Under large driving forces of less than - 0.4 eV we are reasonably sure that this condition is met, especially since k_{obs} ranges around $3 \times 10^{10} \text{ M}^{-1}\text{s}^{-1}$; i.e., diffusion control. However, for the xylenes as electron donors this condition may not be fully achieved since k_{obs} is significantly less than $3 \times 10^{10} \text{ M}^{-1}\text{s}^{-1}$. The hindered donors provide a comparison to check this condition. Under diffusion controlled conditions, the k_{obs} should be a function of both R_{eff} and D_{AD} according to eq 10.6. Because the computed R_{eff} is invariant with respect to steric effects (Table 10.1), the change in k_{obs} must be correlated with changes in D_{AD} if $k_{obs} = k_{diff}$. The hindered benzenes are expected to reduce the magnitude of D_{AD} due to the fact that a species' diffusion coefficient is inversely proportional to its size (eq 10.7). Therefore, the ratio of the diffusion coefficients and k_{obs} (or K_{SV}) of unhindered vs. hindered benzenes, should be the same within experimental error. It is unlikely that under reversible conditions the k_{obs} ratio will be similar to the diffusion coefficient ratio.

Table 10.4 lists the K_{SV} (Table 10.1) and D_{DA} ratios. D_{DA} was calculated from the R_{eff} evaluation listed in Table 10.1. From inspection of Table 10.4, the excellent agreement between the K_{SV} and D_{DA} ratios provides support for the assumption that fluorescence quenching of singlet excited DBMBF₂ by mesitylene and xylenes is diffusion controlled. This is further demonstrated by the toluene / t-butylbenzene pair where the fluorescence quenching is not diffusion controlled, hence the K_{SV} ratio is significantly different from the D_{DA} ratio. Therefore, the xylenes can be assumed to be diffusion controlled and their computed R_{eff} values have some validity.

The meaning of the effective fluorescence quenching distance can be shown by a modification of Scheme 10.1 (Scheme 10.2), which is based on the recent work of Stevens et al. [208] (vide supra). Scheme 10.2 includes the penetration of the donor and acceptor through their mutual solvent shell to form a collision complex of random orientation which then undergoes reorientation to the relaxed exciplex configuration. Based on Scheme 10.2, the effective fluorescence quenching distance is given by [208]

$$R_{eff} = \sigma + \frac{\beta (R_o - \sigma)}{\beta + \gamma (1 - \beta)} \quad (10.8)$$

where β and γ (eqs 10.9) are the efficiencies of SSRIP formation from the encounter complex, $^*A(S)D$, and exciplex formation from the collision complex, $^*(AD)$, respectively. R_o and σ represent the donor-acceptor distance of the SSRIP and exciplex, respectively. Equation 10.8 follows the expected trend where R_{eff} lies in the range of $\sigma \leq R_{eff} \leq R_o$. According to eq 10.8, R_{eff} no longer represents the most probable quenching distance but

$$\beta = k_{et} / (k_{et} + k_{cc}) \quad (10.9a)$$

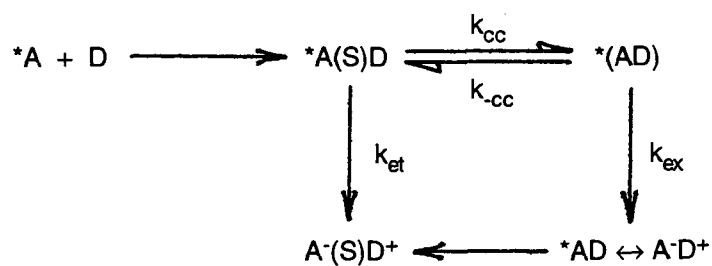
$$\gamma = k_{ex} / (k_{ex} + k_{cc}) \quad (10.9b)$$

Table 10.4: Evidence for Diffusion Controlled Fluorescence Quenching of Singlet Excited

DBMBF₂ by Benzenes

Donor Pair	K _{SV} Ratio	D _{DA} Ratio
Toluene / t-Butylbenzene	2.17 ± 0.07	1.11
p-Xylene / 4-t-Butyltoluene	1.10 ± 0.03	1.09
Mesitylene / 5-t-Butyl-m-xylene	1.09 ± 0.03	1.08
1,2,4-TMB / 4-t-Butyl-o-xylene	1.15 ± 0.03	1.08
1,2,3,5-TMB / 5-t-Butyl-1,2,3-TMB	1.08 ± 0.03	1.07

Scheme 10.2



rather the dynamic weighted average of the formation probabilities in the SSRIP and exciplex.

In Table 10.1, the xylenes must be near the limit of $\beta \rightarrow 0$ since $R_{\text{eff}} \approx 3.3 \text{ \AA}$. This suggests that exciplex formation occurs up to an exothermicity ($\Delta G_{\text{ET}}^{\circ}$) of -0.3 eV , which is partially corroborated by the observation of weak exciplex emission (Figure 10.2). This is consistent with the observations of Stevens et al. [208], Gould and co-workers [191], Peters and co-workers [193] and Kukichi and co-workers [196]. There is no apparent steric effect in this region where R_{eff} is the same within experimental error of that of the unhindered donor. Since R_{eff} is interpreted to represent the dynamic weighted average between the formation probabilities and not the actual most probable quenching distance, steric effect information is obscured.

Because R_{eff} increases with larger driving forces, the SSRIP efficiency is also increasing on the basis of Scheme 10.2. This is indicative of a gradual change in the dominance of exciplex over SSRIP formation from the encounter complex. This is also consistent with the work of Stevens, et al. [208], Gould and co-workers [191], Peters and co-workers [193] and Kukichi and co-workers [196] where SSRIP formation is controlled by the system's reorganization energy, which is usually between -1.0 to -1.8 eV (Chapter Two). Hence the rate for electron transfer does not become appreciable until the driving force is sufficiently large. When $\Delta G_{\text{ET}}^{\circ} = \lambda = -1.0$ to -1.8 eV k_{et} reaches its maximum [45,191].

Sophisticated explanations have been presented for the apparent failure of Marcus theory to rationalize why k_{obs} remains at the diffusion controlled limit well into the inverted region [209-214]. However, some groups have realized that a more explanation can rationalize the observations within the framework of Marcus theory [208,211,215]. As shown in Scheme 10.1 the encounter complex has two pathways: CRIP/exciplex and SSRIP. As a consequence of the CRIP and SSRIP reorganization energies being different by ca. 1 eV , the CRIP inverted region is masked by a favorable k_{et} (cf. Figure 2.3). The

SSRIP inverted region may be obtainable if driving forces of - 3.0 eV can be delivered. However, at such powerful driving forces the charge transfer and ground state potential surface strongly interact (i.e., the energy differences between the ground and charge transfer surfaces in this section is about 3 eV) resulting in significant EDA complex formation. The excited state reaction from direct excitation of the EDA complex (static quenching) is thus obscured.

10.2.3 Endergonic Region

In the endergonic region of Figure 10.2 ($\Delta G_{ET}^{\circ} \geq 0$ eV) the departure from RW behavior is due to more energetically favorable exciplex formation with intermediate and weak CT character (Table 6.2). However, the observed deviation shows a linear relationship with respect to ΔG_{ET}° with a slope of -1.7 eV $^{-1}$. The expected slope of the RW curve in this region is $1 / RT$ (≈ 16.9 eV $^{-1}$ at 298 K). Similar linear relationships between $\log k_{obs}$ and ΔG_{ET}° in the endergonic region have been interpreted in the past to represent fluorescence quenching via an exciplex with partial charge transfer character where k_{obs} is correlated with the donor's IP or E_{ox} potentials (eq 10.10) [216-222].

$$\ln(k_{obs}) = \alpha E_{ox} + \text{Constant} \quad (10.10)$$

The percentage of charge transfer within the exciplex is represented by α , it follows that for a slope of -1.7 eV $^{-1}$, the percentage of charge transfer for DBMBF $_2$ / substituted benzene exciplexes is 10 percent ($= 1.7 / 16.9 \times 100\%$). Although eq 10.10 was fitted to the observed data points, the constant charge transfer exciplex character assumption, intrinsic in eq 10.10, is most certainly not correct (cf. Table 6.2) since the DBMBF $_2$ / substituted benzene exciplexes show decreasing CT character with increasing ΔG_{ET}° .

Involvement of exciplexes with ΔG_{ET}° -dependent CT character has been postulated by Föll et al. [225] and by Kuzmin and co-workers [226] to explain non-RW behavior. We will only discuss Kuzmin's model and point out any differences with Föll et al.'s model. Kuzmin and co-workers were successful in deriving an expression relating the exciplex enthalpy to ΔG_{ET}° as shown in eq 10.11 (in the derivation of Föll et al.'s, eq 10.11 contains an additional term), assuming ΔS_{ex} can be neglected; the neglect of ΔS_{ex} was partially substantiated by the small values found for the exciplex equilibrium K_{ex} .

$$\Delta H_{ex} \cong \Delta G_{ET}^{\circ} / 2 - \{ (\Delta G_{ET}^{\circ})^2 / 4 + \beta^2 \}^{1/2} \quad (10.11)$$

Equation 10.11 is merely a rearranged form of eq 2.35 where ΔG_{ET}° was substituted for the $E_{CT} - E_{LE}$ and β is equal to $H - SE_{EX}$; the influence of electronic coupling appears in eq 10.8 through the β term ($H = \langle A^*D^+ | H | A^*D \rangle$). Equation 10.11 predicts that the exciplex heat of formation is small ($-0.1 < \Delta H_{ex} < 0$ eV) in the endergonic region. The behavior of eq 10.11 can be appreciated by observing how this function behaves as β is varied from zero to a non-zero value. For a CRIP, where β is essentially zero, it is clear that ΔH_{ex} is zero and the fluorescence quenching kinetics converge to the RW model. For intermediate and weak CT exciplexes, where β is expected to be quite large ($\beta = 0.05$ to 0.15 eV [71c,d,225]), ΔH_{ex} is negative for both negative and positive values of ΔG_{ET}° . This suggests that exciplex formation can still be energetically favorable even when electron transfer is endothermic.

Unfortunately Kuzmin and co-workers and Föll et al. were unable to experimentally verify their models beyond the indirect evidence for exciplex intermediates. Direct evidence should consist of the following four points: i) direct evidence of an exciplex participating in the fluorescence quenching (i.e., emission), ii) other quenching mechanisms can be ruled out (i.e., energy transfer), iii) demonstration of the exciplex's intermediate or weak CT character and iv) observed deviation from a RW plot. The

DBMBF₂ / benzene system satisfies all four requirements (Chapters Five and Six) thus establishing the exciplex hypothesis, but not any assumptions used to derive these models.

On the basis of Kuzmin's model in the endergonic and weakly exergonic regions, the exciplex decay to reactants AD is the rate limiting step (i.e, the condition is $k_{-ex} \gg k_{ex}^{nr} + k_{ex}^{rad}$) and the fluorescence quenching rate constant is given by eq 10.12 [226].

$$\log k_{obs} \equiv -\Delta H_{ex} / 2.3RT + \log (0.86 / \tau_{ex}) \quad (10.12)$$

$$\text{where } \tau_{ex} = 1 / \sum k_{dex}$$

This condition ($k_{-ex} \gg k_f^{ex} + k_{nr}^{ex}$) appears to be reasonable due to the lack of oxygen quenching on the exciplex's emission (cf. Chapter Seven, eq 7.9). Equation 10.12 shows that the fluorescence quenching is controlled by both the exciplex's enthalpy of formation and lifetime; Kuzmin's model assumes τ_{ex} is constant whereas Föll et al. set the exciplex lifetime as a function of the exciplex CT character, as observed in Chapter Eight. Because exciplex electronic coupling (β) and exciplex lifetime are different between different donor-acceptor systems, these different systems will show varying degrees of non-RW behavior. This behavior is mostly influenced by the exciplex lifetime since the contribution of ΔH_{ex} is calculated to be less than one $\log k_{obs}$ unit on the basis of eq 10.11. For example, exchanging structurally similar DBMBF₂ to DBMBO, results in RW behavior (Figure 10.2). For τ_{ex} 's of greater than one nanosecond, the observed fluorescence quenching rate constant will be smaller than $10^9 \text{ M}^{-1}\text{s}^{-1}$. Therefore, RW behavior can be approached if the exciplex lifetime becomes larger. It follows that agreement with the RW model does not unambiguously demonstrate fluorescence quenching by electron transfer. As an example, the DBMBO / benzene system displays RW behavior (Figure 10.2) but R_{eff} supports exciplex formation to a ΔG_{ET}° of - 0.4 eV.

The linear free energy type relationship observed in Figure 10.3 may be a result of an indirect relationship between $\log k_{obs}$ and ΔG_{ET}° through eqs 10.11 and 10.12. Plots of

$\log k_{\text{obs}}$ vs. $\Delta G_{\text{ET}}^{\circ}$ based on Kuzmin's (and Föll et al.) model show significant nonlinear relationships that is easily observed over a $\Delta G_{\text{ET}}^{\circ}$ range of 0.6 eV. The best fit of the experimental data to Kuzmin's model ($\beta = 0.10$ eV and $\tau_{\text{ex}} = 2$ ns), using eqs 10.10, 10.11 and 10.13 is shown by the solid line in Figure 10.3.

$$1/k_{\text{calc}} = 1/k_{\text{diff}} + 1/k_{\text{obs}} \quad (10.13)$$

Equation 10.13 takes into account that the upper limit to bimolecular rate constants is equal to k_{diff} . These calculations show that k_{calc} approaches k_{diff} faster than the RW model and that sigmodal behavior is predicted with a limiting $\log k_{\text{obs}}$ of 8.6 ($\Delta G_{\text{ET}}^{\circ} \rightarrow +\infty$). Kuzmin's model obviously does not fit the experimental data; this disagreement is most likely due to the assumption that τ_{ex} and β are constant on the basis that the exciplex lifetime (cyclohexane) was dependent on the extent of CT (i.e., the lifetime increased with increasing exciplex dipole moment as proposed by Föll et al. [225]). If we use the value for β of 0.10 eV [71c,d] and eq 10.11, the $-\Delta H_{\text{ex}} / 2.3RT$ term in eq 10.11 only contributes about 1; i.e., a small enthalpic driving force which is confirmed by the small red-shifts in $h\nu_{\text{max}}$. Using the k_{obs} values from Table 10.1 and eq 10.12, the weak CT exciplexes are estimated to have lifetimes ranging from 3 to 2 nanoseconds; for smaller values of β , τ_{ex} becomes less than one nanosecond.

Both Kuzmin's and Föll et al.'s models provide a beginning to explain the deviation from RW behavior in the endergonic region, which is supported by the observations here. However, the assumptions (exciplex lifetime and neglect of exciplex entropy of formation) utilized to derive kinetic expressions are less than satisfactory since they do not reproduce the commonly observed linear $\log k_{\text{obs}}$ vs. $\Delta G_{\text{ET}}^{\circ}$ plots.

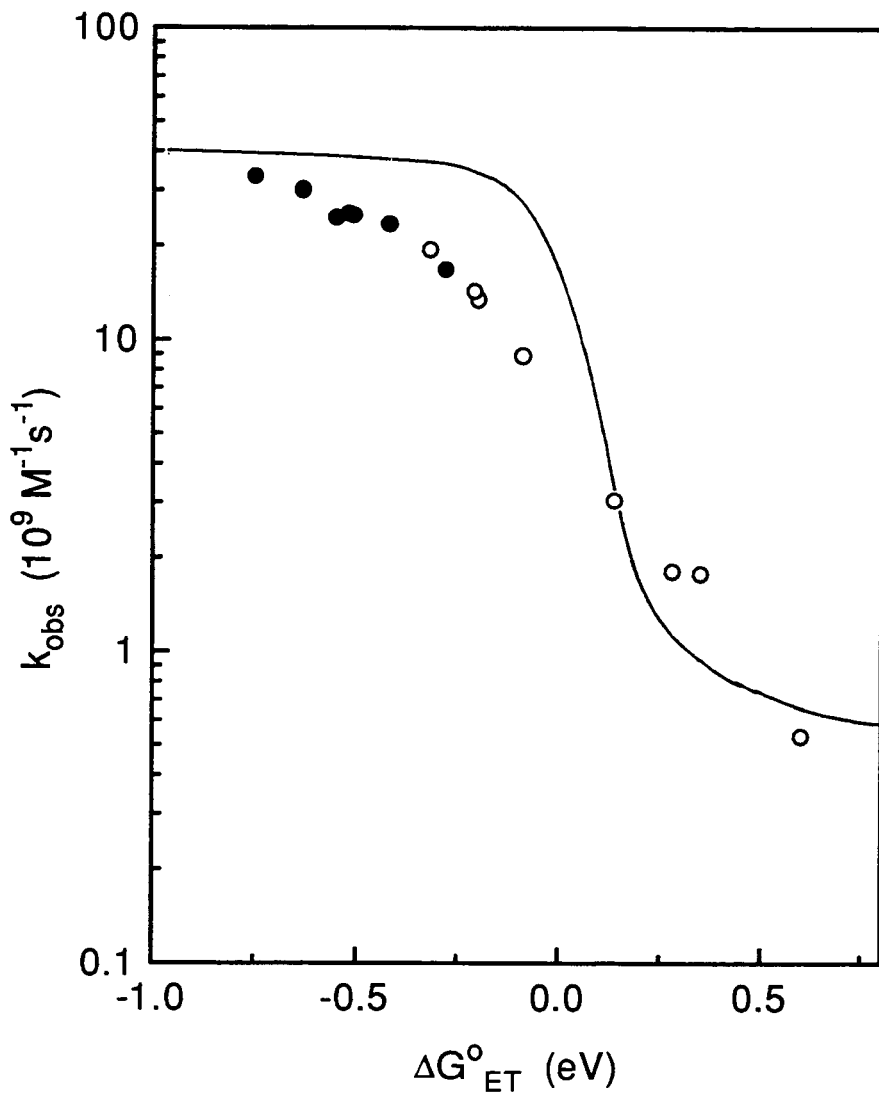


Figure 10.3: Best fit of the Kuzmin Model to the Observed Fluorescence Quenching of Singlet Excited DBMBF₂ by Benzenes in Aerated Acetonitrile.

CHAPTER ELEVEN

EXPERIMENTAL

11.1 General

Unless otherwise stated the following experimental procedures were used. Melting points (m.p.) were measured on a Fisher-Johns melting point apparatus (uncorrected). Infrared spectra (IR) were recorded on a Perkin-Elmer 559B spectrophotometer (Nujol Mull). Gas chromatography-mass spectra (GC-MS) were recorded on a Hewlett-Packard 5985 GC-MS system, equipped with a DB-1 capillary column (30 m × 0.25 mm), by either electron impact (EI) or chemical ionization (CI). Proton nuclear magnetic resonance (^1H NMR) spectra were recorded on either a Bruker WM-400 or WM-100 spectrophotometer. Chemical shifts (δ) are reported in parts per million (ppm) by comparison with tetramethylsilane and coupling constants (J) in Hertz. The coupling patterns are presented as s (singlet), d (doublet), t (triplet), q (quartet), dd (doublet doublet), and m (multiplet). The chemical shifts of ^{13}C NMR spectra are also reported by comparison with tetramethylsilane. Elemental analysis was carried out by Mr. M.K. Yang on a Carlo Erba Model-1106 Elemental Analyzer.

11.2 Chemicals

Spectrograde solvents were used as received, except as noted: acetonitrile (BDH), methanol (Caledon), chloroform (Fisher), dichloromethane (Mallicrodkt, Caledon or Fisher), carbon tetrachloride (Fisher, analytical reagent), dioxane (Acachemia), ethyl ether (BDH anhydrous), 2-propanol (Fisher) and methyl cyclohexane (BDH, reagent grade).

Commercially available reagents, cyanobenzene (MCB), methyl benzoate (MCB), benzene (Fisher), o-xylene (MCB), m-xylene (MCB), 4-t-butyltoluene (Eastman), t-butylbenzene (MCB), 1,2,4-trimethylbenzene (Aldrich, 98%), isodurene (Aldrich, 95%), prebnitene (Aldrich, 85+%) and mesitylene (MCB) were distilled prior to use. Commercially available reagents' durene (Aldrich, 98%), biphenyl (Acachemia, 99%), hexamethylbenzene (Eastman-Kodak) were purified by recrystallization from acetonitrile. The following reagents were used as received: toluene (Fisher, spectrograde), p-xylene (Fisher, spectrograde), 5-t-butyl-m-xylene (TCI, 99+%) and 4-t-butyl-o-xylene (TCI, 99+%).

β -Diketones for preparation of boron complexes were used as received: dibenzoylmethane (Aldrich); 4-methoxy-4'-t-butyl-dibenzoylmethane (Givaudan).

11.3 Boron Complexes

β -Diketonatoboron complexes were prepared from their corresponding β -diketones.

11.3.1 Dibenzoylmethanatoboron Difluoride (DBMBF₂)

DBMBF₂ was prepared according to the procedure described by Cheng [36]. BF₃-etherate (0.77 g, 6.0 mmol) was added to a stirred solution of dibenzoylmethane (1.00 g, 4.45 mmol) in CH₃CN (25 mL) at room temperature under nitrogen. After 12 hours the yellow solution was flash evaporated and the resulting yellow solid recrystallized twice from acetonitrile giving yellow needle crystals of DBMBF₂ (0.90 g, 74% yield). m.p. 191-193 °C (uncorrected; Lit 193-194 °C [9], 197 °C [10]).

11.3.2 4-Methoxy-4'-t-butyl-dibenzoylmethanatoboron difluoride (MBDBF₂)

MBDBF₂ was prepared similarly as described in 4.3.1. BF₃-etherate (1.4 mL, 10.9 mmol) was added to a stirred solution of 4-methoxy-4'-t-butyl-dibenzoylmethane (3.05 g, 10.2 mmol) in acetonitrile (40 mL) at room temperature. After six hours the resulting solution was flash evaporated and the collected yellowish-green solid recrystallized from acetonitrile giving yellow-green needles of MBDBF₂ (2.65g, yield 75%). m.p. 241.5-242.5 °C. MS (EI), m/e (relative intensity): 358 (M⁺, 67), 343 (M⁺ - CH₃, 100), 327 (7), 315 (14), 255 (M⁺ - t-butylphenyl, 11), 135 (61). IR (Nujol mull), ν_{\max} : 1608(s), 1562(w), 1551(w), 1535(s), 1488(s), 1360(s), 1300(m), 1266(s), 1236(s), 1185(s), 1160(m), 1133(m), 1118(m), 1095(m), 10709m), 1045(s), 1018(m), 968(m), 867(m), 800 (s). ¹H NMR (100 MHz, CDCl₃), δ : 1.38 (s, 9H, C(CH₃)₃), 3.95 (s, 3H, -OCH₃), 7.05 (d, 2H, J = 8.5 Hz), 7.09 (s, 1H), 7.57 (d, 2H, J = 8.5 Hz). 8.12 (t, 4H, J = 8.5 Hz). ¹³C NMR (400 MHz, CDCl₃), δ : 31.00; 35.43; 55.76; 92.23; 114.65; 124.44; 126.69; 129.57; 131.46; 159.20; 165.60; 181.60; 181.76. MA, cal. 67.1% C, 5.9% H; found 67.1% C, 6.0% H.

11.3.3 Other β -diketonatoboron complexes

Various β -diketonatoboron complexes were prepared by other members of Professor Y.L. Chow's group and they are listed in Table 11.1.

11.4 EDA Complex

11.4.1 Sample Preparation

Samples for EDA complex studies were prepared in five mL volumetric flasks; the benzene donor was added first and the flask was half filled then swirled (solid benzenes required 10 minutes to completely dissolve). One mL of DBMBF₂ stock solution (0.45 M)

Table 11.1: Other β -Diketonatoboron Complexes and Their Source

Complex	Prepared by:	Properties
BABF ₂	X.E. Cheng	m.p. 152-154 °C; Lit. 153-154 °C ^a
AABF ₂	X.-X. Ouyang	m.p. 42.5-43.0 °C; Lit. 43 °C ^a
Me-AABF ₂	X.-X. Ouyang	m.p. 92.5-94.0 °C; Lit. 85-86 °C ^b
ACHBF ₂	X.-X. Ouyang	m.p. 79.0-79.5 °C
D-t-BBF ₂	X.-X. Ouyang	m.p. 82-83 °C; Lit. 83 °C ^b
DBMBO	Y.-H. Zhang	63.5 %C, 3.4 %H; cal. 63.4 %C, 3.4 %H
BABO	Y.-H. Zhang	55.4 %C, 3.5 %H; cal. 55.5 %C, 3.4 %H
AABO	Y.-H. Zhang	42.2 %C, 3.5 %H; cal. 42.6 %C, 3.4 %H
MBDBO	Y.-H. Zhang	64.7 %C, 5.2 %H; cal. 64.9 %C, 5.1 %H
DBMBC	Y.-H. Zhang	See Table 3.1
BABC	Y.-H. Zhang	m.p. 208-210 °C; Lit. 188 °C ^c , 218 °C ^c
AABC	Y.-H. Zhang	m.p. 175-176 °C; Lit. 192 °C ^c , 194 °C ^d
MBDBC	Y.-H. Zhang	72.9 %C, 5.9 %H; cal. 73.0 %C, 5.9 %H
DBMBN	Y.-H. Zhang	76.3 %C, 4.3 %H; cal. 76.6 %C, 4.4 %H
BABN	Y.-H. Zhang	See Table 3.1
AABN	Y.-H. Zhang	67.0 %C, 5.2 %H; cal. 67.0 %C, 5.0 %H
MBDBN	Y.-H. Zhang	75.3 %C, 5.7 %H; cal. 75.3 %C, 5.6 %H
DBMBM	Y.-H. Zhang	64.4 %C, 3.9 %H; cal. 64.3 %C, 3.9 %H
BABM	Y.-H. Zhang	56.9 %C, 4.0 %H; cal. 57.0 %C, 4.0 %H
AABM	Y.-H. Zhang	45.3 %C, 4.3 %H; cal. 45.2 %C, 4.2 %H
MBDBM	Y.-H. Zhang	65.4 %C, 5.5 %H; cal. 65.6 %C, 5.5 %H

^a Morgan, G.T.; Tunstall, R.B. *J. Chem. Soc.* **1963**, 25, 1924. ^b Ref. 10. ^c Ref. 14e.

^d Ref. 17a.

was then added and the solution diluted to the mark; $[\text{DBMBF}_2] = 0.009 \text{ M}$. Because the solubility of DBMBF_2 is very low in cyclohexane, samples were initially prepared in dioxane (0.05 M), which serves as a carrier solvent. The cyclohexane stock solution was prepared by syringing 25 μL of the DBMBF_2 dioxane stock solution into 25 mL of cyclohexane; $[\text{DBMBF}_2] = 10^{-4} \text{ M}$. The benzene concentration was typically between 0.1 to 0.3 M (acetonitrile and cyclohexane). In acetonitrile the donor concentration was adjusted, whenever possible, to yield an absorbance between 0.2 and 0.8; for cyclohexane solutions the absorption was less than 0.2.

11.4.2 Association Equilibrium Constants

For those donors where the charge transfer band was sufficiently resolved from the nearby intense DBMBF_2 absorption, their association equilibrium constants for ground state complex formation were determined by UV-Vis spectroscopy in acetonitrile. UV-Vis spectra were recorded on a Varian Cary 210 spectrophotometer using matched one centimeter pathlength cells (Canlab No. 7) with the solvent as a reference. The association equilibrium constants K_a were obtained from the standard Benesi-Hildebrand analysis [55] under the experimental condition that the benzene concentration $[\text{D}]$ was greater than that of $[\text{DBMBF}_2]$. Temperature of the UV cell was maintained at 24.0 ± 0.5 °C using an external water bath (Haake Model FJ) where the solution temperature was measured using a thermocouple (Cole-Parmer Model 8528-20 with K type thermocouple).

11.4.3 Enthalpy of EDA Formation

The heat of EDA complex formation was determined in acetonitrile and cyclohexane according to the method of Tamres [113]. In the method of Tamres, the CT

band absorption at λ_{mon} is followed as a function of temperature according to eq 4.2 where ΔAbs is

$$\ln \Delta\text{Abs} = -\Delta H_a / RT + \text{constant} \quad (4.2)$$

defined as $\ln \Delta\text{Abs} = \ln \text{Abs} - \ln[D]$. The $\ln [D]$ term compensates for the change in the donor concentration due to expansion of the solvent with temperature. The change in $[D]$ was calculated from tabulated tables of solvent density vs. temperature [30a].

The UV-Vis spectrophotometer was a Cary 210 where the baseline is recorded electronically. The spectrophotometer was balanced using matched UV cells (Canlab No. 7) filled with solvent. The baseline was stable for several hours, which was longer than the time required to perform the experiments. The experiments were conducted with spectrophotometer parameters of; Bandwidth = 1.0 nm; Pen Period = 10 seconds; Range = 1.0. The high pen period was used to damp the Abs reading such that the absorbance could be read directly from the readout to the fourth decimal place.

The UV cell temperature was maintained using a water cooled / heated cell jacket by way of an external water bath (Haake Model FJ), which was incremented in temperature by approximately 8 °C units; the experimental temperature range was ≤ 60 °C. The cell was equilibrated at each temperature for at least 30 minutes (an independent experiment revealed that the temperature in the cell reached equilibrium within 15 minutes). The UV cell temperature was determined by a secondary UV cell (filled with water) along side the UV cell containing the DBMBF₂ / benzene solution where the temperature in the former cell was measured using thermocouple (Cole-Parmer Model 8528-20 with K type thermocouple). The temperature was found to fluctuate within ± 0.2 °C.

11.5 Steady State Fluorimetry

11.5.1 Instrument and Setup

Unless otherwise stated, the following describes the instruments and general setup considerations. Steady state fluorimetry was performed on either a Perkin-Elmer MPF-44B (uncorrected) or a PTI LS-100 (corrected). The MPF-44B was used for kinetic and thermodynamic studies where corrected spectra are unnecessary. The LS-100 was used for determining the exciplex λ_{\max} and $\Phi_{\text{ex}}^{\infty}$. The sample optical path used in all studies is shown in Figure 11.1.

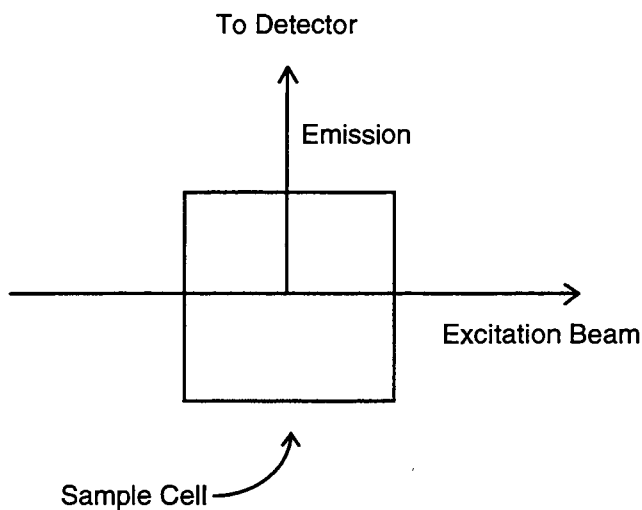


Figure 11.1: Relationship of Excitation / Emission to Detector Orientation Used in Fluorescence Studies.

The 90° orientation requires low concentrations such that inner filter effects are negligible.

Inner filter effect is a result of the attenuation of the excitation beam due to excitation light absorption by the sample. It can be shown that the fluorescence intensity is given by [227]

$$I_F = I^0 \Phi_F (1 - 10^{-\epsilon I c})$$

$$I_F = I^0 \Phi_F [2.303 \epsilon I c - [2.303 \epsilon I c]^2 / 2! + \dots] \quad (11.1)$$

where the latter equation expands the first equation to a power series. I_F , I^0 , ϵ , I and c represent the fluorescence intensity, excitation lamp intensity, molar extinction coefficient, cell path length and fluorophor concentration, respectively. The inner filter effect is represented by the later terms in eq 11.1, $[2.303 \epsilon I c]^2 / 2! + \dots$. At large concentrations the I_F approaches zero. At low concentrations, for which inner filter effects are negligible, eq 11.1 can be truncated after the first term

$$I_F \cong 2.303 \epsilon I c I^0 \Phi_F \quad (11.2)$$

where the fluorescence intensity is proportional to the fluorophor's concentration. Equation 11.2 is a fundamental equation of quantitative fluorimetry.

The working DBMBF₂ concentration was experimentally assessed to be 1 to 4 x 10⁻⁶ M (Figure 11.2). Below 10⁻⁶ M the signal to noise was poor and above 4 x 10⁻⁶ M inner filter effects became significant; i.e., the plot begins to significantly curve downward.

11.5.2 Sample Preparation and Conditions

Unless otherwise stated, the samples were prepared as follows. For β -diketonatoboron complex fluorescence quantum yield studies, samples were prepared in five mL volumetric flasks, from concentrated stock solutions (for nonpolar solvents,

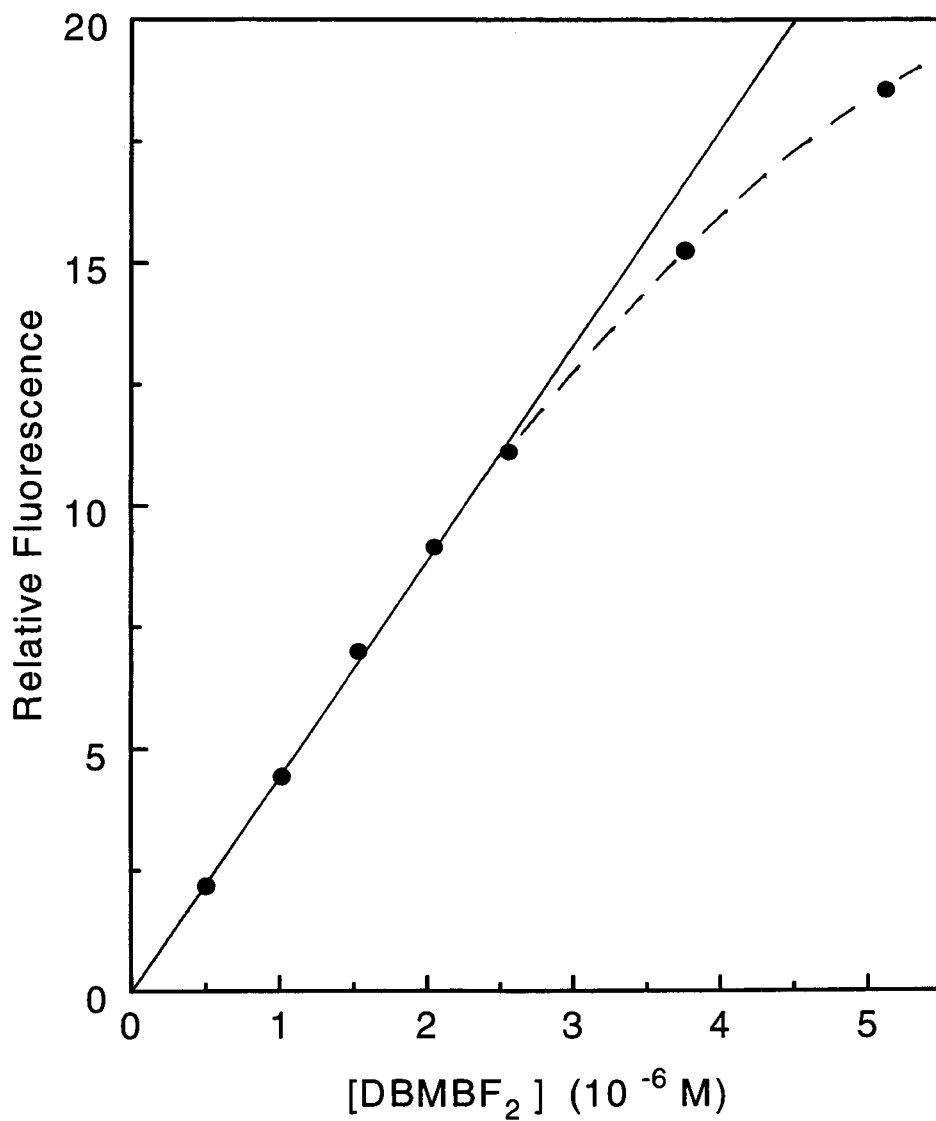


Figure 11.2: Plot of Relative Fluorescence Intensity of DBMBF₂ vs. [DBMBF₂] in Aerated Acetonitrile.

DBMBF₂ stock solution was prepared in 1,4-dioxane that serves as a carrier solvent), and diluted until the concentration was near 10⁻⁶ M (for DBMBF₂, MBDBF₂, DBMBO, MBDBO, DBMBN and DBMBC) or ≥ 10⁻⁵ M (for the remaining complexes). Concentrations were chosen that UV-Vis absorptions at the excitation wavelength were less than 0.01. A three mL aliquot was transferred to a one centimeter fluorimetry cell fitted with a rubber septum. Samples were then purged with argon for several minutes to remove dissolved oxygen.

For fluorescence quenching and exciplex emission studies, samples were prepared by transferring solids or liquids and stock DBMBF₂ solution (2 x 10⁻³ M, 10 μL) directly in tared five mL volumetric flasks and filling to the mark with solvent; [DBMBF₂] less than 10⁻⁵ M. Aliquots (three mL) were then transferred to a one centimeter pathlength fluorimeter cell, sealed with a rubber septum, and purged with argon for several minutes. For fluorescence quenching studies in acetonitrile the samples were not purged with argon; the presence of oxygen did not affect the fluorescence intensity of DBMBF₂.

11.5.3 Exciplex Emission and Resolution of Unresolved Fluorescent Bands

In many of the fluorescence quenching experiments the exciplex emission was well resolved from DBMBF₂'s emission and the exciplex λ_{max} determination was unimpaired. However, in a number of cases DBMBF₂ and its exciplex fluorescence bands are severely overlapped such the exciplex's λ_{max} could not be determined. Resolution of these two fluorescence bands requires knowledge of at least one of the band's line shape. Experimentally, the fluorophor's profile is known in the absence of quencher and any reaction intermediate fluorescence profile can be approximated by the observed fluorescence at high concentrations if solvatochromic effects can be shown to be negligible. Due to exciplex emission solvatochromism, the experimental DBMBF₂ fluorescence profile was used to resolve the exciplex emission from that of DBMBF₂.

The algorithm for resolving two fluorescence bands where one is known is detailed in the following flow scheme in Figure 11.3. This procedure relies on the assumption that the known fluorophor's emission does not significantly change in the presence of quencher. Since DBMBF₂'s solvatochromism is known to be weak and that the overall emission profile in nonpolar and weakly polar solvents is similar, less than one molar concentration of benzenes is not expected to significantly affect DBMBF₂'s emission relative to that without quencher. The comparison of the extracted fluorophor emission and that of the known emission is used as a criterion to judge if the correct multiple was used. Improper choice would be revealed as a nonlinear and non-horizontal division plot, which is a result of the extracted fluorophor emission containing significant proportion of the exciplex emission.

11.5.4 Fluorescence Quenching in Acetonitrile

DBMBF₂ fluorescence quenching was performed according to a method discussed by Caldwell et al. [139]. Ten microlitres of a stock solution of DBMBF₂ in acetonitrile (0.002 M) was syringed into five mL of acetonitrile ([DBMBF₂] = 4 × 10⁻⁶ M). Two mL of this solution was pipetted into a fluorimeter cell and the fluorescence of DBMBF₂ was recorded. The quencher (neat solution for liquids or a concentration solution in acetonitrile for solids) was then syringed (2-5 μL) into the fluorimeter cell and the fluorescence recorded. For large additions of quencher (a total of 20 μL or more) the I⁰ was corrected for dilution of DBMBF₂ concentration on the basis that the fluorescence intensity and [DBMBF₂] is linearly related (Figure 11.2). The presence of molecular oxygen does not affect the fluorescence intensity of either DBMBF₂ or its exciplex with benzenes (I_{ex}⁰ / I_{ex} and I_A⁰ / I_A are less than 1.01: cf. Chapter Seven) therefore Σk_{dex} and Σk_{dm} (= k_f + k_{nr}) are not significantly affected.

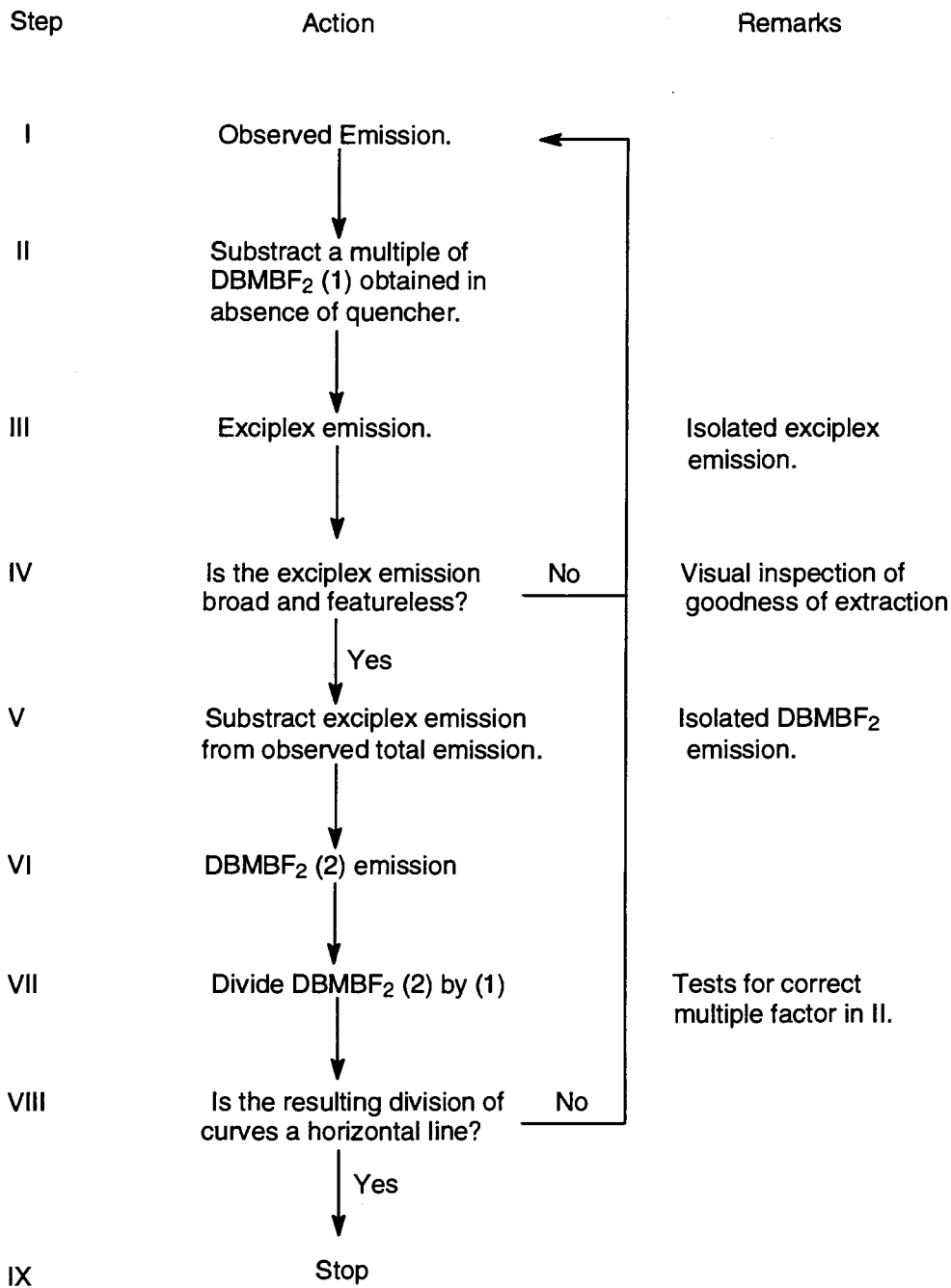


Figure 11.3: Algorithm for the Resolution of the Overlapping DBMBF₂ and its Exciplex Fluorescence.

11.5.5 Exciplex Enthalpy of Formation

Exciplex enthalpy of formation experiments were performed on single cyclohexane solutions of DBMBF₂ plus benzene where these solutions were subjected to various temperatures ranging from 6 to 60 °C where the temperature was incremented from 6 to 60 °C in approximately 8 degree units.

For the strong electron donating benzenes, their concentration was chosen from a separate fluorescence quenching experiment where the ideal [benzene] was achieved when DBMBF₂'s fluorescence intensity (390 nm) was one third the exciplex's fluorescence intensity at its λ_{max} . This one third ratio was chosen on the basis that the exciplex's fluorescence intensity is temperature sensitive where the DBMBF₂ / exciplex fluorescence ratio usually increases from one third to near unity from 6 to 60 °C; this facilitated more accurate analysis. For the weaker electron donating benzenes the benzene concentration was kept less than 0.5 M to minimize the change in solvent polarity.

The fluorimetry cell temperature was maintained using a jacketed cell holder by way of an external water bath (Lauda NB-515). The fluorimetry cell was equilibrated at each temperature for at least 30 minutes. The fluorimetry cell temperature was determined by a secondary cell (filled with water) along side the sample fluorimetry cell where the temperature in the former cell was measured using thermocouple (Cole-Parmer Model 8528-20 with K type thermocouple). The temperature was found to fluctuate by \pm 0.1 °C.

11.5.6 Fluorescence Center of Gravity

The calculation of exciplex emission rate constant (k_f^{ex}) in Chapter Nine required knowledge of DBMBF₂'s emission center of gravity (ν_{ave}). This value was determined from the corrected fluorescent spectrum of DBMBF₂ according to eq 9.13

$$v_{ave} = \int v I(v) dv / \int I(v) dv \quad (9.13)$$

The fluorescence spectrum of DBMBF₂ was manually converted to an energy scale (cm⁻¹) (Figure 11.4) and the unresolved peaks v_{pmax} located using the second derivative of Figure 11.4. With these v_{pmax} the spectrum in Figure 11.4 was fitted to both Gaussian and Lorentzian line shapes, using MircoCal Origin (version 3.0), where Gaussian line shapes gave an excellent fit (Figure 11.5) whereas Lorentzian line shapes gave a poor fit (not shown). Using Gaussian line shapes eq 9.13 can be converted to a summation

$$v_{ave} = \sum v_i A_i / \sum A_i$$

$$\text{where } A_i = (\sqrt{\pi} / 2 \ln 2) \Delta v_{1/2}(i) I_{max}(i) \quad (11.3)$$

where $\Delta v_{1/2}(i)$ and $I_{max}(i)$ are the *i* th Gaussian peak's FWHM and fluorescence intensity at v_i , respectively.

Table 11.2: Parameters determined from the Gaussian fitting of DBMBF₂'s fluorescence in Figure 11.5

Peak	v_i (cm ⁻¹)	I_{max} (i)	$\Delta v_{1/2}$ (i) (cm ⁻¹)
1	25510	323.3	1270
2	24155	381.4	1540
3	22779	117.3	1180
4	21787	68.6	2300
5	19157	6.5	2230

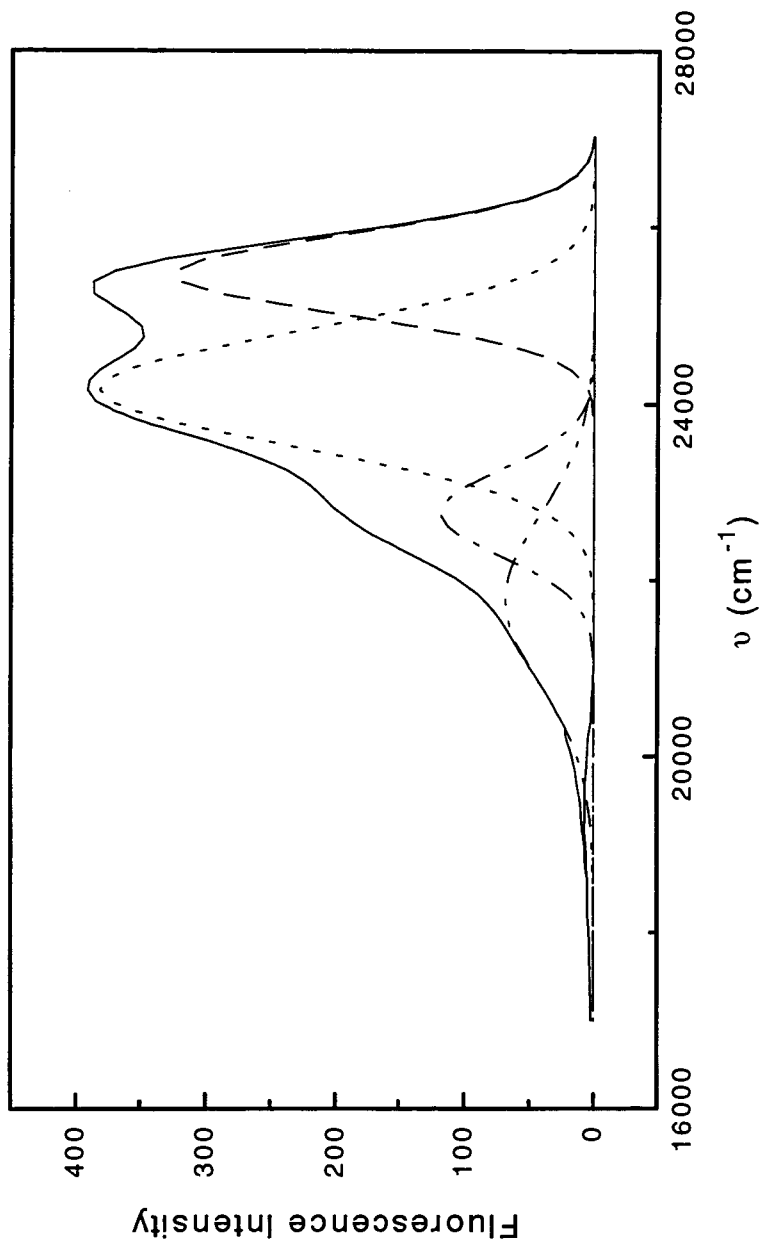


Figure 11.4: Deconvolution of DBMBF₂ Fluorescence Profile (Aerated Acetonitrile) into Five Gaussians. The Solid Line Represents the Summation of the Gaussian Curves.

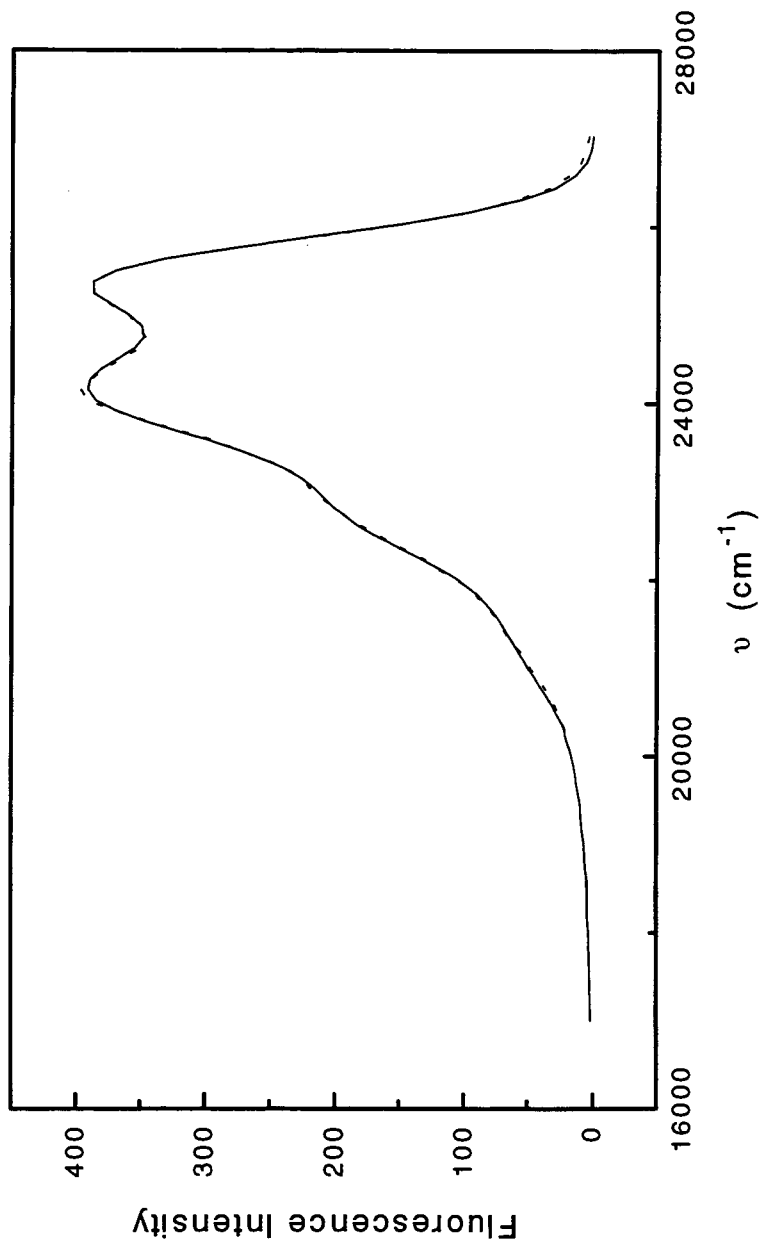


Figure 11.5: Comparison of the Observed (Solid Line) and Calculated (Dashed Line) of DBMBF₂ Fluorescence Profile in Aerated Acetonitrile.

From the data in Table 11.2 and eq 11.3 ν_{ave} is calculated to be 24,100 cm^{-1} .

11.5.7 Exciplex Fluorescence Quantum Yield ($\Phi_{\text{ex}}^{\infty}$)

DBMBF₂ / Benzene exciplex $\Phi_{\text{ex}}^{\infty}$ was evaluated according to eq 9.9.

$$\Phi_{\text{ex}}^{\infty} = \Phi_{\text{F}}^{\circ} [A_{\text{ex}} / (A_{\text{A}}^{\circ} - A_{\text{A}})] \quad (9.9)$$

where Φ_{F}° is the fluorescence quantum yield of DBMBF₂ (Table 3.2) and A_{ex} , A_{A}° and A_{A} are the integrated fluorescence areas of the exciplex, DBMBF₂ in the absence and presence of benzene, respectively. The integrated fluorescence areas were determined using the integrated area option in the PTI LS -100 steady state luminescence software package.

For well resolved DBMBF₂ / exciplex emissions, A_{A} was determined by

$$A_{\text{A}} = (I / I^{\circ}) A_{\text{A}}^{\circ} \quad (11.4)$$

where the fluorescence intensities I and I° were measured at 390 nm. A_{ex} was calculated from the difference between the total integrated fluorescent area (A_{T}) and A_{A}

$$A_{\text{ex}} = A_{\text{T}} - A_{\text{A}} \quad (11.5)$$

For unresolved DBMBF₂ / exciplex emissions the spectral separation method discussed in section 11.5.3 gave the A_{ex} and A_{A} , which their fluorescent areas are integrated directly.

The $\Phi_{\text{ex}}^{\infty}$ was determined for at least three concentrations of added benzene and the averaged value reported in Table 9.1. There was no detectable correlation between

$\Phi_{\text{ex}}^{\infty}$ and benzene concentration (shown as the ratio in Figure 11.6); this is consistent with the observation that plots of $\ln(I_{\text{ex}}/I_{\text{A}})$ vs. $\ln[D]$ (eq 5.2) were linear with unity slopes (cf. Figure 5.3).

11.5.8 Excited State Energies and Fluorescence Quantum Yields

Singlet energies were estimated from the cross-over point (λ_{co}) between normalized excitation, or UV-Vis absorption, and fluorescence spectra. These energies were calculated according to eq 11.6 [69].

$$E_{\text{S}} = 28,600 / \lambda_{\text{co}} \quad (\text{in kcal / mol}) \quad (11.6)$$

Because λ_{co} generally occurs between the absorption onset and the 0,0 peak, non-fluorescent complexes' λ_{co} was estimated from one third up the UV-Vis absorption band onset. The triplet energies (E_{T}) were calculated from eq 11.6 where λ_{co} was estimated one third up the phosphorescence emission profile.

The relative fluorescence quantum yields (Φ) were determined according to eq 11.7 [228].

$$\Phi_{\text{F}} = \Phi^{\text{std}} (A^{\text{unk}} / A^{\text{std}})(\text{Abs}^{\text{std}} / \text{Abs}^{\text{unk}}) (n_{\text{unk}}^2 / n_{\text{std}}^2) \quad (11.7)$$

The capital A represents the integrated fluorescence area and n represents the solvent's refractive index. The fluorescent standard is denoted by std, the compound under study is denoted by unk. The last term in eq 11.7, $n_{\text{unk}}^2 / n_{\text{std}}^2$, corrects for the medium's refractive index influence on the measured fluorescence intensity as it passes out of the fluorimeter cell; anthracene's fluorescence intensity was measured in cyclohexane ($n = 1.4235$ [30a]) whereas most of the β -diketonatoboron complex's fluorescence intensities

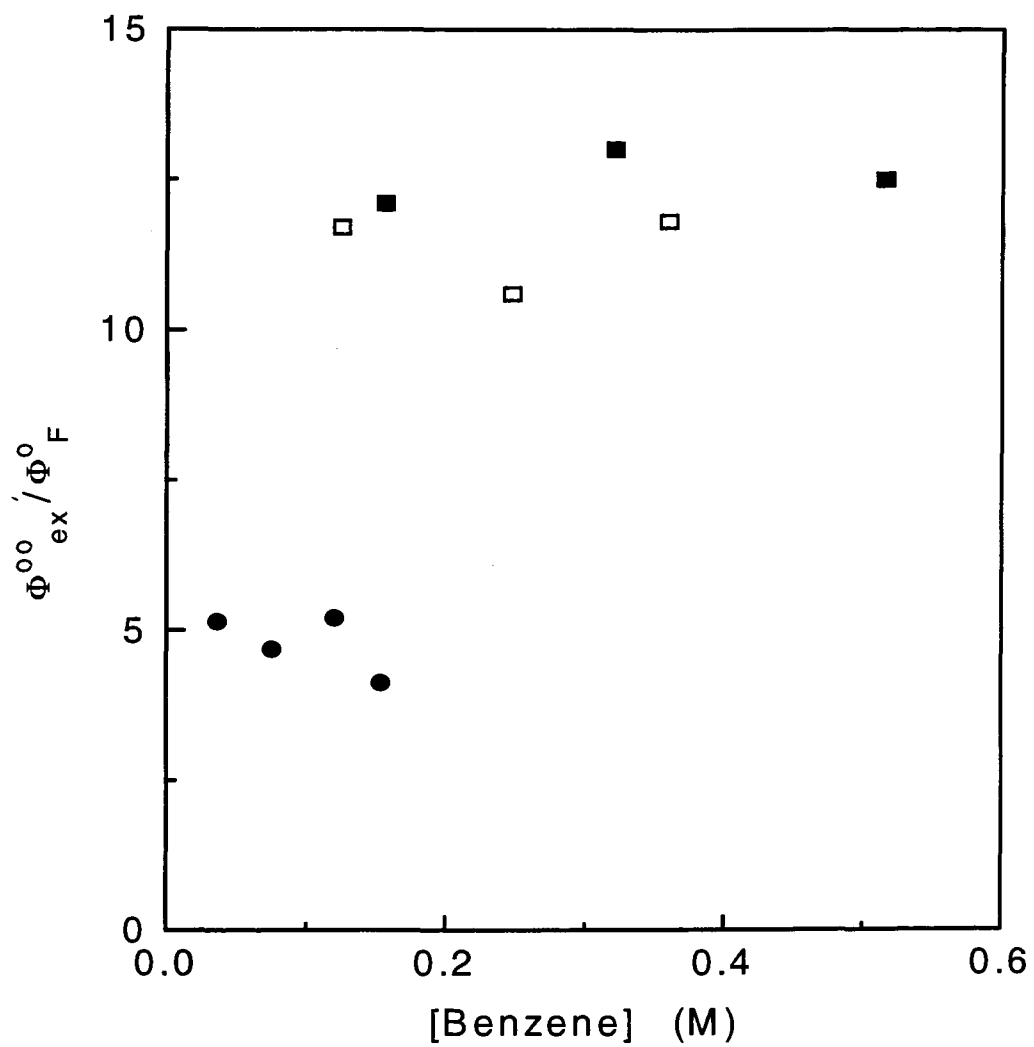


Figure 11.6: The Ratio of $\Phi_{ex}^{\infty} / \Phi_F^{\infty}$ vs. Benzene Concentration in Argon Purged Cyclohexane. Donors are: (■) Benzene; (□) Toluene; (●) Durene.

were measured in acetonitrile ($n = 1.3416$ [30a]). Following a suggestion of Morris, Mahaney and Huber [229] the slits (emission and excitation) were as small as possible (typically 1-2 nm) such that the refractive index correction is valid.

For DBMBF₂ and MBDBF₂, anthracene ($\Phi_F = 0.25$ in aerated cyclohexane, which was obtained from $\Phi_F^0 = 0.30$ [230] and $\Phi_F^0 / \Phi_F = 1.22$ [231]) was used as a fluorescent standard; for BABF₂ and ACHBF₂, methyl 2-naphthoate ($\Phi_F = 0.30$ in acetonitrile [232]) was used as a fluorescent standard. These standards were chosen on the basis that the excitation between standard and sample was identical and that the standard's fluorescence profile was in the same region as the sample's. Anthracene (Eastman, scintillation grade) was purified by recrystallization from ethanol (95 %) and then sublimed. Methyl 2-naphthoate was prepared from the acid catalyzed esterification of 2-naphthoic acid in methanol then recrystallized from acetonitrile.

11.5.9 Total Emission and Phosphorescence

Total and phosphorescence emission were recorded on a Perkin-Elmer MPF-44B with the Hitachi phosphorescence unit. Samples for total emission and phosphorescence were prepared similarly to those for fluorescence studies; however, the fluorimeter cell used was a cylindrical quartz cell with an i.d. of 0.3 mm and contained a sample volume of approximately 0.5 mL. The solvent was methylcyclohexane that gave a clear glass at 77 K; the quality of the glass was checked for each sample and spectra discarded if the glass showed any cracks.

Phosphorescence spectra were recorded at 77 K (liquid nitrogen) with a chopper speed of approximately 1000 rpm. Varying the chopper speed did not affect the phosphorescence intensity. Total emission spectra were recorded under identical condition except that the chopper was removed.

11.6 Time-Resolved Fluorimetry

11.6.1 Time-Correlated Single Photon Counting

A schematic diagram of a simplified single photon counting setup is shown in Figure 11.7. A generalized sequence for single photon counting is as follows: the clock generates a start pulse to the time to amplitude converter (TAC) and simultaneously triggers a lamp flash. This represents time zero. The lamp excites the sample and emission from the sample is detected by the photon multiplier tube (PMT). The detection of a photon by the PMT generates a stop signal to the TAC, in which during the start pulse and stop pulse the voltage was increasing linearly with time. This TAC voltage is translated as a single count into a memory channel of the multichannel analyzer (MCA). This process is repeated until a decay is constructed, one photon at a time. The discriminators shown in Figure 11.7 clean the start (leading edge (L.E.) discriminator) and stop pulses (constant fraction (C.F.) discriminator).

11.6.2 The LS-1 [233]

The PTI LS -1 uses a hydrogen flash lamp operating at a gas pressure of - 50 kPa, an electrode voltage of 4.5 kV and a flash rate of 22-25 kHz. The lamp electrodes are made of tungsten with an electrode spacing of approximately two millimeters. The LS -1 uses grating monochromators and a R928 PMT tube, which is housed in a cryocooled PMT housing. The electronics consists of a Tennelec TC 455 quad discriminator (C.F. and L.E.), Tennelec TC 536 counter, Ortec 457 TAC, Ortec 462 time calibrator, Ortec VT120c pre-amp and a Nucleus PCA II MCA.

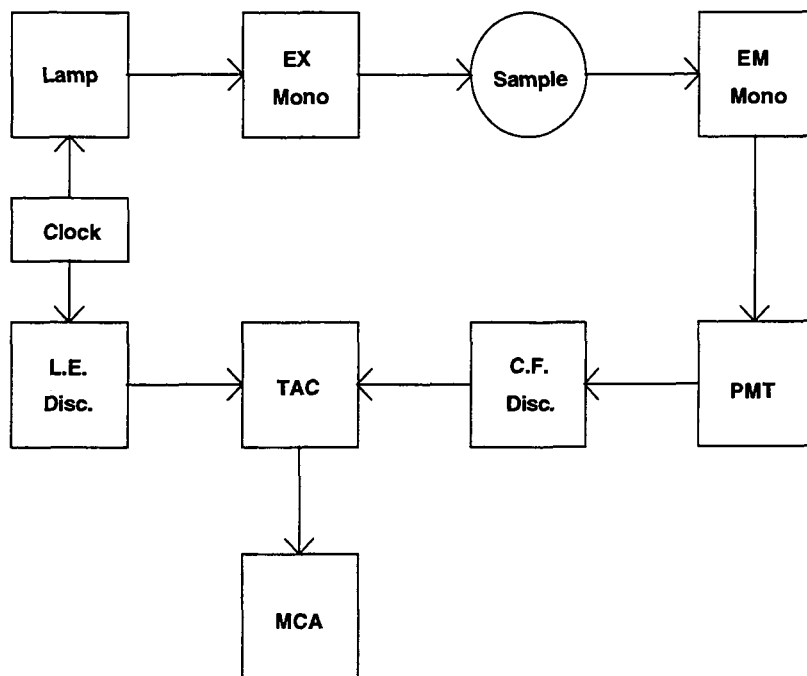


Figure 11.7 : Schematic Overview of the LS-1 Single Photon Counter. Adapted from References 148 and 233.

11.6.3 Calibration and Time Resolution

The LS-1 was calibrated by two methods: the Ortec 462 calibrator and comparison with fluorescence lifetime standards. The Ortec 462 calibrator calibrates the multi-channel analyzer in picoseconds per channel. This calibration was further checked by determining the lifetime of several compounds where these lifetimes are known; other factors, such as instrument instability, time resolution (picoseconds per channel) and software bugs will manifest themselves in the determined lifetime. Radio frequency noise was suppressed by the L.E. discriminator and adjusted until the autocorrelation appeared random. Pulse pile-up was avoided by collecting counts less than five percent (typically two percent) of the

lamp pulse frequency [148]; that is, the lamp pulse frequency lies between 22 to 25 kHz. Thus acquiring counts greater than 1100 to 1250 per second (five percent) will result in pulse pile-up. The lifetime standards were chosen on the basis that a significant lifetime range could be covered which includes the subnanosecond region. Table 11.3 lists the lifetime standards and compares the determined and reported lifetimes for these compounds. The good agreement between the reported and observed fluorescence lifetimes clearly indicates that reliable data can be obtained.

Table 11.3: Compounds, and Their Fluorescence Lifetimes, Used in Evaluating the PTI

LS -1

Compound	Solvent	τ_{obs} (ns)	χ^2	DW	τ_{fit} (ns)	Ref.
DBMBF ₂	CH ₃ CN	0.28	1.46	1.43	0.295	109
DBMBO	CH ₃ CN	1.35	1.26	1.71	1.4	14f
Anthracene	CH ₃ CN	5.07	1.12	1.78	5.0	231
Methyl 2 - naphthoate	CH ₃ OH	11.6	1.09	1.82	11.0	232

Due to the lamp pulse width (FWHM typically 2.0 ns), the lower limit was investigated to establish the LS-1's subnanosecond lifetime capabilities. In principle, any lifetime can be extracted by deconvolution of the signal and lamp profile [148]. The literature suggests that the detection limit ranges from 1 / 10 to 1 / 15 th of the lamp profile FWHM [149,234,235] but strongly dependent on the experimental conditions employed. The LS -1 detection limit was evaluated by deconvoluting the lamp profile from another lamp profile. It is expected that under ideal conditions a zero lifetime will be found but

instrumental instabilities, inherent distortions (due to experimental conditions) and software will introduce a finite lifetime. Two identical solutions containing non-dairy creamer, one used as a sample and the other as a scattering solution, were used to test this assumption. Deconvolution resulted in a lifetime of 0.10 ns. Since the scattering solution in the sample position of the turret does not contain a lifetime, the observed finite lifetime is limited by the time resolution of the LS-1 to lifetimes greater than 0.10 ns.

11.6.4 Data Analysis [148,233]

The observed fluorescence decay profile, $I(t)$, has the form:

$$I(t) = \int_0^t P(t') G(t - t') dt' \quad (11.8)$$

which is known as the convolution integral. $P(t')$ is the instrument response function (the lamp profile) and $G(t)$ is the true decay of the fluorophor. $P(t')$ is determined experimentally using a scattering solution. Since both $I(t)$ and $P(t')$ are known $G(t)$ can be determined. The observed true fluorophor decay was assumed to follow the following fitting law:

$$G(t) = \sum a_i \exp(-t/\tau_i) \quad (11.9)$$

The fitting procedure uses a non-linear weighted least squares procedure based on the Marquardt algorithm to find the minimum in the reduced χ^2 , which is calculated according to eq 11.10. $Y(i)$ is the number of counts in channel i and $I(t_i)$ is the calculated number of counts in channel i . n_1 and n_2 represent the first channel and last channel, respectively.

$$\chi^2 = \sum_{i=n_1}^{n_2} \{ [Y(i) - l(t_i)]^2 / Y(i) \} \quad (11.10)$$

$$\text{reduced } \chi^2 = \chi^2 / (n_2 - n_1 + 1)$$

The goodness of the fit of eqs 10.8 and 10.9 to the experimental data was judged on the basis of four statistical tests. Since acceptable values of reduced χ^2 are obtained for poor fits, the weighted residual, autocorrelation and Durbin-Watson parameter were also used to provide evidence for the goodness of fit. The weighted residual, r_i , was calculated by

$$r_i = w_i (Y(i) - l(t_i))^2 \quad (11.11)$$

where w_i is the weighting factor (reciprocal of the number of counts in channel i). The autocorrelation was calculated according to

$$C_{r_j} = \frac{(1/m) \sum_{i=n_1}^{n_1+m-1} r_i r_{i+j}}{(1/n_3) \sum r_i^2} \quad (11.11)$$

where r_i is given by eq 11.11, n_3 number of channels and $m = n_3 - j$. The Durbin-Watson parameter was calculated by eq 11.13.

$$DW = \frac{\sum_{i=n_1+1}^{n_2} (r_i - r_{i-1})}{\sum_{i=n_1+1}^{n_2} r_i^2} \quad (11.13)$$

$$i = n_1$$

The residuals and autocorrelation are more sensitive tests of the goodness of fitting than the reduced χ^2 ; however, they are subjective visual tests hence subject to personal bias. However, the autocorrelation is particularly useful in analyzing for rf noise where this noise appears as a sinusoidal wave imposed on top of the fluorescence decay curve. The Durbin-Watson test was included as a nonsubjective test where for 512 channels a good fit is demonstrated if $DW \geq 1.65$ and 1.75 for a single and biexponential fit, respectively; rf noise reduces the DW value significantly.

11.7 UV-Vis Absorption

The UV-Vis absorption spectra of various β -diketonatoboron complexes, and their corresponding β -diketones, were recorded on a Varian Cary 210 spectrophotometer. Samples were weighed into 25 mL volumetric flasks and a measured aliquot was diluted until an absorption between 0.2 and one was achieved. The solutions were referenced against the solvent with matched 1 cm quartz UV cells (Canlab No.7).

11.8 Cyclic Voltammetry

Cyclic Voltammetry was performed using a three electrode arrangement with a SCE reference electrode (Fisher), a stationary Pt working electrode (surface area 0.018 cm²), and a Pt counter electrode (Figure 11.8). The electronics included a Princeton Applied Research (PAR) Model 173 Programmer, a PAR Model 178 Electrometer and a PAR Model 173 Potentiostat/Galvanostat equipped with a PAR Model 179 Digital Coulometer. Cyclic voltammograms were recorded on an Allen recorder. The electrochemical cell was based on the design of Kissinger and Heinemann [236], but

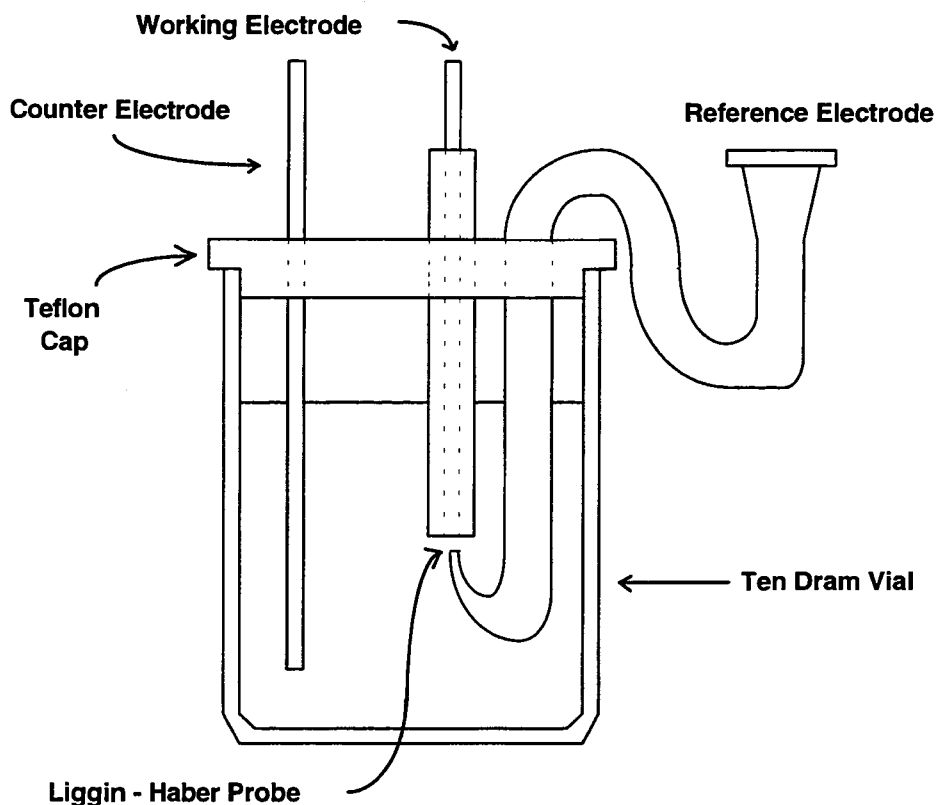


Figure 11.8: Illustration of the Cyclic Voltammetry Set-up.

adapted with a Luggin-Haber probe to reduce the ohmic drop. CH_3CN was refluxed and distilled over CaH_2 under argon. Concentration of the electroactive species was between one and three mM. The supporting electrolyte was tetraethylammonium perchlorate (GFS Chemicals, support electrolyte grade, 0.1 M).

The reported redox potentials were calibrated with respect to a number of calibrants (*vide infra*). The experimental range of the apparatus was determined, in the absence of an electroactive species, to be - 2.5 to + 3 volts (100 mV/s). The linear range of the system was investigated using four compounds that almost expanded across the

electrochemical window (- 2.5 to + 3 Volts); the linear response was observed from - 2 to + 2.6 Volts (Table 11.4).

Table 11.4: Cyclic Voltammetry Calibration

Compound	Observed	Reported	Comments	Ref.
Anthracene	1.28 ± 0.05	1.35, 1.20	Irreversible	238
Anthracene	$- 2.01 \pm 0.05$	- 2.04	Reversible	239
Ferrocene	0.37 ± 0.05	0.38	Reversible	240
Nitrobenzene	$- 1.17 \pm 0.05$	- 1.18	Reversible	239
Benzene	2.65 ± 0.05	2.62	Irreversible	238

With the exception of anthracene's oxidation potential, the observed redox values were within error (0.05 V) of the reported values thus establishing the linear range of the system. The SCE reference electrode is known to have a liquid junction potential (LJP) that varies with time. This is due to the precipitation of KCl on the acetonitrile side of the liquid junction that increases the LJP up to 50 mV [237]. The change in the LJP is the largest source of error, therefore the assigned errors of the reported potentials are ± 0.05 V.

The cyclic voltammograms were similar in appearance regardless of the number of cycles in all cases. No electrochemical intermediate could be detected up to a maximum scan rate of 2 volts per second (the fastest scan rate that the chart recorder could follow). Inspection of the platinum electrodes after a number of oxidation and reduction cycles showed no evidence of a coating. Therefore, no detectable electrochemical reaction product was deposited on the electrodes. The anodic limit (+3 V) of the apparatus is known to be due to the oxidation of the perchlorate anion (from the supporting electrolyte).

11.9 Fitting of Exciplex Dipole Moment to Theory

In this study the DBMBF₂ / benzene exciplex wavefunction is chiefly composed of two configurations, the charge transfer and locally excited state configurations:

$$\Psi_{EX} = a |A^{\cdot}D^{\cdot+}\rangle + c |^{\cdot}AD\rangle \quad (2.30)$$

Assuming the exciplex dipole moment is due to the charge transfer configuration only (i.e., $a^2 = \mu_{ex} / \mu_{CRIP}$), the exciplex dipole moment can be calculated if the coefficient a is known. The coefficient a can be determined via eq 2.30 by minimizing the energy (cf. Chapter 2.3.2). The resulting equations are:

$$E_{EX} = \frac{-B \pm \sqrt{D}}{2A} \quad (2.39)$$

$$\begin{aligned} \text{where} \quad A &= (1 - S^2) \\ B &= 2HS - E_{EL} - E_{CT} \\ C &= E_{LE}E_{CT} - H^2 \\ D &= B^2 - 4AC \end{aligned}$$

$$c/a = (E_{CT} - E_{EX}) / (H - E_{EX}S) \quad \text{if } E_{CT} < E_{LE} \quad (2.40a)$$

$$= (E_{LE} - E_{EX}) / (H - E_{EX}S) \quad \text{if } E_{LE} < E_{CT} \quad (2.40b)$$

The charge transfer (E_{CT}) and locally excited (E_{LE}) configuration energies are given by

$$E_{CT} = E_{ox}(D) - E_{red}(A) + 0.15 \text{ eV} \quad (2.33)$$

$$E_{LE} \equiv E_S$$

and the configuration mixing integral, H, can be calculated by

$$H \equiv -S(\Gamma_D + E_S) \quad (2.35)$$

where $\Gamma_D \equiv -20 \text{ eV} + \text{IP}(\text{Donor})$

Of the equations above only the configuration overlap integral, S, is unknown.

The simple program listing, in Basic, is provided in Figure 11.9 and the memory listing is provided in Figure 11.10. This program returns the B - \sqrt{D} root (eq 2.39), the lowest energy root, and then proceeds to calculate the exciplex coefficient ratio, c/a. Once this ratio calculated, coefficient a and the exciplex dipole moment are calculated. Finally, the program returns the U_{stab} .

Using the experimental μ_{ex}^0 values listed in Table 6.2 and the program shown in Figure 11.9, the S integral (to the closest two significant figures) was calculated by trial and error (Table 11.11). The mean S value (Table 11.11) was then used to calculate the 'best fit' dash line shown in Figure 6.4. The increasing trend of the S values from HMB to toluene follows the decreasing number methyl substituents. This suggests that steric hindrance may be reducing the overlap between the donor and acceptor.

11.10 Estimation of Errors

Unless otherwise noted, the reported errors from plots are one standard deviation as obtained from least squares analysis; standard deviations were calculated using the MicroCal Origin Scientific and Technical Graphics in Windows (version 3.0) by MicroCal Software, Incorporated. The error in lifetime measurements was estimated to be 5 and 10 percent for lifetimes greater than and less than 1 nanosecond, respectively, based on duplicate measurements.

The propagation of random errors was calculated by standard methods [241]:

Figure 11.9: Exciplex Dipole Moment Calculation Program Listing

```

3 : REM **** INPUT OF VARIABLES ***
5 : INPUT "SINGLET ENERGY"; G
10 : INPUT "OVERLAP"; S
20 : INPUT "DONOR'S IP; IF YOU WISH TO QUIT ENTER 0"; I
22 : INPUT "DIFFERENCE IN HOMO-HOMO ENERGIES = "; H
25 : REM **** CALCULATIONS ****
30 : IF V = 0 GOTO 130
40 : V = I - 20.5 + G; V = -1 * S * V
50 : B = (2 * S * V) - (2 * G) - H; A = 1 - S ^ 2
60 : C = G * (G + H) - V ^ 2; D = (B ^ 2) - (4 * A * C); D = D ^ .5
70 : Z = (-1 * B - D) / (2 * A); Y = G - Z
80 : REM W = (-1 * B + D) / (2 * A); W = G - W
90 : E = (G - Z) / (V - Z * S); F = 1 + (S * 2 * E) + E ^ 2; F = 1 / F
100 : M = F * 13.8
105 : REM **** PRINTING OF CALCULATION ***
110 : PRINT "DIPOLE MOMENT IS": PRINT M: PRINT "Ustab IS"
120 : PRINT Y: GOTO 10
130 : STOP

```

Table 11.5 : Memory Listing

Memory	Remarks
A	$1 - S^2$
B	$2HS - E_{EL} - E_{CT}$
C	$E_{EL}E_{CT} - H^2$
D	$(2HS - E_{EL} - E_{CT})^2 - 4(1 - S^2)(E_{EL}E_{CT} - H^2)$
F	$1 / a$
G	E_S
I	IP
M	μ_{ex}
S	overlap
V	H
Y	U_{Stab}
Z	E_{EX}

Figure 11.6: Calculation of the Overlap Integral for DBMBF₂ / Benzene Exciplexes

Donor	IP (eV) ^a	E _{ox} (V) ^a	ΔE _{HOMO} (eV) ^b	μ _{ex} ^o (D) (Exp.) ^a	μ _{ex} ^o (D) (Calc.) ^c	S ^c
HMB	7.85	1.59	0.86	13.3	13.28	0.025
PMB	7.92	1.71	0.74	12.9	12.90	0.030
Durene	8.05	1.79	0.66	12.5	12.48	0.035
1,2,3,5-TMB	8.06	1.83	0.62	12.4	12.36	0.035
1,2,3,4-TMB	8.14	1.82	0.63	12.2	12.17	0.039
1,2,4-TMB	8.27	1.92	0.53	11.5	11.50	0.044
Mesitylene	8.42	2.02	0.43	10.1	10.12	0.058
p-Xylene	8.44	2.06	0.39	11.1	11.13	0.039
m-Xylene	8.56	2.14	0.31	10.5	10.49	0.040
o-Xylene	8.56	2.13	0.32	10.2	10.21	0.045
Toluene	8.82	2.25	0.20	9.2	9.16	0.045
Chlorobenzene	9.07	2.48	-0.03	4.2	-- ^d	-- ^d
Benzene	9.23	2.62	-0.17	2.9	2.87	0.024
Methyl benzoate	9.34	2.69	-0.24	2.3	2.26	0.027
Cyanobenzene	9.70	2.94	-0.49	1.1	1.11	0.033
Mean						0.037

^a Values from Table 6.2. ^b Difference in redox potentials [E_{ox} (DBMBF₂) - E_{ox} (Benzenes)]; E_{ox} (DBMBF₂) = 2.45 V (Table 3.4). ^c Calculated from the program listed in Figure 11.9. S was varied until the calculated exciplex dipole matched the experimental value. ^d This value was not calculated due to sensitivity; a small change in ΔE_{HOMO} results in a large change in the calculated S.

(A) For $F = ax \pm by \pm cz$,

$$\sigma^2(F) = a^2\sigma^2(x) + b^2\sigma^2(y) + c^2\sigma^2(z) \quad (11.14)$$

(B) For $F = axyz$ (or axy/z etc.)

$$\sigma^2(F) / F^2 = \sigma^2(x) / x^2 + \sigma^2(y) / y^2 + \sigma^2(z) / z^2 \quad (11.15)$$

σ represents the error of the associated variable.

REFERENCES

- [1] Mehrotra, R.C.; Bohra, R.; Gaur, D.P. *Metal β -Diketonates And Allied Derivatives*; Academic Press: New York, 1978.
- [2] (a) Barnum, D.W. *J. Inorg. Nucl. Chem.* **1961**, *21*, 221.
(b) Barnum, D.W. *J. Inorg. Nucl. Chem.* **1961**, *22*, 183.
- [3] Belford, R.L.; Martell, A.E.; Calvin, M. *J. Inorg. Nucl. Chem.* **1956**, *2*, 11.
- [4] Fackler, J.P. *Progr. Inorg. Chem.* **1966**, *7*, 361.
- [5] Verdu, J.; Blanco, C.A. *Inter. J. Chem. Kin.* **1994**, *26*, 743.
- [6] Girolami, G.S.; Jeffries, P.M.; Dubois, L.H. *J. Am. Chem. Soc.* **1993**, *115*, 1015.
- [7] Marciniak, B.; Hug, G.L. *J. Photochem. Photobiol. A:Chem.* **1994**, *78*, 7.
- [8] (a) Chow, Y.L.; Cheng, X. *J. Chem. Soc. Chem. Commun.* **1990**, 1043.
(b) Chow, Y.L.; Cheng, X. *Can. J. Chem.* **1991**, *69*, 1331.
- [9] Toporcer, L.H.; Dessy, R.E.; Green, S.I.E. *Inorg. Chem.* **1965**, *4*, 1649.
- [10] Brown, N.M.D.; Bladon, P. *J. Chem. Soc. (A)* **1969**, 526.
- [11] Gerrard, W.; Lappert, M.F.; Shafferman, R. *Chem. Ind.* **1958**, 722.
- [12] (a) Burford, N.; Kennepohl, D.; Cowie, M.; Ball, R.G.; Cavell, R.G. *Inorg. Chem.* **1987**, *26*, 650.
(b) Private communication.
- [13] Diltthey, W.; Edwardof, F.; Schumacher, F. *Liebigs. Ann. Chem.* **1905**, *344*, 300, 326.
- [14] (a) Ilge, H.-D.; Faßler, D.; Hartmann, H. *Z. Chem.* **1984**, *24*, 218.
(b) Ilge, H.-D.; Faßler, D.; Hartmann, H. *Z. Chem.* **1984**, *24*, 292.
(c) Hartmann, H.; Schumann, T.; Dusi, R.; Bartsch, U.; Ilge, H.-D. *Z. Chem.* **1986**, *26*, 330.
(d) Ilge, H.-D.; Hartmann, H. *Z. Chem.* **1986**, *26*, 399.
(e) Hartmann, H. *J. Prakt. Chem.* **1986**, *328*, 755.

- (f) Ilge, H.-D.; Birckner, E.; Fassler, D.; Kozmenko, M.V.; Kuz'min, M.G.; Hartmann, H. *J. Photochem.* **1986**, *32*, 177.
- (g) Schade, W.; Ilge, H.-D.; Hartmann, H. *J. Prakt. Chem.* **1986**, *328*, 941.
- [15] Halm, J.M. *Tappi*, **1977**, *60*, 90.
- [16] Mikhailov, B.M., *Pure Appl. Chem.* **1977**, *49*, 749.
- [17] (a) Bally, I.; Balaban, A.T. *Studii Cere. Chim.* **1969**, *17*, 431.
- (b) Balaban, A.T.; Bally, I.; Minkin, V.I.; Usachev, A.I. *Tetrahedron* **1977**, *33*, 3265.
- (c) Trestianu, A.; Niculescu - Majewska, H.; Bally, I.; Barabas, A.; Balaban, A.T. *Tetrahedron*, **1968**, *24*, 2499.
- [18] Berestova, S.S; Shapet'ko, N.N.; Shigorin, D.N.; Medvedeva, V.G.; Skoldinov, A.P.; Plakhina, G.D.; Andreichikov, Yu. S. *Theor. Eksper. Khim.* **1978**, *15*, 575.
- [19] Boese, R.; Köster, R.; Yalpani, M. *Chem. Ber.* **1985**, *118*, 670.
- [20] Hanson, A.W.; Macaulay, E.W. *Acta. Cryst.* **1972**, *B28*, 1961.
- [21] Cotton, F.A.; Ilsley, W.H. *Inorg. Chem.* **1982**, *21*, 300.
- [22] Haddon, R.C.; Chichester, S.V.; Marshall, J.H. *Tetrahedron* **1986**, *42*, 6293.
- [23] Kopteva, T.S.; Medvedeva, V.G.; Rodionov, A.N.; Ruch'eva, N.I.; Skoldinov, A.P.; Shigorin, D.N. *Zh. Obshch. Khim.* **1978**, *48*, 1587.
- [24] Borisenko, A.V.; Vovna, V.I.; Gorachakov, V.V.; Korotkikh, O.A. *Zh. Strukt. Khim.* **1987**, *28*, 147.
- [25] Calvin, M.; Wilson, K. *J. Am. Chem. Soc.* **1945**, *67*, 2005.
- [26] Holm, R.H.; Cotton, F.A. *J. Am. Chem. Soc.* **1958**, *80*, 5658.
- [27] Medvedeva, V.G.; Skoldinov, A.P.; Shapet'ko, N.N. *Zh. Obshch. Khim.* **1969**, *39*, 460.
- [28] Skoldinov, A.P.; Shigorin, D.N.; Medvedeva, V.G.; Ryabchikova, T.S. *Zh. Obshch. Khim.* **1963**, *33*, 3110.
- [29] Smith, J.A.S.; Wilkins, E.J. *J. Chem. Soc. (A)* **1966**, 1749.

- [30] (a) Riddick, J.A.; Bunger, W.B.; Sakano, T.K. In *Techniques of Chemistry, Volume II: Organic Solvents, Physical Properties and Methods of Purification*; Weissberger, A, Ed.; Wiley: New York, 1986.
- (b) Miukin, V.I.; Osipov, O.A.; Zhdanov, Y.A. *Dipole Moments in Organic Chemistry*; Plenum: New York, 1970.
- [31] Okada, K.; Hosoda, Y.; Oda, M. *J. Am. Chem. Soc.* **1986**, *108*, 321.
- [32] (a) Chow, Y.L.; Cheng, X. *Can. J. Chem.* **1991**, *69*, 1575.
- (b) Chow, Y.L.; Ouyang, X. *Can. J. Chem.* **1991**, *69*, 423.
- (c) Chow, Y.L.; Wu, S.P.; Ouyang, X. *J. Org. Chem.* **1993**, *59*, 421.
- [33] Lui, Z.-L.; Zhang, M.-X.; Yang, L.; Liu, Y.-C.; Chow, Y.L.; Johansson, C.I. *J. Chem. Soc. Perkin Trans. 2* **1994**, 585.
- [34] de Mayo, P. *Acc. Chem. Res.* **1971**, *4*, 41.
- [35] Nozaki, H.; Kurita, M.; Mori, T.; Noyori, R. *Tetrahedron* **1968**, *24*, 1821.
- [36] Cheng, X. Ph. D. Thesis, Simon Fraser University, April 1990.
- [37] Marcus, R.A. *Angew. Chem. Int. Ed. Eng.* **1993**, *32*, 1111 and references cited therein.
- [38] Bhattacharyya, K.; Chowdhury, M. *Chem. Rev.* **1993**, *93*, 507 and references cited therein.
- [39] Kochi, J.K. *Adv. Phys. Org. Chem.* **1994**, *29*, 185.
- [40] (a) Marcus, R.A. *Ann. Rev. Phys. Chem.* **1964**, *15*, 155.
- (b) Marcus, R.A. *J. Phys. Chem.* **1963**, *67*, 853.
- (c) Marcus, R.A. *J. Phys. Chem.* **1968**, *72*, 891.
- (d) Marcus, R.A. *Faraday Discuss. Chem. Soc.* **1982**, *74*, 7.
- [41] Newton, M.D. *Chem. Rev.* **1991**, *91*, 767.
- [42] (a) Hwang, J.-K.; Warshel, A. *J. Am. Chem. Soc.* **1987**, *109*, 715.
- (b) Kuharski, R.A.; Bader, J.S.; Chandler, D.; Sprik, M.; Klein, M.L.; Impey, R.W. *J. Chem. Phys.* **1988**, *89*, 3248.

- [43] McLennan, D.L. *J. Chem. Educ.* **1976**, *53*, 348.
- [44] Scandola, F.; Indelli, M.T.; Chiorboli, C.; Bignozzi, C.A. *Top. Curr. Chem.* **1990**, *1158*, 73.
- [45] Maslak, P. *Top. Curr. Chem.* **1993**, *168*, 1.
- [46] Gould, I.R.; Moody, R.; Farid, S. *J. Am. Chem. Soc.* **1988**, *110*, 7242.
- [47] Suppan, P. *Top. Curr. Chem.* **1992**, *163*, 95.
- [48] Bolton, J.R.; Archer, M.D. In *Electron Transfer in Inorganic, Organic and Biological Systems*; Bolton, J.R.; Mataga, N.; McLenden, G., Eds.; American Chemical Society Advances in Chemistry Series 228; American Chemical Society: Washington, D.C., 1991; Chapter 2.
- [49] (a) Dewar, M.J.S.; Hashmall, J.A.; Trinajstić, N. *J. Am. Chem. Soc.* **1970**, *92*, 5555.
- (b) Chen, E.C.M.; Wentworth, W.E. *J. Phys. Chem.* **1975**, *63*, 3183.
- (c) Pysh, E.S.; Yang, N.C. *J. Am. Chem. Soc.* **1963**, *85*, 2124.
- [50] Mulliken, R.S.; Person, W.B. *Molecular Complexes, A Lecture and Reprint Volume*; Wiley: New York, 1969.
- [51] Briegleb, G. *Elektronen - Donator - Acceptor - Komplexe*; Springer - Verlag: Berlin, 1961.
- [52] Mulliken, R.S.; Person, W.B. *J. Am. Chem. Soc.* **1969**, *91*, 3409.
- [53] Förster, T. In *The Exciplex*; Gordon, M.; Ware, W.R., Eds.; Academic: New York, 1975.
- [54] Weller, A. In *The Exciplex*; Gordon, M.; Ware, W.R., Eds.; Academic: New York, 1975.
- [55] Benesi, H.A.; Hildebrand, J.H. *J. Am. Chem. Soc.* **1949**, *71*, 2703.
- [56] Brackmann, W. *Rec. Trav. Chim.* **1949**, *68*, 147.
- [57] Mantione, M.J. *Theor. Chim. Acta* **1969**, *15*, 141.
- [58] Lippert, J.L.; Hanna, M.W.; Trotter, P.J. *J. Am. Chem. Soc.* **1969**, *91*, 4035.

- [59] (a) Frey, J.E.; Cole, R.D.; Kitchen, E.C.; Suprenant, L.M.; Sylwestrzak, M.S. *J. Am. Chem. Soc.* **1985**, *107*, 748.
- (b) Frey, J.E.; Andrews, A.M.; Ankoviac, D.G.; Beaman, D.N.; Du Pont, L.E.; Elsner, T.E.; Lang, S.R.; Oosterbaan Zwart, M.A.; Seagle, R.E.; Torreano, L.A. *J. Org. Chem.* **1990**, *55*, 606.
- [60] Gould, I.R.; Noukakis, D.; Gomez - Jahn, L.; Young, R.H.; Goodman, J.L.; Farid, S. *Chem. Phys.* **1993**, *176*, 439.
- [61] Hanna, M.W. *Quantum Mechanics in Chemistry*, 3rd ed.; Benjamin / Cummings: Menlo Park, CA, 1981.
- [62] Wentworth, W.E.; Drake, G.W.; Hirsch, W.; Chen, E. *J. Chem. Educ.* **1964**, *41*, 373.
- [63] Weller, A. *Z. Phys. Chem. N.F.* **1982**, *130*, 129.
- [64] Leonhardt, H.; Weller, A. *Ber. Bunsenges. Phys. Chem.* **1963**, *67*, 791.
- [65] Stevens, B. *Adv. Photochem.* **1971**, *8*, 161.
- [66] Mataga, N.; Ottolenghi, M. In *Molecular Association*; Foster, R., Ed.; Academic: New York, 1979.
- [67] Verhoeven, J.W.; Scherer, T.; Willemse, R.J. *Pure Appl. Chem.* **1993**, *65*, 1717.
- [68] Helsen, N.; Viaene, L.; van der Auweraer, M. *J. Phys. Chem.* **1994**, *98*, 1532.
- [69] Turro, N.J. *Modern Molecular Photochemistry*; Benjamin / Cummings: Menlo Park, CA, 1978.
- [70] Weller, A. *Z. Phys. Chem. N.F.* **1982**, *133*, 93.
- [71] (a) Beens, A.; Weller, A. *Acta. Phys. Polon.* **1968**, *4*, 593.
- (b) Knibbe, H. Ph.D. Thesis, Free University of Amsterdam, September 1969.
- (c) Beens, H. Ph.D. Thesis, Free University of Amsterdam, January 1970.
- (d) Beens, H.; Weller, A. In *Organic Molecular Photophysics, Volume Two*; Birks, J.B., Ed.; Wiley: New York, 1975; p 159.

- [72] Michl, J.; Bonacic - Koutecky, V. *Electronic Aspects of Organic Photochemistry*; Wiley: New York, 1990.
- [73] Rehm, D.; Weller, A. *Z. Phys. Chem. N.F.* **1970**, *69*, 183.
- [74] Reichardt, C. *Solvents and Solvent Effects in Organic Chemistry*; VCH: New York, 1988.
- [75] Böttcher, C.J.F. *Theory of Electronic Polarisation*; Elsevier: New York, 1952.
- [76] Davis, K.M.C. In *Molecular Association*; Foster, R., Ed.; Academic: New York, 1975.
- [77] Beens, H.; Knibbe, H.; Weller, A. *J. Chem. Phys.* **1967**, *47*, 1183.
- [78] (a) Marcus, R.A. *J. Chem. Phys.* **1963**, *38*, 1858.
(b) Marcus, R.A. *J. Chem. Phys.* **1965**, *43*, 1261.
(c) Marcus, R.A. *J. Phys. Chem.* **1989**, *93*, 3078.
- [79] van der Zwan, G.; Hynes, J.T. *J. Phys. Chem.* **1985**, *89*, 4181.
- [80] (a) Brunshwig, B.S.; Ehrenson, S.; Sutin, N. *J. Phys. Chem.* **1986**, *90*, 3657.
(b) Brunshwig, B.S.; Ehrenson, S.; Sutin, N. *J. Phys. Chem.* **1987**, *91*, 4714.
- [81] Ooshika, Y. *J. Phys. Soc. Jpn.* **1954**, *9*, 594.
- [82] Lippert, E. *Z. Naturforsch.* **1955**, *10a*, 541.
- [83] McRae, E.G. *J. Phys. Chem.* **1957**, *61*, 562.
- [84] Liptay, W. In *Modern Quantum Chemistry, Istanbul Lectures*; Sinanoglu, O., Ed.; Academic: New York, 1965; Parts II and III.
- [85] Basu, S. *Adv. Quantum Chem.* **1964**, *1*, 145.
- [86] Amos, A.T.; Burrows, B.L. *Adv. Quantum Chem.* **1973**, *7*, 289.
- [87] Onsager, L. *J. Am. Chem. Soc.* **1936**, *58*, 1486.
- [88] Létard, J.-F.; Lapouyade, R.; Rettig, W. *J. Am. Chem. Soc.* **1993**, *115*, 2441.
- [89] Longuet - Higgins, H.C.; Pople, J.A. *J. Chem. Phys.* **1957**, *27*, 192.
- [90] (a) Kamlet, M.J.; Abboud, J.L.; Taft, R.W. *J. Am. Chem. Soc.* **1977**, *99*, 6027.
(b) Abboud, J.L.; Kamlet, M.J.; Taft, R.W. *J. Am. Chem. Soc.* **1977**, *99*, 8325.

- [91] Charge transfer interactions, vide infra.
- [92] Zelent, B.; Durocher, G. *Can. J. Chem.* **1982**, *60*, 2442.
- [93] Lakowicz, J.R. *Principles of Fluorescence Spectroscopy*, Plenum: New York, 1983.
- [94] (a) Kubota, T.; Miyazaki, H.; Ezumi, K.; Yamakawa, M. *Bull. Chem. Soc. Jpn.* **1974**, *47*, 491.
- (b) Kubota, T.; Miyazaki, H.; Yamakawa, M.; Ezumi, K.; Yamamoto, Y. *Bull. Chem. Soc. Jpn.* **1979**, *52*, 1588.
- (c) Kubota, T.; Uno, B.; Kano, K.; Kawakita, T.; Goto, M. *Bull. Chem. Soc. Jpn.* **1990**, *63*, 516.
- [95] Loutfy, R.O.; Loutfy, R.O. *Can. J. Chem.* **1976**, *54*, 1454.
- [96] Wittel, K.; McGlynn, S.P. *Chem. Rev.* **1977**, *77*, 745.
- [97] Michl, J.; Thulstrup, E.W. *Tetrahedron*, **1976**, *32*, 205.
- [98] Ilge, H.-D.; Kozmenko, M.V.; Kuzmin, M.G. *J. Photochem.* **1987**, *36*, 27.
- [99] (a) Gustav, K.; Storch, M. *Z. Chem.* **1988**, *28*, 406.
- (b) Gustav, K.; Storch, M.; Schreiber, H. *Monatsh. Chem.* **1989**, *120*, 473.
- (c) Gustav, K.; Storch, M. *Monatsh. Chem.* **1990**, *121*, 437.
- (d) Gustav, K.; Storch, M. *Monatsh. Chem.* **1990**, *121*, 447.
- [100] (a) Shapkin, N.P.; Korotkikh, O.A.; Karasev, V.E.; *Russ. J. Inorg. Chem.* **1985**, *30*, 1069.
- (b) Karasev, V.E.; Korotkikh, O.A. *Russ. J. Inorg. Chem.* **1985**, *30*, 1290.
- (c) Karasev, V.E.; Korotkikh, O.A. *Russ. J. Inorg. Chem.* **1986**, *31*, 493.
- [101] Brouwer, A.M.; Bakker, N.A.C.; Wiering, P.G.; Verhoeven, J.W. *J. Chem. Soc. Chem. Commun.* **1991**, 1094.
- [102] (a) Emsley, J.; Freeman, N.J. *J. Mole. Struct.* **1987**, *161*, 193.
- (b) Mills, S.G.; Beak, P. *J. Org. Chem.* **1985**, *50*, 1216.
- (c) Apeloig, Y. In *The Chemistry of Enols*; Rappoport, Z., Ed.; Wiley: New York, 1990; p 1.

- (d) Toullec, J. In *The Chemistry of Enols*; Rappoport, Z., Ed.; Wiley: New York, 1990; p 323.
- [103] (a) Veierov, D.; Bercovici, T.; Mazur, Y.; Fischer, E. *J. Org. Chem.* **1978**, *43*, 2006.
- (b) Veierov, D.; Bercovici, T.; Fischer, E.; Mazur, Y.; Yogev, A. *J. Am. Chem. Soc.* **1977**, *99*, 2723.
- (c) Markov, P.; Petkov, I. *Tetrahedron* **1977**, *33*, 1013.
- (d) Markov, P. *Chem. Soc. Rev.* **1984**, 69.
- (e) Nakanishi, A; Morita, H.; Nagakura, S. *Bull. Chem. Soc. Jpn.* **1977**, *50*, 2255.
- (f) Pascal, F.A. Ph.D. Thesis, Louisiana State University, August 1982.
- [104] Jaffé, H.H.; Orchin, M. *Theory and Applications of Ultraviolet Spectroscopy*, Wiley: New York, 1962.
- [105] Gacoin, P. *J. Chem. Phys.* **1972**, *57*, 1418.
- [106] Seitz, W.R. *Treatise on Analytical Chemistry; Part One, Theory and Practice*; Elving, P.J.; Meehan, E.J.; Kolthoff, I.M., Eds.; Interscience: New York, 1981.
- [107] Marcantonatos, M.; Gamba, G.; Monnier, D. *Helv. Chim. Acta* **1969**, *52*, 538.
- [108] Berlman, I.B. *J. Phys. Chem.* **1970**, *74*, 3085.
- [109] Harju, T.O.; Erostryak, J.; Chow, Y.L.; Korppi - Tommola, J.E.I. *Chem. Phys.* **1994**, *181*, 259.
- [110] Bard, A.J.; Faulkner, L.R. *Electrochemical Methods, Fundamentals and Applications*; Wiley: New York, 1980.
- [111] Wiley, J.R.; Chen, E.C.M.; Chen, E.S.D.; Richardson, P.; Reed, W.R.; Wentworth, W.E. *J. Electroanal. Chem.* **1991**, *307*, 169.
- [112] Chow, Y.L.; Cheng, X.; Johansson, C.I. *J. Photochem. Photobiol. A:Chem.* **1991**, *57*, 247.
- [113] Tamres, M.; Strong, R.L. In *Molecular Association*; Foster, R., Ed.; Academic: New York, 1979; p 331.

- [114] Gur'yanova, E.N.; Gol'dshtien, I.P.; Romm, I.P. *Donor - Acceptor Bond*; Wiley: New York, 1975.
- [115] Marks, A.P.; Drago, R.S. *J. Am. Chem. Soc.* **1975**, *97*, 3325.
- [116] Seal, B.K.; Sil, H.; Mukherjee, D.C. *Spectrochim. Acta A* **1982**, *38A*, 289.
- [117] Person, W.B. *J. Am. Chem. Soc.* **1965**, *87*, 167.
- [118] Deranleau, D.A. *J. Am. Chem. Soc.* **1969**, *91*, 4044, 4050.
- [119] Johnson, G.D.; Bowen, R.E. *J. Am. Chem. Soc.* **1965**, *87*, 1655.
- [120] Connors, K.A. *Chemical Kinetics, The Study of Reaction Rates in Solution*; VCH: New York, 1990.
- [121] Hamilton, T.D.S.; Naqvi, K.R. *Chem Phys. Lett.* **1968**, *2*, 374.
- [122] Al - Wattar, A.J.H.; Lumb, M.D. *Chem. Phys. Lett.* **1971**, *8*, 331.
- [123] Murov, S.L. *Handbook of Photochemistry*; Marcel Dekker: New York, 1973.
- [124] Berlman, I.B. *Handbook of Fluorescence Spectra of Aromatic Molecules*; Academic: New York, 1971.
- [125] Gaweda, E.; Prochorow, J. *Chem. Phys. Lett.* **1975**, *30*, 155.
- [126] Haque, R.; Coshov, W.R.; Johnson, L.F. *J. Am. Chem. Soc.* **1969**, *91*, 3822.
- [127] Walker, M.S.; Bednar, T.W.; Lumry, R. *J. Chem. Phys.* **1967**, *47*, 1020.
- [128] de Lange, M.C.C.; Leeson, D.T.; van Kuijk, K.A.B.; Huizer, A.H.; Varma, C.A.G.O. *Chem. Phys.* **1993**, *174*, 425.
- [129] Beens, H.; Weller, A. *Chem. Phys. Lett.* **1968**, *2*, 140.
- [130] Suppan, P. *Chem. Phys. Lett.* **1983**, *94*, 272.
- [131] Edward, J.T. *J. Chem. Educ.* **1970**, *47*, 261.
- [132] Trotter, P.J. *J. Am. Chem. Soc.* **1966**, *88*, 5721.
- [133] (a) Baumann, W. *J. Mol. Struct.* **1978**, *47*, 237.
(b) Baumann, W.; Bischoff, H.; Fröhling, J.C. *J. Lumin.* **1981**, *24/25*, 555.
(c) Baumann, W.; Nagy, Z. *Pure Appl. Chem.* **1993**, *8*, 1729.
- [134] Knibbe, H.; Rehm, D.; Weller, A. *Ber. Bunsenges. Phys. Chem.* **1969**, *73*, 839.

- [135] (a) Mataga, N.; Okada, T.; Yamamoto, N. *Chem. Phys. Lett* **1967**, *1*, 119.
- (b) Okada, T.; Matsui, H.; Oohari, H.; Matsumoto, H.; Mataga, N. *J. Chem. Phys.* **1968**, *49*, 4717.
- (c) Taniguchi, Y.; Nishima, Y.; Mataga, N. *Bull. Chem. Soc. Jpn.* **1972**, *45*, 764.
- [136] (a) Ware, W.R.; Richter, H.P. *J. Chem. Phys.* **1968**, *48*, 1595.
- (b) Kuzmin, M.G.; Guseva, L.N. *Chem. Phys. Lett.* **1969**, *3*, 71.
- (c) McDonald, R.J.; Selinger, B.K. *Aust. J. Chem.* **1971**, *24*, 1797.
- (d) Talyor, G.N. *Chem. Phys. Lett.* **1971**, *10*, 355.
- (e) Ottolenghi, M. *Acc. Chem. Res.* **1973**, *6*, 153.
- (f) Tavares, M.A.F. *J. Chem. Phys.* **1980**, *72*, 43.
- [137] (a) Cohen, M.; Selinger, B. *Mol. Photochem.* **1969**, *1*, 371.
- (b) McDonald, R.J.; Selinger, B.K. *Mol. Photochem.* **1971**, *3*, 99.
- [138] (a) O'Connor, D.V.; Ware, W.R. *J. Am. Chem. Soc.* **1976**, *98*, 4708.
- (b) O'Connor, D.V.; Ware, W.R. In *12th Informal Conference on Photochemistry*; NBS Special Publication 526; United States Department of Commerce, NBS: Washington, D.C., October, 1978.
- (c) O'Connor, D.V.; Ware, W.R. *J. Am. Chem. Soc.* **1979**, *101*, 121.
- (d) Cheung, S.T.; Ware, W.R. *J. Phys. Chem.* **1983**, *87*, 466.
- [139] Caldwell, R.A.; Creed, D.; DeMarco, D.C.; Melton, L.A.; Ohta, H.; Wine, P.H. *J. Am. Chem. Soc.* **1980**, *102*, 2369.
- [140] Chow, Y.L.; Johansson, C.I. *Res. Chem. Intermed.* **1993**, *19*, 191.
- [141] Saltiel, J.; Atwater, B.W. *Adv. Photochem.* **1988**, *14*, 1.
- [142] Isaacs, N.S. *Physical Organic Chemistry*; Longman; New York: 1987; Table 8.5.
- [143] Itoh, M.; Furuya, S.; Okamoto, T. *Bull. Chem. Soc. Jpn.* **1977**, *50*, 2509.
- [144] Dresner, J.; Prochorow, J. *J. Lumin.* **1981**, *24/25*, 539.
- [145] Chow, Y.L.; Johansson, C.I. *J. Chin. Chem. Soc.* **1993**, *40*, 531.
- [146] Demas, J.N. *Excited State Lifetime Measurements*; Academic: New York, 1986.

- [147] (a) deMelo, J.S.; Macanita, A.L. *Chem. Phys. Lett.* **1993**, *204*, 556.
(b) Heidt, G.K. *J. Photochem.* **1976/77**, *6*, 97.
- [148] O'Connor, D.V.; Phillips, D. *Time-Correlated Single Photon Counting*, Academic: New York, 1984.
- [149] Cramer, L.E.; Spears, K.G. *J. Am. Chem. Soc.* **1978**, *100*, 221.
- [150] Fleming, G.R. *Chemical Applications of Ultrafast Spectroscopy*, Oxford: New York, 1986.
- [151] Birks, J.B. *Prog. React. Kin.* **1970**, *5*, 181.
- [152] Person, W.B. *J. Am. Chem. Soc.* **1962**, *84*, 536.
- [153] Kapinus, E.I.; Aleksankina, M.M.; Dilung, I.I. *Chem. Phys. Lett.* **1985**, *114*, 507.
- [154] Elisei, F.; Aloisi, G.G.; Masetti, F. *J. Chem. Soc. Faraday Trans. 2* **1989**, *85*, 789.
- [155] Zachariasse, K.A.; Duveneck, G. *J. Am. Chem. Soc.* **1987**, *109*, 3790.
- [156] Albright, T.A.; Burdett, J.K.; Whangbo, M.H. *Orbital Interactions in Chemistry*, Wiley: New York, 1985.
- [157] Lim, B.T.; Okajima, S.; Chandra, A.K.; Lim, E.C. *Chem. Phys. Lett.* **1981**, *79*, 22.
- [158] Deperasińska, I.; Prochrow, J.; Sobolewski, A. *Chem. Phys.* **1978**, *32*, 257.
- [159] Birks, J.B. *Photophysics of Aromatic Molecules*, Wiley: New York, 1970.
- [160] Yardley, J.T. *Introduction to Molecular Energy Transfer*, Academic: New York, 1980.
- [161] Bixon, M.; Jortner, J. *J. Chem. Phys.* **1968**, *48*, 715.
- [162] Henry, B.R.; Siebrand, W. *Organic Molecular Photophysics, Volume 1*; Birks, J.B., Ed.; Wiley: New York, 1973; p 153.
- [163] Siebrand, W. *J. Chem. Phys.* **1967**, *46*, 440; *47*, 2411.
- [164] Freed, K.F.; Jortner, J. *J. Chem. Phys.* **1970**, *52*, 6272.
- [165] Engleman, R.; Jortner, J. *Mol. Phys.* **1970**, *18*, 145.
- [166] Fong, F.K. *Acc. Chem. Res.* **1976**, *9*, 433.
- [167] Avouris, P.; Gelbart, W.M.; El-Sayed, M.A. *Chem. Rev.* **1977**, *77*, 793.

- [168] Ali, M.A. *J. Chem. Phys.* **1989**, *91*, 2892.
- [169] Nguyen, K.A.; Gordon, M.S.; Montgomery, Jr., J.A. *J. Chem. Phys.* **1993**, *98*, 3845.
- [170] Kono, H. *Chem. Phys. Lett.* **1993**, *214*, 137.
- [171] Scholes, G.D.; Ghiggino, K.P. *J. Chem. Phys.* **1994**, *101*, 1251.
- [172] Strickler, S.J.; Berg, R.A. *J. Chem. Phys.* **1962**, *37*, 814.
- [173] Birks, J.B.; Dyson, D.J. *Proc. Roy. Soc., A*, **1963**, *275*, 135.
- [174] Ware, W.R.; Baldwin, B.A. *J. Chem. Phys.* **1964**, *40*, 1703.
- [175] Seybold, P.G.; Gouterman, M.; Callis, J. *Photochem. Photobiol.* **1969**, *9*, 229.
- [176] Amirav, A.; Castella, M.; Piuizzi, F.; Tramer, A. *J. Phys. Chem.* **1988**, *92*, 5500.
- [177] Van der Auweraer, M.; Grabowski, Z.R.; Rettig, W. *J. Phys. Chem.* **1991**, *95*, 2083.
- [178] Zarchariasse, K.A. Ph.D. Thesis, Free University of Amsterdam, January, 1972.
- [179] (a) Prochorow, J.; Siegoczyński, R. *Chem. Phys. Lett.* **1969**, *3*, 635.
- (b) Prochorow, J. *Chem. Phys. Lett.* **1973**, *19*, 596.
- (c) Prochorow, J. *J. Lumin.* **1974**, *9*, 131.
- (d) Prochorow, J.; Bernard, E. *J. Lumin.* **1974**, *8*, 471.
- [180] Formosinho, S.J. *Mol. Photochem.* **1976**, *7*, 41.
- [181] Kobayshi, T.; Yoshihara, K.; Nagakura, S. *Bull. Chem. Soc. Jpn.* **1971**, *44*, 2603.
- [182] Van, S.-P.; Hammond, G.S. *J. Am. Chem. Soc.* **1978**, *100*, 3895.
- [183] (a) Van der Auweraer, M.; Swinnen, A.M.; DeSchryver, F.C. *J. Chem. Phys.* **1982**, *77*, 4110.
- (b) Helsen, N.; Viaene, L.; Van der Auweraer, M.; DeSchryver, F.C. *J. Phys. Chem.* **1994**, *98*, 1532.
- [184] Davis, H.F.; Chattopadhyay, S.K.; Das, P.K. *J. Phys. Chem.* **1984**, *88*, 2798.
- [185] Verhoeven, J.W.; Kroon, J.; Paddon - Row, M.N.; Warman, J.M. In *NATO Science Forum on Supramolecular Chemistry*, Balzani, V.; Decola, L., Eds.; NATO ASI Series; Kluwer: Dordrecht, 1992, p 181.

- [186] (a) Gould, I.R.; Farid, S.; Young, R.H. *J. Photochem. Photobiol. A:Chem.* **1992**, *65*, 133.
- (b) Gould, I.R.; Mueller, L.; Farid, S. *Z. Phys. Chem. (München)* **1991**, *170*, 143.
- [187] McGlynn, S.P.; Azumi, T.; Kinoshita, M. *Molecular Spectroscopy of The Triplet State*; Prentice-Hall: Englewood Cliffs, New Jersey, 1969.
- [188] (a) Watkins, A.R. *Chem. Phys. Lett.* **1976**, *43*, 299.
- (b) Watkins, A.R. *J. Phys. Chem.* **1979**, *83*, 1892.
- [189] (a) Shibuya, T. *Chem. Phys. Lett.* **1983**, *103*, 46.
- (b) Shibuya, T. *J. Chem. Phys.* **1983**, *78*, 5175.
- [190] Mattes, S.; Farid, S. *Science* **1984**, *226*, 917.
- [191] (a) Gould, I.R.; Ege, D.; Mattes, S.L.; Farid, S. *J. Am. Chem. Soc.* **1987**, *109*, 3794.
- (b) Gould, I.R.; Moser, J.E.; Ege, D.; Farid, S. *J. Am. Chem. Soc.* **1988**, *110*, 1991.
- (c) Gould, I.R.; Moser, J.E.; Armitage, B.; Farid, S.; Goodman, J.L.; Herman, M.S. *J. Am. Chem. Soc.* **1989**, *111*, 1917.
- (d) Gould, I.R.; Farid, S. *J. Am. Chem. Soc.* **1988**, *110*, 7883.
- (e) Gould, I.R.; Ege, D.; Moser, J.E.; Farid, S. *J. Am. Chem. Soc.* **1990**, *112*, 4290.
- (f) Gould, I.R.; Young, R.H.; Moody, R.E.; Farid, S. *J. Phys. Chem.* **1991**, *95*, 2068.
- (g) Chung, W.-S.; Turro, N.J.; Gould, I.R.; Farid, S. *J. Phys. Chem.* **1991**, *95*, 7752.
- (h) Gould, I.R.; Farid, S. *J. Phys. Chem.* **1992**, *96*, 7635.
- (i) Gould, I.R.; Gomez - Jahn, L.; Goodman, J.L.; Farid, S. *J. Am. Chem. Soc.* **1993**, *115*, 4405.
- (j) Gould, I.R.; Farid, S. *J. Am. Chem. Soc.* **1993**, *115*, 4814.

- (k) Gould, I.R.; Farid, S. *J. Phys. Chem.* **1993**, *97*, 13067.
- [192] (a) Mataga, N. *Pure Appl. Chem.* **1984**, *56*, 1255.
(b) Mataga, N.; Okada, T.; Kanda, Y.; Shioyama, H. *Tetrahedron* **1986**, *42*, 6143.
(c) Ojima, S.; Miyasaka, H.; Mataga, N. *J. Phys. Chem.* **1990**, *94*, 7534.
(d) Kakitani, T.; Yoshinori, A.; Mataga, N. *J. Phys. Chem.* **1992**, *96*, 5385.
(e) Mataga, N. *Pure Appl. Chem.* **1993**, *85*, 1605.
- [193] (a) Goodman, J.L.; Peters, K.S. *J. Am. Chem. Soc.* **1985**, *107*, 1441.
(b) Goodman, J.L.; Peters, K.S. *J. Phys. Chem.* **1986**, *90*, 5506.
(c) Peters, K.S.; Angel, S.A.; O'Driscoll, E. *Pure Appl. Chem.* **1989**, *61*, 629.
(d) Peters, K.S.; Lee, J. *J. Phys. Chem.* **1992**, *96*, 8941.
(e) Li, B.; Peters, K.S. *J. Phys. Chem.* **1993**, *97*, 7648.
(f) Peters, K.S. *J. Am. Chem. Soc.* **1993**, *115*, 3643.
- [194] Thompson, P.A.; Simon, J.D. *J. Am. Chem. Soc.* **1993**, *115*, 5657.
- [195] Baggott, J.E. In *Photoinduced Electron Transfer, Part B*; Fox, M.A.; Chanon, M., Eds.; Elsevier: New York, 1988; p 385.
- [196] Steiner, U.E.; Wolff, H.-J. In *Photochemistry and Photophysics, Volume IV*; Rabek, J.F., Ed.; CRC Press: Boca Raton, 1991; p 1.
- [197] (a) Rehm, D.; Weller, A. *Isr. J. Chem.* **1970**, *8*, 259.
(b) Rehm, D.; Weller, A. *Ber. Bunsenges. Phys. Chem.* **1969**, *73*, 834.
- [198] Ware, W.R.; Lewis, C. *J. Chem. Phys.* **1972**, *57*, 3546.
- [199] Rice, S.A. In *Comprehensive Chemical Kinetics: Diffusion - Limited Reactions, Volume 25*; Bamford, C.H.; Tipper, C.F.H.; Compton, R.G., Eds.; Elsevier: Amsterdam, 1985.
- [200] Szabo, A. *J. Phys. Chem.* **1989**, *93*, 6929.
- [201] (a) Ware, W.R. *Pure Appl. Chem.* **1975**, *41*, 635.
(b) Nemzek, T.L.; Ware, W.R. *J. Chem. Phys.* **1975**, *62*, 477.
(c) Viriot, M.L.; André, J.C.; Ware, W.R. *J. Photochem.* **1980**, *14*, 133.

- (d) Ware, W.R.; Novros, J.S. *J. Phys. Chem.* **1966**, *70*, 3246.
- (e) Andre, J.C.; Niclause, M.; Ware, W.R. *Chem. Phys.* **1978**, *28*, 371.
- [202] Stevens, B.; McKeithan, D.N. *J. Photochem. Photobiol. A:Chem.* **1987**, *40*,1; **1989**, *47*, 131.
- [203] Eads, D.D.; Dismar, B.G.; Fleming, G.R. *J. Chem. Phys.* **1990**, *93*, 1136.
- [204] Song, L.; Dorfman, R.C.; Swallen, S.F.; Fayer, M.D. *J. Phys. Chem.* **1991**, *95*, 3454.
- [205] Dutt, G.B.; Periasamy, N. *J. Chem. Soc., Faraday Trans.* **1991**, *87*, 3815.
- [206] Weller, A. *Z. Phys. Chem. N.F.* **1957**, *13*, 335.
- [207] Chan, T.C.; Chan, M.L. *J. Chem. Soc., Faraday Trans.* **1992**, *88*, 2371.
- [208] Stevens, B.; Biver III, C.J.; McKeithan, D.N. *Chem. Phys. Lett.* **1991**, *187*, 590.
- [209] (a) Efrima, S.; Bixon, M. *Chem. Phys. Lett.* **1974**, *25*, 34.
(b) Efrima, S.; Bixon, M. *Chem. Phys.* **1976**, *13*, 449.
- [210] Ulstrup, J.; Jortner, J. *J. Chem. Phys.* **1975**, *63*, 4358.
- [211] Siders, P.; Marcus, R.A. *J. Am. Chem. Soc.* **1981**, *103*, 748.
- [212] Zachariasse, K.; Weller, A. *Chem. Phys. Lett.* **1971**, *10*, 590.
- [213] (a) Kakitani, T.; Mataga, N. *Chem. Phys. Lett.* **1986**, *124*, 437.
(b) Kakitani, T.; Mataga, N. *J. Phys. Chem.* **1986**, *90*, 993.
- [214] van Duyne, R.R.; Fisher, S.F. *Chem. Phys.* **1974**, *5*, 183.
- [215] Arnaut, L.G.; Formosinho, S.J. *J. Mol. Struct.* **1991**, *233*, 209.
- [216] Katitani, T.; Yoshimori, A.; Mataga, N. *J. Phys. Chem.* **1992**, *96*, 5385.
- [217] Tachiya, M.; Murata, S. *J. Phys. Chem.* **1992**, *96*, 8441.
- [218] Wagner, P.J.; Leavitt, R.A. *J. Am. Chem. Soc.* **1973**, *95*, 3669.
- [219] Schore, N.E.; Turro, N.J. *J. Am. Chem. Soc.* **1975**, *97*, 2482.
- [220] Loutfy, R.O.; Dogra, S.K.; Yip, R.W. *Can. J. Chem.* **1979**, *57*, 342.
- [221] Jones II, G.; Santhanam, M.; Chiang, S.-H. *J. Photochem.* **1980**, *12*, 267.
- [222] Pac, C.; Yasuda, M.; Shima, K.; Sakurai, H. *Bull. Chem. Soc. Jpn.* **1982**, *55*, 1605.

- [223] Mattay, J.; Gerdorf, J.; Buchkremer, K. *Chem. Ber.* **1987**, *120*, 307.
- [224] Loeff, I.; Treinin, A.; Linschitz, H. *J. Phys. Chem.* **1992**, *96*, 5264.
- [225] Föll, R.E.; Kramer, H.E.A.; Steiner, D.E. *J. Phys. Chem.* **1990**, *94*, 2476.
- [226] (a) Kuzmin, M.G. *Pure Appl. Chem.* **1993**, *65*, 1653.
(b) Sadovskii, N.A. Poster presented at the 16th International Conference of Photochemistry, Vancouver, B.C., August 1993; Paper P90.
- [227] Rendell, D. *Fluorescence and Phosphorescence Spectroscopy*; Wiley: New York, 1987.
- [228] Eaton, D.F. *Pure Appl. Chem.* **1988**, *60*, 1107.
- [229] Morris, J.V.; Mahaney, M.A.; Huber, J.R. *J. Phys. Chem.* **1976**, *30*, 969.
- [230] Hui, M.-H.; Ware, W.R. *J. Am. Chem. Soc.* **1976**, *98*, 4718.
- [231] Chojnowski, A.; Wiczak, W.M.; Latowski, T. *Z. Naturforsch.* **1991**, *46a*, 707.
- [232] Green, S.A.; Simpson, D.J.; Zhou, G.; Ho, P.S.; Blough, N.V. *J. Am. Chem. Soc.* **1990**, *112*, 7337.
- [233] *The PTILS - 100 Luminescence System: Reference Manual*; Photon Technology International: New Jersey, 1992.
- [234] Love, L.J.C.; Shaver, L.A. *Anal. Chem.* **1980**, *52*, 154.
- [235] O'Connor, D.V.; Ware, W.R.; Andre, J.C. *J. Phys. Chem.* **1979**, *83*, 1333.
- [236] Kissinger, P.T.; Heineman, W.R. *J. Chem. Educ.* **1983**, *60*, 702.
- [237] Mann, C.K. in *Electroanalytical Chemistry, Volume 3*; Bard, A.J., ed.; Marcel Dekker: New York, 1969; p 57.
- [238] Howell, J.O.; Goncalves, J.M.; Amatore, C.; Klasinc, L.; Wightman, R.M.; Kochi, J.K. *J. Am. Chem. Soc.* **1984**, *106*, 3968.
- [239] Meites, L.; Zuman, P. *CRC Handbook Series in Organic Electrochemistry, Volume 1*; CRC Press: Cleveland, Ohio, 1976.
- [240] Gagné, R.P.; Koval, C.A.; Lisensky, G.C. *Inorg. Chem.* **1980**, *19*, 2855.

[241] Shoemaker, D.P.; Garland, C.W.; Steinfeld, J.I. *Experiments in Physical Chemistry*; McGraw - Hill: New York, 1981.